![University of Nottingham logo — UK | CHINA | MALAYSIA]

Faculty of Engineering

Department of Chemical and Environmental Engineering

Technical and economic assessment of process integration in gasoline production

Tasneem Muhammed (BSc, MSc)

A thesis submitted to the University of Nottingham for the degree of

Doctor of Philosophy

March 2021

Abstract

In chemical engineering, process design is a fundamental attribute that includes process definition, simulation, and optimization. Commonly, superstructure approaches are used for process design. These approaches represent the process by integrating simpler unit blocks described by physical and chemical properties to retrofit complex chemical processes. The superstructure approaches follow certain objectives (e.g. economic, environmental and social) that can be optimized. This makes the implementation of superstructure approaches in process design a challenging task.

In this thesis, a superstructure-optimization framework is proposed considering economic criteria. The proposed superstructure representation divides the process into sections and then links these sections using a switch. This generates several pathways that are economically evaluated and then optimized. The framework is modelled using the HYSYS®-MATLAB® hybrid software platform. This platform implements two or more software programs and applications, each of which has a different specialist feature, to obtain a wider overview oi the process constraints, variables and conditions.

The proposed platform is applied in a case study. After generating process pathways, a trade-off between capital and operating costs are determined and then optimized employing the genetic algorithm (GA) method, which mimics the natural process of selection. The algorithm selects the most practical and economical process configuration design,

considering alternative operating conditions, process pathways, materials and energy efficient units.

Gasoline production through isomerisation process of light naphtha was chosen as the case study, because the isomerisation process fulfils strict environmental regulations that call for lower energy consumption and cleaner fuel (e.g. fewer carcinogens substances such as aromatics). The process mainly converts the straight chain of normal paraffin to iso-paraffin. The isomerisation process superstructure was made of two sections: frontend and backend. The frontend process flowsheet includes three catalysts: chlorinated alumina-based, sulphated metal oxide-based, and zeolite. The backend process flowsheet includes five independent separation units, consisting of distillation column (DIS), eight-bed simulated moving bed adsorption (SMB), and three energy efficient side-stream distillation processes: absorption (AHP), bottom flash (BF) and vapour recompression (VRC) heat pumps.

The front end and backend flowsheets were linked by using the switch method, which connects the selected element(s) of the superstructure process without interacting with the other options. This adds up to 15 pathways made of the combination of the frontend and backend processes to produce gasoline. This enables the proposed platform to economically evaluate and optimize each combination independently.

As a result of evolving the process for 100 populations and 20 generations, a maximum net present value (NPV) of \$220 million and maximum gasoline research octane number (RON) of 95 were obtained for the combination of sulphated metal oxide-based catalyst and the

SMB flowsheet. However, coupling AHB and zeolite base catalyst to produce gasoline only achieved $180 million NPV and 90 RON. Also, the overall energy consumed (i.e. heating and electricity) and production cost of the optimal flowsheet combination were 0.33 GJ and $1.67 million per barrel gasoline, respectively. Thus, the developed method reduces the energy consumption and production costs by approximately 20% and 30% respectively over the conventional refinery.

In conclusion, our approach increases the gasoline production process NPV by approximately 15% over the base case. Applying the method for other applications and processes is recommended as long as the energy consumption and product quality are considered.

Acknowledgements

Thank you to my supervisors Prof Alex Conradie, Dr Begum Tokay and Dr Paul Langston for their patience, helpful guidance, constructive criticism notes and feedback, and endless support. It is truly a privilege and indeed a great honour to work under their supervisions. I am delighted to thank Dr Buddhika Hewakandamby for sharing his knowledge and wisdom.

Dedication

I dedicate this thesis to my beloved parents Abd-elfatah and Salma ...

Declaration

No part of this thesis has previously been submitted for a degree or other qualification at this or any other university.

Table of Contents

List of Figures

List of Tables

List of algorithms

Nomenclature

Latin Symbols

A   Pre-exponential factor (s^{-1})

A   The payment per interest period ($M)

A   Heat transfer area (m^2)

A_n Net area (m^2)

b   Adsorption affinity constant (kPa^{-1})

b^0 frequency factor of the affinity constant (kPa^{-1})

c_i Concentration of component i in the fluid ($kmol/m^3$)

C_p Specific heat capacity (J/mol K)

Cv   Valve constant (kmol/kPa h)

D_{ax} Axial mass dispersion coefficient (m^2/s)

D_m Molecular diffusion coefficient (m^2/s)

E   Activation energy or interaction energy (kJ/mol)

F   Molar flowrate (kmol/h)

G_f Specific gravity of the fluid

i   Interest rate (%)

k   Kinetic constant (s^{-1})

Latin Symbols- continue

k_{MTCi}	Effective mass transfer coefficient of component i (s^{-1})
M_w	Molecular weight
m	Number of front end flowsheets (e.g. Catalysts)
n	Number of back end flowsheets (e.g. Separators)
n	Number of components
n	Plant lifetime (year)
n	Number of interest period (year)
n	Number of column trays
p_i	Partial pressure of sorbate i (kPa)
P	Present worth ($M)
P	Pressure (kPa)
P_o	Operating pressure (kPa)
P_d	Design pressure
ΔP	Pressure drop (kPa)
$\overline{q_i}$	Average amount of solute i adsorbed ($kmol/kg_{ads}$)
q_i^*	Equilibrium loading of component i ($kmol/kg_{ads}$)
q_i	Amount adsorbed of component i (mol/m^3)

Latin Symbols- continue

q_m	Saturation loading of component i (mol/m^3)
Q	Volumetric flowrate (m^3/h)
Q	Heat transfer (J/mol)
r	Reaction rate (mol/m^3.s)
r_p	Particle radius (m)
R	Gas constant (8.314 J/mol.K)
Rc	Internal column radius (m)
t	Time (s)
ΔT_{lm}	Temperature logarithmic mean
T	Temperature (K)
U	Overall heat transfer coefficient
v_g	Gas velocity (m/s)
V	Reactor volume (m^3)
W	Work (kWh)
W	Tower weight (kg)
x	Space (m)
x	Component fraction (%)

Abbreviations

AOC	Annual operating cost
BPD	Barrel per day
C_B	Base cost ($M)
C_p	Purchase cost ($M)
C_{pl}	Stairs and platform cost ($M)
C_{tr}	Trays cost ($M)
C_V	Empty Vessel cost ($M)
D_i	Inner Diameter (m)
E	Welding efficiency (%)
EMPC	Economic model predictive control
F_L	Length tube correction factor
F_M	Material type factor
F_P	Pressure factor
F_T	Pump type factor
FC	Fixed cost
FDM	Finite difference method
BTCS	backward time centred space

Abbreviations-continue

GA	Genetic algorithm
GDP	Generalized disjunctive programming
H	Height (m)
H	Pump head (m)
HEN	Heat exchanger network
HQI	Health quotient index
IRR	Internal rate of return
ISI	Inherent safety index
IOHI	Inherent occupational health index
L	Length(m)
LCA	Life cycle assessment
LP	Linear programing
MINLP	Mix integer non-linear programing
MPC	Model predictive control
MP	Medium pressure steam
NLP	Non-linear programing
NPV	Net present value ($M)

Abbreviations-continue

PBP	Payback period
P_B	Brake power (kW)
P_c	Power consumed (kW)
P_T	Theoretical power (kW)
PC	Production cost ($M)
PCR	Potential chemical risk
PDEs	Partial differential equations
PR	Peng-Robinson equation-of-state
PSO	Particle swarm optimization
QRA	Quantitative risk assessment
RON	Research Octane Number
RC	Recycle convergence
S	Size factor
S	Maximum material stress allowable
SA	Simulated annual
SEN	State-equipment network
STN	State-task network

Abbreviations-continue

SQP	Sequential Quadratic Programming
t_p	Wall thickness (m)
t_s	The stage height (m)
TAC	Total annual cost ($M)
TEA	Techno-economic analysis
TCI	Total capital investment
TIP	Total isomerisation process
VC	Variable cost ($M)

List of Components

c-	Cyclo-
HC	Hydrocarbon
i-	Isomer
n-	Normal
nC4-	Butane and lighter HC
nC5	Pentane
nC6	Hexane
nC7+	Heptane and heavier HC

List of Components-continue

iC4   Iso-butane

iC5   Iso-pentane

2MC5   2-methylpentane

3MC5   3-methylpentane

22DMC4   2,2-dimethylbutane

23DMC4   2,3-dimethylbutane

2MC6   2-methylhexane

3MC6   3-methylhexane

iC7+   Iso-heptane and heavier HC

cC4   Cyclo-butane

cC5   Cyclo-pentane

McC5   Methylcyclopentane

cC6   Cyclo-hexane

cC7+   Cyclo-heptane and heavier HC

Columns and beds

AHP   Absorption heat pump

BF   Bottom flashing heat pump

DIH   Deisohexanizer

DIP   Deisopentanizer

DIS   Distillation

DP   Depentaneizer column

PSA   Pressure swing adsorption

SMB   Simulated moving bed

VRC   Vapour recompression heat pump

Programs & licence

ACM   Aspen custom modeler

Aspen   Advanced System for Process Engineering

ASW   Aspen simulation workbook

COM   Component object model

HYSYS   Hyprotech System

MATLAB   Matrix Laboratory

UOP   Universal Oil Products

VBA   Visual Basic for Applications

Sub- and Super- script

b   Bulk

g   Gas phase

H   High

i   Component

in   Inlet

j   Site

L   Low

p   Particle

s   Solid phase

out   Outlet

v   Vapour

Greek Symbols

ε_b Interparticle voidage (m^3_{void}/m^3_{bed})

ε_t Intraparticle voidage ($m^3_{void+bed}/m^3_{bed}$)

ρ Construction material density (kg/m^3)

ρ_b Adsorbent bulk density (kg/m^3)

ρ_g Gas phase density (kg/m^3)

Δ Change (step size)

η Efficiency (%)

η_M Electric motor efficiency (%)

η_P Pump efficiency (%)

γ Ratio of specific heat

μ_g Dynamic viscosity ($N\ s/m^2$)

Ω_D Diffusion collision integral

σ Collision diameter (Å)

Mathematical symbols

∂   Partial differential

Σ   Summation

π   Mathematical constant (3.142)

exp   Exponential function

n!   Factorial function which equals [n× (n-1) ×… × 2×1]

f   Function

j   Time coordinate index

i   Axial coordinate index

ln   Natural logarithm

m   Number of time elements

n   Number of space elements

Chapter 1   Introduction

1.1 General overview

70-80% of chemical process design problems were predicted by Grossmann et al. (1987) involve process retrofitting. Process retrofitting is a way to generate a considerable number of alternatives that can be evaluated and optimized (Grossmann et al., 1987). Superstructure optimization-based approaches involve associating process networks to be optimized according to economic, environmental, and/or social objectives (Grossmann, 1989, Umeda et al., 1972, Biegler et al., 1997). These approaches have been widely used in chemical process retrofitting syntheses (Mencarelli et al., 2020, Sitter et al., 2019), for example, to synthesise a rigorous distillation sequence (Cui and Sun, 2019), a reactor network (Martinez-Gomez et al., 2017) and a heat exchanger network (Aguitoni et al., 2018). However, investigation of the combination of such syntheses has been quite scarce in the literature. It is somewhat surprising that this combination has not been previously studied for a field-scale superstructure flowsheet and optimized economically.

1.2 Proposed method

This study aims to develop a superstructure optimization method that solves and optimizes a case study. Modelling level, economic evaluation level and optimization level are the proposed sequence to retrofit the case study. These levels are explained as follows.

1.2.1 Modelling level

To our knowledge, there are no previous studies that used the superstructure method to fully model and optimize a chemical process. As superstructure approaches describe the process implications, these approaches are significant to find the optimal flowsheet design (Chen and Grossmann, 2017). The main two challenges to achieve this are: the process/unit alternative simulations and the flowsheet superstructure organization (Chen and Grossmann, 2017).

First, sequential modular (SM) software such as Aspen HYSYS®, Aspen PLUS® and ProII® are commonly used to simulate the chemical process (Marchetti et al., 2001). Although these software support numerous build-in models, they do not satisfy the user needs, especially in biochemical, polymer, and specialty industrial processes (Shacham et al., 1982). To customize these process/unit, mathematical oriented (EO) software such as ACM®, MATLAB®, GAMS® and gPROMS® are used (Ponce-Ortega and Hernandez-Perez, 2019). Then, SM and EO software were integrated to generate a comprehensive superstructure flowsheet.

To tackle the second challenge, this research suggested a generic superstructure flowsheet. Several methods have been developed to represent superstructure processes (Chapter 2). This thesis aims to introduce a novel switch method instead of the traditional methods to represent a superstructure process easier, reduce the computational approaches, and minimize the optimization steps. Thus, the proposed

superstructure flowsheet can comprehensively represent the process network association.

1.2.2 Economic evaluation level

In this thesis, a techno-economic analysis, i.e. net present value (NPV), was associated with the process, since the different scale was proposed. Capital cost (CAPEX), total capital investment (TCI) and operating cost (OPEX) detailed calculations were covered in Chapter 5.

1.2.3 Optimization level

Choosing the appropriate flowsheet design and operating conditions from a plethora of alternatives with respect to sustainable criteria is an example of the design challenges in the chemical process (Lam et al., 2011). Optimization methods find the best solution from several alternatives, considering the sustainable objective function, i.e. the NPV equation, (Segovia-Hernández and Gómez-Castro, 2017). Interaction between alternatives creates a nonconvex problem with a high number of degrees of freedom that are expected to have multiple local optimal solutions (Segovia-Hernández and Gómez-Castro, 2017).

Therefore, advanced optimization tools such as stochastic algorithms that search for global solutions have been employed (Carroll, 1961). However, such algorithms are not available in SM software, e.g. Aspen PLUS® and HYSYS®, which only support deterministic methods such as sequential quadratic programming (SQP) (AspenTech, 2019). Fortunately, stochastic methods either can be easily programmed in EO software or are available within these program toolboxes. Thus, in this

study, the hybrid simulation-optimization platform was applied to solve the process retrofitting.

The proposed platform linked both MATLAB® and Aspen HYSYS® and then the process was optimized using the genetic algorithm (GA), which is built in to MATLAB®. GA optimization is the process of mimicking the natural life of selection (Martinez-Gomez et al., 2017). This stochastic optimization tool has a great ability to find global optima (Segovia-Hernández and Gómez-Castro, 2017).

Figure 1-1 describes the GA procedure to obtain the global optimal solution (Haupt and Haupt, 2004, McCall, 2005). To begin with, the first population is generated randomly. This is followed by evaluating each individual in the population using an objective function. Then, the algorithm checks whether the termination condition is met or not. If the termination condition is not met, the algorithm generates the next generation via three operators, namely, selection, crossover and mutation. The selection step is randomly choosing two parents/individuals/chromosomes. To select these individuals, several methods are used such as roulette wheel, tournament, ranking, and random selections (Abualigah, 2018).

This step is followed by the crossover step, where offspring are generated by swapping two gens at one point, two points, and uniform crossover. The probability of the generated offspring using the crossover is ranged between 0 and 1 (Abualigah, 2018). The following step is the mutation step, where the one point or uniform flips methods are used to flip gens. This leads to improve the produced children. The probability of

mutated children is between 0 and 1 (Abualigah, 2018). These new offspring replace old parents to generate new generation. Then the loop closes by returning these data to the evaluation step and repeat until termination condition is met. Finally, the algorithm stops and delivers the optimal solution. A reflection of GA on a process model-encoding example is available in Appendix A.
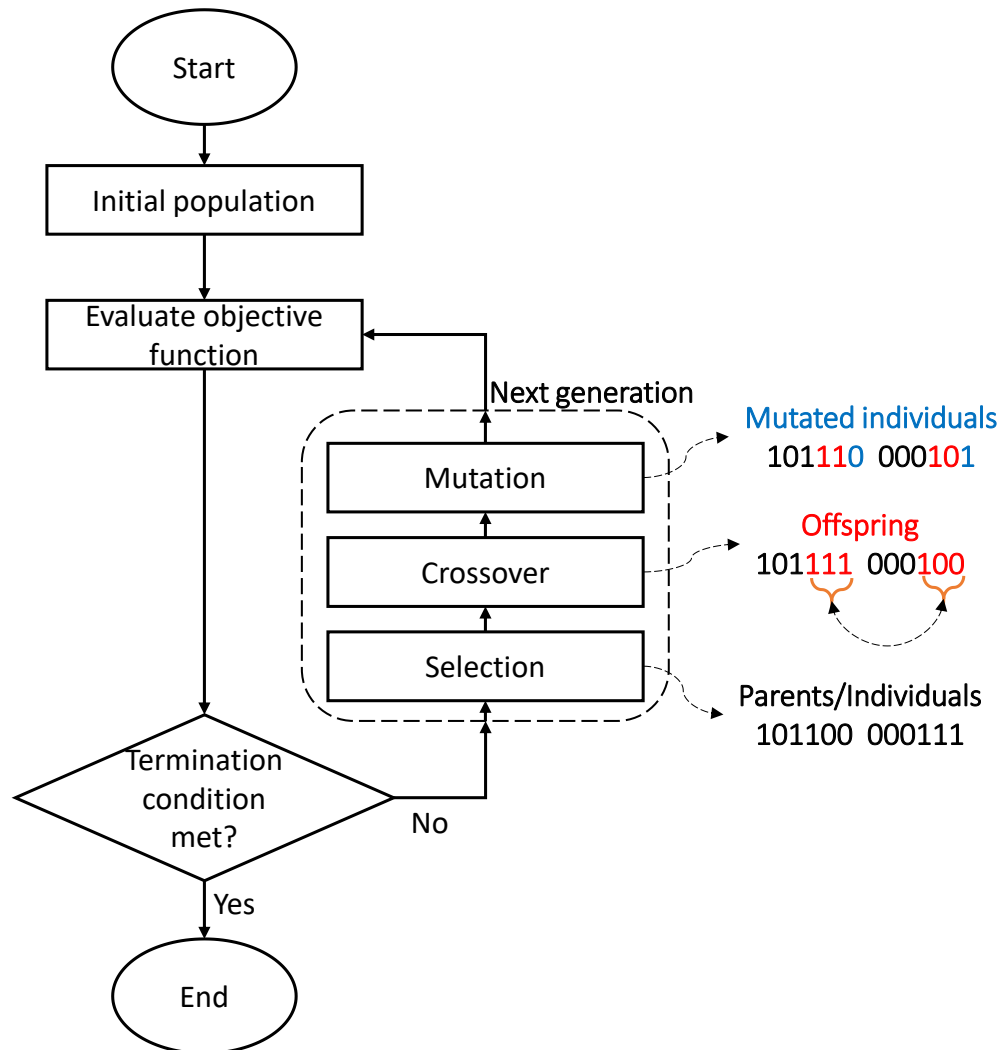
Figure 1-1 Genetic Algorithm flow diagram

1.3 Case study: Isomerization of light naphtha process

1.3.1 General background of the case study

Gasoline is one of the global economy pillars (Hancsók et al., 2020). Due to the strict environmental and economic criteria, the production of

gasoline has to consume less energy (Haynes, 1979) with high-quality products (Szoboszlai and Hancsók, 2011, Chekantsev et al., 2014). The gasoline specification research octane number (RON) required in the market is a minimum of 95 (Oils, 2015). RON is a measure of the knocking (pinking) of the gasoline occurs in spark-ignition engines. A high-octane number obtains high resistance of the auto-ignition in an internal combustion engine. RON is determined by comparing their knocking with n-heptane (0 RON) and iso-octane (2, 2, 4-trimethylpentane) (100 RON) (Mohamed A. Fahim et al., 2010, Ross, 2012). Components additive, such as alcohol and ethers (anti-knocking) are used to increase the RON. However, these components are toxic, air pollutants and cause cancer for humankind (Szoboszlai et al., 2012, Naqvi et al., 2018). Moreover, natural gasoline components, such as aromatics (e.g. benzene), gives a higher quality too, however, it has a carcinogen impact.

Isomerization of light naphtha process considers environmentally friendly and economically attractive to produce gasoline. The reasons of this are the process converts normal paraffin to isomers, which enhances the gasoline RON up to 93, breaks aromatics to basic components and converts sulphur into HS, which easier to be treated (Meyers, 2004). The importance of investing in the isomerization process has been increased in the last 10-15 years (Hunter, 2003). The global stock naphtha market value is predicted to increase to around $200 billion with compound annual growth rate (CAGR) 3.5% for the period 2016-2030 (Charliegefen, 2017).

This case study is a good problem to test the proposed superstructure optimization platform against for the following reasons:

- Economic and environmental impact of the process and the potential money and energy saving that can be made.
- The industrial importance of the process scale.
- The complex nature of reaction kinetics.
- Paraffin recycle to increase the RON against the capital cost (i.e. adding separator unit).
- Hydrogen recycle trade-off between capital and operating costs.
- High potential of energy saving.

1.3.2 The isomerization process flowsheet

Figure 1-2 shows the process flowsheet, which is described as follows. The light naphtha feed stream, which has about 70 RON and mostly contains normal pentane and hexane (Chekantsev et al., 2014), is pumped and mixed with the hydrogen make-up stream. The mixture is preheated and charged to a fixed bed catalytic reactor conducted in the vapour phase at low temperature to isomerize the normal paraffin. Then, the reactants stream is cooled using air cooler to recycle the hydrogen. The liquid product is discharged to stabilizer column to separate the off gases from the gasoline (78-80) RON. To increase the RON, the product is discharged by a separation unit that recycles the low RON product and withdraws the high RON gasoline (Sullivan et al., 2015).
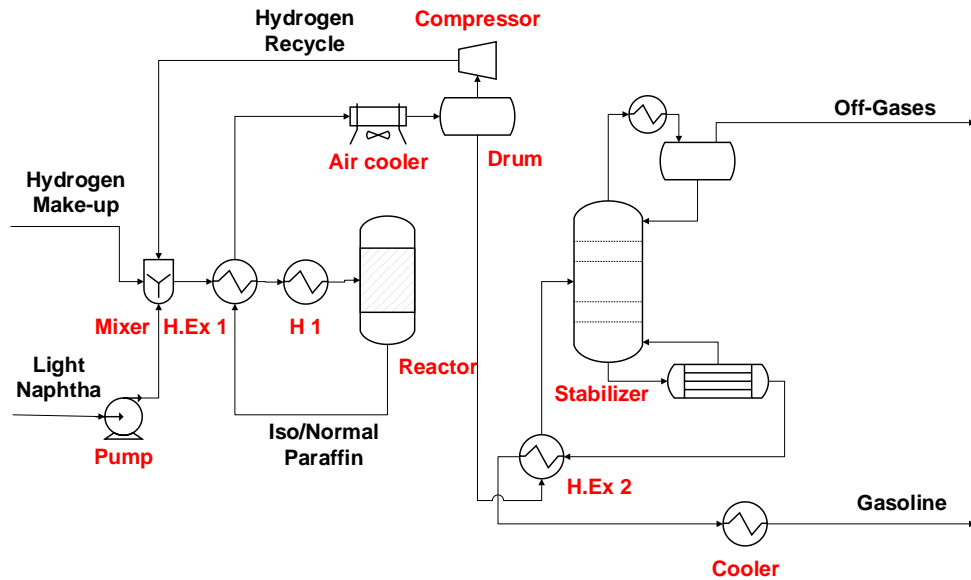
Figure 1-2 Generalized diagram of the isomerization process

Several catalysts and separation units were developed in the literature to upgrade the gasoline RON. However, these studies were examined the RON upgrading experimentally, modelled at lab scale, and did not simulate all available operating conditions and separation unit options. Furthermore, these studies did not associate and compare the process path-ways economic feasibilities or optimized the process in a field scale.

Therefore, in this thesis, to optimize the process, a superstructure optimization approach was proposed to include a variety of catalysts namely chlorinated alumina-based, sulphated metal oxides based and zeolite catalysts and separation units namely distillation column, moving bed adsorption (SMB), and heat integrated distillation processes compressing the vapour recompression heat pump (VRC), the bottom flashing heat pump (BF) and the absorption heat pump (AHP). This superstructure was then utilised within a comprehensive optimization framework using the techno-economics as the objective function to arrive at the optimal equipment selection and operating conditions.

1.4 Aims and objectives

The aim of this project is to develop a comprehensive superstructure flowsheet representation and an optimization method that considers wider operating variables and unit operations. This was achieved through the following objectives:

- Re-build and rescale a comprehensive superstructure simulation of the isomerisation process, using the developed switch method.

- Model an eight-simulated moving bed (SMB) in a field scale using a numerical method.

- Accommodate energy-efficient distillations.

- Investigate the interaction between a steady-state system and dynamic system in a hybrid software.

- Insert a rigorous techno-economic assessment to the process case study, which evaluates the process by using net present value (NPV).

- Propose an optimization platform using a genetic algorithm (GA) that overcomes the changes in designing a chemical engineering process by estimating the trade-off between the capital and operating costs.

1.5 Thesis roadmap

Thesis roadmap is outlined as follows (Figure 1-3). Chapter 2 collects and reviews the historical information about superstructure methods and summaries the previous studies of different optimization tools, objective functions and hybrid software. Chapter 3 describes the methodologies that were used throughout the thesis. The chapter comprises the

numerical solution to model the 8-simulated moving bed adsorption using backward time centred space (BTCS) method and the interface between MATLAB® and Aspen HYSYS® in hybrid optimization platform.

Referring to Section 1.2, detailed steps of each level of the methodology sequence are also presented in Figure 1-3. First, modelling level, to have a comprehensive and reliable superstructure model of the isomerisation process, chapter 4 begins collecting the design and operating data for each alternative unit of the isomerization process. The reliability of these preliminary unit-designs was tested and validated against the available literature. Moreover, equipment, namely, heat integrated distillation processes and simulated moving bed were rescaled and integrated by using the switch method to complete the overall superstructure model.

Then, the economic evaluation level, in chapter 5, discusses and details the techno-economic analysis, builds-up the objective function and its implementations in the HYSYS® spreadsheet (Figure 1-3). Followed by the optimization level that discusses the hybrid optimization platform results, and compares the outcomes of applying different GA parameters on the final decision in chapter 6 (Figure 1-3).

Chapter 7 Concludes and summarises the findings from this thesis as well as provides recommendations and suggestions for future developments.
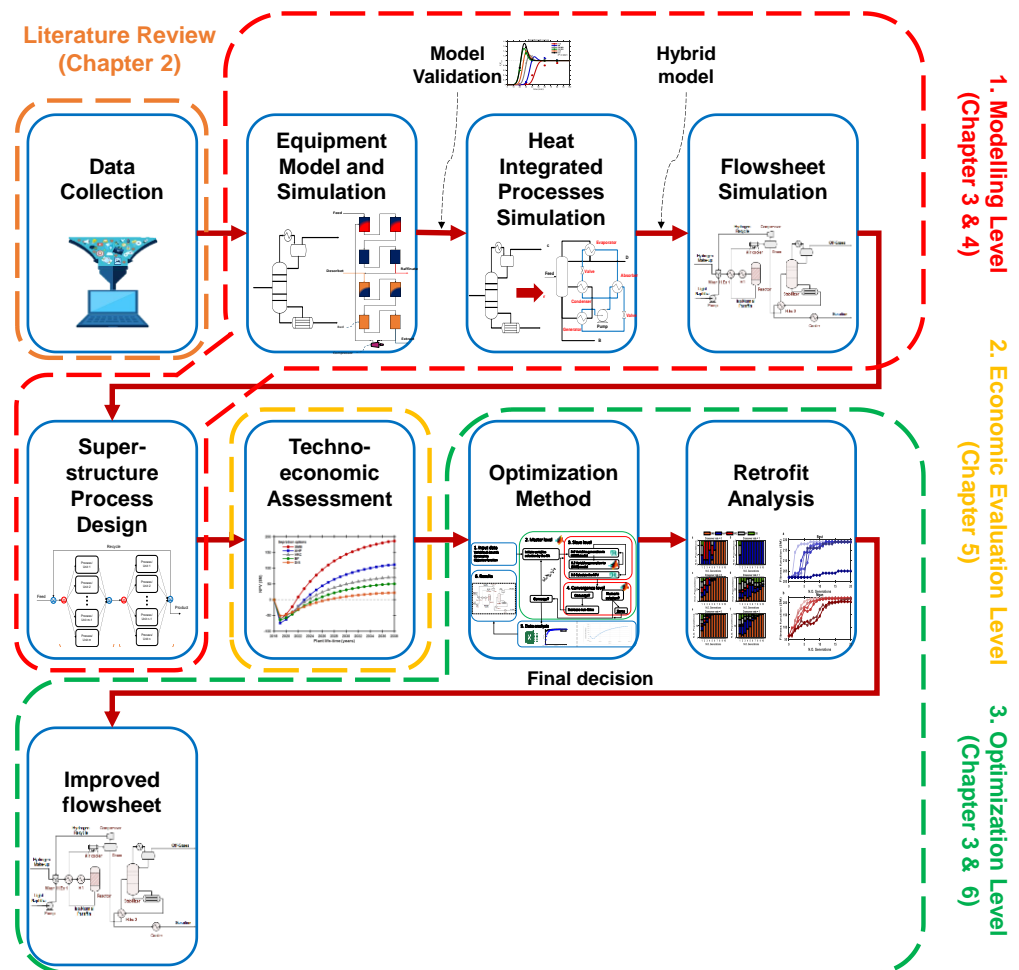
Figure 1-3 Thesis roadmap

Chapter 2   Literature review

2.1 Introduction

There is substantial research on superstructure flowsheets and optimization methods due to the increasing demands on creating sustainable processes. The majority of publications focused on superstructure representation of sub-flowsheet processes such as heat exchanger network, mass exchange network, reactors network and distillation sequences. Therefore, the current literature review conducts the history of the process synthesis designing and modelling methods. Moreover, a discussion of suitable criteria to evaluate the process synthesis expressed as an objective function is provided.

In addition, the chapter compares optimization approaches, namely, deterministic, stochastic, and hybrid that are usually evaluated the superstructure flowsheet. Furthermore, in the last decade, studies highlighted the importance of using hybrid software, which links two or more software, to model, optimize and control chemical processes. These hybrid software are also reviewed in this chapter.

2.2 Process synthesis

Since the 1970s, the definition of designing a chemical process with respect to synthesis has been developed over the years. Process synthesis is the art of generating the optimal configuration of a process associating the process economic, environmental and/or social impacts (Skiborowski, 2018, Sitter et al., 2019). Process synthesis design is based in two methods, which are hierarchical decomposition

approaches (Siirola and Rudd, 1971, Douglas, 1985) and superstructure approaches (Umeda et al., 1972, Chen and Grossmann, 2017). The distinctions between these approaches are elaborated in the following subsections.

2.2.1 Decomposition methods

Decomposition methods are based on a sequence stages of making decisions (Douglas, 1985). These decisions are made by engineering judgment, at each stage (Mencarelli et al., 2020). These methods distribute the process design into five stages/levels (Douglas, 1985), which are:

- Batch vs. continues.
- Input-output flowsheet
- Recycle and reactor contracture considerations
- Separation level
- Heat exchanger network

An onion model was developed by Smith and Linnhoff (1988), which is an example of decomposition methods. Figure 2-1 illustrates the method hierarchical, which selects the reactor (e.g. type) and then adds separation and recycle structure and so on (Smith and Linnhoff, 1988). The main advantage of the method is the ability to control the simple selections and cooperate with the process design as it develops maintains the method attentiveness (Smith and Linnhoff, 1988). The reason of this is that the method separated the making decisions process into levels; each level dealt with its particular challenges (Foo and Ng, 2013).
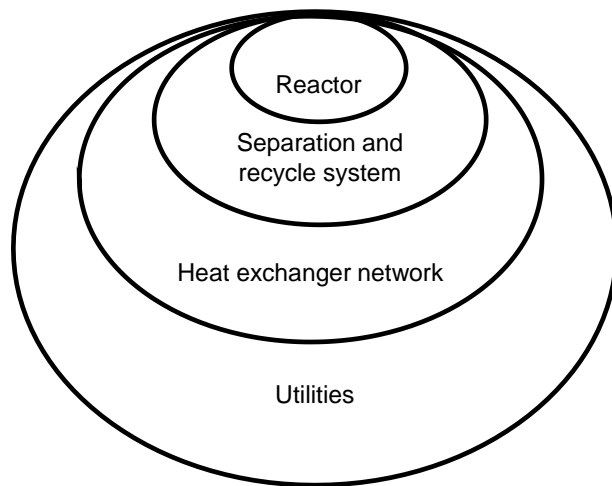
Figure 2-1 The onion model (Smith and Linnhoff, 1988)

As sustainable processes are required mainly for environmental reasons, resent advancements on the onion model were introduced by several researshers (Foo and Ng, 2013, Gundersen, 2002, Klemes, 2011). In order to obtain a sustainble chemical process (e.g. minmize the process emissions), Klemes (2011) added an external layer to the onion model that called ambient layer. The ambient layer, where the process emissions and effluent are treated prior to being disposed to the environment, which can benefit the ecosystem (Klemes, 2011).

For more sustainability, process technologies such as process integration (PI) and purification systems are gradually improved over the years. Therefore, Foo and Ng (2013) extended the onion model to include material recovery system, heat recovery system, energy utility system layers, which deal with mass and heat integrations (Figure 2-2). Adding treatment-systems layer to deal with pre- and post- treatment was also included (Foo and Ng, 2013), as shown in Figure 2-2. Further development was carried on considering the safety, health and environmental impacts within each layer instead of insert these impacts in an outer separated layer (Teh et al., 2019). Moreover, process integration (PI) is a systematic method for designing an efficient use of

14

energy and reducing environmental impacts of processes (IEA, 1993). As the utilities layer is the center of the process (Figure 2-1), these utilities (e.g. heating, cooling and power) need to be integrated with the different process sites. Therefore, Gundersen (2002) established the interaction between the onion leyers (Figure 2-3). The study proposed exchange of utilites between layers (Gundersen, 2002, Wiertzema et al., 2020).
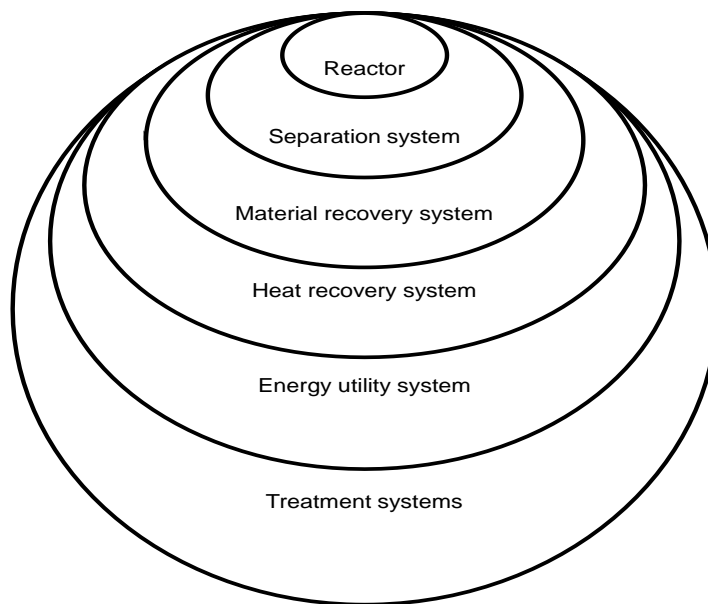
Figure 2-2 The extended onion model (Foo and Ng, 2013)

Although significant endeavors to develop the decomposition method were introduced by the aforesaid researchers, interaction between these levels is not fully recovered (Chen and Grossmann, 2017). The abovementioned models ignore the upstream effects and disconnect the logical flow of information between the onion core and outer layers (Gundersen, 2002, Wiertzema et al., 2020). Moreover, optimization is only allowed after reaching the last level, which makes it difficult to evaluate each alternatives, especially alternatives closer to the onion

core (e.g. reactor design/operating conditions) (Smith and Linnhoff, 1988).
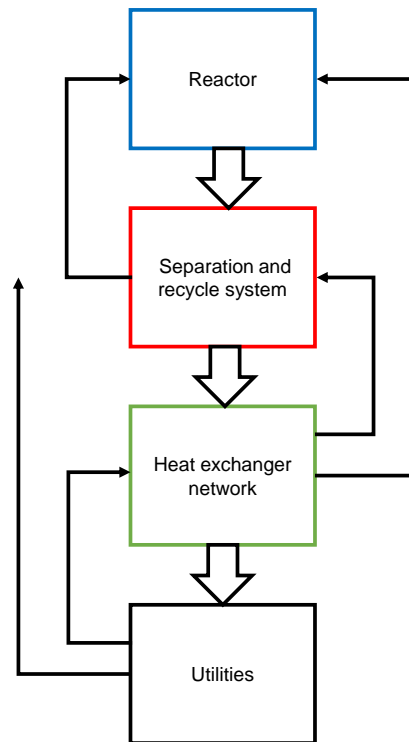
Figure 2-3 The onion model with interacted layers (Gundersen, 2002)

For these reasons, a poor process flowsheet representation is generated. Also, the flowsheet representation can lead to inaccurate and unfavorable outcomes, which strongly misses the process evaluation (e.g. financial feasibility, environmental influence). Therefore, superstructure representation methods are introduced.

2.2.2 Superstructure representation methods

Superstructure methods are the way of representing and finding an optimal process scheme by means of a proposed design (Umeda et al., 1972). These methods obtain three steps (Chen and Grossmann, 2017), which are:

- Postulation of a superstructure.
- Mathematical model.

- Optimization solution by solving the mathematical model.

In the following subheadings, the most common superstructure representation approaches are reviewed and compared by providing a three components sharp split distillation example for each approach.

2.2.2.1 State-task network (STN)

State-task network (STN) represents the process as nodes, namely, states and tasks (Figure 2-4) (Kondili et al., 1993). States imply physical and chemical properties (e.g. Temperature and pressure) of process streams such as feed, intermediate, or product streams (Yeomans and Grossmann, 1999). Tasks imply process operations (e.g. reactions and adsorption) between states, where physical and chemical transformations happen (Yeomans and Grossmann, 1999). To construct a process, all unit alternatives of the process are considered as tasks and connecting them via status to generate different process routes.
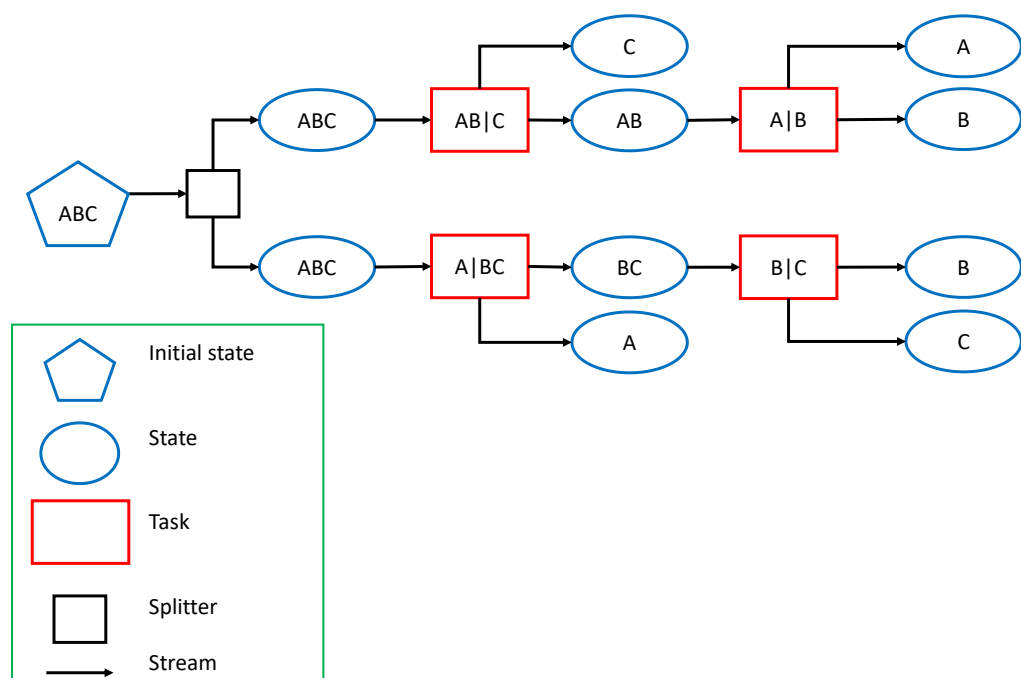
Figure 2-4 State-task network (STN) for 3 components separation (Mencarelli et al., 2020)

17

2.2.2.2 State-equipment network (SEN)

Similarly, state-equipment network (SEN) represents the process as nodes, namely, states and equipment (Figure 2-5) (Smith and Pantelides, 1995). The term equipment can be defined as the physical devices that implement a given task (e.g. reactor and adsorber) (Smith and Pantelides, 1995). Using SEN to represent superstructures decreases the number of nodes needed, compared to STN by ratio of 10:4 (STN:SEN) as concluded by Yeomans and Grossmann (1999). For 3 componets sharp spliter distillation given example the node raio were 4:2 for STN:SEN (Mencarelli et al., 2020).
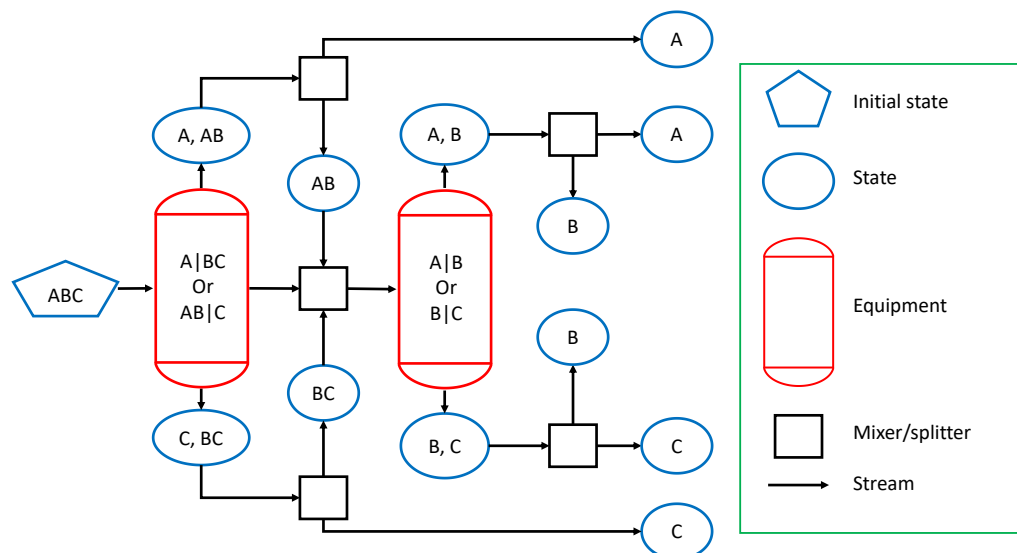
Figure 2-5 State-equipment network (SEN) for 3 components separation (Mencarelli et al., 2020)

2.2.2.3 P-graph network superstructure (PNS)

Process graph (P-graph) constructs the process as nodes, namely, material (M-type) and operation unit (O-type) in a bipartite graph (Figure 2-6) (Friedler et al., 1992a, Friedler et al., 1992b). The nodes in the PNS method is similar to STN; material nodes resemble state nodes while operator nodes resemble tasks nodes (Friedler et al., 1993). The method

is a systematic (i.e. polynomial) algorithm for constructing the P-graph that can provide the maximal structure generation (Friedler et al., 1993). Although the key advantage of the P-graph method is the mathematical accuracy for building the superstructure, its closed implementation and complex notation make it hard to be applied to chemical processes (Mencarelli et al., 2020).
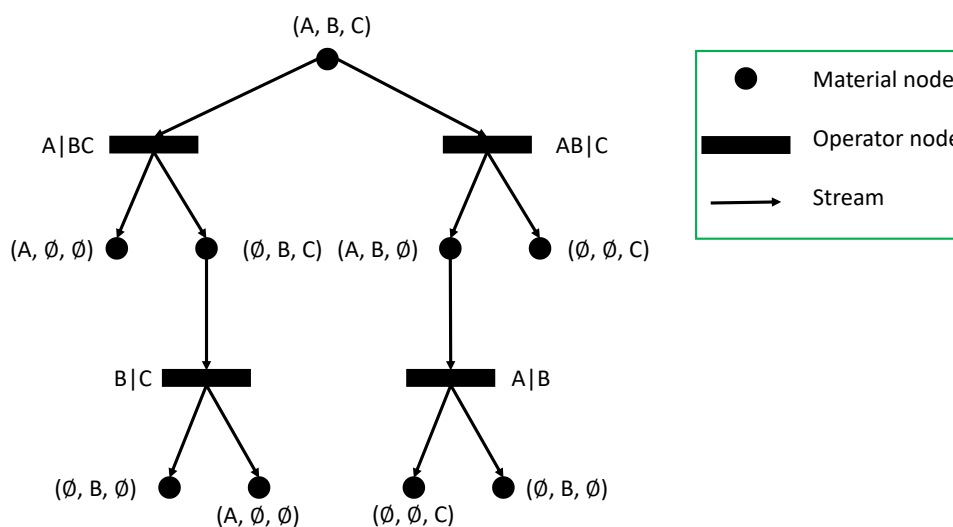
Figure 2-6 P-graph network superstructure (PNS) for 3 components separation (Mencarelli et al., 2020)

2.2.2.4 State-space representation (SSR) superstructure

State-space representation (SSR) was inspired from "state space" theory (Zadeh and Desoer, 1979). The SSR constructs the process as functions, which are (1) mixing and splitting of input/output streams in the distribution network (AKA state), and (2) unit operations which determine the process operator (AKA space) (Bagajewicz and Manousiouthakis, 1992). Figure 2-7 illustrates the connection between state (arrows) and space (blocks), using SSR to separate 3 components.

Process integration (PI) (i.e. heat, mass and power exchange) is the most popular form of SSR (Figure 2-7) (Klemeš et al., 2018). The PI are implemented widely in chemical process applications. For instance, PI

19

was applied for optimizing heat exchanger network (Klemeš and Kravanja, 2013), fresh/waste water network (Muhammed and Wagialla, 2016), reactors network (Chen and Grossmann, 2017), membranes network (Khor and Shah, 2011), distillations sequence (Dutta et al., 2018) and mass-heat integrations (Pham and El-Halwagi, 2012). Moreover, hydrogen distribution network (Marques et al., 2017) and carbon dioxide emission reduction networks (Chen et al., 2018, Dhole and Linnhoff, 1993) are also examples of subsystems that implemented the PI method. However, the SSR is closed and limited to solve PI problems, which is the main disadvantage of the SSR method (Mencarelli et al., 2020).
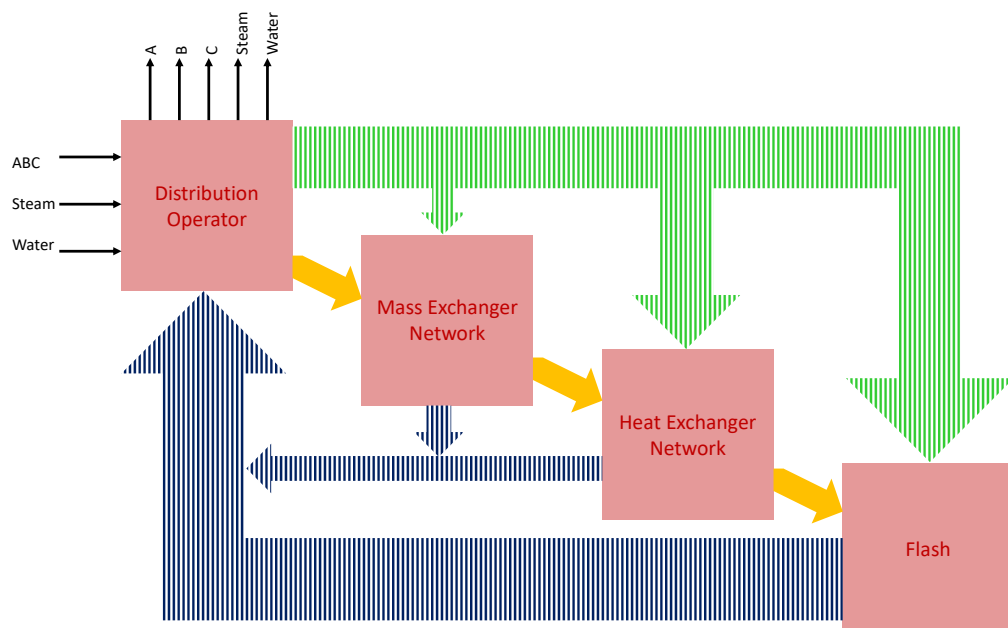
Figure 2-7 State-space representation superstructure (SSR) for 3 components separation (Mencarelli et al., 2020)

After representing the process using the above-named methods, a mathematical model has to be formulated based on (1) the process design, which are described by conservation, equilibrium and rate equations, and (2) interactions between these units, which are described by the transport phenomenon equations (Chen and Grossmann, 2017).

The mathematical model includes nonconvex and nonlinear equations (Segovia-Hernández and Gómez-Castro, 2017). Solving these equations can be overwhelming, especially, in the case of a highly complex process flowsheet (Mencarelli et al., 2020). Therefore, superstructure-free approaches are proposed.

2.2.2.5 Superstructure-free approaches

Nishida et al. (1981) introduced the evolutionary superstructure-free approach, as way to resolver process synthesis problems. The superstructure-free methods combine "two level of decomposition methods, separating the discrete selection decision and the detailed flowsheet evaluation" (Chen and Grossmann, 2017, Nishida et al., 1981). The two levels are (1) evolutionary algorithm that generates superstructure (upper level), and (2) determinsitic optimization (commonly MINLP), which evaluates each alternative (lower level), (Kocis and Grossmann, 1989). For instance, superstructure-free approaches were used to economically optimize a hydro-formylation process (the evolutionary algorithm for the upper level and NLP for the lower level) (Steimel et al., 2014, Steimel et al., 2013) and a production of light olefins process (NLP for the upper level and MILP for the lower level) (Onel et al., 2016).

Although superstructure-free approaches avoid the excessive use of mathematical model, it does not guarantee the global optimal solution at the lower level (Mencarelli et al., 2020). As the thesis aims to optimize an industrial-scale plant that includes a vast variety of unit operations

and operation conditions, developing a comprehensive superstructure method that can fully and fairly represents the plant is proposed.

2.3 Objective Function

Objective functions are an expression(s) to determine a process performance to service the process purposes (e.g. environment, economic) (Segovia-Hernández and Gómez-Castro, 2017). These expressions can be an equation or multiple equations, linear or non-linear functions. To evaluate the chemical process, common forms are used such as performance, economic, energy, environmental, process control and other criteria. These criteria were reviewed and explained by Rangaiah et al. (2020) as shown in the following subsections.

2.3.1 Performance criteria

This criterion comes very handy when establishing new processes or using an innovation unit/process, due to the criterion keen to evaluate physical and chemical performances of the unit/process. Performance criteria are often associated with reactor and separation units (Rangaiah et al., 2020). Conversion, yield, batch process time, product purity, recovery and productivity rate functions are some examples of performance criteria (Rangaiah et al., 2020).

2.3.2 Economic criteria

Economic criteria are the most used to construct a process economically. Commonly, total capital investment (TCI) and annual operating cost (AOC) are used as an objective function (Rangaiah et al., 2020). TCI is representing costs such as the purchase cost and installed

cost, while the AOC is related to variable cost (e.g. raw materials, electricity and steam) (Rangaiah et al., 2020). Rigorous techno-economic model (e.g. net present value (NPV), internal rate of return (IRR) and payback period (PBP)) can also consider as economic criteria, which were detailed in many books (Perry and Green, 1999, Peters and Timmerhaus, 1991, Pikulik and HE, 1977, Seider et al., 2017, Turton et al., 2009).

2.3.3 Energy criteria

This criterion is often used to protect, save, or minimise polluting natural resources such as water. In energy criteria, the process energy obtains a maximum efficiency by justifying the amount of steam, fuel and electricity, applying thermodynamic laws as an objective function (Rangaiah et al., 2020).

2.3.4 Environmental criteria

As processes should be accompanied by sustainability and life cycle assessment (LCA) rules, environmental impacts must be considered. Eco-indicator 99 (ECO99), the potential environmental impact, impact assessment of chemical toxics 2002+ (IMPACT), green degree and inherent environmental toxicity hazard are most common indicators that are used as an objective function (Rangaiah et al., 2020).

2.3.5 Control criteria

Traditionally, the process design is based on the optimized steady-state system, associating the economic feasibility. However, controlling this system may result in a poor dynamic process operation. This is due to

ignoring the process disturbances, while optimizing the steady-state system. Therefore, a tread-off between process design, process optimization and process control is conducted (Rangaiah et al., 2020). Controllability index-based approach, a dynamic optimization-based approach, and a robust control-based approach are methods that serve these criteria (Ricardez-Sandoval et al., 2009). In addition, model predictive control (MPC) is constructing a trajectory that predicts the process performance instead of just responding to sudden changes, where occurs in PID controller (Camacho and Bordons, 2007). Recently, economic model predictive control (EMPC) was developed to include the economic factors (Ellis et al., 2014). The tuning of the MPC is treated as an objective function for process design (Feng et al., 2018).

2.3.6 Other criteria

Other criteria are often related to social impacts such as safety, health, and chemical and operating risks. The possible objective functions are inherent safety index (ISI) (Heikkilä, 1999), inherent occupational health index (IOHI) (Hassim et al., 2010), health quotient index (HQI) (Teh et al., 2019), quantitative risk assessment (QRA) (Eini et al., 2016) and potential chemical risk (PCR) (Mio et al., 2018).

The current thesis aims to economically evaluate the case study (Chapter 5) since it is nearly impossible or impossible to attract investment without conducting the financial feasibility.

2.4 Optimization approaches

Optimization can be defined as "selecting the best alternative amongst a set of possibilities" (Segovia-Hernández and Gómez-Castro, 2017). The optimization solution is to find the maximum or minimum point(s) of the proposed objective function within available conditions and constraints (Sitter et al., 2019). Types of the solution methods are deterministic, stochastic and hybrid (Sitter et al., 2019).

2.4.1 Deterministic approaches

Deterministic methods are based on systematic and mathematical programming. Tradition methods such as sequential quadratic programming (SQP), mix-integer nonlinear programming (MINLP) and generalized disjunctive programming (GDP) are often used for process optimization (Grossmann, 1989, Chen and Grossmann, 2017).

The SQP is a powerful tool to optimize non-linear problems (Chaves et al., 2016, Fletcher, 2010). In chemical engineering, this nonlinearity is consequences of describing unit operating as a model includes transport phenomenon, kinetics, and thermodynamics (Chaves et al., 2016). The MINLP is widely proposed and used in chemical process superstructure optimization especially for process integration (Morar and Agachi, 2010, Klemeš and Kravanja, 2013). This method works well to overcome problems that involve nonlinear relationships, binary or integer variables (discrete variables), and continuous variables (Chaves et al., 2016).

Generalized disjunctive programming (GDP) is similar to MINLP with the advantage of including Boolean variables (Chen and Grossmann, 2017).

A recently study made by Navarro-Amorós et al. (2014) considered using the GDP framework to optimize a methanol production configuration from a syngas stream, economically. However, their superstructure flowsheet was very simple, which cannot represent and solve complex interactions and multiple choices (Navarro-Amorós et al., 2014). Also, a subsystem optimization of distillation sequence optimization was examined using the GDP (Caballero, 2015). The study proposed a framework to optimize distillation sequence by manipulating columns theoretical trays and reflux ratios (Caballero, 2015). However, these papers concluded that the GDP framework cannot guarantee the global optima and full-scaled process should be included.

In all, the determination nature of the deterministic approaches that allows the method to find the local optima, which is the main drawback. Therefore, this thesis investigates on stochastic approaches.

2.4.2 Stochastic approaches

Stochastic approaches are methods "in which the parameters are varied according to probabilistic instead of the deterministic rules" (Schwefel, 1981). These approach are considered better than the deterministic method, because of the random selection, which let the stochastic approach escapes the local optima(s) (Fang, 2007). Although there are many recent developed stochastic methods such as differential evolution (Storn and Price, 1997), simulated annealing (Kirkpatrick et al., 1983), and particle swarm optimization (Kennedy and Eberhart, 1995), this thesis did not set out to compare these methods. Thus, the thesis choses

the most common and original stochastic method: genetic algorithm (GA).

2.4.2.1 Genetic algorithms (GA)

Genetic algorithm (GA) is a global optimization technique developed by John Holland in 1975, which is based on the survival of the fittest theory by Herbert Spencer (1859).

The algorithm are applied on many applications such as engineering design (Gen and Cheng, 2000, Rasheed and Gelsey, 1996), traffic signal timing and shipment routes (Gen and Cheng, 2000), molecular design (Gen and Cheng, 2000), computer games (Gen and Cheng, 1997), dynamic system and control (Valadi and Siarry, 2014), and finance and investment strategies (Suman and Giri, 2015, Gen and Cheng, 1997). On the contrary, the use of GA on chemical engineering has been quite scarce because the majority of optimization applications were based on deterministic approaches. However, in the last decade, the interest increased on applying stochastic methods due to its proven efficiency of finding the global optima and method simplicity. Heat exchanger networks, reactor networks and distillation sequences optimization are some of the examples that implement the GA in chemical engineering, which are elaborated as follows.

2.4.2.1.1 Heat exchanger networks

The heat exchanger network (HEN) topology and maximum load recovary was optimized sumiltanuosly by using GA (Dipama et al., 2008). A new modified method that includes GA was developed for heat

27

exchanger network to minimise the total annual cost (Aguitoni et al., 2018). Their method considered non-isothermal mixing and stream splitting. Moreover, refrigerant heat exchangers networks was optimized using GA with respect to energy for liquified natural gas (LNG) process (Alabdulkarem et al., 2011). Their model compared pinch temperatures on saving the process energy.

2.4.2.1.2 Reactor networks

Martinez-Gomez et al. (2017) proposed a method that incorporates the genetic algorithm for syngas production from shale gas. Their method determined the optimal reactor superstructure and operating conditions, considering the safety factor and economic estimation (Martinez-Gomez et al., 2017).

2.4.2.1.3 Rigorous distillation sequences

Cui and Sun (2019) suggested an optimizer platform for rigorous extractive distillation columns, using genetic algorithm. Their method calculated the minimum total annual cost (TAC), considering the column operating pressures (Cui and Sun, 2019).

Although stochastic approaches overcome the local optima disadvantage that was caused by deterministic methods, they consumed a considerable time to find the global optima (Sitter et al., 2019). The thesis carried on using a stochastic method (i.e. GA) to optimize the economic objective function, despite the stochastic method drawback. The reason of this is that the process economic evaluation usually requires high outcome accuracies.

2.4.3 Hybrid optimization approach

Hybrid approaches is a combination of deterministic methods and stochastic methods (Tula et al., 2017). Farrokhpanah (2009) proposed a hybrid method to optimize a subsystem of distillation processes at low temperatures. Their study combined simulated annealing and linear programming (LP) to minimize the operational expenses of the process (Farrokhpanah, 2009). Simulated annealing is a stochastic method that is based on a single solution investigation (Kirkpatrick et al., 1983). Hybrid methods significantly reduce the computing time; however, these methods were investigated on small scaled processes and more studies are needed for complex and larger scale processes (Sitter et al., 2019).

2.5 Software tools: hybrid simulation-model

The rapid acceleration in the development of chemical process technologies, comprising modeling, optimization and control, creates shortages in sequential modular (SM) software; it becomes impotent to integrate SM software with equation oriented (EO), as mention in Section 1.2.1. The hybrid software technique combines the advantages of two or more software (Ponce-Ortega and Hernandez-Perez, 2019). Appendix A provides several chemical process applications that implement hybrid software for modeling, optimization and control. The distinction between EO software and SM software, and the interfacing techniques between these software are provided as follows.

2.5.1 Equation-oriented (EO) software

Equation- oriented (EO) software such as ACM®, MATLAB®, GAMS® and gPROMS® that solve a mathematical set of equations which suggests an approximation solution of a system (Maria, 1997, Lam et al., 2011). These systems can be deterministic, stochastic, dynamic, and steady state model (Maria, 1997).

2.5.2 Sequential modular (SM) software

Sequential modular (SM) software such as Aspen HYSYS®, Aspen PLUS® and ProII® simulate the process as blocks to study the behaviour of the system (Maria, 1997). Moreover, the simulation packages are very useful in technical and economic decision-making for planning, designing and operating a new or existing sub-system/system (Maria, 1997, Lam et al., 2011). Moreover, these software are used for designing process flowsheets and sup-flowsheets, estimating chemical and physical properties, calculating mass and energy balance, optimizing/analysing processes and process control and dynamic (West et al., 2008). These programs are usually using the visual interaction of the equipment (e.g. heat exchanger and distillation) for easing the simulation practising (Lam et al., 2011).

2.5.3 Hybrid simulation-model techniques

As the thesis focuses only on modelling and optimization applications, they are elaborated in the following subheadings.

2.5.3.1 Hybrid simulation-model for modelling process

There are two common techniques to model a chemical process using hybrid model, which are user-defined block model and software interface. These techniques are discussed as follows.

2.5.3.1.1 User-defined block model

Although simulator programs support numerous build-in models, simulators do not satisfy the user needs, especially in biochemical, polymer, and specialty industrial processes (Segovia-Hernández and Gómez-Castro, 2017). This increases the necessity of customizing and defining a unit operation model, considering physical/chemical properties, sizing, and costing, inside the simulator. For example, Aspen PLUS® and Aspen HYSYS provide an aspen custom modular (ACM), which allows the user to implement her/his developed code and fulfils the needs of the unit design (Segovia-Hernández and Gómez-Castro, 2017).

It is noteworthy that the degrees of freedom have a significant role in solving model equations of the newly-created unit (Rangaiah, 2016). However, the ACM lacks the build-in equation solver such as ODE15 and ODE23 provided by MATLAB®, which reduces the programming timing. Therefore, the hybrid model is a relatively easy and fast tool to be employed by users.

2.5.3.1.2 Softaware interface

Generally, the communication structure between SM and EO software is direct or indirect via MS Excel®, as can be seen in Figure 2-8. EO program acts as a master while SM (and MS Excel®, in case of the indirect communication) runs as a slave(s) (Claumann et al., 2015). This allows the master to read and write from slave(s). Although the direct interaction considers easier and reduces the miss communication between programs than the indirect, the need of applying MS Excel® strongly depends on the type of EO and SM couple. The interface is achieved by embedding the component object module (COM) technology. The COM technology generates a client-server interface such as ActiveX (provided by MATLAB®) and object linking and embedding (OLE) (provided by visual basic for applications® (VBA)) that allows the applications to behave as an automation server (Birnbaum and Vine, 2007). These interfaces require a scripting language such as VBA® (provided by MS Excel®) and visual studio® (Ponce-Ortega and Hernandez-Perez, 2019).

For example, coupling Aspen PULS® with MATLAB® needs Excel® interface (Fontalvo, 2014, Claumann et al., 2015), while coupling Aspen HYSYS® with MATLAB® does not require the intermediate slave. The reason for this is MATLAB® creates the link to Aspen HYSYS® MS Excel® via the COM (MathWorks, 2019), while for Aspen PULS® the link is created via objective variable exposer (OVE) (AspenTech, 2011, Claumann et al., 2015).

a

b
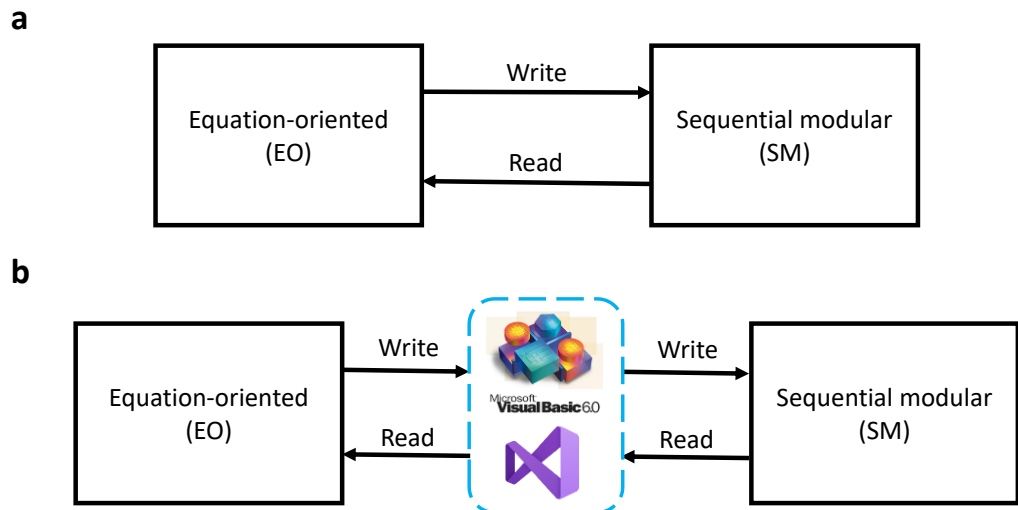
Figure 2-8 Interfacing between EO and SM. (a) Direct interface (b) Indirect interface.

2.5.3.2 Hybrid software for optimization process

Choosing the appropriate flowsheet design and operating conditions between a plethora of alternatives with respect to sustainable criteria are examples of the designing challenges in the chemical process (Lam et al., 2011). Optimization methods find the best solution among several alternatives, considering sustainable objective function(s), e.g. economy, society, and environment (Segovia-Hernández and Gómez-Castro, 2017). Interaction between alternatives creates a nonconvex problem with a high number of degrees of freedom that expected to have multiple local optimal solutions (Segovia-Hernández and Gómez-Castro, 2017).

Therefore, advanced optimization tools such as stochastic algorithms that search for global solutions have been practised (Carroll, 1961). However, such algorithms are not available in SM software, e.g. Aspen PLUS® and HYSYS®, which only support the deterministic methods such as sequential quadratic programming (SQP) (AspenTech, 2019). Fortunately, stochastic methods either can be easily programmed in EO

software or available within these programs' toolbox. Therefore, an interface between software is required.

As mentioned in Section 2.5.3.1.2, the programs are connected directly or indirectly via MS Excel®. Additionally, in optimization processes model convergence must be considered (Rangaiah, 2016). Rangaiah (2016) simplified the optimization process when using hybrid models via MS Excel® into three steps (Figure 2-9), which are:

1. Importing of decision variables values from an Excel® worksheet to a process simulator.
2. The process simulation activation or deactivation from Excel.
3. Exporting of the selected stream and/or unit data back to Excel worksheet.
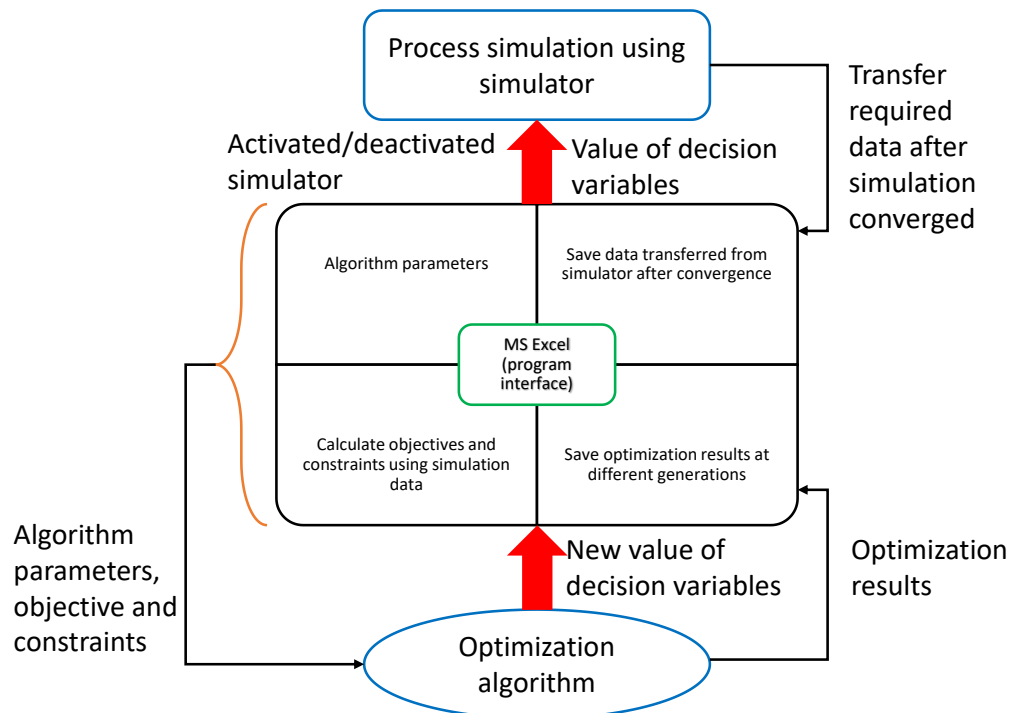
Figure 2-9 Hybrid software interfacing via MS Excel® for optimization process (developed from (Rangaiah, 2016)).

There are many types of hybrid software, comparing between them is out of the current research scope, as any combination will serve the

research purpose. Moreover, software availability and researcher experiences are the key features to choose between these software. Therefore, this thesis conducts the direct interface between Aspen HYSYS®, MATLAB®, and Microsoft Excel® for the modeling-optimization platform.

Chapter 3   Methodology

3.1 Introduction

This chapter explains the proposed methodology adopted in this thesis. Briefly, the proposed optimization-based superstructure hybrid platform is detailed in this chapter, embedding Aspen HYSYS®, MATLAB® and Microsoft Excel® programs to economically optimize the case study using the genetic algorithm (GA) and accomplish the study objectives. The platform proceeds through six levels: input data, master, slave, convergence, data analysis, and presentation levels. These levels are elaborated in the following sections.

In addition, the switch superstructure representation approaches to build the case study superstructure and the numerical method (i.e. backward time centred space method (BTCS)) to simulate the SMB are also described in detail.

3.2 Platform elements

Aspen HYSYS®, MATLAB®, and Microsoft Excel® software are linked to construct the optimization hybrid platform using genetic algorithm. These programs are explained as follows.

3.2.1 Aspen HYSYS® software

Aspen HYSYS® (which stand for **A**dvanced **S**ystem for **P**rocess **En**gineering; **Hy**protech **Sys**tem) is the most convenient tool to simulate hydrocarbon system because of the inclusive variety of thermodynamic packages (Lam et al., 2011). Moreover, HYSYS® spreadsheet

automatically manipulates and updates the design and economic calculations whenever changes are made in the process flowsheet model (AspenTech, 2019).

3.2.2 MATLAB® software

MATLAB® (**Mat**rix **Lab**oratory) is the most favourite program to be used because it can provide an accurate solution, manipulate matrices, plotting of functions and data, implementing algorithms and interfacing with programs in other languages (Lam et al., 2011). Also, MATLAB® mainly contains large and powerful built-in functions that are used to solve linear programming (LP) problem and partial differential equations (PDEs), Simulink, graphical illustration tools, and global optimization toolboxes (MathWorks, 2019). In chemical engineering, MATLAB® is used in various applications such as process modelling, heat and mass integration, process dynamic and control, optimization and analysis (Martín, 2015, Rangaiah, 2016).

3.2.3 Microsoft Excel® software

The main features of Microsoft Excel® are calculation, graphing tools, tables, and a macro programming language (Visual Basic for Applications (VBA)) (Martín, 2015). Also, it interfaces with other languages such as MATLAB® and link any two or more software (Martín, 2015). Moreover, MS Excel® includes built-in routines, which support basic calculations such as trigonometric functions, average, and summation. A recent example of using Microsoft Excel® in chemical engineering is developing a novel method to reduce and recycle water and wastewater in chemical processes using pinch technology,

calculating and plotting the composite curve (CC) (Muhammed and Wagialla, 2016).

3.3 Hybrid optimization software using GA

Figure 3-1 illustrates the levels/steps of the data flow between HYSYS®, MATLAB®, and MS Excel® on the platform model. The link between the programs was operated via the command ActiveX (Actxserver) excluded in the component object model (COM) server (Khan et al., 2011).

The platform proceeds as follows (Figure 3-1). First, define the input data such as process decision variables (operation conditions (OC) and superstructure variables (SS)) and optimizer settings in MATLAB®. This level is followed by the master level, where the optimizer (i.e. GA) imports a random set of decision variables to the slave level and then receives the objective function (NPV) outcome from the convergence level. The slave level is the process simulation level, where superstructure flowsheets are generated in the HYSYS®-MATLAB® hybrid model based on the OC and SS data received from MATLAB® and the NPV is calculated based on OC and equipment sizing (ES). While the convergence level ensures the convergence of these flowsheet models and protects these models from crashing.

The optimizer checks whether the maximum number of generations is reached or not. If not, optimizer generates a new of variables to be sent to the slave and convergence levels. This will continue until the maximum number of generations is attained. Data analysis level, after each check, MATLAB® stores in MS Excel® file the decision variables and the obtained NPV for each generated flowsheet throughout

generations. Final level, presentation level, represents the improved process flowsheet. More details for each level are elaborated as follows.

3.3.1 Input data level

After collecting data from available resources, the data were inserted in MATLAB®. The data were grouped into the following categories:

1. Insert the decision variables which includes OC (e.g. temperature) and SS (e.g. recycling ratio and unit selection). Also, the upper and lower boundaries for each decision variable was implemented as vectors.

2. Call constraints (see Section 3.3.1.1).

3. Call the objective function.

4. Select the optimization tool (i.e. genetic algorithm (GA)) and define whether to maximise or minimize the objective function.

5. Set the optimizer solver parameters. For GA these parameters are number of populations, number of generations, crossover rate.
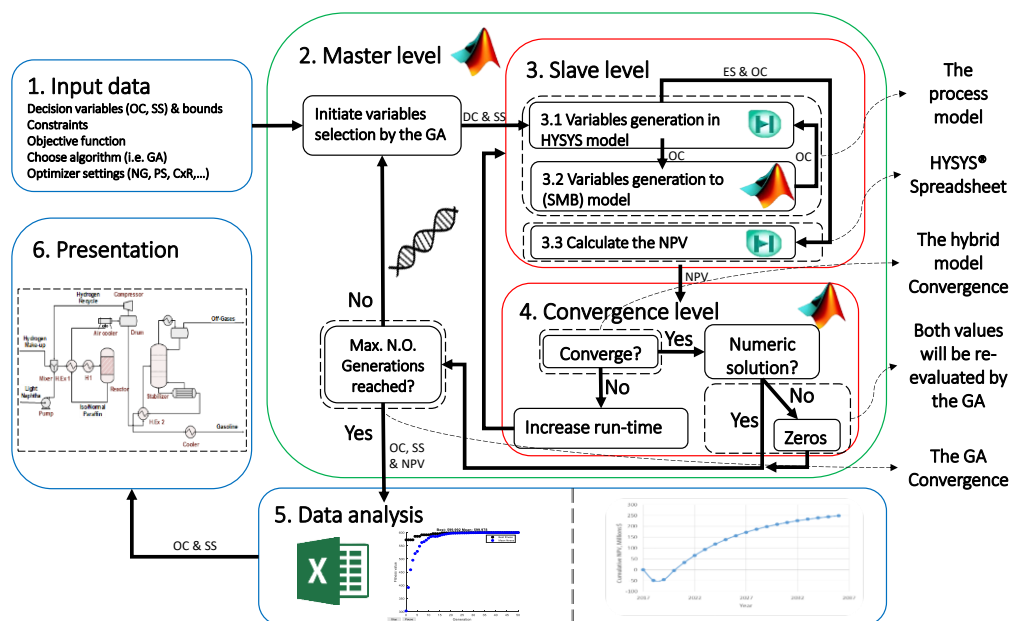
Figure 3-1 Hybrid optimization platform using GA. Note: OC=operating variables, SS=superstructure variables, ES= equipment sizing

39

3.3.1.1 Placing Constraints

Constraints are restricted relationships that must be satisfied for the optimization process (Takayama and Akira, 1985). As the simulation, in this thesis, had many levels, most of the simulation constraints were added within their section or level, as condition statements (i.e. if and while statements) to avoid simulations crashing and reduce CPU time. Therefore, placing constraints were limited to unit selections. The choice between the available options, to build the superstructure flowsheet, was done by using two techniques. The reason of that is elaborated in Section 3.3.3.1.

First, the selection between the three reactors was stated as a molar ratio of 0 or 1, when the ratio equals 1 the flowrate was fully fed to that reactor specifically and via versa. For three reactors, the equality constraint equation was a ratio function Equation (3-1), which always equals one. This guaranteed that only one reactor was chosen, which prevents HYSYS® simulation from crashing. Secondly, the selection between the five separations was numbered from 1 to 5. These numbers had to be integers and randomly generated by GA.

$$\sum_{i=1}^{n} x_i = 1 \qquad\qquad (3\text{-}1)$$

where x_i is the flowrate ratio for reactor i (x_i = 0 or 1) and n is the maximum number of reactors.

3.3.2 Master level (Optimization)

As described in Chapter 2, optimization is used to maximize or minimize the objective function by manipulating the process decision variables (i.e. OC and SS) within a set of constraints. Therefore, the main role of this level was to ensure a rigorous interface to solve the optimization problem by maintaining to export the data to the slave level and import from convergence levels. After receiving data from the previous level, the Master level was processed as follows. The genetic algorithm, which is available in MATLAB®, generated a random set of decision variables, also known as the initial chromosome (also called individuals/ parents) each chromosome contained number of genes. Each gene presents a variable. Figure 3-2 presents examples of some chromosomes, which are adopted in this research. After the chromosome was generated by the GA in MATLAB®, it was delivered to the slave level.

Chrom.	Gene1 Reactor Temp.	Gene4 Recycle Ratio	Gene5 Reactor ratio 1	Gene6 Reactor ratio 2	Gene7 Reactor ratio 3	Gene8 Sept. options
Chrom1	120	0.2	1	0	0	3
Chrom2	180	0.9	0	1	0	5

Operating conditions   1st constraint   2nd constraint

Superstructure design parameters

Figure 3-2 Chromosomes example

3.3.3 Slave level (Simulation)

Slave level is the third step in the methodology data transfer sequence, yet it must be prepared first by the researcher. This level focused on the building and simulating the case study superstructure flowsheet, employing the data were received from the GA optimizer in MATLAB®, switch superstructure method and process simulation in the hybrid software. The decision variables (i.e. OC and SS) were sent to the HYSYS® spreadsheet, which exports these variables to the superstructure flowsheet. Then these data were proceeded as follows.

3.3.3.1 Variables generation in the process superstructure

Technically, the SS variables were presented as a vector of ratio in-silico. Each index of the vector presented the molar ratio of a specific flowrate stream that was sent to a specific unit (i.e. reactor and separator). Keeping in mind that the summation of ratios must equals to one, these ratios varied between 0 and 1. This was used in combining units or using units simultaneously, which is outside the scope of this thesis. In this study, the distribution was limited to a one unit at a time, which numerically means the vector elements are all zeros except for one.

However, practically, HYSYS® simulation did not converge when zero flowrate streams inserted to the process simulation. Therefore, minimum ratio of 5% to solve the problem was suggested. However, increasing the number of units cased error accumulation. For example in case of 4 units found, 5% of the flowrate mass was withdrawn to each of the undesired units, which left 80% of the flowrate to the selected unit. This

means 20% of the outcome was treated differently, which leads to inaccurate process presentation and finance losses.

To solve this issue a switch method was developed. In this method the flowrate stream switched between units instead of being a ratio (Figure 3-3). This implied that the vector elements must be integer numbers instead of a range between 0 and 1. This allowed each flowsheet to be selected, converged, economically optimized, and analysed separately, more efficiently and accurately. Figure 3-3 shows the process network example using the switch method.

Sep.	1	2	...	n
1	1	0	...	0
2	0	1	...	0
⋮	⋮	⋮	⋰	⋮
n	0	0	...	1
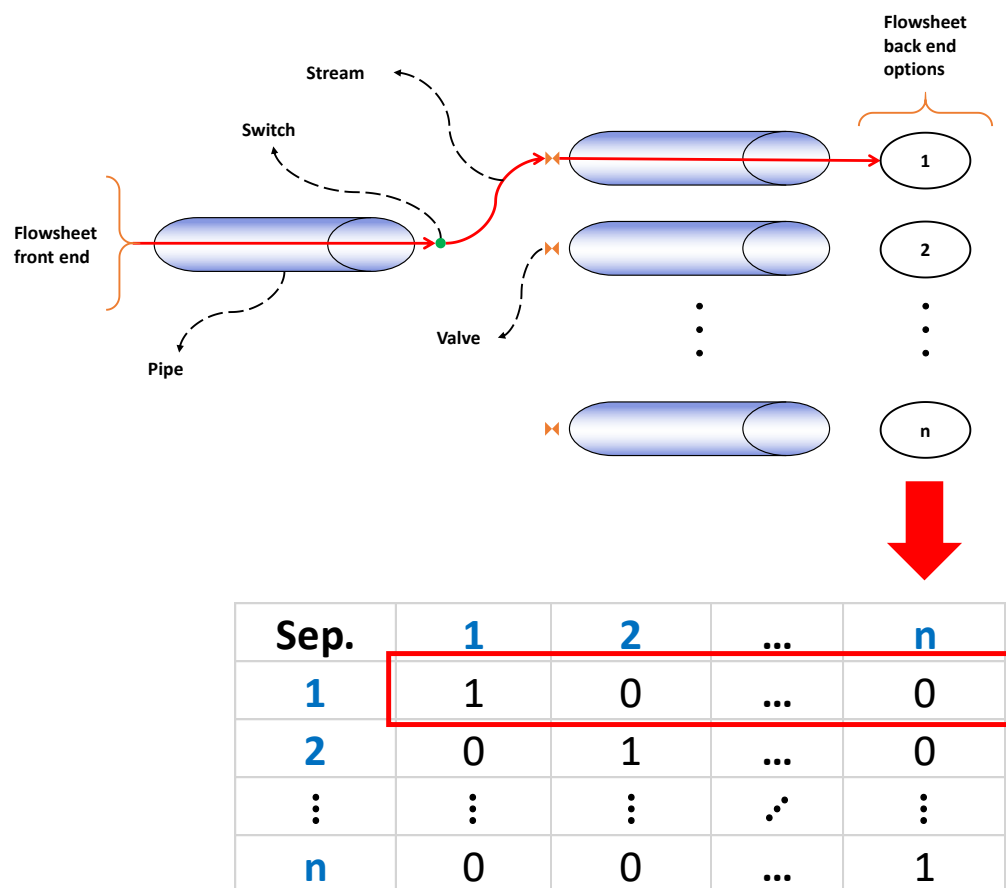
Figure 3-3 Suggested switch method

However, in case of a more complex problem such as a superstructure flowsheet with 10 reactors and 15 separations, the flowsheet will be simulated 10 X 15 times to allow interactions between units. It is strongly advisable to use a different method or simulator.

Figure 3-4 applies the switch method on the three components sharp split distillation example. This example showed that the feed can be switched between two separation processes. Each option had two separation units. The feed was switched to the first option (process). In this option, component A was separated from a mixture of B and C. The mixture was sent to the next unit where B and C are produced. This allowed to economically evaluate the first option. Then, switch was obtained to operate the second option, which also can be economically evaluated. After this, a comprehensive economic comparison between these options can be outlined.
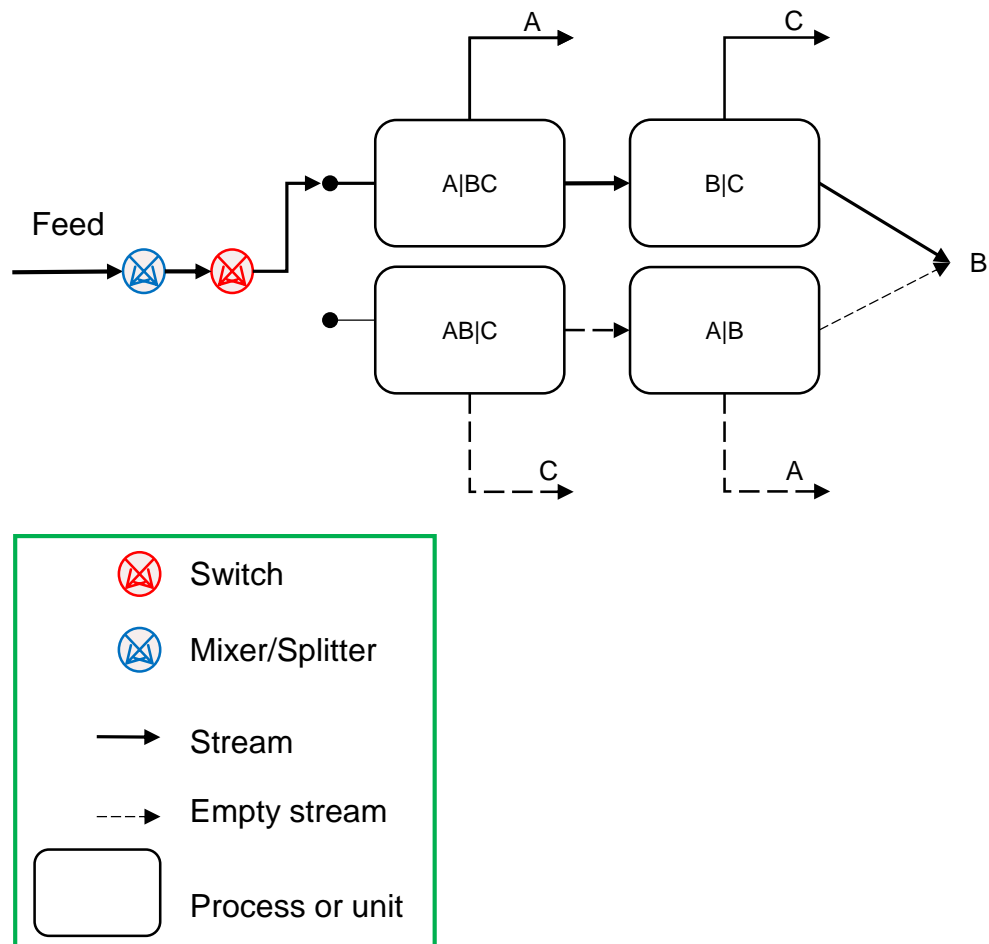
Figure 3-4 Switch method for three components separation

Figure 3-5 represents the switch superstructure representing a general chemical process. The process was presented as several sections. Typically, these sections are pre-treatment, frontend, backend, purification, post-treatment, and others. Each section can be done using many process/unit options, which construct the superstructure flowsheet. These options can be a single unit or a process (multiple units). Inlet and outlet stream from each option were reconnected in a node and the outlet was sent toward the next process step(s). In this thesis, the aim of introducing a novel switch method instead of traditional node methods is to represent a superstructure process easier, reduce the computational approaches, and minimize the optimization steps.
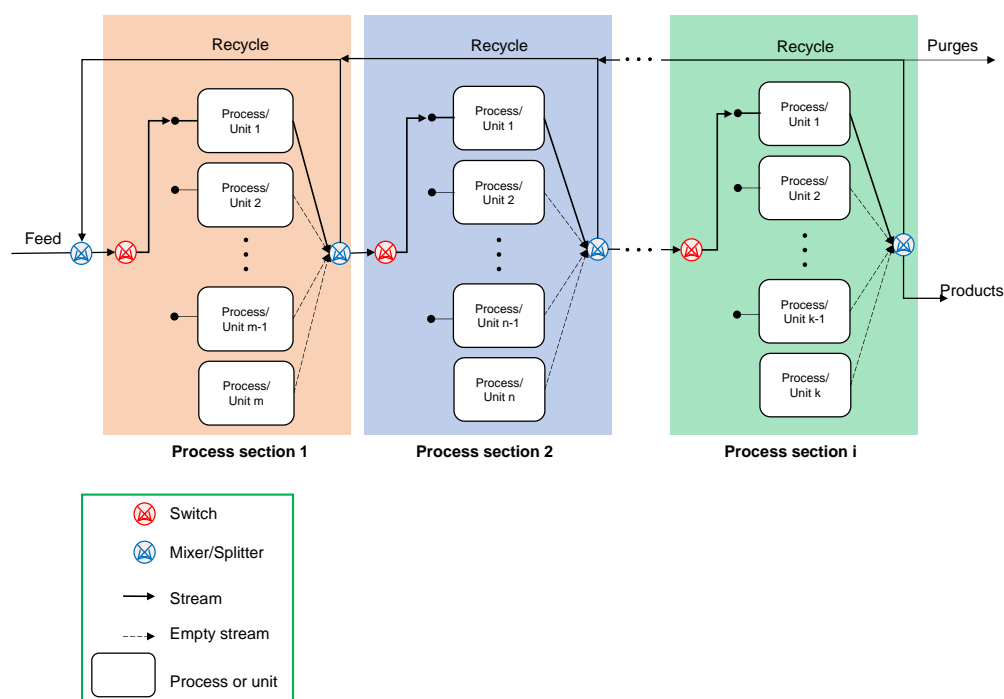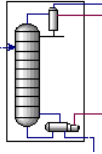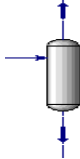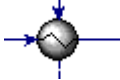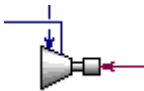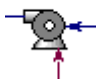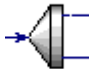
Figure 3-5 The generic superstructure network using the switch method.

3.3.3.2 Variables generation in HYSYS model

The process was simulated in HYSYS® using blocks that present an equipment. Some examples of this blocks were shown in Table 3-1. After HYSYS® converge, the data were returned MATLAB®.

Table 3-1 HYSYS® symbolic equipment examples

Reactor	Distillation Column	Drum	Heat Exchanger

Air Cooler	Compressor	Pump	Mixer/ Splitter

3.3.3.3 Variables generation in SMB model

After receiving the data from HYSYS®, the simulated moving bed (SMB) model was used to recycle the unconverted materials and discharge the converted substances to gasoline pool. The SMB model got the input data such as temperature, pressure, flowrate and component fractions from HYSYS® spreadsheet. The MATLAB® model is described as follows.

The simulated moving bed is a dynamic system includes a highly nonlinear partial differential equations (PDEs) set that can be solved by using analytical or numerical methods. Analytical methods give the exact solution(s), however, they are time consuming and difficult to be applied (Gonstantinides and Mostoufi, 2000). Instead, numerical approaches give an approximate result(s), do not consume significant time, and are easy to use (Gonstantinides and Mostoufi, 2000). There are numerous numerical methods such as first order up-wind (FOU), Lax-Wendroff,

leap-frog, and forward time centred space (FTCS) schemes that are used to solve the PDEs (Causon and Mingham, 2010, Ames, 2014), comparing these methods is out of the current research scopes.

According to Subiyanto et al. (2013) who compared forward and backward time centred space, backward time centred space (BTCS) was more stable and performed well when it was tested against longer time duration. Therefore, in this thesis, the BTCS (Figure 3-6), which couples the finite difference method (FDM) (Equation (3-2) and Equation (3-3)) and backward Euler's method (Equation (3-4)), was used to solve the partial differential equations (PDEs) set. The BTCS method derivatives from Taylor series are available in Appendix C. Finite difference method (FD) is replacing the area, that the independent variable is defined, by a finite grid (also known as a mesh) (Ames, 2014, Subiyanto et al., 2013). The BTCS fixes the time (t) derivative and solves the PDEs for space (x) derivative using FD and then solves the PDEs considering the time using Euler's method with constant x.
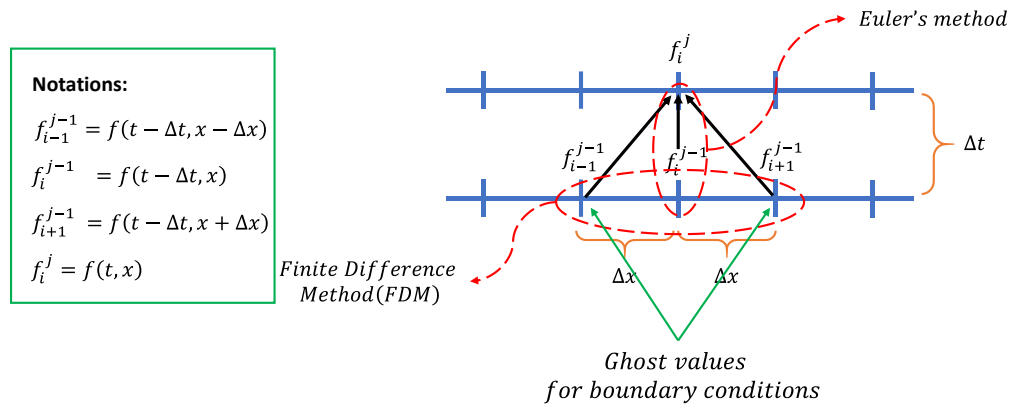
Figure 3-6 Numeric solution for BTCS (developed from (Smith et al., 1985))

In addition, the BTCS sets initial and final points (also known as ghost values) as solution boundary conditions (Causon and Mingham, 2010).

47

The centred finite difference method (FDM) for first order derivative can be calculated by using Equation (3-3)

$$\frac{\partial f}{\partial x} \approx \frac{f(x + \Delta x) - f(x - \Delta x)}{\Delta x} \qquad (3\text{-}2)$$

where $\partial f/\partial x$ is the first partial derivative of function f with respect to x, x is the space and Δx is the change in x.

The centred finite difference method (FDM) for second order derivative can be calculated by using Equation (3-3)

$$\frac{\partial^2 f}{\partial x^2} \approx \frac{f(x + \Delta x) - 2 * f(x) + f(x - \Delta x)}{\Delta x^2} \qquad (3\text{-}3)$$

where $\partial^2 f/\partial x^2$ is the second partial derivative of function f with respect to space (x).

The backward Euler's method can be calculated by using Equation (3-4)

$$\frac{\partial f}{\partial t} \approx \frac{f(t) - f(t - \Delta t)}{\Delta t} \qquad (3\text{-}4)$$

where $\partial f/\partial t$ is the first partial derivative of function f with respect to t, t is the time and Δt is the change in t.

In this thesis, number of t and x elements were assumed to be 18 and 10 per bed. Ghost values were assumed to be related to inlet and outlet flowrates at each zone. Although this thesis was limited for investigating eight beds economic feasibility, the SMB model can solve any number of beds. Figure 3-7 illustrates a proposed solution strategy to model the eight-SMB for this thesis. The strategy is proceeded as follows.

1. The simulated moving bed (SMB) was assumed to be a long bed, which was divided to 4 zones. Each zone included 2 beds and each bed was discretized to space (x) and time (t) elements (also known as indices).

2. At the first bed, the initial concentrations were reset to be the feed concentrations and the initial load at the solid phase was assumed to be zero.

3. The PDEs set was solved with respect to space (x) by using FDM and then was solved with respect to time (t) by using explicit Euler's method.

4. The solved concentrations and bed loads were reset (switched) as initial conditions to the next bed. Then, equations ware solved by step 3.

5. Step 4 was repeated until the last bed, considering adding desorbent stream and discharging raffinate and extract streams. The key difference between these zones was assumed to be adjusted by the pressure.

6. At the last bed, the extract stream was collected and stored in a tank and concentrations and bed loads were and switched to the first bed to start a new cycle (repeat from step 2).

7. After the maximum number of cycles was reached and outlet concentrations were steady, then outlet streams date can be sent to HYSYS®.
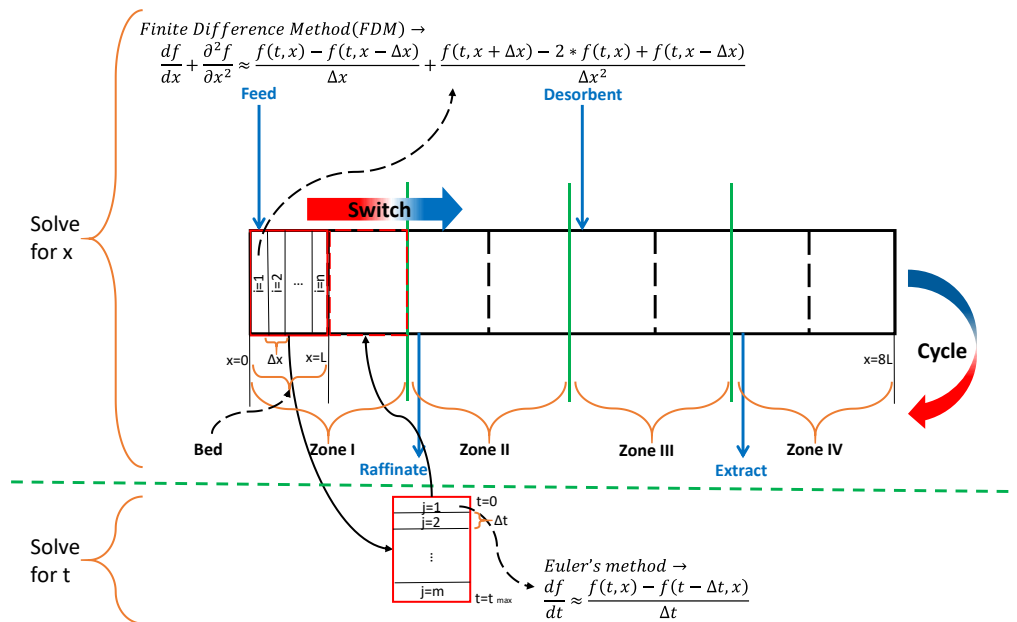
Figure 3-7 Solution strategy

3.3.4 Convergence level

This level maintains the convergence of the hybrid process model (HYSYS®-MATLAB®). Recycling data to HYSYS® caused an overall materials imbalance. To tackle the process imbalanced, a full recycle convergence (Algorithm 3-1) was inserted in MATLAB®. The algorithm continuously imported data to run the SMB model and then exported to recycle unconverted components to a reactor in HYSYS® until the overall inlet flowrate and outlet flowrates were equals. if-condition statement that checks whether HYSYS® solver is running (using "issolving" command in MATLAB®). HYSYS® solver replied with true or false signals. If a true signal was received in MATLAB®, then the Algorithm 3-1 paused for time t seconds. After that, the SMB re-ran until the HYSYS® solver sent a false signal and the convergence was reached. In case of no convergence the hybrid simulation outcomes were considered to be zeros. In this thesis, after many trials and error, it was found that the suitable time to let HYSYS®-MATLAB® model converge without crashing was 180 seconds.

```
Algorithm 3-1 Convergence level (CL)

1.  // Overall inlet flowrates (Fi)

2.  // Overall outlet flowrates (Fo)

3.  // Time in seconds (t)

4.  while Fi ~= Fo do

5.  CL=Solver.issolving

6.      if CL==True

7.          pause (t)

8.          re-run (SMB)

9.      end if

10. end while
```

3.3.4.1 Calculate the TEA

After solution of the LC loop was obtained, the objective function was calculated in the HYSYS® spreadsheet and then exported to MATLAB®. The techno-economic analysis (TEA), namely, net present value (NPV) was determined by the process model outcomes such as amount of steam and outlet flowrates. These outcomes depended on the operation conditions such as temperature and recycling ratio. To avoid HYSYS® from crashing, a condition statement was constructed as shown in Algorithm 3-2. The statement checks the emptiness of a cell (i.e. A5), which occurs because of an invalid calculation in HYSYS®. For non-numerical inputs avoidance such as an empty cell, the outcome at this situation is zero.

Algorithm 3-2 Empty cell in HYSYS®
1. if cell(A5) == Forgetting then
2.   cell(A5) =0
3. end if

After MATLAB® received the NPV and stored it in GA, the GA in the master level repeated the sequence of generating random decision variables set, processing them into the slave and convergence levels and calculate the TEA. This continues for next chromosomes till the full population size is completed (i.e. 100). Then the GA evaluates and ranks each chromosome to pass on the elite individuals to the next generation, from these individuals the GA randomly selects parents (Table 3-2) for crossover (Abualigah, 2018). In crossover, the children get half of each parent gens, an example of crossover is shown in Table 3-2 and Table 3-3.

The crossover represents the reproduction rate, which varies between 0 and 1. While 1 means all children are produced from crossover and 0 means all children are mutated, excluding the elite children (MathWorks, 2019). Elite children have the best fitness value that allow them to survive to the next generation (MathWorks, 2019). The probability of the mutation children are specified by using the Gaussian distribution in MATLAB® (MathWorks, 2019). The amount of mutation is added to each chromosome vector, which decreases across generations. Example of mutated child is shown in Table 3-3 (pink box). Table 3-4 presents the new chromosome for the next generation, which was delivered to the

slave level and repeated the process till the maximum number of generations is reached.

Table 3-2 Selcted parents

	Gene1	**Gene4**	**Gene5**	**Gene6**	**Gene7**	**Gene8**
Chrom.	Reactor Temp.	Recycle Ratio	Reactor ratio 1	Reactor ratio 2	Reactor ratio 3	Sept. options
Chrom1	**160**	**0.2**	**0**	**0**	**1**	**2**
Chrom2	**180**	**0.9**	**0**	**1**	**0**	**5**

Table 3-3 Crossover

	Gene1	**Gene4**	**Gene5**	**Gene6**	**Gene7**	**Gene8**
Chrom.	Reactor Temp.	Recycle Ratio	Reactor ratio 1	Reactor ratio 2	Reactor ratio 3	Sept. options
Chrom1	**160**	**0.2**	**0**	**1**	**0**	**5**

Table 3-4 Mutation

	Gene1	**Gene4**	**Gene5**	**Gene6**	**Gene7**	**Gene8**
Chrom.	Reactor Temp.	Recycle Ratio	Reactor ratio 1	Reactor ratio 2	Reactor ratio 3	Sept. options
Chrom1	160	0.8	0	1	0	5

3.3.5 Data analysis level

The information of each individuals were collected from MATLAB® and stored Excel® (using *xlswrite* command), including number of individual, number of generation, crossover rate, OC, SS and TEA, to be reviewed and applied further analysis. The data collection was to investigate the effect of the optimization parameters, namely, different crossover rates and population sizes, against fitness function.

3.3.6 Presentation level

The optimal flowsheet and operating conditions are illustrated in this level.

Chapter 4   Process simulation model

4.1 Introduction

This chapter briefly reviews the light naphtha isomerization process to produce gasoline background. Also, the chapter synthesizes the process superstructure in order to emulate the field-scale industry, including 15 routes. The detail of the switch synthesizing representation approach was described in Chapter 3 (Section 3.3.3.1). The superstructure simulation was programmed in the HYSYS®- MATLAB® hybrid platform (Section 3.3.3). Each route of the simulation superstructure was compared and validated against published studies whenever possible. In addition, the performance of the process superstructure hybrid simulation platform evaluation, analysis, and results are described in this chapter.

4.2 Background overview

4.2.1 Isomerization of light naphtha
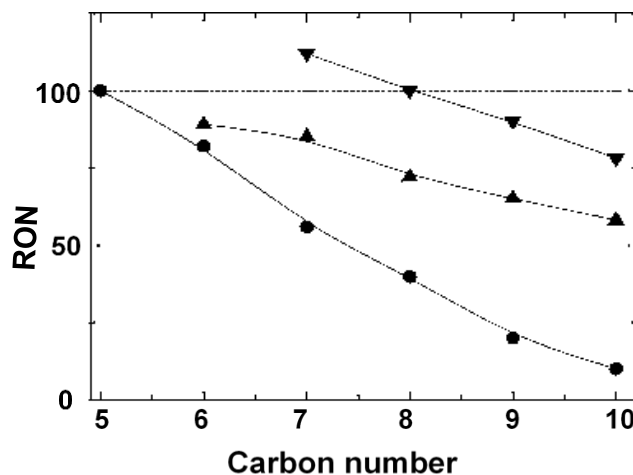
Figure 4-1 RON vs carbon number for mono (●), di (▲) and tri-branched (▼) (Busto et al., 2011)

Isomerisation is a process of upgrading a low RON paraffin, mainly C4, C5, and C6, occurs by converting the straight chain of paraffin to produce mono-, dual- and tri- branched isomers, which has a higher RON values (Mohamed A. Fahim et al., 2010).

Figure 4-1 shows octane numbers increase proportionally to the number of branched and reverse proportional to the carbon number (Busto et al., 2011). The gasoline research octane number is calculated following Equation (4-1) (Chuzlov et al., 2019).

$$RON = \sum_{i=1}^{n} RON_i x_i \qquad (4\text{-}1)$$

where RON is the gasoline octane number, RON_i is the individual octane number of component i, x_i is the weight fraction of component i and n is the number of components.

4.2.1.1 Isomerization reaction

The main reactions taking place in the isomerization process are: isomerisation of normal paraffin, ring-opening of naphthenes, benzene saturation and hydrocracking (Valavarasu and Sairam, 2013). These reactions and their interactions depend on many factors such as the type of catalyst and feed compositions. Both experimental and modelling studies are reviewed as follows.

4.2.1.1.1 Experimental studies

The skeleton isomerization has been a topic of many studies (Ali et al., 2001, Busto et al., 2012, Busto et al., 2008, Chekantsev et al., 2014, Chuzlov et al., 2014, Chuzlov et al., 2017, Dhar et al., 2017, Ivanova et

al., 2002, Pather and Lokhat, 2014, Silva-Rodrigo et al., 2015, Sullivan et al., 2015, Valavarasu and Sairam, 2013). The isomerization catalysts are mono-functional (acidic sites) and bi-functional mechanism (metallic and acidic sites) (Valavarasu and Sairam, 2013, Leprince and Travers, 2001). Hydrogenation /dehydrogenation reactions occur in a metallic sites catalyse while isomerization/hydrocracking reactions occur in acidic sites (Ali et al., 2001, Valavarasu and Sairam, 2013).

The most active, stable and impurities resistant catalysts were examined including metals such as palladium (Pd) (Dzhikiya et al., 2016) and platinum (Pt) (Busto et al., 2012, Watanabe et al., 2005, Watanabe et al., 2004) based on different support material such as zeolite, chlorinated-alumina and sulphated metal oxides (Section 4.2.1.3) (Busto et al., 2012, Busto et al., 2008, Dhar et al., 2017, Ivanova et al., 2002, Pather and Lokhat, 2014, Silva-Rodrigo et al., 2015, Sullivan et al., 2015). Moreover, hybrid catalysts combine the abovementioned supported materials (Dzhikiya et al., 2016, Kimura, 2003, Watanabe et al., 2005, Watanabe et al., 2004) and add extra metals such as Nobel metal and tungsten oxide with and without chlorine (Ali et al., 2001), gallium, zirconium and silicon (Tailleur and Platin, 2008). In addition, the skeletal rearrangements of the isomerisation reactions at different acidities have been investigated experimentally by several researchers (Li et al., 2017, Volkova et al., 2007, Ejtemaei et al., 2018). In general, the most desirable catalyst should have a suitable distribution balance between acid and metal sites.

In addition, the effect of feed impurities on catalysts is speed up catalyst deactivation, which disrupts the process continuity and leads to financial

losses. Experimentally, the effect of isomerizing the sulphur contained in the process and the deactivation of the main three types of commerce catalysts (i.e. chlorinated alumina-based, sulphated metal oxides based and zeolite catalysts) were studied by Szoboszlai and Hancsók (2010). The investigation showed that aluminium- and sulphated-based catalysts were potentially decaying with a higher sulphur contain in the feed at 5-20 mg/kg for 1-2 days (Szoboszlai and Hancsók, 2010). For lower sulphate content ≤ 5 mg/kg, the activity rate of the catalyst was slightly decreased (Szoboszlai and Hancsók, 2010). Moreover, the zeolite catalyst demonstrated a higher isomerisation activity up to 2.3 years when increasing the Pt content from 0.35% to 0.45% (Szoboszlai and Hancsók, 2010).

4.2.1.1.2 Model studies

The mathematical model of the skeletal of the isomerization reaction to predict reaction kinetics parameters has been investigated by several authors (Chuzlov et al., 2017, Chekantsev et al., 2014, Chuzlov et al., 2014), using software programs such as MATLAB® (Hayati et al., 2014, Pather and Lokhat, 2014), Aspen Plus® (Pather and Lokhat, 2014), HYSYS® and IZOMER® (Chuzlov et al., 2014), and gPROMS® (Ahmed et al., 2018). Then results have been compared with industrial (Chekantsev et al., 2014, Chuzlov et al., 2017), pilot plant (Hayati et al., 2014) and lab-experimental data (Pather and Lokhat, 2014, Kazantsev et al., 2016). In order to calculate the optimal values of the kinetic parameters an optimization method minimizing the sum of least square error between product mole fractions and estimated/calculated values was used (Hayati et al., 2014, Chekantsev et al., 2014). The error

between the predicted and actual data has been minimised from 6.1%-21.2% (Koncsag et al., 2011) to 5% (Chekantsev et al., 2014). A most recent study was obtained the minimum error of 1-2%, which is the most realistic estimation of reaction kinetics (Chuzlov et al., 2017). Their reactions pathway (Figure 4-2) included a sum up of 35 possible reactions occurring (Chuzlov et al., 2017). This enhanced the reaction rate predictions (Chuzlov et al., 2017).
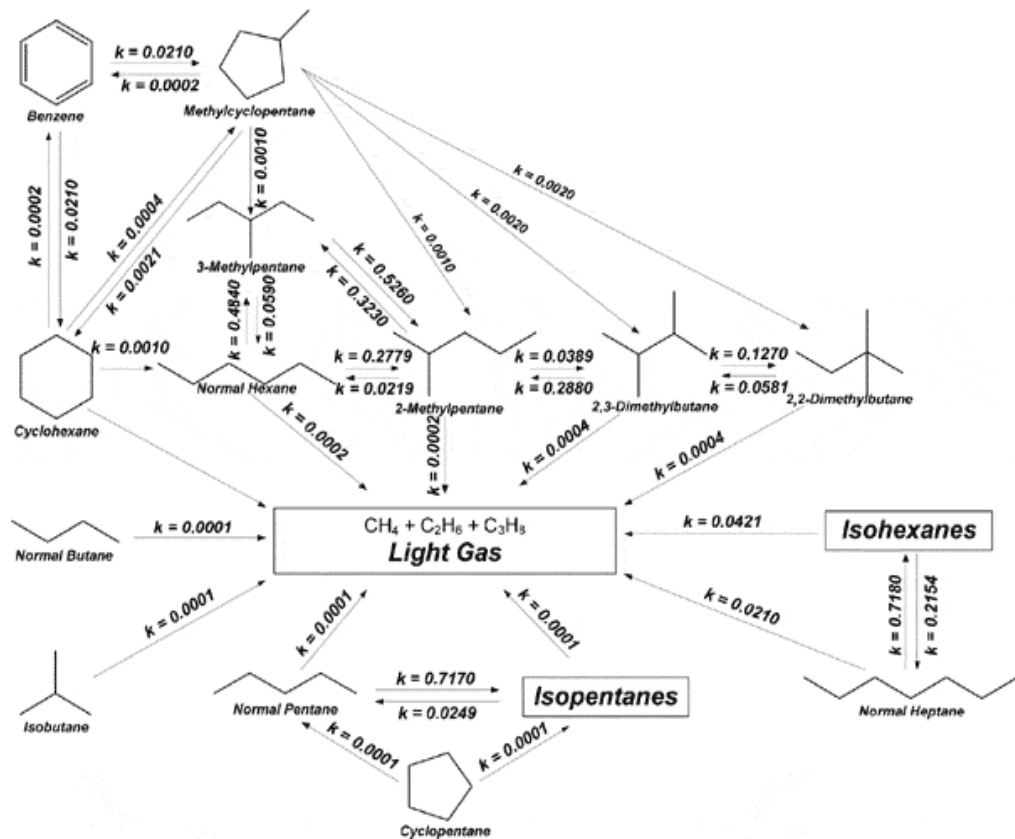
Figure 4-2 Isomerization reaction scheme (Chuzlov et al., 2017)

As the reaction mechanism pathways are complex to be applied into HYSYS®, a simple form of these reactions was considered in this thesis. These reactions with components RON are listed as follows.

- **The isomerization of pentane (nC5):** Equation (4-8) (Naqvi et al., 2018, Valavarasu and Sairam, 2013):

$$\begin{matrix} nC5 \\ (62) \end{matrix} \leftrightarrow \begin{matrix} iC5 \\ (90) \end{matrix} \qquad (4\text{-}2)$$

59

- **The isomerization of hexane (nC6):** there are several expressions for hexane isomerization reaction (Macht et al., 2009) due to the nature of mono/bi-function catalyst, the possible hydrocarbon species produce from the reaction are shown in Equation (4-3) and (4-4) (Busto et al., 2011, Chekantsev et al., 2014):

$$
\begin{array}{cc}
nC6 & 2MC5 \quad 3MC5 \\
(25) \leftrightarrow (74) \quad or \quad (75)
\end{array}
\tag{4-3}
$$

$$
\begin{array}{cc}
nC6 & 22\mathrm{D}MC4 \quad 23\mathrm{D}MC4 \\
(25) \leftrightarrow (94) \quad or \quad (100)
\end{array}
\tag{4-4}
$$
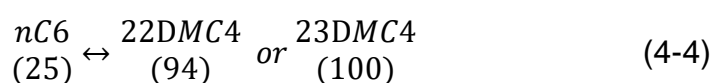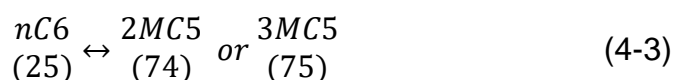
- **Ring-opening of naphthenes** is to convert cyclohexane (cC6) to normal hexane (nC6) which occurred at high temperature (Valavarasu and Sairam, 2013), Equation (4-5)

$$
\begin{array}{c}
cC6 \quad nC6 \\
(83) + H_2 \leftrightarrow (25)
\end{array}
\tag{4-5}
$$

- **Benzene saturation** is the desired reaction to reduce benzene contained in gasoline by converting it to naphthenes and hexane (Valavarasu and Sairam, 2013). However, It is a highly exothermic reaction resulting in increasing reactor temperature, which is not favorable for the equilibrium reaction of normal paraffin (Vuković, 2013), Equation (4-6).

$$
\begin{array}{cccc}
Benzene & cC6 & McC5 & nC6 \\
(102) \leftrightarrow (83) & \leftrightarrow (91) & \leftrightarrow 25
\end{array}
\tag{4-6}
$$
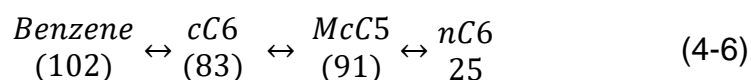
4.2.1.2 Reaction thermodynamic

In general, the isomerization reaction is a slightly exothermic (-4 to -20 kJ/mol) (Lamprecht and Klerk, 2009) and occurs in equilibrium mode

(Mohamed A. Fahim et al., 2010). The reaction would not influence by the alteration of pressure because the unity on stoichiometric ratio between the isomerisation reactant and product and the reaction occurs in a gas phase (Leprince and Travers, 2001, Mohamed A. Fahim et al., 2010). To achieve a higher RON the reactor should operate at low temperature (Section 4.2.1.3) (Mohamed A. Fahim et al., 2010). The conversion of pentane and hexane in optimal conditions are 60-65% (Chekantsev et al., 2014) and 65-75% (Adžamić et al., 2011, Yashima et al., 1996), respectively. These phenomena become thermodynamically preferred in the industry due to the low temperature condition (Chekantsev et al., 2014, Pather and Lokhat, 2014), and indicate that the catalyst must be active enough to achieve the highest conversion in the lowest possible temperature.

4.2.1.3 Catalysts and reactor operation conditions

Chlorinated alumina-based, sulphated metal oxides based or zeolite are the main types of catalysts that can be used in isomerization reactor (Pather and Lokhat, 2014, Pestryakov et al., 2016). These catalysts and operation conditions (Table 4-1) are briefly described as follows:

- **Zeolite catalysts** have relatively high resistance of the feed impurities, so the feed does not need to pre-treatment. However, the catalysts have low reaction activity and operate in a high operation temperature (220-300 ºC), which increases the feed RON by only (10-12) points. The process configuration, when the zeolite is used, needs fire heater to preheat the inlet feed,

hydrogen-rich gas separator and compressor to recycle hydrogen-rich gas.

- **Chlorinated alumina based catalysts** solve the problem of the activation. The reactor operates at a low temperature (120 -180 ºC) and increases the RON by (4-5) points higher than zeolite. However, they need a high feed purity (Table 4-2), because of their high sensitivity towards impurities such as water, sulphur and nitrogen. Therefore, feed pre-treatments are required. Organic chlorine injection such as CCl_4 and $AlCl_3$ are needed to maintain the activity of the catalyst. However, continuously adding the chlorine can cause corrosion problems (Yasakova et al., 2010). Moreover, discharging the hydrochloric acid in a scrubber is necessary. However, this can cause disposal caustic issues in refineries which increases the treatment cost (Yasakova et al., 2010).

- **Sulphated metal oxides based catalysts** solve both previous issues as they resist the feed impurities (Table 4-2), operate in relatively low-temperature conditions (180-240 ºC) and produce RON more than (2-4) points higher than zeolites. The drawback of using these catalysts is that they need a separator and compressor to recycle hydrogen-rich gas.

Table 4-1 Operating conditions for the process (Chuzlov et al., 2014, Kimura, 2003, Valavarasu and Sairam, 2013, Weyda and Köhler, 2003)

	Chlorinated alumina	Sulphated metal oxide	Zeolite
Temperature (°C)	120-180	130-210	220-300
Pressure (bar)	20-30	15-30	15-30
LHSV (hr^{-1})	1-3	1-3	1-3
H_2/HC (mol %)	0.1-2	< 0.1	1.5-4
Yield (Wt %)	99	98.5	98
RON	82-85	81-84	76-80

The comparison of the operation conditions, excessive hydrogen, yields and RON of using each catalyst in the process are presented in Table 4-1. The table shows the sulphated metal oxide is the intermediate catalyst in a matter of condition and product quality. Moreover, the liquid hourly space velocity and operating pressure are almost the same for the three catalysts which are 1-3 h^{-1} and 15-30 bar, respectively. Table 4-2 shows the sensitivity of each catalyst against the feed impurities. Chlorinated alumina showed the highest sensitivity, zeolites have the highest resistance and sulphated metal oxide has both intermediate sensitivity and resistance of impurity. Also the table presents the effect of each impurity on catalyst and humankind. In this thesis, these catalysts are modelled to design the superstructure flowsheet.

4.2.1.4 Isomerization reactor(s) design

The selection of using one or two reactor(s) in the isomerization process is related to the required performance (Sullivan et al., 2015). Fixed bed reactor is used when the catalyst is active enough (Meyers, 2004). Two trickle bed reactors sequence is used, for higher RON requirements and lower benzene contains (Valavarasu and Sairam, 2013, Vuković, 2013). A lead reactor, which is the first reactor, operated in high temperature (200-220 ⁰C) to improve the reaction rate (Sullivan et al., 2015) and hydrate benzene (Valavarasu and Sairam, 2013). A lag reactor, which is the second reactor, operated in lower temperature (110-150 ⁰C) to increase the isomerate formulation due to its equilibrium limitation (Valavarasu and Sairam, 2013, Sullivan et al., 2015). The optimal reactors temperature for isomerization process was studied by Vuković, 2013 (Vuković, 2013) and Said et al., 2014 (Said et al., 2014). Also, the optimal benzene contain, liquid hour space velocity, and hydrogen to hydrocarbon ratio was justified by Fathy and Soliman, 2019 work (Fathy and Soliman, 2019). Two reactors demonstrated the best performance while increasing the capital (e.g. addition catalyst loaded) and operational costs (e.g. addition hot/cold utilities) (Sullivan et al., 2015). Therefore, this thesis focuses on modelling one reactor per catalyst.

Table 4-2 Feed limitations for the industrial isomerization catalysts (Kimura, 2003, Valavarasu and Sairam, 2013)

	Chlorinated alumina	Sulphated metal oxide	Zeolite	Effects
Water (ppm)	<0.1	<30	<200	Deactivates catalyst, Promotes corrosion and Irreversible poison and reduce catalyst lifetime
Sulphur (ppm)	<0.1	<20	<200	Deactivates catalyst, increases cracking and repair of activity by a sulphur removal
Aromatics /benzene (Wt %)	<2	<2	<10	Cause cancer
C_7^+ (Wt %)	<2	<2	<5	--

4.2.1.5 Catalyst regeneration

Deactivations occurred mainly because of the impurities and coke accumulated on the catalyst (Valavarasu and Sairam, 2013). Catalysts life time is related to operation conditions, such as high hydrogen-hydrocarbon ratio and lower reactor temperature (Ancheyta, 2011). Also, catalyst lifetimes, which varies from 6 months to 8 years (Ancheyta, 2011, Klerk, 2008). This thesis focuses on the economical investigation of catalyst regenerations.

4.2.2 Octane upgrading technologies

The single-pass isomerization process increases RON to only 78-80 and requires a low capital investment (Sullivan et al., 2015, Valavarasu and Sairam, 2013). However, separation and recycling of the normal alkane assists achieving full conversion of the feed, thereby increasing the product RON to 88-93 (Yasakova et al., 2010). Therefore, recycling procedures have been applied to the process (Graeme and Ross, 2004). The three main techniques used in the process to separate normal/iso-paraffin are adsorption, distillation, or combination of the two techniques (Graeme and Ross, 2004, Yasakova et al., 2010). These techniques are described as follows.

4.2.2.1 Adsorption separation

Since mid-1960s, adsorption is a separation process happens when a gas molecule moves from fluid bulk to bond with a solid surface (Figure 4-3) (Kikkinides et al., 1993). This bond might occur because of molecule size and shape, interaction strength or chemical reaction (Knaebel and Hill, 1985, Ruthven et al., 1994). This process has two phases, which are adsorbate (liquid or vapor phase) and sorbent (solid phase) (Seader and Henley, 2006). There are two types of adsorptions, which are physical adoption and chemical adsorption. This research focuses on the physical adsorption.

In gasoline production via isomerization process, the highest possible gasoline octane number is demanded, which is obtained by improving the materials and technologies. A various type of adsorbents has been developed by several authors (see the next subsection). Moreover,

technologies such as a fixed bed adsorption, pressure swing adsorption (PSA) and moving bed adsorption (SMB) are used to boost the paraffin separation qualities. These materials and technologies separate straight chain paraffin from the desired product which increases the RON (Leprince et al., 2001b). A mini review of several adsorbents, adsorption technologies and adsorption theoretical framework is provided as follows.

4.2.2.1.1 Adsorbent

Various adsorbents are used to increase the adsorbent capacity. To predict the adsorption/adsorbent behaviour, simulation and mathematical models are used widely to determine equilibrium isothermal constants and transfer parameters by comparing breakthrough curves with experimental studies. Experiment and simulation studies of different types of adsorbents that applied for upgrading naphtha are reviewed as follows.

- **Experimental studies**

Studies compared different types of zeolites to investigate the relationship between structures and adsorption performance regarding the adsorption operating pressure (Fu et al., 2018, Abdelrasoul et al., 2017). These investigations are followed by analyse done by using Grand canonical Monte Carlo simulations (GCMC) (Fu et al., 2018, Abdelrasoul et al., 2017). Bárcia et al. (2007) discovered new adsorbent (i.e. zeolite beta). The adsorbent can separate iso/normal paraffin effectively due to its tri-site nature (Bárcia et al., 2007).   Also, experimental data at different temperature degrees was tested against

67

a mathematical model to predict the kinetic and thermodynamic parameters of the tri-site Langmuir equations (Bárcia et al., 2007).

Moreover, a lab-scale PSA with 5 bar high pressure and 0.5 low pressure was investigated to separate nC6 and nC5 from their isomers on zeolite 5 A (Silva and Rodrigues, 1997, Silva et al., 2000). This study focused on the effect of the purge to feed mole ratio on the process performance, which was 0.25 with recovery 70% and purity 100%. Then the study compares the experimental PSA with a mathematical model which uses orthogonal collocation techniques to solve sets of partial differential equations. In this simulation work Adsim was used to estimate all PSA behaviours (Bárcia et al., 2010a).

In addition, Zeolitic Imidazolate framework material (ZIF-8) was suggested to separate n/iso pentane because it has a higher selectivity at low temperature 361 K which is lower than 5A molecular sieve by about 30-80 K (Zhang et al., 2015). They also developed the Langmuir equation which showed high accuracy with their lab tests. Also, separation of hexane isomers on ZIF-8 adsorbent was investigated by Henrique et al., 2018 (Henrique et al., 2018). They use Sips isotherm equation to define the experimental data. Their breakthrough curves were compared to a mathematical model which was designed by using the method of lines (MOL). The results were highly agreed. Their study showed the potential of using ZIF-8 adsorbent to upgrade the gasoline RON.

Moreover, normal pentane adsorption on mesoporous silica was investigated by Gor et al. (2013). They extended the quantitative theory

of adsorption-induced deformation to determine solvation pressure and strain isotherms for SBA-15 and MCM-41 silica which have weak solid−fluid interactions (Gor et al., 2013). The theoretical study showed high agreement with experimental data (Gor et al., 2013).

- **Simulation studies**

Simulation studies are used to calculate the isotherm constants, parametric study and the PSA behaviours and scale-up the column without waste time and money in design the column. Most studies were done on Aspen Adsim 2006.5 which is a powerful tool to simulate adsorption columns that is provided by AspenTech, Inc (Bárcia et al., 2010b, Bárcia et al., 2010a). A two layered bed using zeolite 5A/zeolite beta to get a higher separation performance was studied by Bárcia et al. (2010b). The study concluded that the layered bed increases the RON by 1 point and at a higher operating temperature the RON can be increased by 0.5 point (Bárcia et al., 2010b). Also, Bárcia et al. (2010a) analysed the dynamic behaviour for a single fixed bed. A re-simulation of Bárcia et al. (2010b) work was done by Wood et al. (2018) on Aspen Adsorption® to validate the breakthrough curves for academic studies.

From the above review, the properties of zeolite beta adsorbent showed a potential to upgrade naphtha among the competitive options. Therefore, this thesis carries on with the zeolite beta.

4.2.2.1.2 Adsorption technologies

A fixed bed adsorption, pressure swing adsorption (PSA) and moving bed adsorption (SMB) are elaborated as follows.

- **Fixed bed Adsorption**

For iso/normal paraffin separation, the bed is operated at 90-450 °C and 15-35 bar and desorption is roughly at same operation condition (Leprince and Travers, 2001). The number of beds usually used for the paraffin separation is 3-4 beds (Leprince et al., 2001b, Silva et al., 2000, Silva and Rodrigues, 1997, Silva and Rodrigues, 1998). A total isomerisation process (TIP) converts the normal paraffin to isomers in a catalytic reactor (i.e. platinum-impregnated catalysts) (Holcombe et al., 1990). This is followed by a molecular sieve separation process (Zeolite 5A) to separate and recycle the unconverted normal paraffin to achieve a higher octane number (Holcombe et al., 1990). The molecular sieve separation process is called IsoSive process, which is an adsorption based separation technology that is provided by UOP (Holcombe, 1980, Stine, 2004). The process uses four adsorption beds which leads to increase the gasoline RON up to 93-94 (Leprince et al., 2001a). To accomplish a continuous processing, the cyclic adsorption is used instead.
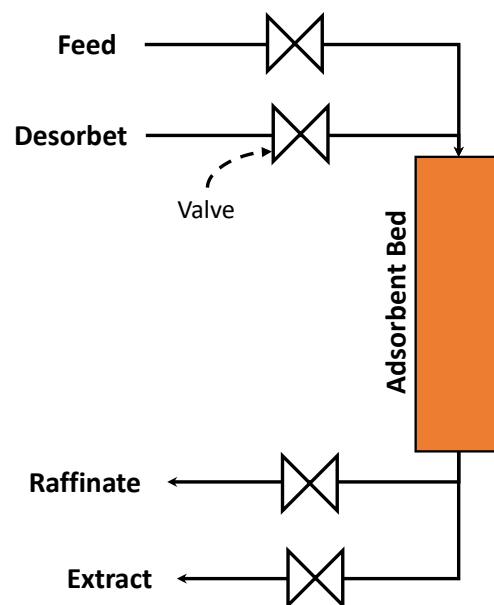
Figure 4-3 Fixed bed Adsorption

- **Pressure swing adsorption (PSA)**

The simplest configuration of the cyclic adsorption is implementing two fixed beds in parallel (Figure 4-4) (Seader and Henley, 2006). Adsorption desorption beds operate alternately to obtain continuous performance and vice versa. The PSA cycle was invented by C.W. Skarstrom (1960) for two beds (Figure 4-4). The Skarstrom cycle is based on an equal duration of four stages, compressing pressurization, adsorption, depressurization (blowdown) and purge. One bed operates for pressurization adsorption, while the other operates for depressurization and purge. For switching between beds, automatic sequencing control valves system is applied (Stine, 2004).
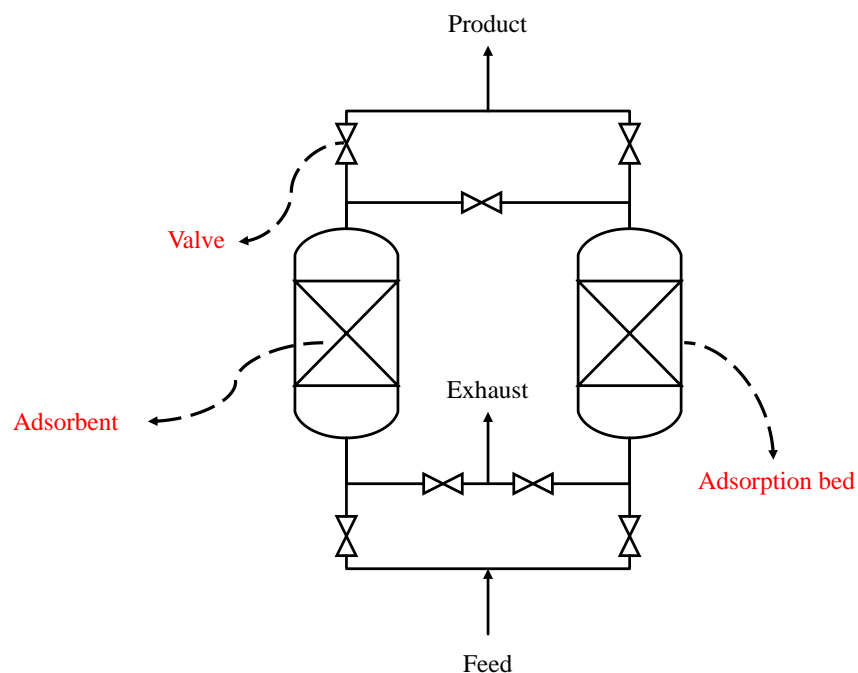
Figure 4-4 Pressure swing adsorption (PSA)

For the straight/branched paraffin separation, several researcher carried on improving the efficiency of the PSA cycle (Evans and Stem, 1988, Haensel, 1975, Stem and Evans, 1987, Zarchy et al., 1993). Moreover,

the PSA is combined with distillation column, which is provided by Axens (please see Section 4.2.2.3).

The main disadvantage of the PSA process that the bed performs one function each time either adsorption or desorption compared to SMB. In the case of adsorption, the equilibrium between the adsorbent and the feed reaches early at the bed entrance. Meanwhile, the raffinate cannot be discharged till the end of the bed (Meyers, 2004). This section of the bed has no use other than pushing the feed downwards the bed. Therefore, the bed requires 3 to 4 times adsorbent amount compare to SMB (Meyers, 2004). In the case of desorption, double the amount of the desorbent is required because of the unproductive bed sections and not allow components to overtake each other (Meyers, 2004).

- **Simulated moving bed (SMB)**

For more than 50 years, simulated moving bed (SMB) has been extensively used for separation technologies (Broughton and Gerhold, 1957). Figure 4-5 shows a four-bed, four zones of the SMB (Lee et al., 2019). Figure 4-5 the adsorbent-filled bed remains fixed, while the fluid rotates stepwise through a rotary valve between a certain number of fixed beds. Number of fixed beds is varied between 4 to 32 columns. Increasing the number of beds increases the mass transfer area, which leads to improve the separation. For process continuity, shortening the switching time between beds can be accomplished by increasing the number of beds and decreasing the bed length. This can justify the reason of the significant SMB separation capabilities improvement,

when compared to the cyclic adsorption. The SMB zones are describes as follows (Figure 4-5) (Seader and Henley, 2006).

Zone I Desorb A. The zone begins with feeding the bed a mixture of A and B. By the end of this zone, component A is discharged into a raffinate stream.

Zone II adsorb B. This zone recycles the adsorbed component B from the previous zone.

Zone III Desorb B. This zone elutes component B using a suitable desorbet.

Zone IV isolation zone. This zone prevents the feed stream from been contaminated by the extract in zone III, as the bed pores are filled with desorbet.

Each zone operates at different flowrates. Thus, accessories equipment such as tank, valve, and compressor are included.
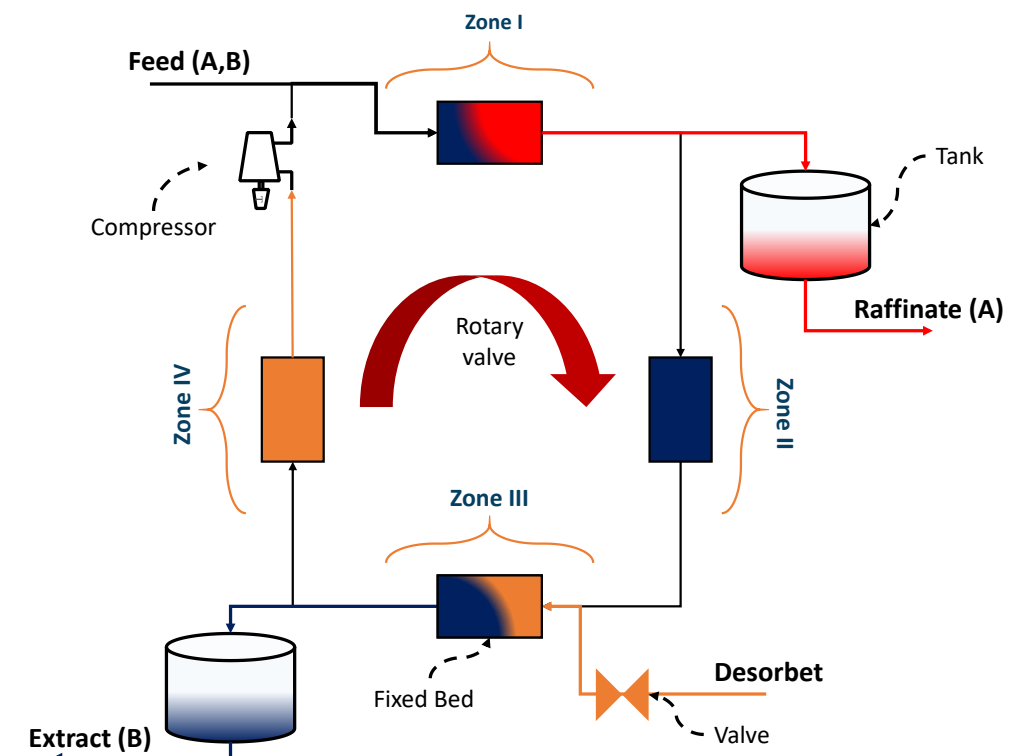
Figure 4-5 Simulated moving bed (SMB)

Sorbex process is a paraffin separation technology that provided by UOP which designs based on the SMB (Figure 4-6) (Meyers, 2004). The separation is held on an adsorption chamber that is divided into number of beds. These beds are separated by grid and flow distributor. Similarly to the SMB, the main active streams are feed, raffinate, desorbet and extract, which ensure the process continuity (Meyers, 2004). The flowrates of these streams are controlled by the amount that is added or withdrew from the chamber for each zone. To circulate the fluid around the chamber, a pumparound pump is used. The rotate valve sends the dilute extraction and dilute raffinate to distillation columns, which are separating desorbent from the extract and the raffinate from the desorbent, respectively (Meyers, 2004). Then, the rotate valve recycle the desorbent back to the chamber (Meyers, 2004).
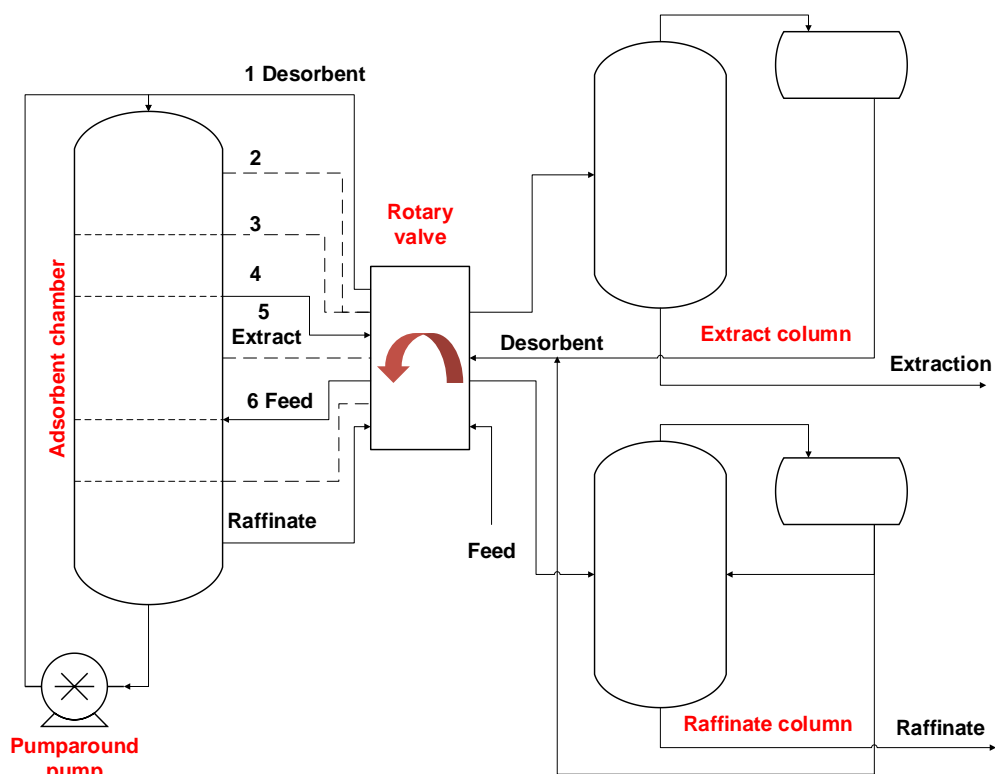
Figure 4-6 Sorbex process flowsheet (Stine, 2004)

Molex process is the naphtha isomerization process that applies Sorbex process. Published studies claimed that the Molex process, is an expensive option for the isomerisation process (Couper et al., 2012, Yasakova et al., 2010). Therefore, this thesis proposes an improvement in the SMB.

4.2.2.1.3 Adsorption governing equations

Several studies described adsorption design equations (Chue et al., 1995, Bárcia et al., 2010b, Knaebel and Hill, 1985), which are expressed as follows.

- **Mass conservation equation**

The general mass balance (Equation (4-7)) demonstrates the mathematical model of the mass balance which was taken from published works (Chue et al., 1995, Knaebel and Hill, 1985).

$$\underbrace{\varepsilon_b D_{ax} \frac{\partial^2 c_i}{\partial x^2}}_{Diffusion/Flux} = \underbrace{\frac{\partial \left(v_g c_i \right)}{\partial x}}_{Convection} + \underbrace{\varepsilon_t \frac{\partial c_i}{\partial t}}_{Accumulation} + \underbrace{\rho_b \frac{\partial \overline{q_i}}{\partial t}}_{Mass\ Transfer} \qquad (4\text{-}7)$$

where ε_b is the inter-particle voidage, c_i is the concentration of component i in fluid, v_g is the gas velocity, ε_t is the total bed voidage, ρ_b is the bulk density, x is the space coordinates, t is the time coordinates, $\overline{q_i}$ is the average amount of i adsorbed and D_{ax} is the axial dispersion coefficient, and it is calculated from Equation (4-8) (Ruthven, 1984, Ruthven et al., 1994).

$$D_{ax} = 0.73 * D_m + \frac{v_g r_p}{\varepsilon_b \left(1 + 9.49 \frac{\varepsilon_b D_m}{2 v_g r_p}\right)} \tag{4-8}$$

where r_b is the particle radius and D_m is the molecular diffusion coefficient which was calculated using Chapman-Enskog theory (Equation (4-9)) (Bird et al., 2006).

$$Dm = \frac{1.86 * 10^{-3} T^{3/2} \left(1/M_A + 1/M_B\right)^{1/2}}{P \sigma_{AB}{}^2 \Omega_D} \tag{4-9}$$

where M_A and M_B are the molecular weights, P is the pressure, σ is the collison diameter in Å and Ω is the diffusion collision integral.

Mass transfer term in Equation (4-7) was calculated using linear driving fource (LDF) , Equation (4-10) (Do and Rice, 1986, Ruthven et al., 1994).

$$\frac{\partial \overline{q_i}}{\partial t} = k_{MTCi}(\overline{q_i} - q_i^*) \tag{4-10}$$

where is k_{MTCi} is the effective mass transfer coefficient of component i and q_i^* the equilibrium loading of component i.

The equilibrium relationship between the sorbent and the adsorbate is called adsorption isotherm. There are five classes that illustrate this relationship (Richardson et al., 2002). In literature, many models were suggested to fit these types. The most commonly used Langmuir isotherm model because it works well within a large range of pressure (Wood et al., 2018). Moreover, the model fixable to be extended to bi- and tri- site Langmuir isotherm basically by adding the basic models in

one equation as shown in Equation (4-11) (Bárcia et al., 2007, Bárcia et al., 2010a).

$$q_i = \sum_j \frac{q_{i,j}^m b_{i,j} p_i}{1 + \Sigma_i\, b_{i,j} p_i} \qquad (4\text{-}11)$$

where q^m is the saturation loading in each site, p_i is the partial pressure for the component i, j is the number of sites and b_i is the adsorption affinity constant of component i in site j. The adsorption affinity constant (b_j) is calculated by using Arrhenius Equation (4-12).

$$b_j = b_j^0\, e^{\left(\frac{-E_j}{RT}\right)} \qquad (4\text{-}12)$$

where is b_j^0 the frequency factor of the affinity constant, E_j is the interaction energy of site j, T is the temperature and R is the universal gas constant.

- **Momentum conservation equation**

Ergun equation (Equation (4-13)) is used to calculate pressure drop, because it is valid for laminar flow as well as turbulent flow (Bárcia et al., 2010a).

$$-\frac{dP}{dx} = \frac{1.5 * 10^{-3} * \mu_g (1 - \varepsilon_b)^2}{\left(2 r_p\right)^2 \varepsilon_b^3} v_g + \frac{1.75 * 10^{-5} * M_w \rho_g (1 - \varepsilon_b)}{\left(2 r_p\right) \varepsilon_b^3} v_g^2 \qquad (4\text{-}13)$$

where P is the pressure, μ_g is the dynamic viscosity and M_w the molecular weights.

- **Mass balance around a tank**

Raffinate and extract streams are storage in tanks. These tanks are modelled according to Equation (4-14) (Vojtesek et al., 2014).

$$\frac{dF}{dt} = F_{in} - F_{out} \qquad (4\text{-}14)$$

where F_{in} and F_{out} is the inlet and outlet flowrate, respectively.

- **The valve model**

For more reliability, the flowrate through the valve is assumed to have a non-linear relationship (Wood et al., 2018) with the pressure drop (ΔP) as shown in Equation (4-15).

$$F = C_v \Delta P = Q \sqrt{G_f \Delta P} \qquad (4\text{-}15)$$

where C_v is the valve constant, Q is the volumetric flowrate and G_f is the specific gravity which was taken from Aspen HYSYS®.

- **Compressor model**

The work of the compressor is calculated using Equation (4-16) (Yang, 2013).

$$W = FRT \frac{1}{\eta} \frac{\gamma}{(1-\gamma)} \left[\left(\frac{P_H}{P_L}\right)^{\frac{\gamma-1}{\gamma}} - 1 \right] \qquad (4\text{-}16)$$

where W is the work, f is the gas flowrate, η is the efficiency which assumed to be 75% and γ is the ratio of specific heat which is 1.334 and it is calculated using HYSYS®.

4.2.2.2 Distillation separation

The separation by distillation relies on the volatility of paraffin (Seader and Henley, 2006). To get a higher RON, it is necessary to recycle unconverted nC5, nC6 and low octane components such as methyl pentane (MC5) back to the reactor. This can increase the RON up to 92 (Leprince and Travers, 2001). A recycle build-up approach recovers approximately 65% of the fresh feed (Graeme and Ross, 2004, Leprince and Travers, 2001, Rice, 2007). Many column configurations were suggested in the literature (Chen et al., 2015, Mohamed et al., 2017, Yasakova et al., 2010). These configurations, which, mainly, depends on feedstock compositions, are listed and discussed as follows (Chen et al., 2015, Mohamed et al., 2017, Yasakova et al., 2010):

- Deisopentanizer column (DIP) is used to separate the isopentane (iC5) at the beginning of the process because it lowers the reaction rate. Normally, it is used when the feed contains more than 13-15% of isopentane. This upgrades the RON to 80-86.

- Recycling of unconverted pentane (nC5) increases the equilibrium reaction towards the products. This increases the RON to 80-86. Depentanizer column (DP) is used in this context.

- Recycling of unconverted hexane (nC6) increases the feed concentration which leads to an increase in the reaction rate. This upgrades the RON to 82-90. Dehexanizer column (DIH) is used in this framework. It is, however, rarely used in industry due to the high conversion of hexane to isomerate.

- Deisohexanizer is a distillation column that separates lighter components such as normal pentane and dimethyl butane

79

(DMC4) in the overhead stream, methyl pentane and hexane in the side stream and the heavier components at the bottom (Rice, 2007). In all, dimethyl butane has a relatively higher octane number than methyl pentane, so methyl pentane will be recycled with the normal hexane (Rice, 2007) and dimethyl butane will be sent to gasoline pools. This increases the gasoline octane number to 82-90.

According to Mohamed et al. (2017) investigation the combination of methods 1, 2 and 4 (Figure 4-3) results the highest RON (91-93) with the highest capital investment (up to $220M).

These schemes have been illustrated, discussed and economically analysed by Mohamed et al. (2017). Their study found that the best and most economical scheme for light naphtha containing 13% mole pentane and 30% mole hexane is a combination of deisopentanizer and dehexanizer column with return on investment (ROI) of 26.6% and RON of 87.4. However, in this thesis, a depentanizer column was developed because nC5 content in the feed is assumed higher than 30%. Also, the column is reported to produce an ROI of 20% and a RON of 84.5, which is among the top-best columns (Mohamed et al., 2017). In this thesis, the focus is on developing distillation column model.
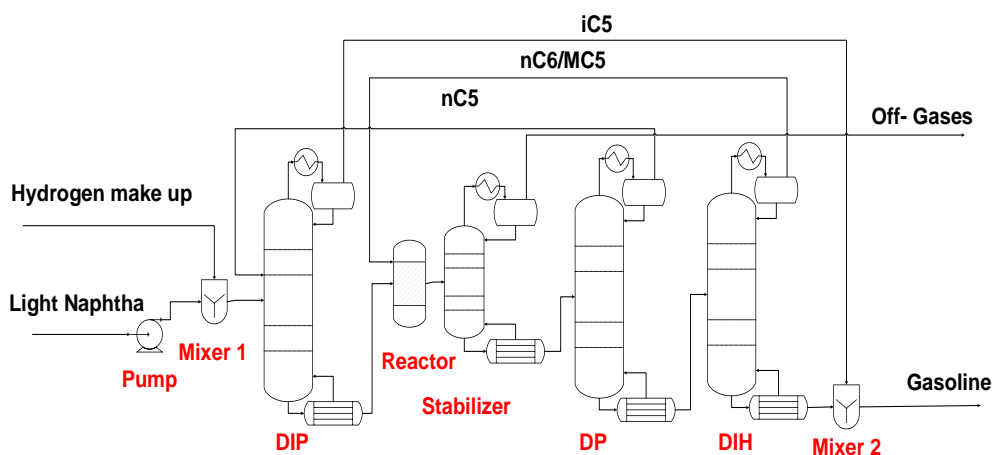
Figure 4-7 Flowsheet diagram for the isomerization unit with deisopentanizer (DIP), depentanizer (DP) and deisohexanizer (DIH) columns (Mohamed et al., 2017)

4.2.2.3 Combination of the two separations

The combination of distillation and pressure swing adsorption is commonly used to increase the gasoline RON up to 90. Using adsorption separations to upgrade gasoline RON is proven to be much better by 3-4 points than distillation columns. However, to desorb the normal alkanes recycled hydrogen was used to reduce the operating cost. This hydrogen contains dissolved materials from the reactor such as chlorine which decay the adsorbent performance (Graeme and Ross, 2004). Thus, combination methods solve this issue by desorbing the adsorption with iso-pentane or methyl pentanes streams which are generated by deisopentanizer and deisohexanizer columns, respectively (Graeme and Ross, 2004). Commercial examples of the combination separations are Ipsorb™ and Hexorb™ which are provided by Axens (Graeme and Ross, 2004, Leprince et al., 2001b, Yasakova et al., 2010). Ipsorb™ is a combination of upper-stream deisopentanizer and down-stream molecular sieve, which upgrade the RON to 88-89 with 0.65 C5:C6 ratio feed (Graeme and Ross, 2004). Hexorb™ process is a combination of upper-stream molecular sieve and down-stream deisopentanizer, which

upgrade the RON to 91-92 with 0.65 C5:C6 ratio feed (Axens, 2009, Graeme and Ross, 2004).

4.2.3 Heat pump distillation

In chemical industries, 90% of separation processes are distillations (Humphrey, 1995), which consume about 36% of petroleum refineries total energy (Haynes, 1979) and 60% of total chemical and petroleum processes (Mix et al., 1981). Reducing this energy is highly requested to obtain low environmental impacts.

Several researchers have suggested different types of heat efficient distillation processes such as multi columns (Masel et al., 2013), thermally coupled distillation (TCD) (Hojjati and Namdari Ghareghani, 2019), heat integrated distillation column (HIDis) (Fang et al., 2018, Ulyev et al., 2018, Kiss, 2016) and divided wall distillation columns (DWC) (Rice and Plaines, 2002, O'Brien and Rice, 2002). Although these studies obtain significant energy reductions, they conclude that these configurations are economically inefficient. Generally, this occurred because the capital cost of implementing a new separating technology is relatively high.

On the other hand, heat pump assisted distillation columns exchange a condenser and/or a reboiler with a compressor, which can maintain the low capital cost (Jana, 2010, Jana, 2014). Heat pump assisted distillation columns replace water, heat and refrigerant utilities (usually consumed by the regular distillation) with little work, which is more sustainable (in case of using solar and wind energy) (Seider et al., 2019). Many comparisons between different types of heat pump assisted distillation

column configurations were investigated by aforementioned studies (Farrokhpanah, 2009, Reddy et al., 2014, Kazemi et al., 2017, Kazemi et al., 2018a, Kazemi et al., 2018b). These studies concluded that vapour recompression, reboiler flashing and absorption heat pump columns are the most efficient configurations in terms of saving energy and money (Figure 4-8).

An economical comparison between these configurations was investigated by Díez et al. (2009) to separate iso/normal butane on a distillation column. The study reported that up to 33% saving energy was achieved when using the bottom flashing heat pump comparing to conventional distillation and vapour recompression heat pump (Díez et al., 2009). However, the absorption heat pump was not economical because it is more suitable for applications with a large temperature difference between condenser and rebuilder (Fonyo and Benko, 1996, Fonyo and Benkö, 1998, Jana, 2014, Tufano, 1997, Xu and Wang, 2017).
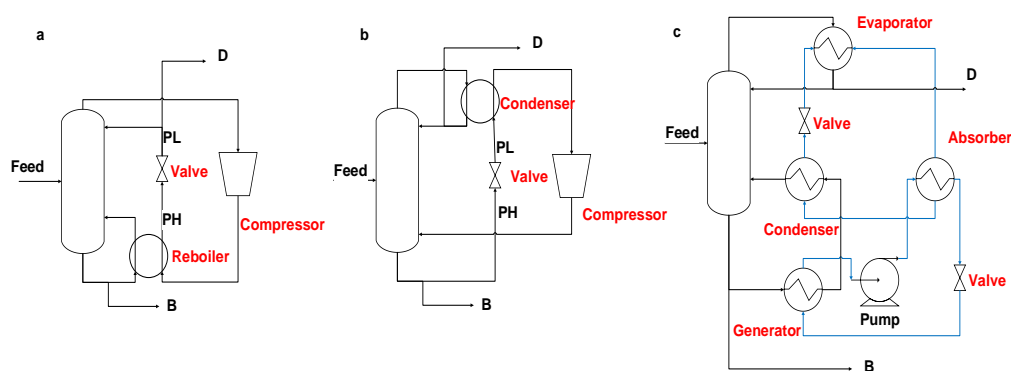
Figure 4-8 Heat pump distillations configurations: (a) vapour recompression, (b) reboiler flashing and (c) absorption (developed from (Kiss et al., 2012a))

Heat pump distillations are applied to reduce the operating cost, in case of the electricity is cheaper than steam or the need of water in other

applications such as agriculture is significantly high. However, they increase the capital cost. Therefore a trade-off between capital cost and operating cost is investigated in this thesis.

4.3 The superstructure process simulation development using hybrid software

As mentioned in Section 1.3.2, a detailed isomerization of light naphtha process model was not available in the literature. Therefore, all parameters (e.g. thermodynamics and kinetics) were conducted and suitable assumptions was estimated to simulate the comprehensive superstructure process. The superstructure process was modelled is made up of two flowsheets: frontend and backend. The frontend flowsheet included preheated, reactors, hydrogen recycle system and light gases separation, where gasoline was produced. The backend flowsheet included iso/normal paraffin separation systems, which enhance the RON of the gasoline. Detailed models were provided as follows.

4.3.1 Frontend flowsheet simulation

The continuous frontend process was simulated in Aspen HYSYS® with capacity of 10,000 BPD (barrel per day) of gasoline production. The process feedstock and hydrogen data were based on the Universal Oil Products (UOP), after excluding impurities such as sulphur and water. Moreover, constant feed molar compositions were assumed. Peng-Robinson was used as a thermodynamic package, as it is suitable for hydrocarbon at varies pressure (Seader and Henley, 2006). The hydrogen to hydrocarbon molar ratio for isomerisation process was

assumed to be 0.5 to 1 (Yasakova et al., 2010). Figure 4-9 illustrates the frontend process simulation in Aspen HYSYS®. The hydrogen and the pumped light naphtha were mixed and preheated. The mixture was sent to a splitter to switch the mixture flowrate into one of the available reactors (i.e. Pt/Al_2O_3–CCl_4, Pt/SO_4–ZrO_2, and $Pt/zeolite$). The pre-products were cooled and sent to a flash drum. Then, the drum recycled the excessive hydrogen back to the reactors and sent the off gases and paraffin to a stabilizer column. The column separated the off gases and sent them to the LPG, and normal/iso paraffine mixture was cooled to obtain the low RON gasoline. The frontend simulation details are provided as follows.
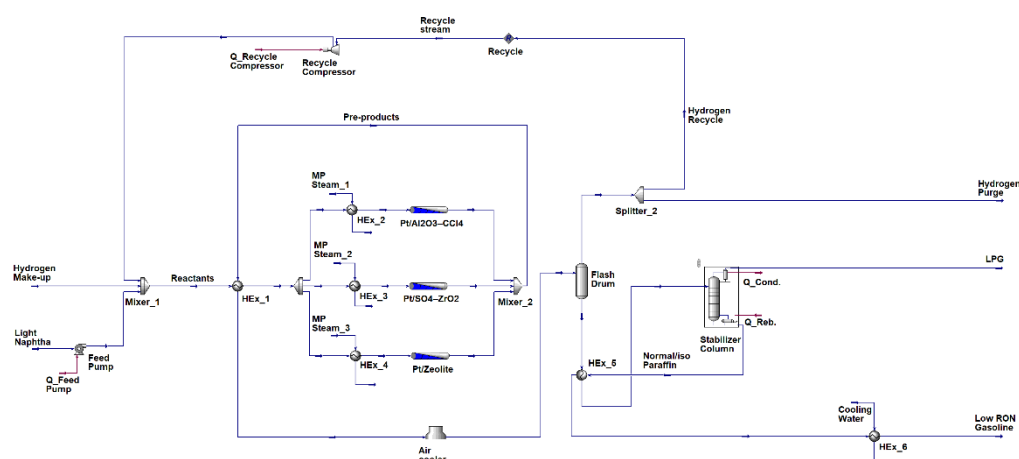
Figure 4-9 Frontend model in Aspen HYSYS®

4.3.1.1 Pumped and preheated model

The light naphtha was provided from atmospheric distillation at temperature of 313 K and pressure of 7 bar (Mohamed et al., 2017). Hydrogen was available in the petroleum refinery at temperature and pressure of 313 K and 30 bar (Meyers, 2004). The fresh feed was operated at temperature of 393 - 573 K and pressure of 30 bar, depending on which catalyst is used, as the isomerization reactions achieve their highest conversion at these conditions (Chuzlov et al.,

2014). The fresh feed was often pumped and heated by using a feed pumped and a heat exchanger (Figure 4-9) (Meyers, 2004). The isomerization reactions are exothermic and release energy up to 4 - 20 kJ/mole (Lamprecht and Klerk, 2009). This energy was integrated by using an extra heat exchanger with the fresh feed for preheating and minimizing the steam requirements, which is beneficially environmentally. The pump and heat exchangers were added prior to the reactors (Figure 4-9).

4.3.1.2 Reactor model

The most common catalysts are used in the gasoline production are $Pt/SO_4–ZrO_2$, Pt/zeolite and $Pt/Al_2O_3–CCl_4$. The reactors were designed based on Abdulbari et al. (2017) work. For the capacity of 10,000 BPD, the reactor volume is 35 m^3 (Toraman et al., 2016), the height to diameter ratio of 10 to allow maximum conversion (Luyben, 2011), hold-up of 75% and Voidage ratio(ε) of 0.4 (Abdulbari et al., 2017). The reactor vessel was sized for continuous operation by dividing the reaction residence time (i.e. 1 hr) by the feed flowrate. The volumes of these catalysts were estimated based on the plant capacity. Catalysts' deactivation was neglected.

$Pt/Al_2O_3–CCl_4$, $Pt/SO_4–ZrO_2$, and Pt/zeolite catalysts were operated at temperature of 422 K, 518 K, and 403 K, and pressure of 34, 27 and 30 bar, respectively (Chekantsev et al., 2014). Vapour phase reactions were assumed under these operation conditions. In addition, Ergun equation, which is built-in HYSYS® function, was used to estimate the pressure drop. As mentioned in Section 4.2.1.1, the isomerization

reactions scheme is complex, including isomerization, ring-opening and reversible reactions, which strongly depends on the type of catalysts. However, the catalytic The reaction rate (r) equations were assumed to be first order (Equation (4-17)), as Aspen HYSYS® only allows these type under the kinetic reaction category.

$$r = k * C - k' * C'$$ (4-17)

where k is the rate constant (s^{-1}) for the forward reaction, k' is the rate constant (s^{-1}) for the reverse reaction, C and C' are the concentrations for the forward reaction and the reverse reaction, respectively.

The reaction rate constants and energy activations for $Pt/SO_4–ZrO_2$ are shown on Table 4-3. Arrhenius equation was used to calculate the pre-exponential factors to apply them to HYSYS®. Arrhenius equation is shown in Equation (4-18)

$$k = A * e^{\frac{-E_a}{RT}}$$ (4-18)

where A is the pre-exponential factor (s^{-1}), E_a is the activation energy (kmol/kJ), R is the universal gas constant (8.314 kJ/kmol.K) and T is the temperature (K). Table 4-4 presents Pt/zeolite and $Pt/Al_2O_3–CCl_4$ catalysts reaction rate constants normalised by $Pt/SO_4–ZrO_2$ (Chekantsev et al., 2014). The difference between the other reactions were negligible (Chekantsev et al., 2014). Table 4-5 presents the kinetic parameters were applied in the current research.

Table 4-3 Kinetic parameters taken from literature for Pt/SO₄–ZrO₂

Reactions	k(s⁻¹) (Chekantsev et al., 2014)	E $_{ref.}$ (kmol/kJ)	References
nC5 → iC5	0.0717	150 ± 20	(Szoboszlai and Hancsók, 2011)
iC5 → nC5	0.0249	150 ± 20	(Szoboszlai and Hancsók, 2011)
nC6 → 2MC5	0.2790	121 ± 1	(Szoboszlai and Hancsók, 2011)
2MC5 → nC6	0.2100	143.42 ± 5.78	(Pather and Lokhat, 2014)
2MC5 → 23DMC4	0.0288	68.4 ± 7.62	(Pather and Lokhat, 2014)
23DMC4 → 2MC5	0.0386	121 ± 1	(Szoboszlai and Hancsók, 2011)
2MC5 → 3MC5	0.3230	152.96 ± 2.73	(Pather and Lokhat, 2014)
23DMC4 → 22DMC4	0.0581	126.5 ± 7.5	(Szoboszlai et al., 2012)
22DMC4 → 23DMC4	0.1270	126.5 ± 7.5	(Szoboszlai et al., 2012)
cC6 +H2 → nC6	0.0010	125 ± 25	(Szoboszlai and Hancsók, 2011)
Benzene + 3 H2 → cC6	0.0210	112.96	(Pather and Lokhat, 2014)

Table 4-4 Reaction rate constants normalised by Pt/SO₄–ZrO₂ catalyst (Chekantsev et al., 2014)

Reactions	Pt/SO₄–ZrO₂	Pt/zeolite	Pt/Al₂O₃–CCl₄
nC5 → iC5	1	0.48	0.31
iC5 → nC5	1	1.43	0.96
2MC5 → 3MC5	1	0.52	1.72
nC6 → 2MC5	1	1.10	0.47
2MC5 → 23DMC4	1	0.91	1.63
22DMC4 → 23MC4	1	1.27	0.85

Table 4-5 Kinetic parameters for current study for Pt/SO$_4$–ZrO$_2$

Reactions	k(s^{-1})	E (kmol/kJ)
nC5 → iC5	0.0717	150
iC5 → nC5	0.0249	130
nC6 → 2MC5	0.2790	120
2MC5 → nC6	0.2100	143.42
2MC5 → 23DMC4	0.0288	68.4
23DMC4 → 2MC5	0.0386	120
2MC5 → 3MC5	0.3230	153
23DMC4 → 22DMC4	0.0581	107
22DMC4 → 23DMC4	0.1270	123
cC6 +H2 → nC6	0.0010	125
Benzene + 3 H2 → cC6	0.0210	112.96

4.3.1.3 Hydrogen recycle model

Excessive amount of hydrogen is required for the isomerisation reaction and, therefore, the hydrogen can be recycled for environmental and economic purposes, as was anticipated from Yasakova et al. (2010). The hydrogen recycle system was proceed as follows. The outlet stream from the reactor was cooled in an air cooler, and then followed by a flash drum to separate the hydrogen from bottom products. The recycled hydrogen was then compressor and fed back to the reactor. The bottom products are sent to stabilizer column.

4.3.1.4 Stabilizer model

Traditionally, light gases are separated from heavy components to be reused for LNG systems. Multistage flash vaporization and distillation columns are the common techniques used for light gases separation (Moghadam et al., 2012, Moghadam and Samadi, 2012, Hashim and Jassim, 2014). Moghadam et al. (2012) combared both processes for

light gases stabilization. Their study found that the distillation consumed less total heat duty and produced much higher condensate recovery. Accordingly, this thesis applied stabilizer column to separate the LPG from paraffine. The column was designed for 30 stages column. The stabilizer column designs were based on principles outlined in the literature (Turton et al., 2009, Seider et al., 2017).

4.3.2 Backend flowsheet simulation

The single-pass process allows for producing a partial conversion due to equilibrium reaction limitation (Chekantsev et al., 2014). So, recycling is a necessity to dilute the fresh feed, which increases the forward reaction (Lamprecht and Klerk, 2009). The backend flowsheet model includes eight simulated moving bed, distillation column and heat efficient distillations (i.e. bottom flashing vapour recompression and absorption heat pump). All these models are described as follows.

4.3.2.1 Eight moving bed-adsorption (SMB)

There are many developed software such as Aspen chromatography® that was used to simulate the SMB (Lee et al., 2019). Although they work very well to represent the dynamic process, they show imbalanced material results (Wood et al., 2018). This made it difficult to adjust the economic calculation fairly for accomplishing the current research aims. Moreover, because of the nature of these software to prevent users from showing and modifying the program equations, it becomes more challenging to debug and solve the imbalance issue. In addition, numerical simulation tools such as PDECOL package was developed by Madsen and Sincovec (1979), which tackles the previous problem.

However, the package can consume up to 90 hours of the CPU time in a CrayJ916 computer (Lu and Ching, 1997, Madsen and Sincovec, 1979).

Therefore, the large scale eight SMB was modeled in MATLAB® by solving the governing equations (Subsection 4.2.2.1.3) using the BTCS method, which was described in Chapter 3. The SMB process was described in subsection 4.2.2.1.2.

4.3.2.1.1 The developed model assumptions

Mass and momentum balance equations were employed in this model, following the one proposed by Bárcia et al. (2010a). the model assumptions are listed as follows:

- Ideal gas.

- The adsorption is an exothermic process with negligible temperature variation (about 5 K). So, beds were assumed isothermal.

- Dead volume on either side of the bed is negligible (Lu and Ching, 1997).

- Linear driving force model describes the mass transfer between the gas and adsorbent (Do and Rice, 1986).

- The axial dispersed plug flow model describes the flow pattern.

- The pressure drop used Ergun equation (Kikkinides et al., 1993).

- The main resistances to mass transfer rate from bulk fluid phase to solid particles are the external fluid film resistance around the particles and the intraparticle diffusion of components (Kikkinides et al., 1993).

- The adsorption data are described by the Tri Langmuir isotherm.

4.3.2.1.2 Isothermal equilibrium model

There are several researchers (see subsection 4.2.2.1.1) estimated the isothermal parameters for paraffin separation. However, the most inclusive and accurate estimation was made by Bárcia et al.(2007-2010). Tri-Langmuir isothermal equilibrium model for hexane branches at zeolite beta adsorbent was first proposed by Bárcia et al. (2007) study. Then, Bárcia et al. (2010a) extended the model to include normal and iso pentane. Their study used the Adsim® simulator to estimate the isothermal parameters. Their isothermal model obtained consistent results at various feed compositions and temperatures for lab-scaled process. Thus, this thesis applied their tri-Langmuir isothermal parameters for field scale SMB.

The mass transfer coefficients and extended Langmuir parameters are shown in Table 4-6 and Table 4-7, respectively. The bed properties are shown in Table 4-8.

Table 4-6 Mass transfer coefficients (k_{MTC} (s^{-1})) (Bárcia et al., 2010a)

T(K)	nC6	3MC5	23DMC4	22DMC4	nC5	iC5
423	0.003	0.006	0.0123	0.0298	0.031	0.067
473	0.038	0.076	0.1268	0.3681	0.209	0.386
523	0.2676	0.5559	0.8165	1.8355	0.959	1.570

Table 4-7 Extended Langmuir model parameter and mass transfer coefficients (Bárcia et al., 2010a)

	nC6	3MC5	23DMC4	22DMC4	nC5	iC5
q_1^m (mmol/g$_{ads}$)	0.529	0.329	0.775	0.797	0.608	0.491
$b_{0,1}$ (*10^9/kPa)	0.5	2	0.86	1.2	10	13
E_1(kJ/mol)	70.3	67.2	67.5	65.9	59.5	59.1
q_2^m (mmol/g$_{ads}$)	0.289	0.195	--	--	0.082	0.354
$b_{0,2}$ (*10^9/kPa)	1.7	0.3	--	--	9.7	20
E_2(kJ/mol)	78.8	84.8	--	--	26.2	52.8
q_3^m (mmol/g$_{ads}$)	0.112	0.406	0.155	0.133	0.257	0.1
$b_{0,3}$ (*10^9/kPa)	$4.6*10^{-3}$	$5*10^{-3}$	0.68	3.2	8.1	18
E_3(kJ/mol)	99.8	87.1	80.2	68.1	65.9	60.3

Table 4-8 Bed properties (Feng et al., 2017, Silva et al., 2000, Al-Juhani and Loughlin, 2003, Hamelinck et al., 2004)

Diameter (m)	3.66
Length (m)	6.67
Bulk porosity (ε_b)	0.49
Adsorbent particle diameter (cm)	0.159
Bulk density (ρ_b) (kg/m^3)	630
ε	0.35

4.3.2.1.3 Eight moving bed adsorption (SMB)

For plant with 10,000 BPD capacity, the regular beds dimensions are 3.33 m and 6.67 m for the bed diameter and length, respectively (Bárcia et al., 2010b). The bed operated low and high pressures were 5 and 15 bar, respectively (Leprince et al., 2001a, Leprince et al., 2001b). The SMB was included four zones each zone contained two beds. The reason of using two beds for each zone was to increase the mass transfer units, which leads to better iso normal paraffin separation (Lu and Ching, 1997). Also, the 8-bed SMB can allow faster adsorption/ regeneration cycles. Hydrogen was used to wash the bed.

Figure 4-10 presents the SMB simulation in HYSYS®-MATLAB® platform. The input stream data was exported from HYSYS® to MATLAB®. MATLAB® processed these data and then sent them back

to HYSYS® for recycling the unconverted paraffin and increasing the gasoline RON. The SMB outlet recycled, and isomers flowrate streams received data from MATLAB® were returned to HYSYS® for each component separately, which is the HYSYS® model limitation.
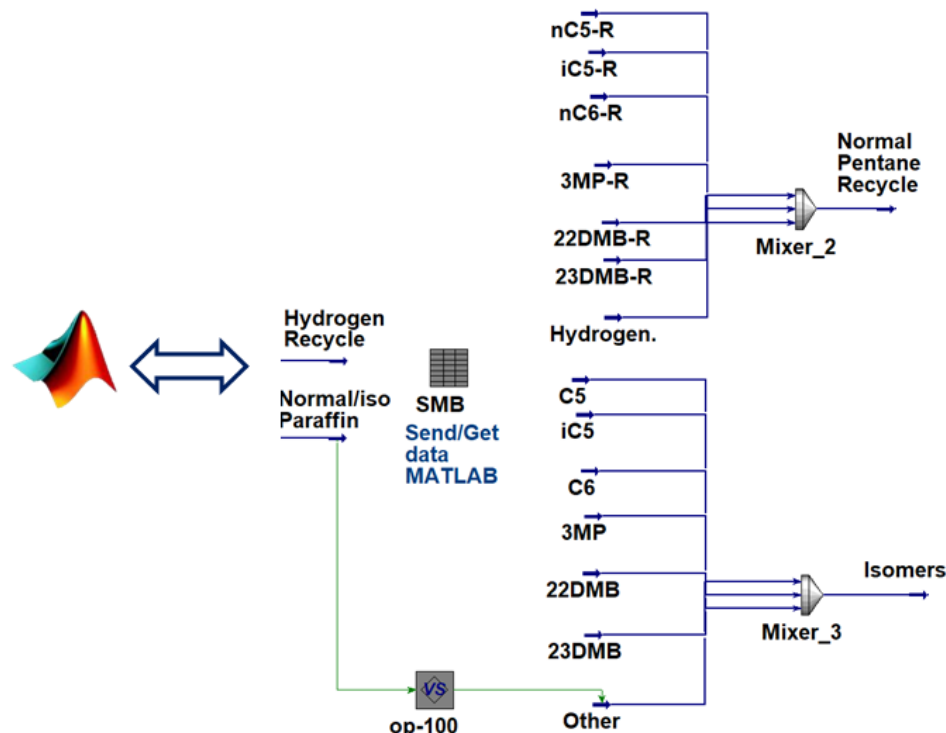
Figure 4-10 Simulated moving bed (SMB)

4.3.2.2 Distillation column (DIS)

Distillation column was used to separate light components from heavy and normal paraffin from isomers (Figure 4-11). The short cut column was used to estimate the column number of trays (90 trays), reflux ratio (10), feed temperature (385 K), feed pressure (25 bar), top pressure (20 bar) and bottom pressure (30 bar). Then, these data were applied to a conventional column. The column had a side stream to recycle normal pentane (nC5). The column design was based on Apostolakou et al. (2009), where the height transfer unit (HTU) and pressure drop were assumed to be 0.5 m and 0.2 bar, respectively.
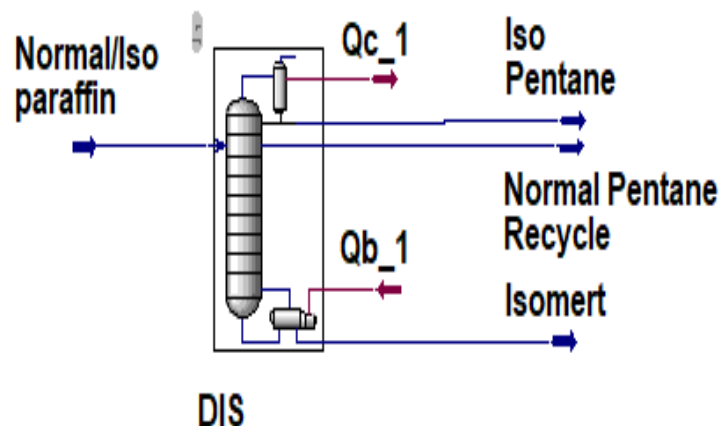
Figure 4-11 Distillation column in HYSYS®

4.3.2.3 Energy efficient distillations model

Three heat pump distillation processes were employed in HYSYS®: vapor recompression (VRC), bottom flashing (BF) and absorption heat pump (AHP). These processes were developed from Díez et al. (2009) study, who applied them to separate iso/normal butane. While this thesis applies them for iso/normal paraffin. These heat pump distillation processes are described as follows.

4.3.2.3.1 Vapor recompression heat pump (VRC)

Figure 4-12 presents the VRC distillation process model in HYSYS®. The VRC replaces the condenser with a compressor, air cooler and valve. The VRC process is elaborated as follows. The main tower was operated similarly to the distillation column. The top product compressed and then cooled by using an air cooler for total condensate fluid. A part of the product was recycled to the top tray of the column. The bottom product exchanged heat with the top product using a heat exchanger. The vapour outlet was recycled to the lower tray of the main tower and withdraw the liquid products. A side-stream was added in this thesis to recycle the normal pentane, which leads to increase the RON.
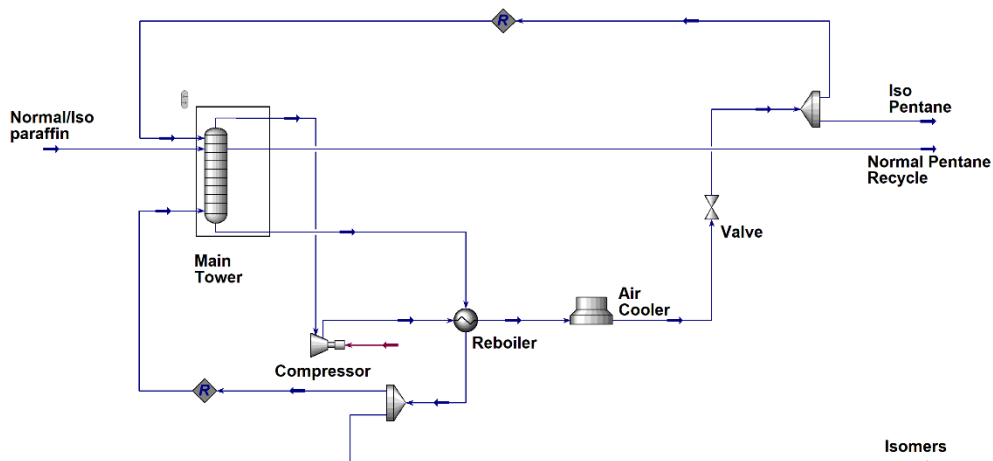
Figure 4-12 Vapor recompression heat pump distillation process in HYSYS®

4.3.2.3.2 Bottom flashing heat pump (BF)

Similarly, the BF replaces the reboiler with a compressor, air cooler and valve (Figure 4-13). The main column was operated similarly to the distillation column. The top product exchanged temperature with lower product on a heat exchanger for total condensate fluid. A reflux was recycled to the column top tray. The bottom product was compressed and then cooled down using the compressor and the air cooler, respectively. Part of the bottom product was recycled to the lowest tray in the column. Also, in this thesis, a side-stream was added to recycle the normal pentane, which leads to increase the gasoline RON.
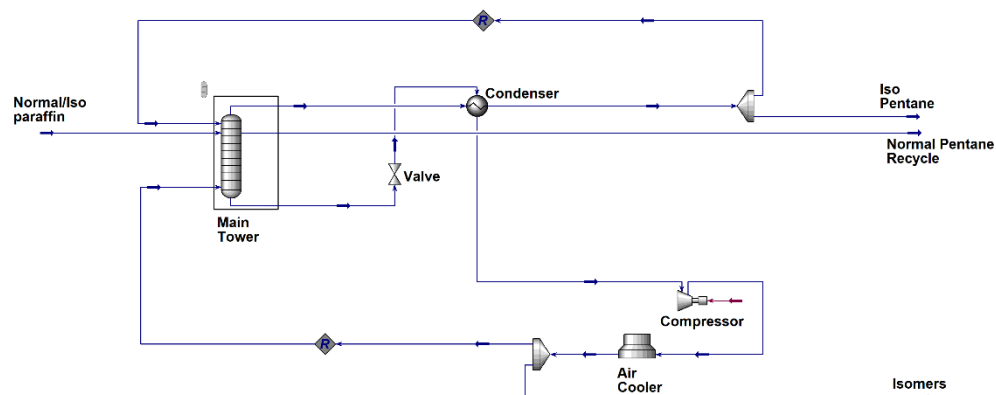
Figure 4-13 Bottom flashing heat pump distillation process in HYSYS®

4.3.2.3.3 Absorption heat pump (AHP)

The AHP process basically includes absorber, desorber (also known as generator), evaporator and condenser (Jana, 2014). Figure 4-14 presents the AHP cycle in the HYSYS® model. The cycle flows as: the released vapour from the generator at high pressure and temperature was sent to the absorber. Then the condensed fluid, which was produced form the absorber, was sent to the evaporator, meanwhile, the condenser energy was used to reboiler the isomers. The fluid from the evaporator and from the bottom of the absorber were cooled to be recycled to the generator, where the cycle starts again. Ammonia – water solution was used because of its many advantages such as it is not corrosive (Fonyo et al., 1995, Jana, 2014). A side-stream was added in this thesis to recycle the normal pentane, which led to increase the RON.
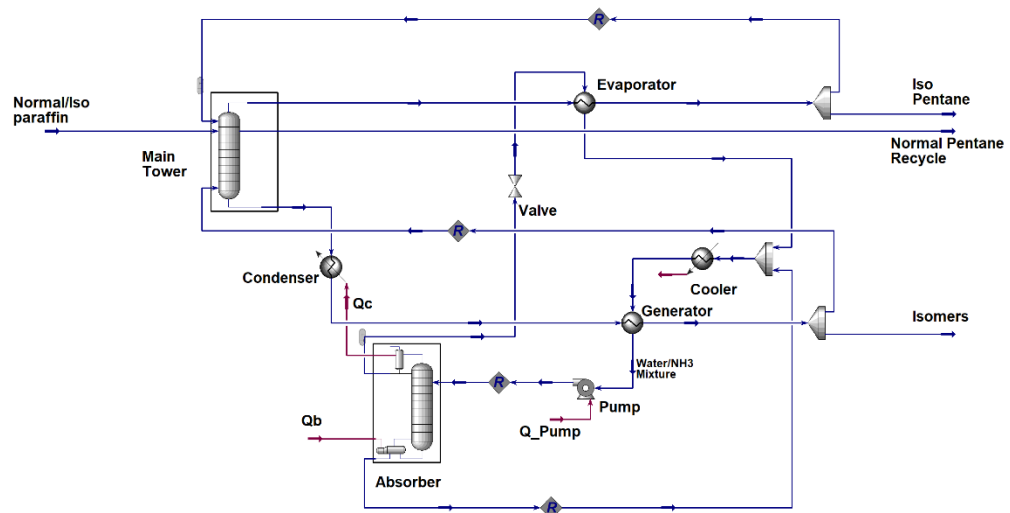
Figure 4-14 Absorption heat pump distillation process in HYSYS®

4.3.3 Hybrid superstructure simulation

Figure 4-15 presents the superstructure process that was simulated in HYSYS®-MATLAB® platform. Light naphtha and hydrogen were processed through the frontend process flowsheet to produce the

preliminary gasoline (RON=~77). Then, the gasoline was cooled to 410 K by using heat exchanger 5 and was sent to the backend process flowsheet to recycle the unconverted pentane and to enhance the gasoline RON. The switch method decides which separation option was been applied. Finally, the high RON gasoline sent to heat exchanger 6 to be cooled to 303 K and then sent to the gasoline pool.

In MATLAB® ensures the superstructure process stability using convergence level (see Chapter 3). The thermodynamic data and equipment sizing data are exported in the HYSYS® spreadsheet to determine the techno-economic analysis (see Chapter 5).
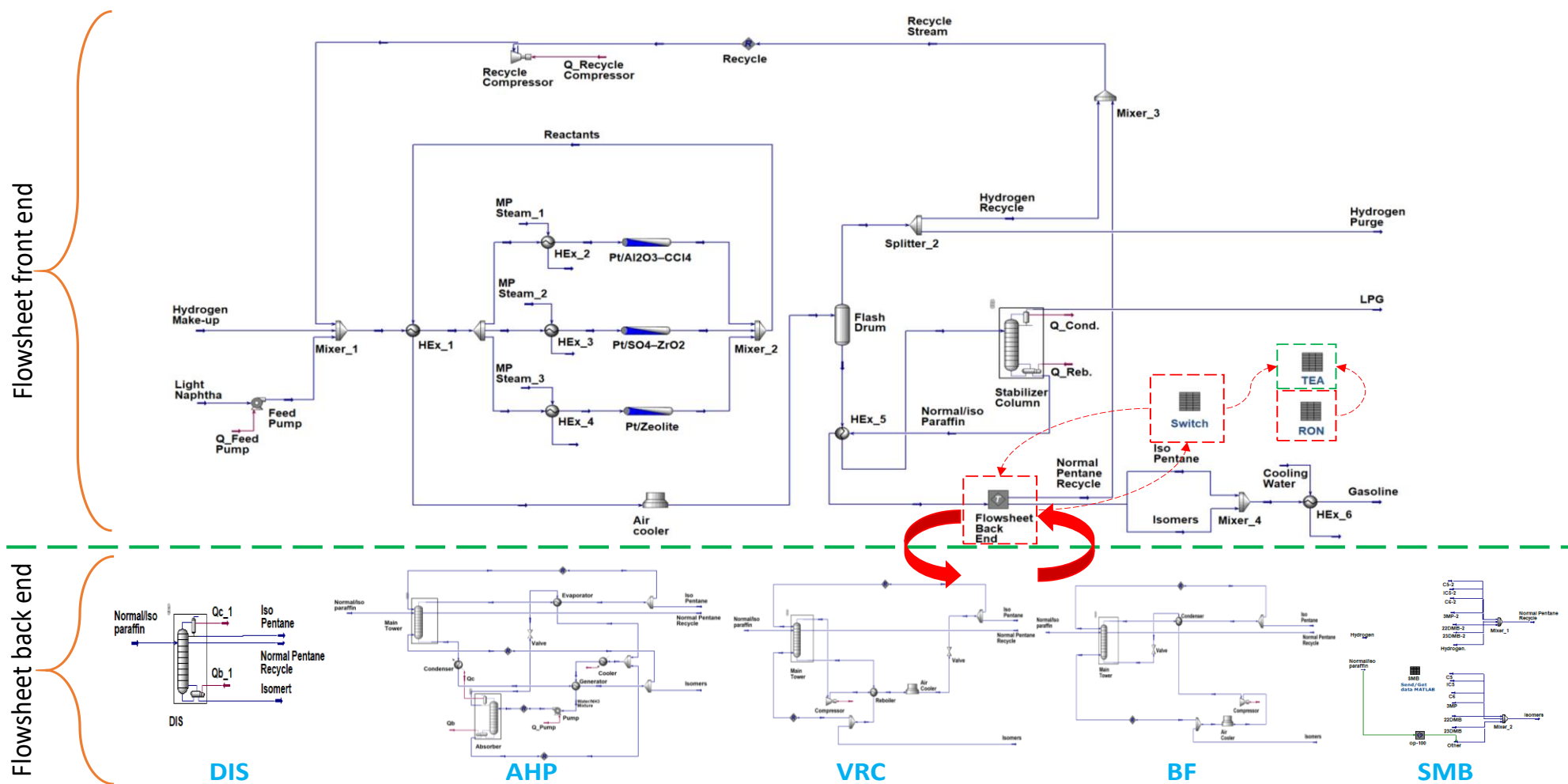
Figure 4-15 The superstructure flowsheet - HYSYS® model

4.4 Results and discussions

4.4.1 Frontend flowsheet model results

Figure 4-16 presents the gasoline RON produced against three catalysts: Pt/SO$_4$–ZrO$_2$, Pt/zeolite and Pt/Al$_2$O$_3$–CCl$_4$. The highest RON was achieved when using Pt/Al$_2$O$_3$–CCl$_4$ at 83.6 RON followed by Pt/SO$_4$–ZrO$_2$ 81.3 RON and then Pt/zeolite at 73.7 RON. Although, these results agreed precisely with Chekantsev et al. (2014) model, the overall error of gasoline compositions between the HYSYS® model and Chekantsev et al. (2014) model was ranged from 5% to 20% (Appendix C). This variation on the results can be explained as the HYSYS® model implements only the first order reaction, while advanced reaction expressions were used in Chekantsev et al. (2014) study.
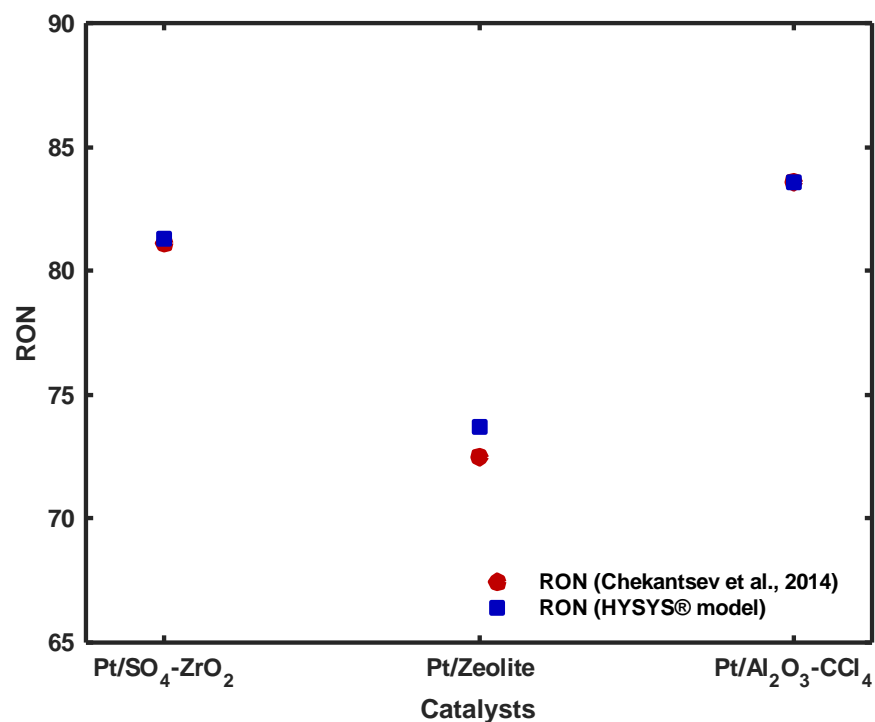
Figure 4-16 comparison between Chekantesev et al., 2014 model and HYSYS® model

4.4.1.1 The effect of inlet reactor temperature on the gasoline RON

Figure 4-17 illustrates the RON is gradually increased along with temperature for the three catalysts. The curve trend remains almost unchanged at 87.5 RON for Pt/Al$_2$O$_3$-CCl$_4$. The trend continue increasing until RON of 86 for Pt/SO$_4$-ZrO$_2$ catalyst. The trend continue increasing to reach a peak of 84.2 RON at temperature of 280 °C for Pt/zeolite catalyst and then slightly decreases, probably because of the thermal cracking. The general RON trends agreed with earlier studies (Said et al., 2014, Hancsók et al., 2020, Aitani et al., 2019). However, these studies used two reactors the scale of increasing the RON was smaller on each reactor which was (84-84.15). Moreover, their experimental works were considered almost 50% of the feed composition is nC5, while this study assumed the nC5 is 30% of the feed. The difference of nC5 content in the feed affected on the iC5 content in the gasoline and the RON.
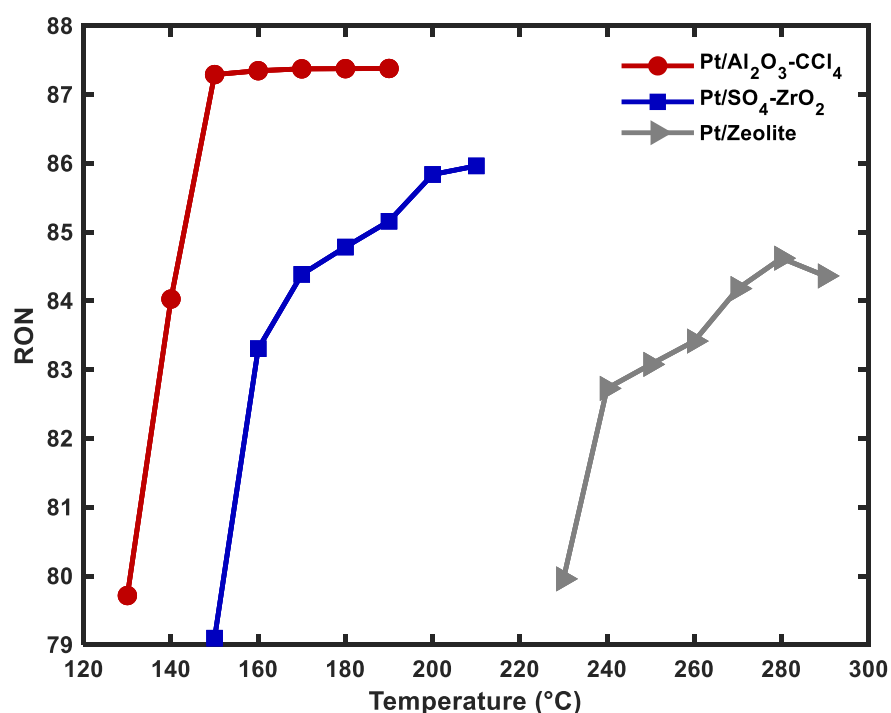
Figure 4-17 The effect of the temprature on catalysts activity.

4.4.1.2 Hydrogen recycle/purge vs compressor power

Figure 4-18 presents the effect of altering the hydrogen recycle ratio on the compressor power (kW) and the amount of hydrogen purge. As the recycle ratio increases results the power of the compressor increases, and the purge rate decreases. This was done for importance of the hydrogen on the economic assessment.
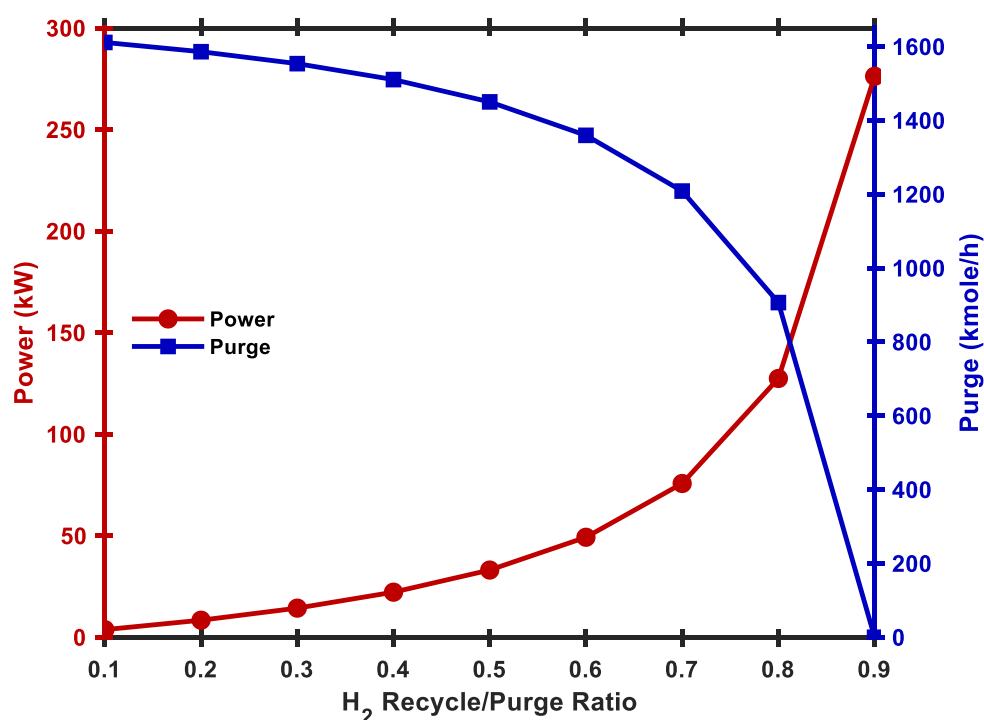
Figure 4-18 The effect of hydrogen recycle ratio on the compressor power and the purge amount

4.4.2 Backend flowsheet model results

This section outlines outcomes from simulated moving bed (SMB) and distillation column (DIS), the vapour recompression heat pump (VRC), the bottom flashing heat pump (BF) and the absorption heat pump (AHP).

103

4.4.2.1 Eight simulated moving bed results

To validate the SMB model, it must be compared to published studies. The closet investigation Adsim® model was made by Bárcia et al. (2010a). Their study was based on a lab scaled adrorption fixed bed, which is oparated at overall presure of 9.7 kPa and varios tempreures of 423 K, 473 K and 523 K (Bárcia et al., 2010a). Therefore, this thesis downscaled the SMB process to be operated similarly to Bárcia et al. (2010a) fixed bed. The combarison of loading and breakthrough curves between the devaloped MATLAB® model and Bárcia et al. (2010a) fixed bed model is discussed as follows.

4.4.2.1.1 Adsorbent loading curve results

Figure 4-19, Figure 4-20 and Figure 4-21 present adsorbent loading against the partial pressure for six components at 423 K, 473 K and 523 K, respectively. Overall, the loading capacity increased gradually as the pressure increased and decreased as the temperature increased, which depended on isothermal bonds between the components and the zeolite beta. For temperature of 423 K and 473 K, the order of components loading in zeolite beta is nC6> 3MC5> 23DMB>2DMB>nC5>iC5, which depends on the filling of adsorbent sites. However, as increasing the temperature changes the adsorption capacity, the order was changed to nC6> 3MC5> 23DMB>2DMB>iC5>nC5 at temperature of 523 K.

The comparison between the developed MATLAB® model and Bárcia et al. (2010a) model was based on the curve regression method. Curve regressions were determined and the coefficient of determination (R^2) was found to be greater than 0.95 for each curve. The coefficient of

determination (R^2) varies from 0 to 1, which represent the worst and the best data-line fitting, respectively. This results fitted perfectly with the results made by Bárcia et al. (2010a).
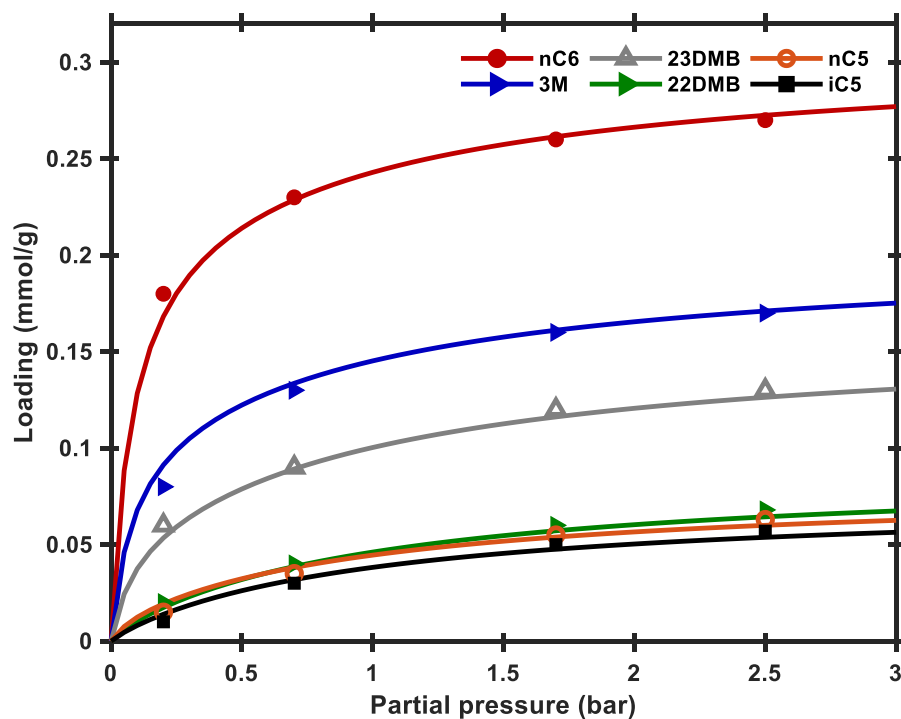
Figure 4-19 Comparison of equilibrium data on zeolite beta between MATLAB® model (line) and Bárcia et al. (2010a) model (symbols) at T=423K
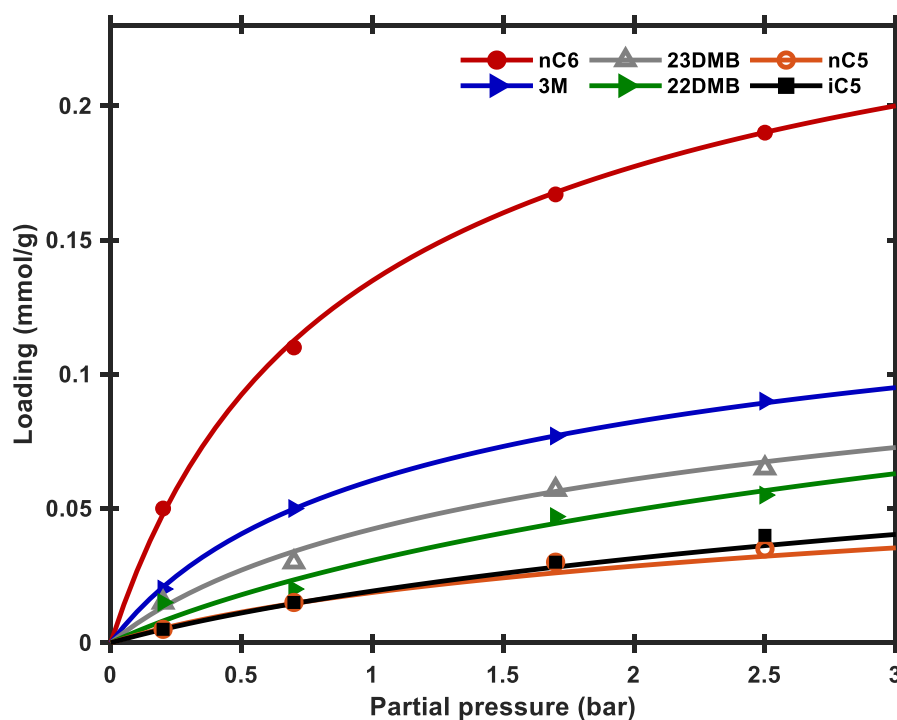
Figure 4-20 Comparison of equilibrium data on zeolite beta between MATLAB® model (line) and Bárcia et al. (2010a) model (symbols) at T=473K
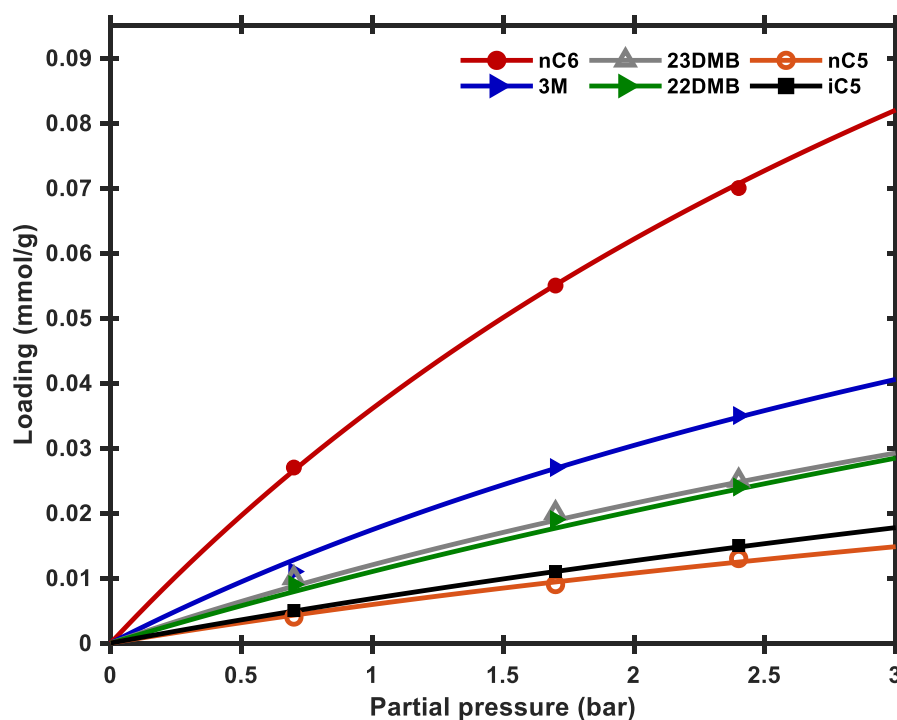
Figure 4-21 Comparison of equilibrium data on zeolite beta between MATLAB® model (line) and Bárcia et al. (2010a) model (symbols) at T=523K

4.4.2.1.2 Breakthrough curve results

Figure 4-22, Figure 4-23 and Figure 4-24 present breakthrough curves for the 6 components, which are generated at 423 K, 473 K and 523 K and at total of pressure 9.8 kPa. The overshoots mean the component elutes first from the column in this order iC5<22DMB<nC5<23DMB< 3M< nC6. Increasing the temperature decreased the breakthrough durations and decreased the elution of nC5, which increases the overall RON. Therefore, higher temperature may suggest better separation performance.

Overall, the breakthrough curves of the developed MATLAB® model show a good agreement with Bárcia et al. (2010a) model. The coefficient of determination (R^2) was found to be greater than 0.9 for each curve. However, normal hexane reached saturation points faster than Bárcia et al. (2010a) and the deviation worsen (R^2=0.83) when increasing the operating temperature. This discrepancy could be attributed to assuming the isothermal method and neglecting the temperature term in conservation equations.
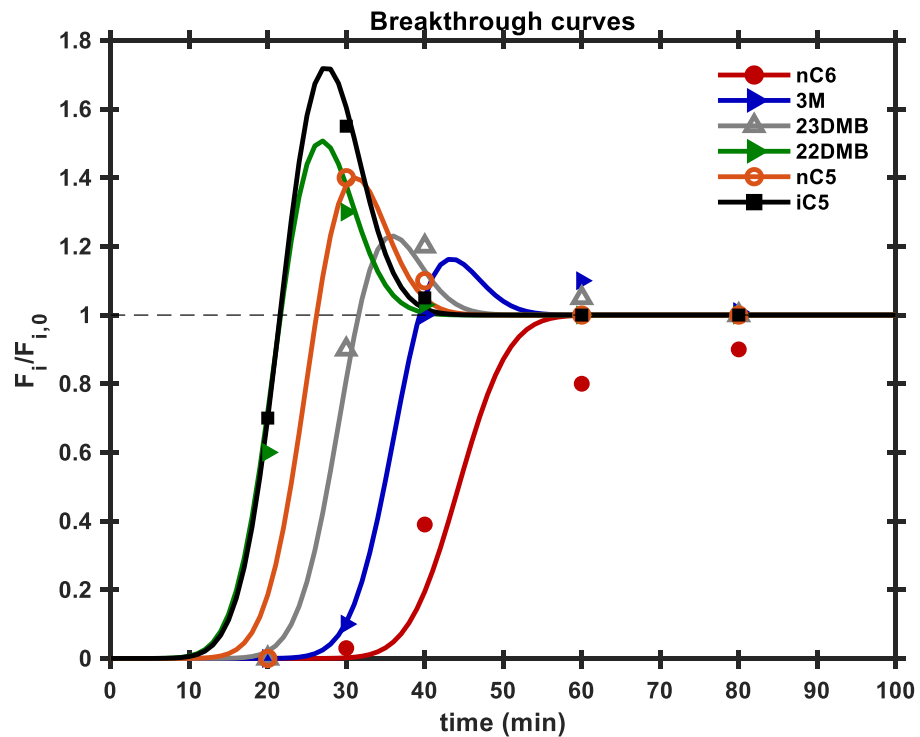
Figure 4-22 Comparison of breakthrough curves between MATLAB® model (line) and Bárcia et al., 2010a model (symbols) at T=423K
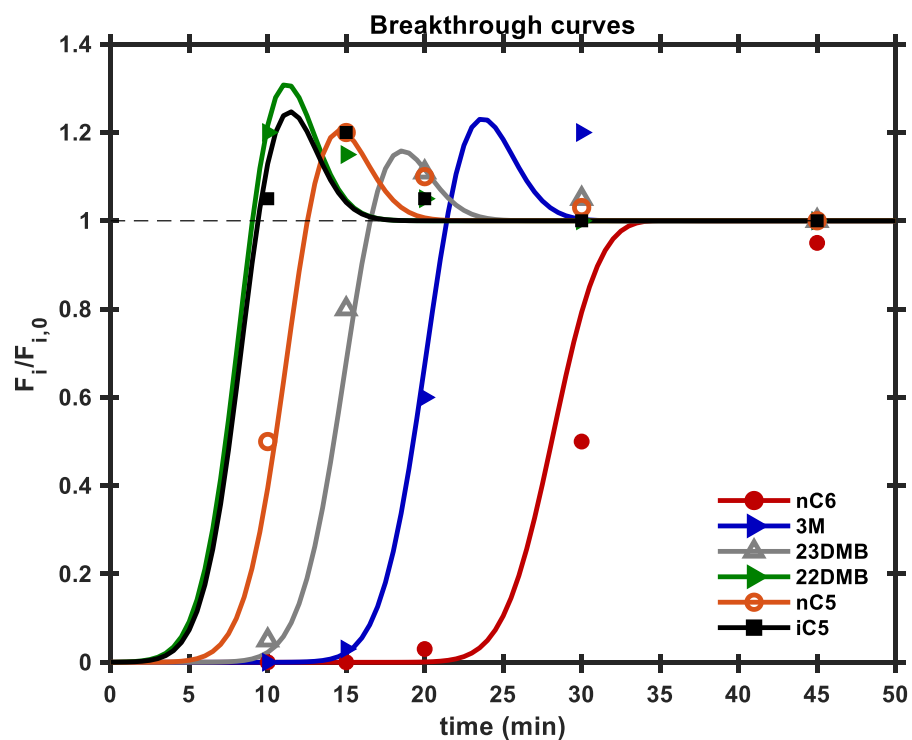
Figure 4-23 Comparison of breakthrough curves between MATLAB® model (line) and Bárcia et al., 2010a model (symbols) at T= 473 K
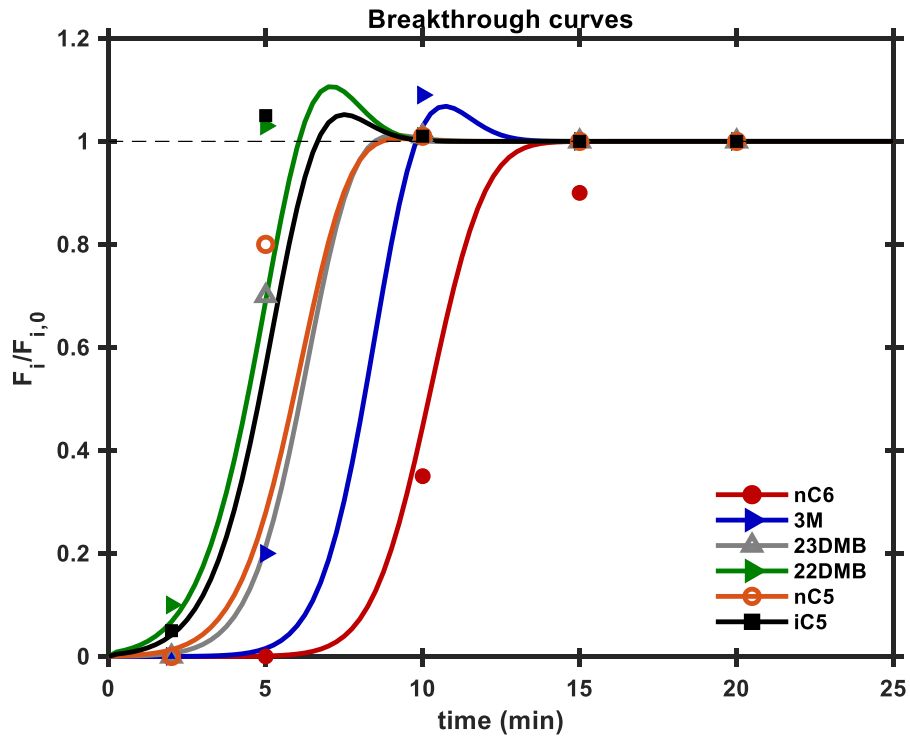
Figure 4-24 Comparison of breakthrough curves between MATLAB® model (line) and Bárcia et al., 2010a model (symbols) at T= 523 K

4.4.2.1.3 Scaled up simulated moving bed

The SMB reached the steady state after 20 cycles (Figure 4-25). Each bed was operated for 7 minutes at temperature 523 K, which means the process consumes about 2.5 hours to reach the steady state and start up. The iC5 concentration in the raffinate and extract streams are about 0.38 kmol/m^3 and 0.05 kmol/m^3, respectively. The nC5 concentration in the raffinate and extract streams are about 0.02 kmol/m^3 and 0.32 kmol/m^3, respectively. Also, the raffinate zone has 92.2 RON, which will be sent to gasoline pool and extract outlets with 62.5 RON to be recycled to an isomerization reactor. Figure 4-26 shows detailed material outlets from the SMB after 20 cycles. Initial assumption can be improved or increased the number of indices to more than 10 to improve the quality.
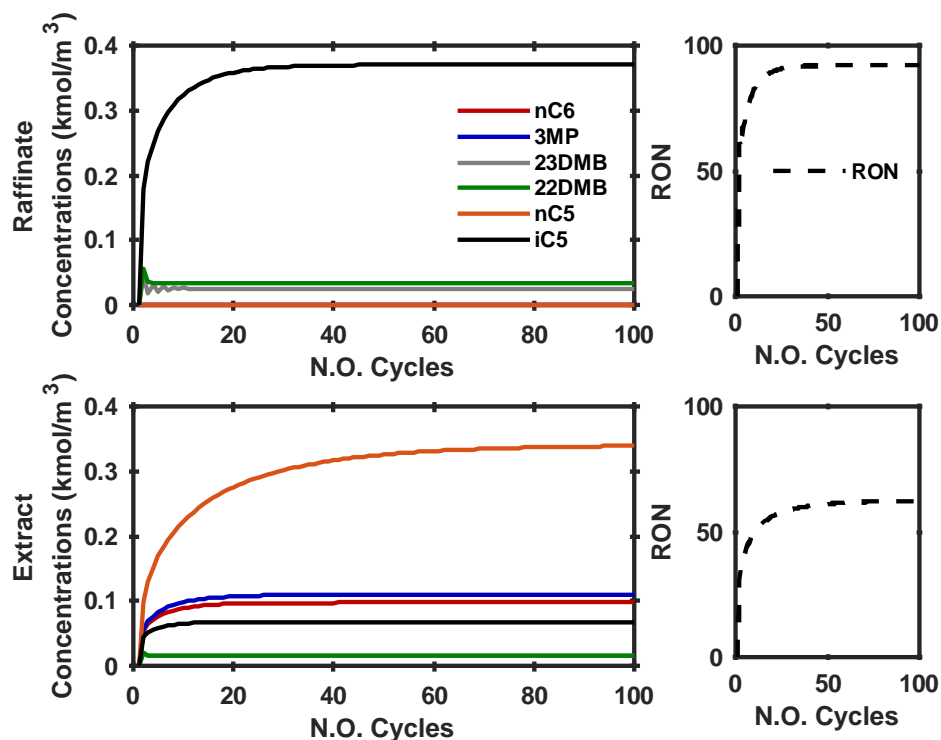
Figure 4-25 Raffinate and extract profile vs concentrations (top) and RON (bottom) for each cycle

Feed

F: 100 kmol/h
T: 523 °K
P: 15 bar
nC6   : 0.08
3MC5   : 0.09
23DMC4: 0.04
22DMC4: 0.05
nC5   : 0.28
iC5   : 0.46
RON   : 76.5

Raffinate

F: 47.0 kmol/h
T: 523 °K
P: 15 bar
nC6   : 0.00
3MC5   : 0.00
23DMC4: 0.06
22DMC4: 0.08
nC5   : 0.00
iC5   : 0.86
RON   : 92.2

Extract

F: 83.0 kmol/h
T: 523 °K
P: 5 bar
H_2 : 0.36
nC6   : 0.10
3MC5   : 0.11
23DMC4: 0.01
22DMC4: 0.01
nC5   : 0.34
iC5   : 0.07
RON   : 62.5

Desorbet

F: 30.0 kmol/h
T: 523 °K
P: 5 bar
H_2 : 1.00
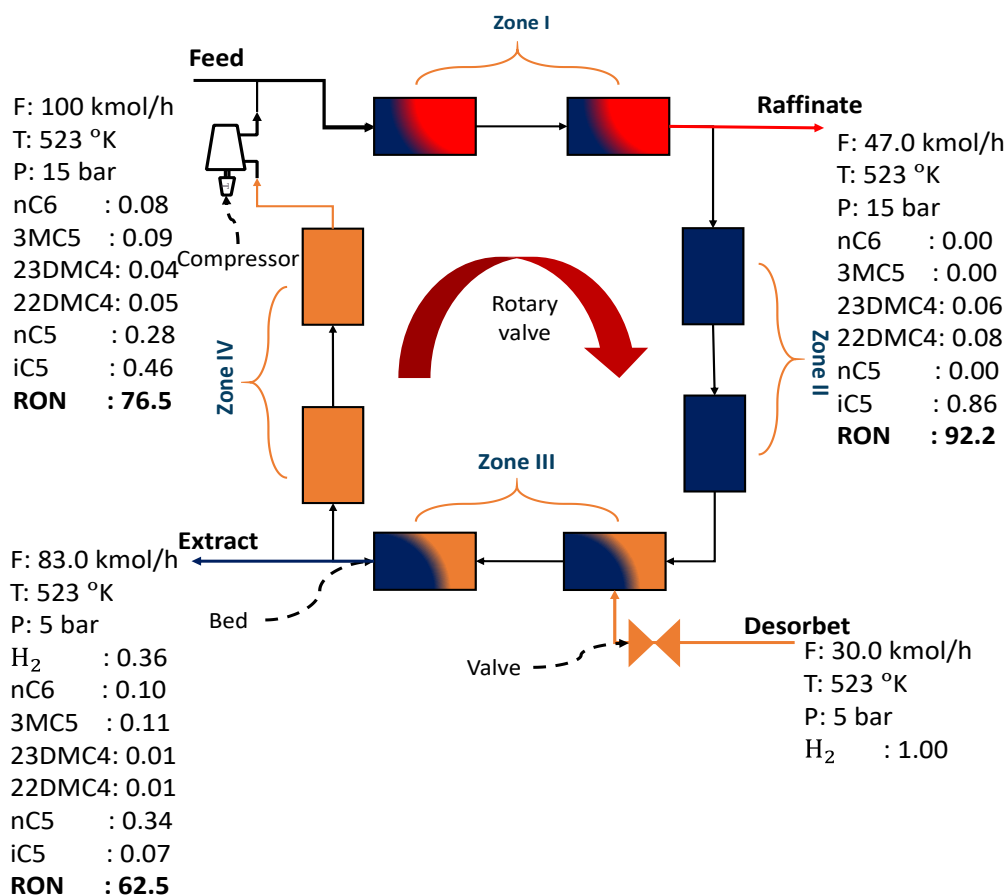
Figure 4-26 Mass balance

4.4.2.1.4 Desorbent to feed ratio analysis

The desorbent to feed (D/F) ratio was investigated against high octane components recovery and purity of the iso components for an 8-bed pressure swing adsorption system. The recovery and purity were calculated by using Equation (4-19) and Equation (4-20), respectively (Bárcia et al., 2010b).

$$\text{Recovery of the iso(molar basis)} \qquad\qquad (4\text{-}19)$$
$$= \frac{amount\ of\ the\ \text{isomers withdrawn in production step}}{amount\ of\ the\ \text{isomers fed}}$$

$$\text{Purity of the iso(molar basis)} \qquad\qquad (4\text{-}20)$$
$$= \frac{amount\ of\ the\ \text{isomers withdrawn in production step}}{aamount\ of\ the\ \text{paraffins withdrawn in production step}}$$

The results on Figure 4-27 shows that the optimal point is at D/F ratio about 0.3 and the purity and recovery are 99.9% and 86.8%, respectively. The key point that should be emphasized is that an appropriate D/F ratio is affected by the type of components and pressure ranges. Moreover, the RON varies between 92.2 and 93.2. Thus, the 8-bed simulated moving bed system is more effective and efficient than industrial competence.

4.4.2.1.5 Adsorption pressure analysis

In the current research, high pressure analysis was curried out to measure the compressor power consumption against the quality and recovery. Figure 4-28 presents the effect of altering adsorption pressure on recovery and purity, and power consumption. The adsorption pressure target, in this thesis, was 11 to 19 bar. During this period the

purity increases to 94% and the recovery decreases to 99%. Moreover, the power increases gradually from 100 kWh to 400 kWh.
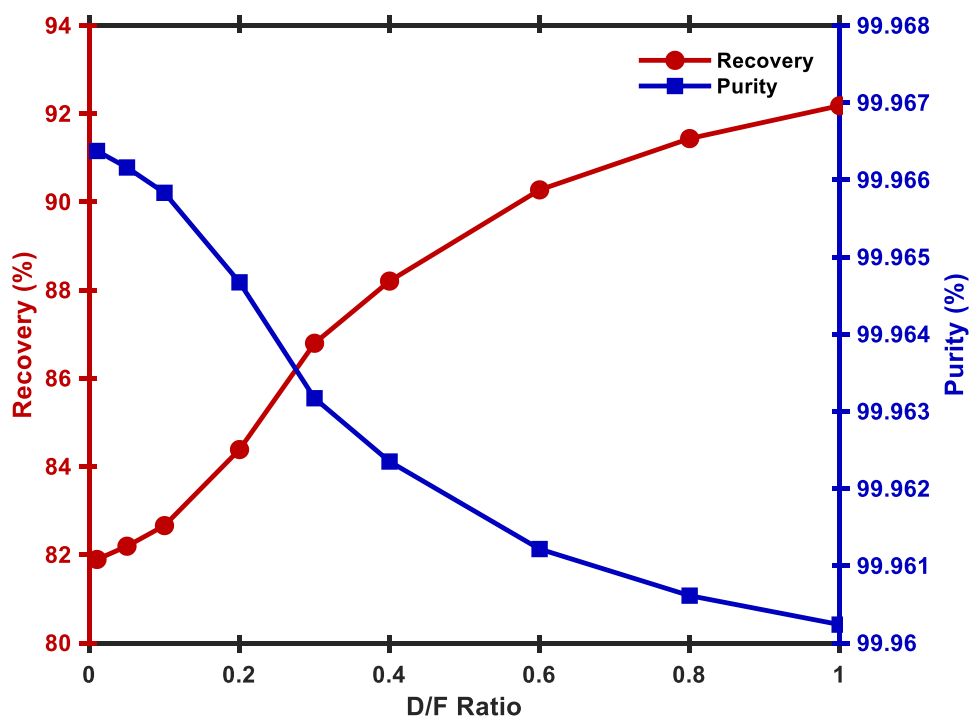
Figure 4-27 Desorbent/Feed ratio of High octane components

4.4.2.2 Distillation column and Energy efficient distillations results

Table 4-9 compares consumed energies by condenser, reboiler and compressor, when using DIS and efficient energy distillations: VRC, BF and AHP. The VRC and the BF eliminated the energy used for the condenser and reboiler, while the VRC and BF increased the compressor power by up to 5500 kW and 5700 kW, respectively. The condenser and reboiler energies of the AHP consumed up to 15% heating and 2% cooling utilities of the DIS column. These results suggest that the AHP was the most energetic option compared to the VRC and the BF. This is the exact observations made by Fonyo and Benko (1996) and Díez et al. (2009) who preferred the AHB over the VRC and the BF for large temperature difference systems. The temperature difference for

this study was 86.9 °C, where the AHB is more suitable than the VRC and the BF.
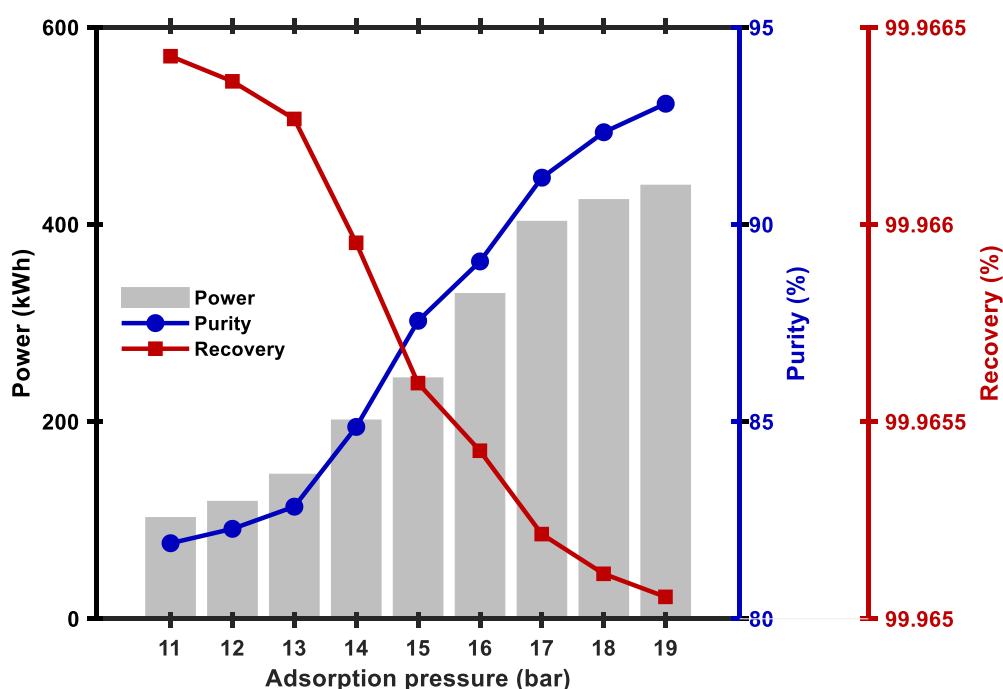
Figure 4-28 The effect of altering adsorption pressure on purity and recovery

Table 4-9 Power consumption comparison

Energy (kW)	DIS	VRC	BF	AHP
Condenser	15,000	--	--	320
Reboiler	16,000	--	--	2400
Compressor	--	5500	5700	24

4.4.3 Hybrid superstructure simulation results

After linking HYSYS®-MATLAB® to have the full flowsheet, the gasoline RON comparison between none recycled normal pentane and recycled normal pentane was made and shown in Table 4-10. Recirculate the normal pentane increases the RON between 1 to 11 points which depends on catalyst and separation selections.

Table 4-10 Gasoline RON with and without recycle

		Pt/Al$_2$O$_3$-CCl$_4$	Pt/SO$_4$–ZrO$_2$	Pt/zeolite
RON Without recycle	Base case	88	86	84
	Distillations group	89	87	86
	SMB	93	93	92
		Pt/Al$_2$O$_3$-CCl$_4$	Pt/SO$_4$–ZrO$_2$	Pt/zeolite
RON With recycle	Base case	--	--	--
	Distillations group	91	89	87
	SMB	95	95	93

4.5 Conclusion

This study has shown that HYSYS® can represent the frontend process flowsheet. After analysing the base case model, we found that the inlet reactor temperature was affecting on the RON and catalyst activity. Also, hydrogen recycle ratio has significantly influenced the compressor consumed power. However, 5% to 20% error of the gasoline compositions was reported. The simple reactions set assumed in the study can be a reason of this. Moreover, the calculation of the process simulation may not really present the actual system because it is based on parameter estimated by HYSYS®.

Traditionally, field-scale simulations cannot be performed directly using the thermodynamic and kinetic parameters obtained from experimental-scale models. Moreover, although the gas at operation conditions of 423-523 K and 5-15 bar is compressed gas (Z factor) = 0.94-0.84 (calculated

using HYSYS®), it was assumed to behave as an ideal gas. However, gasoline RON enhancement using the SMB through volume upscaling construct the next conclusion. The SMB increased the RON by up to 95, which is 11 points better than the base case. Moreover, the SMB consumed less energy compared to heat efficient distillation processes. The desorbent to feed (D/F) ratio analysis showed that maximum 99.9% purity and 92% recovery were achieved at ratios of I and 0, respectively. The maximum purity of 94% was obtained at high pressure of 19 bar with energy consumption of 400 kW, while maximum recovery of 99% was obtained at high pressure of 11 bar with energy consumption of 100 kW.

For large temperature system (ΔT= 86.9 ℃), the AHB was performed better than the VRC and the BF by consuming up to 15% heating and 2% cooling utilities of the DIS column consumption. From the superstructure process hybrid platform, the maximum tolerance for the convergence was 0.02%, which was achieved after running the "while" loop for 3-5 times, which can be a limitation of the platform. The gasoline RON can be increased up to 11 points when following Pt/Al$_2$O$_3$-CCl$_4$ and SMB flowsheet route. Thus, embedding the SMB to the isomerization process flowsheet in HYSYS® and the trade-off between capital and operating costs are explicated to associate the process performance in Chapter 5

Chapter 5   Techno-economic analysis

5.1 Introduction

The techno-economic analysis of the isomerization superstructure process is detailed in this chapter in order to build the objective function (Chapter 3). The HYSYS® spreadsheet was used host the economic calculations and analysis, and the objective function. The estimation methods and factors of total capital cost (CAPEX) and operating expenditures (OPEX) are addressed. In addition, the economic analysis method, namely, the net present value (NPV), and results are discussed in this chapter.

5.2 Estimation of total capital costs (CAPEX)

Five main methods estimate the total capital cost: order of magnitude estimate, study estimate, preliminary estimate, definitive estimate, and detailed estimate (Table 5-1). Table 5-1 shows the accuracy, the speed to be obtained, and the purpose of each method. As this thesis focus on the preliminary design of the chemical process, the "study estimate" method was applied. The method is based on the overall factor method of Lang (1947 a, b and 1948), which multiplies the predicted costs of equipment by overall factors. Moreover, the method requires full knowledge of the process design, compressing mass and energy balance, equipment sizing and equipment construction materials (Pikulik and HE, 1977). To apply the "study estimate" method, more time is considered compared to the order of magnitude estimate. However, a higher accuracy (up to ±30%) is obtained (Peters and Timmerhaus, 1991).

Table 5-1 Categories of total capital cost estimates (Perry and Green, 1999, Peters and Timmerhaus, 1991, Pikulik and HE, 1977)

Estimate	Based on	Error%	Obtain	Used
Order of magnitude (Ratio estimate)	Method of Hill, 1956. Production rate and PFD with compressors, reactors and separation equipment. Based on similar plants	40-50	Very fast	Profitability analysis
Study	Overall Factor Method of Lang, 1947. Mass & energy balance and equipment sizing.	25-40	Fast	Preliminary design
Preliminary	Individual Factors Method of Guthrie, 1969, 1974. Mass & energy balance, equipment sizing, construction materials and P&ID. Enough data to budget estimation.	15-25	Medium	Budget approval
Definitive	Full data but before drawings and specifications.	10-15	Slow	Construction control
Detailed	Detailed Engineering	5-10	Very slow	Turnkey contract

Using thermodynamic and equipment sizing results from Chapter 4, the economic model (based on the "study estimate" method) was developed to evaluate the equipment cost as follows. The presentations of the base cost (C_B) of each equipment are estimated in the form of graphs or equations (Seider et al., 2017). Graphs present the effect of size factors on the cost estimation easy to catch. Size factors (e.g. pressure factor and temperature factor) affect the equipment size and alter the equipment cost. However, equations are more consistent and suitable

for computational models (Seider et al., 2017). The equipment cost equations for the thesis are available in Appendix E.

Generally, each equipment follows Equation (5-1) to estimate its purchase cost (C_p) (Seider et al., 2019).

$$C_P = C_B * F_P * F_T * F_i * F_M * F_L \qquad \text{(5-1)}$$

where is F_p is the pressure factor, F_T is the temperature level factor, F_i is the installation factor, F_M is the material factor and F_L is the length tube correction factor (Seider et al., 2019).

After obtaining these costs, purchase costs are then allocated (location factor =1 for US gulf coast) and objectified to the design year $C_{P,y}$ by using Equation (5-2) (Seider et al., 2019).

$$C_{P,y} = C_{P,b} * \frac{I_y}{I_b} \qquad \text{(5-2)}$$

where $C_{P,b}$ is the purchase cost at base year, I_y is the cost index at the design year and I_b is the cost index at the base year.

In the current study, the design year and based year were 2018 and 2014, respectively. Nelson-Farrar cost index is the most stable index for petroleum processes for economic estimation (Oil & Gas, 2018). The NF cost indices for years 2018 and 2014 are equal to 2690 and 2555, respectively (Kaiser et al., 2019).

5.3 Operating cost (OPEX)

The operating expenditure (OPEX) is the sum of fixed operating cost (FC) and variable operating cost (VC). OPEX is calculated as follows.

5.3.1 Fixed operating costs (FC)

The fixed operating cost is calculated per year throughout the plant time life. FC factors are shown in Table 5-2. These factors were adapted from Seider et al. (2017).

Table 5-2 Fixed operating cost factors

Costing factor	Calculation
Operators per shift	1 (5 shifts)
Direct wages and benefits	$40/ operator hour
Direct salaries and benefits	15% of direct wages and benefits
Operating supplies and services	6% of direct wages and benefits
Technical assistance of manufacturing	$6*10^7$ per year, for each operator per shift
Control laboratory	$6.50*10^7$ per year, for each operator per shift
Wages and benefits	3.5% of total depreciable capital
Salaries and benefits	25% of maintenance wages and benefits
Materials and services	100% of maintenance wages and benefits
Maintenance overhead	5% of maintenance wages and benefits
Operating overhead	22.8% of maintenance and operation wages and benefit
Property taxes and insurance	2% of total depreciable capital

5.3.2 Variable operating cost (VC)

The Variable operating cost (VC) calculations, including the cost of raw materials, utilities, catalysts and adsorbent, are described as follows.

5.3.2.1 Raw materials and Utilities costs

Raw materials and utilities costs are listed on Table 5-3. The medium pressure stream and the cooling water are maintained at pressure of 2.4 bar, 0.4 bar and temperature of 210 °C and 6 ºC, respectively (Turton et al., 2009).

Table 5-3 Cost of the process raw materials

Chemicals	Specification	Price	Ref.
Light naphtha ($/kg)		0.628	(Mohamed et al., 2017)
Hydrogen ($/kg)	90% mole	3.6	(Mohamed et al., 2017)
Utilities			
Electricity ($/kW)		0.06	(Turton et al., 2009)
MP stream ($/GJ)	10 bar 184 °C	14.2	(Turton et al., 2009)
Cooling Water ($/1000 kg)	30 °C	0.067	(Turton et al., 2009)

5.3.2.2 Catalyst and adsorbent regeneration

The costs of Pt/Al_2O_3, $Pt/SO_4–ZrO_2$, Pt/zeolite catalysts and zeolite beta adsorbent are 160, 80, 70 and 60 ($/kg), respectively (Zauba Technologies & Data, 2013, Brownel, 2017). The lifetime of these catalysts and the adsorbent are assumed to be 3, 4, 5 and 5 years for Pt/Al_2O_3, $Pt/SO_4–ZrO_2$, Pt/zeolite catalysts, and zeolite beta adsorbent,

respectively (Gary et al., 2007). This means Pt/Al$_2$O$_3$, Pt/SO$_4$–ZrO$_2$, Pt/zeolite catalysts and zeolite beta adsorbent were regenerated for 6, 5, 4 and 4 times during the 20 years of the plant lifetime. Therefore, to maintain the economic stability of the process, the regeneration costs per annual are calculated by using Equation (5-3) (Seider et al., 2017).

$$\frac{A}{P} = \frac{i * (1 + i)^n}{(1 + i)^n - 1} \tag{5-3}$$

where A is the payment per interest period, P is the present worth, i is the interest rate of the catalyst/adsorbent (15%), and n is the number of interest years. The number of interest years is equal to 3,4 or 5 years, which is dependent on catalyst/adsorbent used.

5.3.2.3 Gasoline prices (sales)

Gasoline prices depend on its RON. Mohamed et al. (2017) reported various gasoline RON and their prices ($/gallon), as shown in Table 5-4. In this thesis, Figure 5-1 shows the data linearization into a formula of Equation (5-4). The equation is then applied into HYSYS® spread-sheet for economical calculations.

Table 5-4 Gasoline prices regarding the RON (Mohamed et al., 2017)

Gasoline RON	81	82.4	84.5	85.1	86.74	87.35	90.8	92.3
Price ($/gallon)	2.06	2.17	2.33	2.37	2.49	2.54	2.8	2.91
Price ($/m^3)	550	570	620	630	660	670	740	770
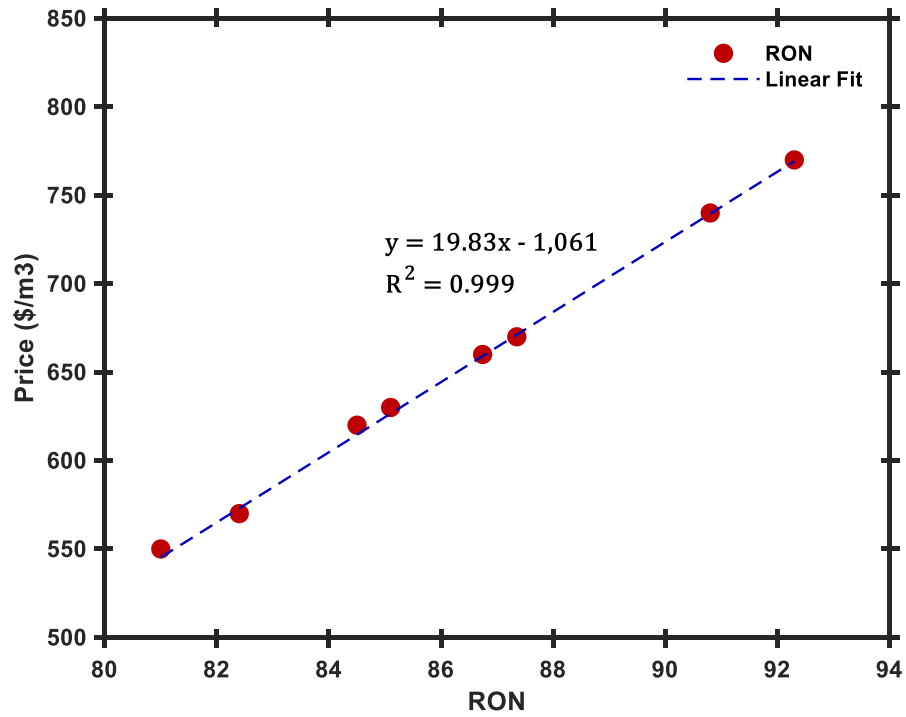
Figure 5-1 Gasoline price vs RON

$$\text{Gasoline price} \left(\frac{\$}{m^3}\right) = 19.8 * \text{RON} - 1{,}061 \qquad (5\text{-}4)$$

5.4 Economic analysis

There are several methods to evaluate and compare the economic feasibility of alternative processes such as net present value (NPV), payback period and internal rate of return (IRR) (Peters and Timmerhaus, 1991). As NPV is well defined and simpler to apply computationally (Seider et al., 2017), it was used in this study. NPV is calculated by using Equation 5-5, which was taken from Seider et al. (2017).

$$NPV = \sum_t \frac{Net\ profit_t}{(1+i)^t} - \frac{Working\ capital\ investment}{(1+i)^n} - \frac{Total\ capital}{investment} \qquad (5\text{-}5)$$

where i is the interest rate and n is the plant-life time.

Net profit calculations involve depreciation, taxel income and taxes. Other capital cost such as site preparation, service facilities, contingencies and constructor fees, land, and plant start-up costs are also considered for the estimation of the total capital investment (TCI). Working capital investment was assumed to be 15% of the TCI. The calculations are detailed in Appendix F

Table 5-5 Total capital investment (TCI)

Total Permanent investment	Calculation
Depreciation	7 years
Cost of site preparation	5% of total equipment cost
Cost of service facilities	5% of total equipment cost
Cost of contingencies and constructor fees	18%5% of total cost of site preparation and service facilities
Cost of land	2% of total depreciable capital
Cost of plant start-up	10% of total depreciable capital

5.5 Results and discussion

The economic model was based on plant capacity of 10,000 BPD gasoline production. Plant annual operating hours was set at 8000 h/y (330 days/y). The plant lifetime (n) was assumed to be 20 years with an interest rate (i) of 15%. The operating conditions for the based case study (isomerization process) is shown in

Table 5-6.

Table 5-6 presents the value of hydrogen/purge ratio, and reactor inlet temperature (notation 1: Pt/Al_2O_3, 2: $Pt/SO_4–ZrO_2$, and 3: Pt/zeolite).

These conditions were constants for the five separations, including SMB, DIS, AHP, VRC and BF.

Table 5-6 List of oprating conditions for the base case study

Variables	Value
Hydrogen/purge ratio	0.5
Reactor 1 inlet temperature (°C)	120
Reactor 2 inlet temperature (°C)	130
Reactor 3 inlet temperature (°C)	220

5.5.1 Capital cost estimation (CAPEX)

The capital expenses of the 15th pathways of the gasoline production via the light naphtha isomerization process was estimated by using the "study estimate" method (Figure 5-2). In addition, the operating cost calculation was based on data given in Section 5.3 (Figure 5-3).
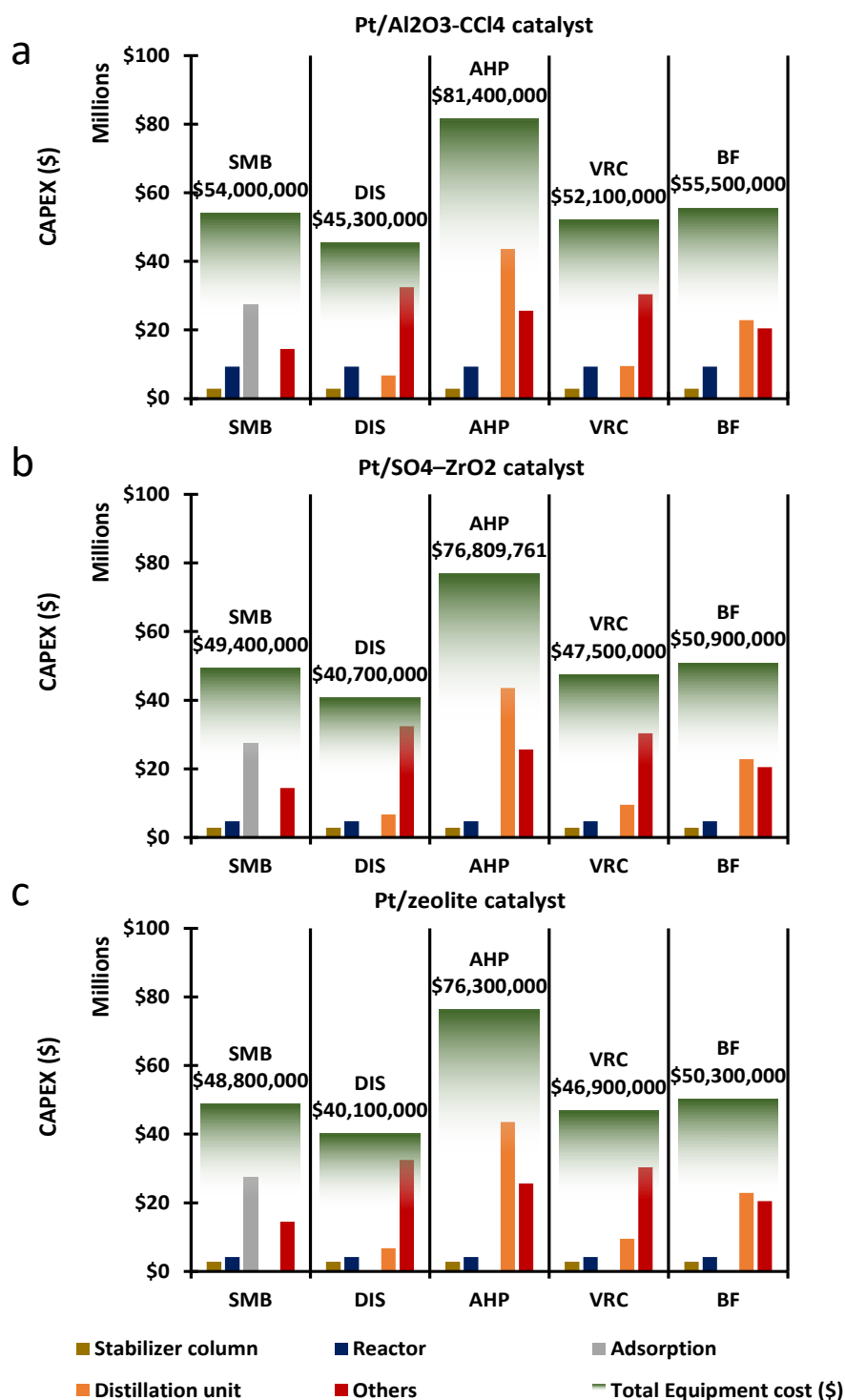
Figure 5-2 The effect of using different catalysts on the process total capital cost (CAPEX), considering different separation technologies. Note: SMB=simulated moving bed, DIS=distillation column, AHP=absorbent heat pump, VRC=vapor recompression column, BF=bottom flashing column

Figure 5-2 presents the total capital cost and main equipment costs for

the isomerization process, considering three catalysts and five

separation technologies. For the three catalysts, i.e. Pt/Al_2O_3-CCl_4, Pt/SO_4–ZrO_2 and Pt/zeolite (overlapping bars), the highest CAPEX was obtained at ~$78 million when combining with the AHP. This was followed by the BF, SMB and VRC at the range of $55-40 million, while the lowest (~$43 million) was achieved for using the DIS.

Figure 5-2 (a) presents the equipment cost of stabilizer column and reactor were fixed at $3 million and $10 million, respectively, throughout different separation options. However, the costs of adsorption, distillation unit (i.e. DIS, AHP, VRC and BF) and others (i.e. air cooler, heat exchangers, flash drum, pumps, and compressors) were varied, depending on the separation technologies. As the adsorption was only applied for the SMB, its cost was $27 million and cost zero in other technologies. DIS, AHP, VRC and BF cost were $7, 44, 10 and 23 million, respectively. The design of separation units influenced the cost of "others", which was varied between $15 million and $33 million.

Discussing Figure 5-2 (a), comparing to SMB, DIS, VRC and BF, the design of the AHP was required extra equipment to be installed, which is resulted in increasing the total capital cost. For DIS, VRC and BF, the total capital cost was subjected to the column accessories (e.g. Heat exchangers and compressors) sizes. For the Pt/Al_2O_3-CCl_4 -DIS process (Figure 5-2 (a)), the CAPEX was $45 million, which is a finding that has also been reported by Mohamed et al. (2017) after excluding their other capital costs such as Instrument, control cost, electrical requirements, piping, erection, utilities connections, off site preparation, civil work, equipment transportation and installation costs. While the other scenarios have not previously been described.

The same trend can be seen in Figure 5-2 (b) and (c), with a total subtraction of $0.6 million and $1.2 million, respectively, for each separation option. This discrepancy could be attributed to consider the cost of other catalysts into account. The most expensive process was detected for AHP process, while the DIS process was the cheapest to produce gasoline from the light naphtha isomerization process. SMB, VRC and BF processes were remained at the middle.
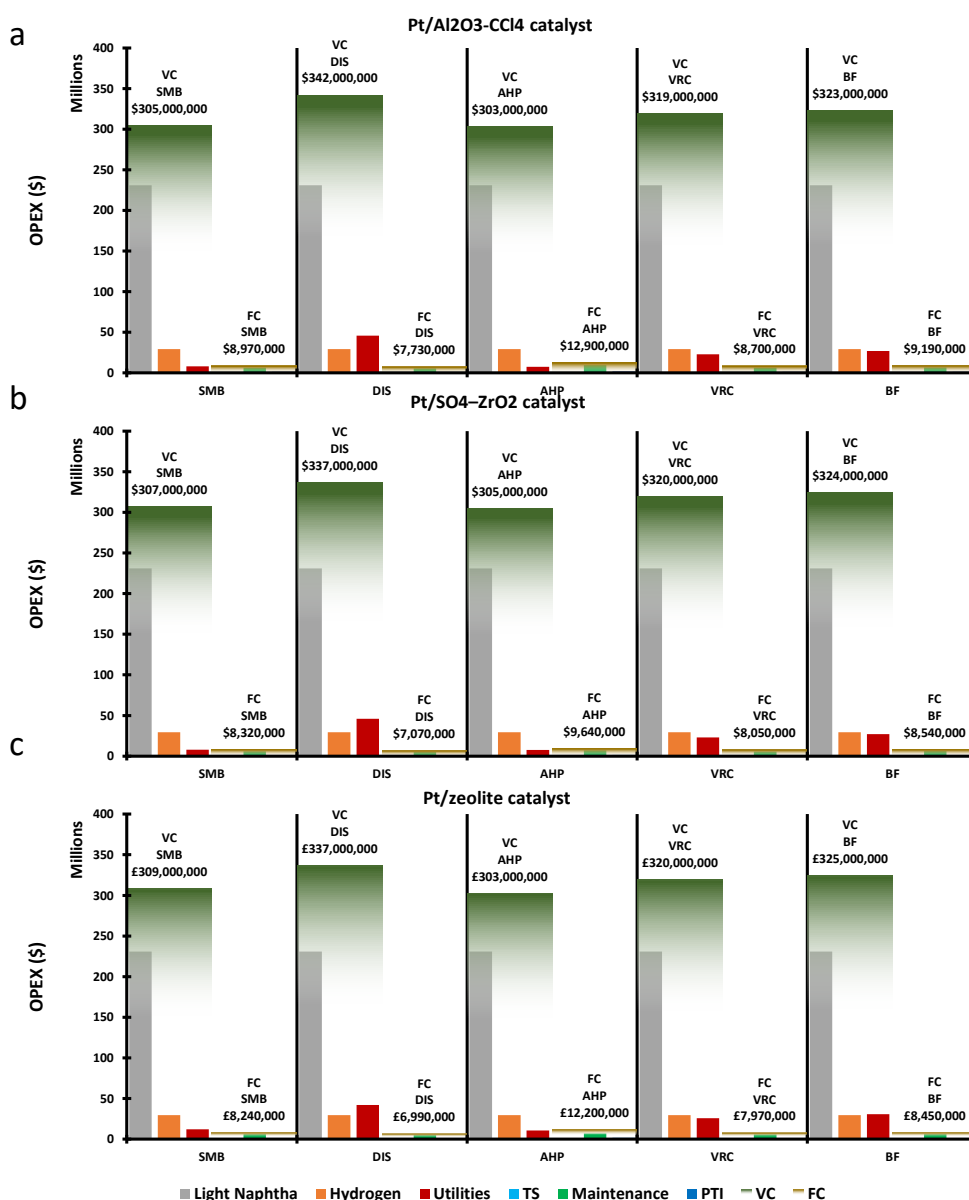
Figure 5-3 The effect of using different catalysts on the process total operating cost (OPEX), considering different separation technologies. Note: TS = Total salaries, PTI = Property taxes and insurance, VC=variable operating cost, FC=fixed operating cost

5.5.2 Operating cost (OPEX)

Figure 5-3 presents the total operating cost (OPEX) for the process, considering three catalysts and five separation technologies. The fixed operating cost (FC) represents 2-4% ($7-13 million) of the OPEX. Using the DIS increased spending of the OPEX to $345 million for all catalyst, while the spending on SMB and AHP were $314 million and $315 million, respectively. Further ~$330 million spending was on VRC and BF process. Almost 70% of the OPEX spending was on the light naphtha, which were remained constant at $230 million throughout processes. This finding was also reported by Mohamed et al. (2017), who investigated on the combination of Pt/Al_2O_3-CCl_4 with DIS for the isomerization process. Hydrogen cost was fixed at $30 million for all process. However, the cost of utilities, namely, medium pressure steam, cooling water, electricity, catalyst and adsorbent, were dependent on each catalyst and separation method.

In term of catalyst, Pt/Zeolite is the cheapest catalyst, however, it consumes a considerable amount of steam, as the catalyst activation temperature is > 220 °C. However, Pt/Al_2O_3-CCl_4 has the highest catalyst expenditure, however, it consumes less energy due to the catalyst activates at temperature < 180 °C. The intermediate performance was practised by Pt/SO_4–ZrO_2 catalyst.

As SMB and AHP were consumed less utilities, the utility costs was dominated by the energy required by the catalyst. The utility costs for SMB process were $8 million, $10 million and $12 million for Pt/Al_2O_3-CCl_4, Pt/SO_4–ZrO_2 and Pt/Zeolite, respectively. The utility one million

dollar lower when using AHP. However, DIS process was demanded more of heating energy, which manipulated the utility cost. The utility costs for Pt/SO$_4$–ZrO$_2$ was \$41 million. Additional spending of \$5 million and \$1 million was detected when using Pt/Al$_2$O$_3$-CCl$_4$ and Pt/Zeolite, respectively. There are no significant changes on the utilities cost when integrating each catalyst with either VRC (\$25 million) or BF (\$30 million). The highest operating expenditure was detected for DIS process, while AHP and SMB achieved the lowest. VRC and BF processes were indicated an intermediate spending.

5.5.3 The net present value (NPV)

The NPV was calculated for the process using three catalysts and five separation approaches (Appendix F). Figure 5-4 compares Pt/Al2O3-CCl4, Pt/SO4–ZrO2 and Pt/zeolite catalyst associating the 5 separation options. The respective maximum and minimum net present values were \$185 million for SMB and approximately \$5 million for the DIS, respectively. The reason of this is that the extensive energy consumed of 31,000 kW by the DIS and the low RON of 89 reduced the NPV, while the SMB obtained less energy of 500 kW and RON of 92. The three catalysts almost achieved similar NPV when coupling with SMB at \$180 million. In addition, Figure 5-4 shows that the Pt/Al2O3-CCl4 catalyst achieved best NPV with VRC and BF at \$70 million and \$50 million, respectively with similar RON of 89. However, the Pt/SO4–ZrO2 performed the best when using AHP and DIS at \$120 million and \$20 million, respectively with RON of 88. Pt/ zeolite obtained the lowest NPV of approximately \$20 million and RON of 91.4 for SMB and 87 for distillation options (DIS, VRC, AHP and BF).
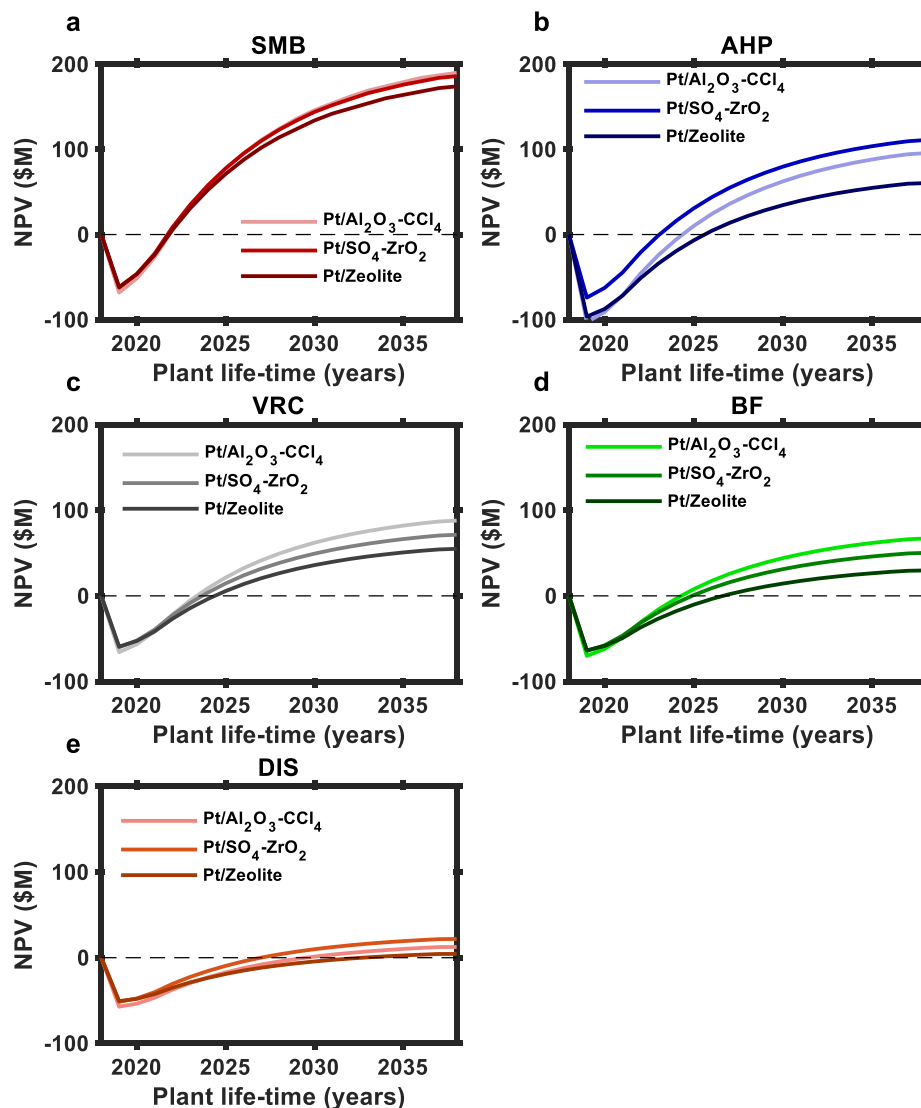
Figure 5-4 A comparison of NPVs using Pt/Al$_2$O$_3$-CCl$_4$, Pt/SO$_4$–ZrO$_2$ and Pt/Zeolite catalysts for each separation technology. Note: SMB=simulated moving bed, DIS=distillation column, AHP=absorbent heat pump, VRC=vapor recompression column, BF=bottom flashing column

5.6 Conclusion

The techno-economic analysis discussed the different costs of using different catalysts and separation methods. This is explained the ability to shape the isomerisation process economic feasibilities by using different materials and equipment. Using Pt/SO$_4$–ZrO$_2$ catalyst in the process increases the variable cost because the catalyst is activated on a relatively higher temperature. Pt/zeolite has the lowest variable cost because of the lower frequent catalyst regeneration, lower catalyst

charge, which increases the income and reduces the variable cost. However, the gasoline RON is the lowest when using the Pt/zeolite catalyst. Pt/Al$_2$O$_3$ catalyst produces the highest RON gasoline at lower temperatures whilst, the catalyst regeneration frequency is higher than the other catalysts and it has the highest expenses. Also, the net present value (NPV) results showed the change of choosing the best route. Therefore, adjusting between the best economic performances and operation conditions of the discussed options should be optimized using stochastic optimization, namely genetic algorithm (GA), which is explained in next chapter.

Chapter 6   Optimization   using   genetic algorithm (GA)

6.1 Introduction

This chapter highlights the economic and technical development of the isomerization process using hybrid genetic algorithm optimization superstructure method. Chapter 4 and Chapter 5 observed the technical performance and economic analysis of the superstructure process, respectively, while this chapter optimizes the superstructure process using the method is described in Chapter 3. In addition, this chapter explains the effect of: applying different crossover rates on the evolution of populations throughout the generations, and the randomness of the stochastic method (i.e. Genetic algorithm) on the objective function (Chapter 4).

6.2 Model settings

Five computers were manually used to optimize the superstructure process (Appendix G provides the MATLAB® optimization model). The properties of each computer are an Intel (R) Core (TM) i3 processor (3.7 GHz) with 8 GB of RAM. The optimizer operating conditions are shown in Table 6-1. The tolerance of the constraint equations was taken 10^{-8}, which is higher than HYSYS® (10^{-6}). The reason of this is that when retuning data from MATLAB® to HYSYS® with tolerance $\leq 10^{-6}$, HYSYS® does not converge. Table 6-2 shows range values of the case study variables that are optimized in this thesis.

Table 6-1 Tuning parameters Value

Number of design variables	8
Population size	5, 50 and 100
Reproduction count	50% of the population size
Elite count	2, 10 and 20
Maximum number of generations	10 and 20
crossover fraction 0.8	0.0, 0.2, 0.4, 0.6, 0.8 and 1.0
Selection method	Stochunif
Tolerance (constraint)	10^{-8}
Number of crossover points	1
Mutation method	Gaussian

Table 6-2 List of optimization variables

N.O.	Variables	Range value
x1	Flowrate ratio to reactor 1	[0 1]*
x2	Flowrate ratio to reactor 2	[0 1]*
x3	Flowrate ratio to reactor 3	[0 1]*
x4	Hydrogen/purge ratio	[0.2 0.9]
x5	Reactor 1 inlet temperature (°C)	[120 180]
x6	Reactor 2 inlet temperature (°C)	[130 210]
x7	Reactor 3 inlet temperature (°C)	[220 300]
x8	Separator option	[1 5]*+

* These values are integers. +Each number refers to the selection of different separation units, not to the number of units.

6.3 Crossover rate and population size analysis

6.3.1 The effect of altering crossover rates on the separators selection

The selection of the crossover rate and the population size is important, because they can affect the probability of finding the global optima. The crossover rate can change between 0-1. In all, zero crossover rate means the new individuals are created by introducing random changes to a single parent, while crossover rate equals one means the new individuals are created by coupling both parent-vectors (MathWorks, 2019). The maximum reported population size was a range of 5 - 50 in literature (Aguitoni et al., 2018, Steimel et al., 2014, Steimel et al., 2013), which applied for optimizing sub-flowsheet using GA.

Figure 6-1 compares the genetic algorithm parameters, namely, population size and crossover rate to find the global optima. The table represents population sizes of 5, 50 and 100 with crossover rates 0 and 1. Local optima were achieved at number of populations equals to 5 and crossover at 1, as the optimizer was trapped in the second-best separation, which is the absorption heat pump (AHP). The optimizer did not show any sing of development after the 2nd generations as MATLAB® stopped due to the low regeneration rates in new mutant offspring. However, at crossover rate equals zero the GA optimizer reached the global optima at the 7th generation.

At population size equal 50, the optimum solution might be reached after the 10th generation and at crossover rate equals 1. However, the global optima was achieved at the 7th generation and zero crossover rate.

On the other hand, the global optima was achieved at population size of 100 at both crossover rate 0 and 1 after 5th and 9th generations, respectively. The GA optimizer selected the best separator, which is the simulated moving bed (SMB). Therefore, applying more mutant populations to the GA can show better performance on the case study.

However, some might argue (Hassanat et al., 2019) a higher number of generations and higher crossover rate could find the global solution, due to the population diversity. To answer that letting an optimizer stuck in an unfavourable solution can increase the rise of system failures, data loses and time waste. Thus, applying a larger number of populations is more stable than a larger number of generations as long as the number of variables is considered.

6.3.2 The effect of altering crossover rates on the catalysts selection

The effect of population dynamic on catalyst selection is shown in Figure 6-2. The optimizer stuck with $Pt/SO_4–ZrO_2$ catalyst for 5 individuals. After increasing the number of individuals to 50, Pt/zeolite is competing with Pt/Al_2O_3-CCl_4 until around the 5th generation and then the Pt/Al_2O_3-CCl_4 took over. At 100-population size Pt/Al_2O_3-CCl_4 overcomes the population at crossover rate equals 1, while $Pt/SO_4–ZrO_2$ catalyst overcomes the population at crossover rate equals 0. Therefore, the case study does challenge the optimizer to find the optimal solution.
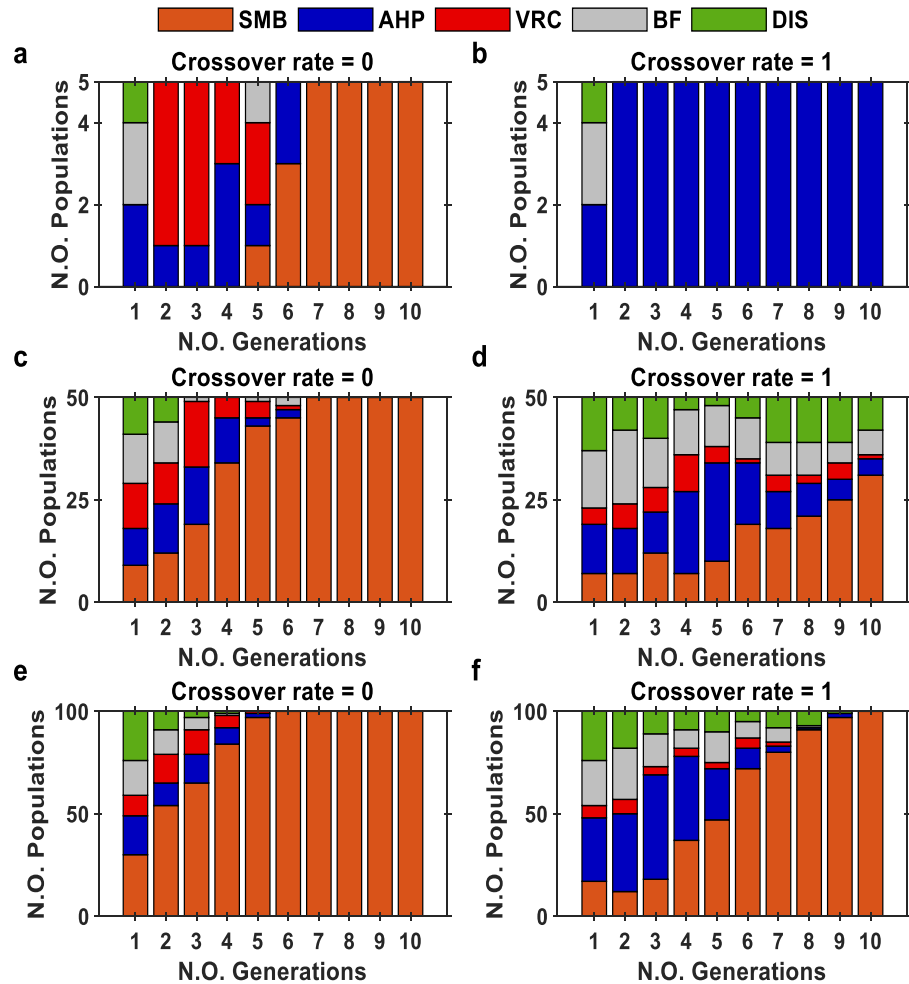
Figure 6-1 Population dynamic vs population size and different crossover rates on separation options

6.3.3 The effect of altering crossover rates on the fitness function

Figure 6-3 shows the effect of altering the crossover rate (i.e. 0.0, 0.2, 0.4, 0.6, 0.8 and 1.0) on the fitness function evolution curves through 20 generations and 100 populations. In all, at crossover rate equals one, the best and mean fitness function are the lowest evolutions because the mutation has been neglected. At crossover rate equals 0.4 and 0.6 the best fitness function curve shows an intermediate evolution speed where its first peak at the 7th generation, however, the mean curve shows a fast peak at generation 7 and then increases slightly to $220 M at the 20th generation. Moreover, at 0.0 crossover rates, the evolution of the

best curves are the highest at 6th generation. Thus, the mean fitness function curves evolution are reversed proportional to crossover rate. Zero crossover showed the best and fastest GA performance on finding the best solution.
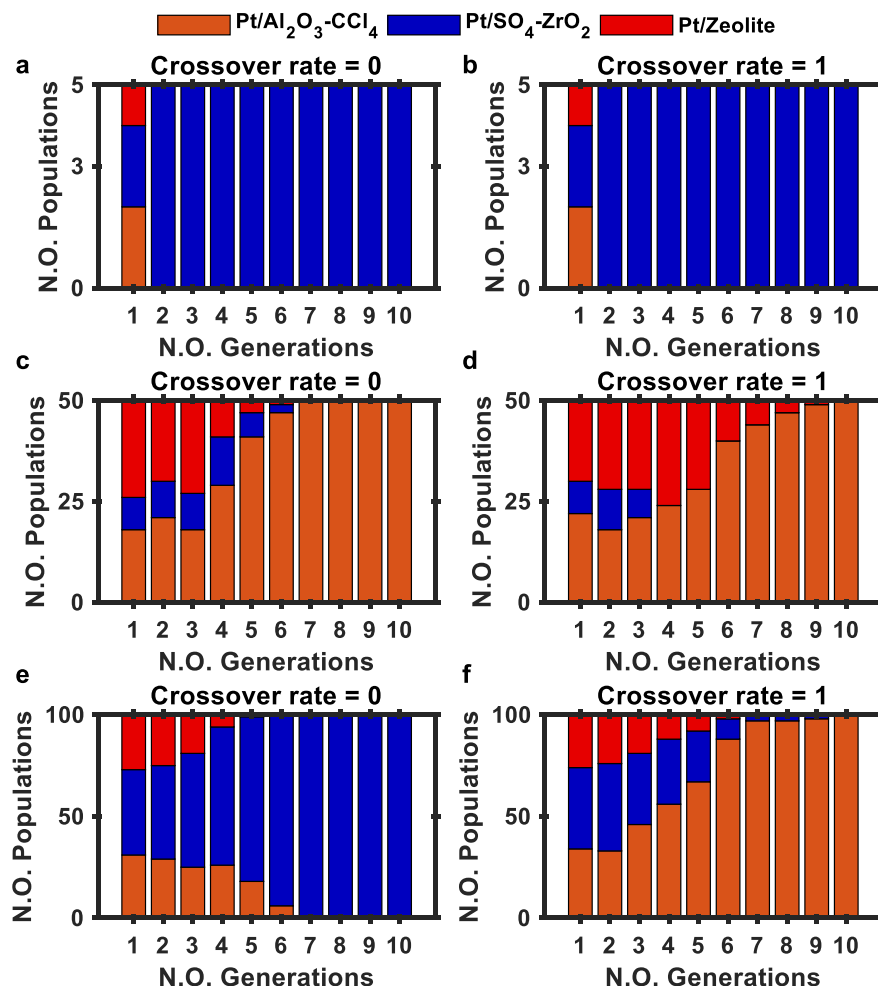
Figure 6-2 Population dynamic vs population size and different crossover rates on catalyst options

It can be observed that the global optimal solution was obtained when applying solver settings of number of generations of 20, the population size of 100 and crossover rate of 0.0. The next section discusses the dynamic of each of the 15th pathways dominates over the population throughout the number of generations.
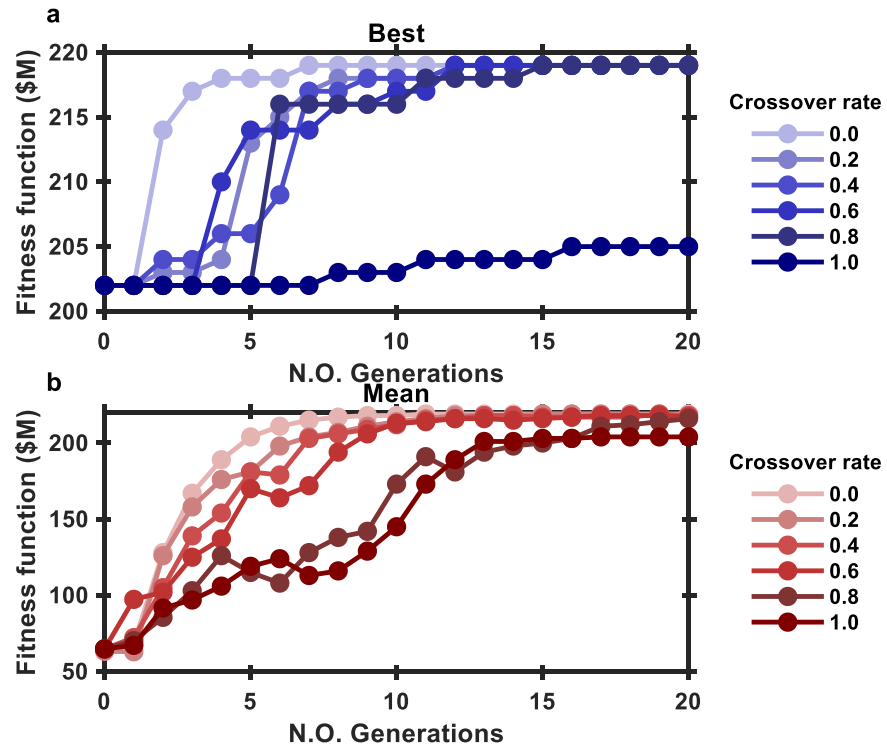
Figure 6-3 A comparison of crossover rates during 20 generation for (a) the best fitness function (blue lines) and (b) the mean fitness function (red lines)

6.4 Genetic algorithm population dynamic

6.4.1 Randomness performances

Figure 6-4 presents the population best and average evolutions via 20 generations, respectively. The SMB has the highest NPV at about $220M followed by heat pump distillations at around $130M and the distillation column NPV at slightly less than $30M.

At generation zero, ±40% was found to be an error because the case study initial conditions were different. Also, Figure 6-4 shows the behaviour of running the GA three times, the result shows the high stability performance of GA abilities on finding the best solution on each generation. However, on distillation options the error bars are showed up because of three of distillation processes did not converge because the TEA outcomes from HYSYS was not stable (not deterministic). This

return zeros if HYSYS did not converge. Newer version of MATLAB (R2019b and latter) offers to solve this problem by asking to not re-evaluate elite values with allowing better value to be generated and be replaced in the newer generations. This the elite offspring will not be affected by the randomness function. This way will ensure the GA converges. These suggestions will cause GA to behave less randomly but will cover up for the gap in the simulation convergence. It also noted that the AHP average curve did not converge with the best curve due to convergence problem.
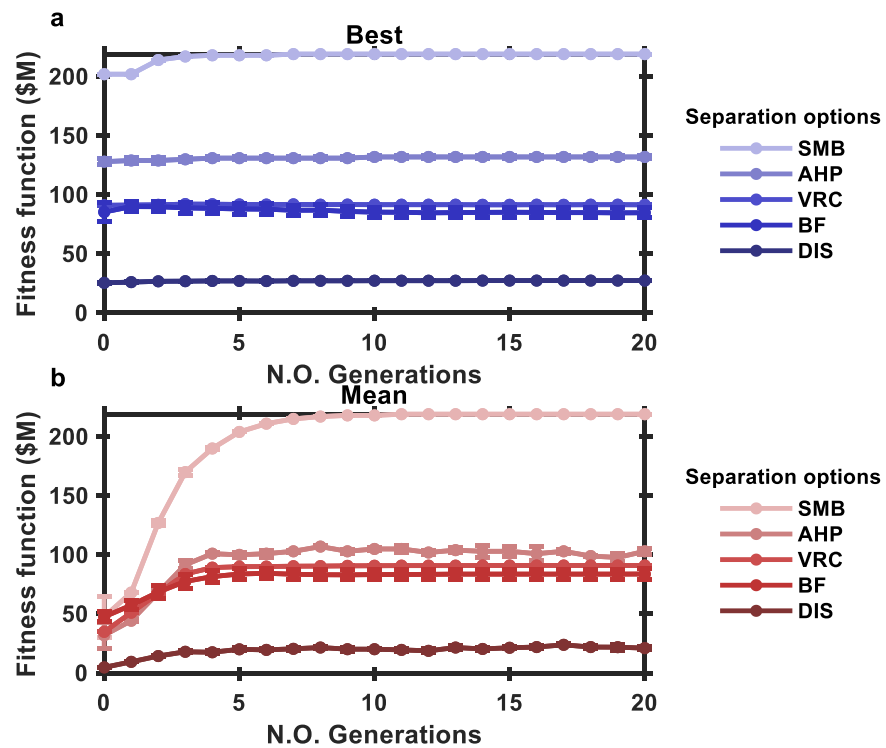
Figure 6-4 GA behaviors: a) after three runs on the best curves (blue lines) and b) after three runs on the average population curves (red lines).

6.4.2 Population dynamic of separations

After applying the recommended population size (i.e. 100) and crossover rate (i.e. 0.0) by this thesis, the population size was examined for four scenarios, which are comparing 5, 4, 3, and 2 separation units.

Figure 6-4 shows the statistical analysis of each separator via 10 generations. Each sub-chart represents when the GA compares 5, 4, 3, and 2 separation options. The genetic algorithm found the global optima in maximum of 5 generations. Unexpectedly, in Figure 6-4 (b), the comparison included absorption heat pump (AHP), which a complex distillation column. The column did not adapt well when having extremely random inputs that causes some convergence complications. These difficulties confuse the GA optimizer and resulting on stochastic problem at each generation, which did not allow the GA to converge and reach the global optima.
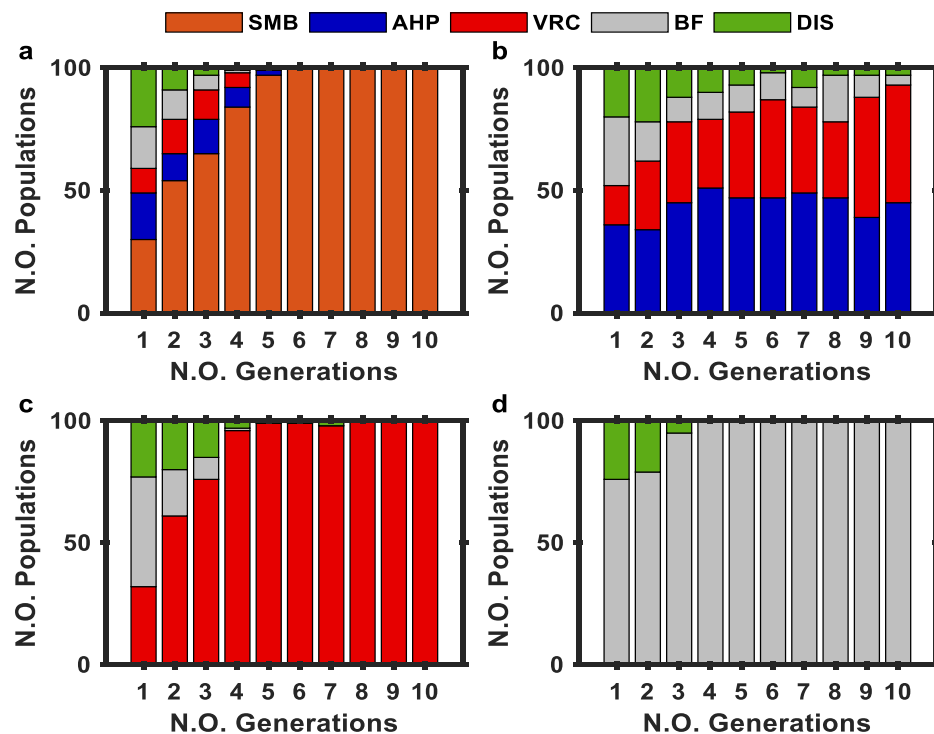
Figure 6-5 The population analysis vs 20 generations. The letters represent the GA comparing (a) 5, (b) 4, (c) 3, and (d) 2 separation units

Therefore, it can be said that the method is powerful in solving superstructure flowsheet problems. Although the superstructure flowsheet is solved at the 5th generation, the progress of developing the process operating conditions were still evolving.

6.4.3 Population dynamic of catalysts

Figure 6-6 compares the selection catalyst by the GA for three scenarios, which are simulated moving bed (SMB), heat pump absorption (AHP) and vapour recompression (VRC). In Figure 6-6 (a), the GA couples the SMB with Pt/SO_4-ZrO_2 catalyst for the isomerization process, at the 7th generation, which obtains in the best NPV. Turning now to the combination of AHP with Pt/Zeolite catalyst in Figure 6-6 (b), at the 7th generation. The reason of that is the GA tries to balance the lowest capital cost (i.e. Pt/Zeolite) with the highest capital investment (i.e. AHP).

In Figure 6-6 (c), the optimizer attempts to couple the VRC with Pt/Zeolite catalyst for the first 8 generations. The Pt/Zeolite catalyst individual rate rises to a high point of 84 individuals and peaks at the 8th generation. A possible explanation for this maybe that the GA tries to balance the lowest capital cost (i.e. Pt/Zeolite) with a relatively higher variable cost option (i.e. VRC). Then, the individual rate falls to zero at the 14th generation, which allows Pt/SO_4-ZrO_2 catalyst to reach 100-population size. The GA re-corrects its selection path to choose Pt/SO_4-ZrO_2 catalyst rather than Pt/Zeolite.

The reason of this can be that the variable cost of Pt/SO_4-ZrO_2 catalyst was lower than Pt/Zeolite. This inconsistency maybe due to the trade-off between the variable cost and the capital cost was difficult. Therefore, this made the GA selection process, to avoid trapping in a local-optima, relatively longer than the SMB and AHP scenarios.

Thus, the results show that the optimizer adapts differently with each scenario to bush the case study process towards its best performance.
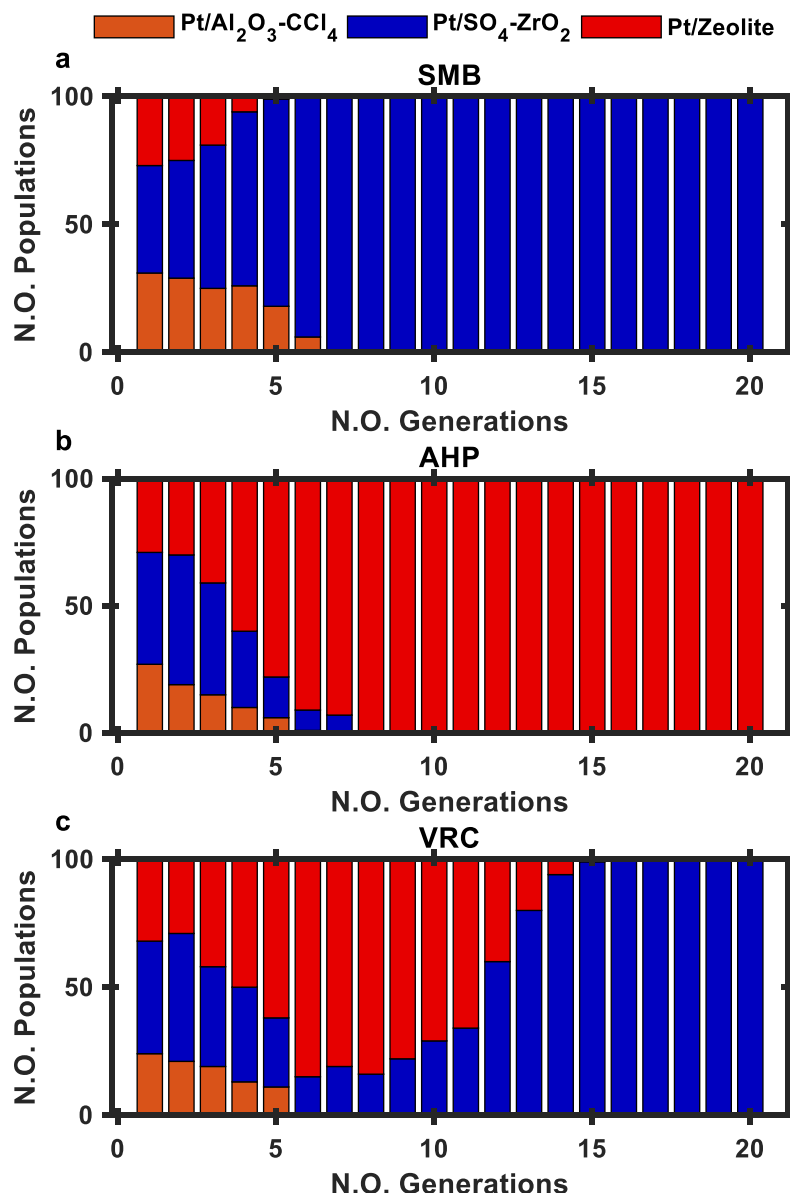
Figure 6-6 The population analysis vs 10 generations. The letters represent when the GA compares (a) SMB, (b) AHP and (c) VRC

6.5 The improved flowsheet

According to the above evidence, the optimizer was operated at the conditions shown in Table 6-3, in this thesis. Table 6-4 compares the base case study variables and objective function against the improved flowsheet. The optimal configuration was a combination of Pt/SO_4-ZrO_2

and SMB. Figure 6-7 illustrates the improved isomerization process. The mixed of the hydrogen and the pumped light naphtha was preheated to 180°C. The mixture was sent to the reactor with $Pt/SO_4–ZrO_2$ catalyst. The air cooler and the flash drum separated the pre-products to recycle 80% of the excessive hydrogen back to the reactor, and sent the off-gases and paraffin to a stabilizer column. The off-gases was sent to the LPG, and normal/iso paraffine mixture was discharged to the 8-SMB. The SMB recycled the unconverted normal paraffin and the iso paraffin was cooled to obtain the high RON gasoline (95). The configuration obtained RON of 95 and NPV of $ 220 million, including capital cost, variable operating cost and fixed operating cost of $58 million, $365 million, and $9 million, respectively.

Table 6-3 Tuning parameters Value

Number of design variables	8
Population size	100
Reproduction count	50% of the population size
Maximum number of generations	20
crossover fraction 0.8	0.0
Selection method	Stochunif
Tolerance (constraint)	10^{-8}
Number of crossover points	1
Mutation method	Gaussian

Table 6-4 List of optimization variables

	N.O.	Base value	Optimized value
	x1	1	0
	x2	0	1
	x3	0	0
	x4	0.9	0.2
Temperature (°C)	x5	180	N/A
	x6	N/A	210
	x7	N/A	N/A
	x8	5	5
Objective function (NPV) ($M)		186	220

Figure 6-7 The improved superstructure flowsheet

6.6 Conclusion

After several analyses were made, the best optimizer settings were 20 generations, 100-population size and zero crossover rate. The proposed method improved the process NPV to $220M with RON of 95, which is up to 15% over the bas case, after considering operating conditions optimization using the GA. The optimal decision variables were reactor temperature of 210℃ and hydrogen recycle ratio of 0.2. The optimal superstructure parameters were Pt/SO$_4$-ZrO$_2$ and SMB. Thus, the method is recommended to be applied into other applications.

The main disadvantage of the proposed method is the considerable time consumption. For 20 generations, the optimizer spent 1.08, 10.4 and 20 days for population sizes of 5, 50 and 100, respectively, to achieve the global optimum solution. This is due to the slow communication between HYSYS® and MATLAB®. The *issolving* command was found broken, due to the connection between HYSYS® and MATLAB® was created by third party. This glitch made the hybrid program run extra 3-5 times. Further development to improve these program communications is needed. Another limitation of the hybrid platform was that HYSYS® was not stable for the complexity of the AHP. Thus, the optimizer might not reach the maximum economic potential of the AHP.

Chapter 7   Conclusion, Recommendation and Future work

7.1 Conclusions

This study offered a method that economically retrofits and optimizes a superstructure chemical process, considering the process design and operating conditions. Results reported in Chapters 4, 5 and 6 clearly demonstrate the successful achievement of the specific objectives highlighted in Chapter 1. Conclusions from these chapters (i.e. 4, 5 and 6) are as follows.

7.1.1 Conclusion from superstructure process simulation

7.1.1.1 Frontend flowsheet

The Aspen HYSYS® model was used to represent the frontend flowsheet of the isomerisation process, which included three separated pathways. Each pathway accommodated one of three catalysts: chlorinated alumina-based, sulphated metal oxides based and zeolite catalysts. The process accessories, namely, pumping and preheating, hydrogen recycle, and stabilizer, were also included in the model. The results showed a high agreement for the gasoline RON between the HYSYS® model and the published studies (see Chapter 4). In addition, investigating the effect of different inlet temperature on the gasoline RON for each catalyst showed a similar trend to published studies. The model also showed that increasing the amount of the recycled hydrogen increased the compressor and decreased the amount of the purge. It is clear that the model was able to represent the frontend flowsheet.

However, up to ~20% error was obtained when comparing the mass compositions of the outlet streams with published studies. This was a consequence of estimating the kinetic parameters from available literature, which obtained these parameters under relatively scattered process conditions. In addition, although the catalytic reactions were complex and revisable, the reaction rate equations were assumed to be first order reactions. For each catalyst, the effect of temperature outside the referenced range may or may not indicate changes on the gasoline RON. Further experimental work is needed to determine the kinetics to develop a robust model to present the complex reactions schemes and to investigate the temperature effect on the gasoline RON.

7.1.1.2 Backend flowsheet

MATLAB® was used to simulate the lab-scaled fixed bed adsorption and the field-scaled eight simulated moving bed (SMB). To predict kinetic isothermal parameters of a fixed bed adsorption the Adsim® simulator was used by Bárcia et al. (2010a). Despite using different software to simulate a fixed bed model to validate the adsorption kinetic isothermal parameters, the results were nearly identical. This showed confidence to scale up the model to full scale SMB. Observations found from purity and recovery analyses on the SMB were satisfactory.

However, in the fixed bed MATLAB® model, the breakthrough curves results revealed that the normal hexane reached saturation a little bit later than the published data (Adsim®). In this thesis, the adsorbent bed was utilized only up to saturation points. Therefore, the model may not represent the fixed bed after these saturation points and it will be

necessary to continue to develop this model in the future. In addition, the SMB model was resized based on lab scale empirical correlations and experimental work is needed to measure these correlations for large scales.

This study appears to be the first study to find that the absorption heat pump (AHP) distillation column offered a higher energy saving than vapour recompression and bottom flashing heat pump distillations. The AHP was determined to minimise the heating and cooling utilities by up to nearly 15% and 2% of the original distillation column, respectively. As the study focuses on particular operating conditions, further investigations are required on the effect of such operating variables as reflux ratios, feed/side-stream ratios, operating pressure and feed/distillate rate ratios are required. Moving further, the AHP configuration can be improved and integrated to other chemical engineering processes.

7.1.2 Conclusion from techno-economic analysis

This study provided the first comprehensive techno-economic assessment for 15th routes of the isomerization process. A trade-off between capital cost and variable cost showed that applying an energy efficient distillation such as absorption heat pump (AHP) could reduce the utility cost by up to 8.95%, which can improve the process sustainability.

7.1.3 Conclusion from the optimization platform

As a result of implementing the hybrid optimization platform using GA for the isomerisation process, the NPV was improved by 15% over the conventional cases. It can be concluded that the hybrid optimization software can be easily encrypted to other process industries. However, this conclusion was based on 3 runs and it is important to increase the number of runs to at least 100 runs for each scenario. This would form a basis for well-grounded conclusions and recommendations.

7.2 Recommendations based on the case study

In addition to the future work suggested in section 7.1, the following recommendations need further research.

7.2.1 Recommendation for superstructure flowsheet modelling

The superstructure flowsheet and case study can be improved by investigating the following applications.

7.2.1.1 Developing materials

A novel material for adsorption and reactor can be developed to achieve better product quality (e.g. RON). The gap between the lab and the commercial material activities are huge (Løften, 2004), thus more investigation is needed. Moreover, although a few papers studied the decay of the catalysts, they did not classify the kinetics rates. Wang et al.'s (2016) study identified the deactivation mechanism for n-butane isomerization over alumina-promoted sulfated zirconia. It is

recommended that their mechanism be promoted for pentane and hexane (Wang et al., 2016).

7.2.1.2 Developing the process condition

Seasonal temperatures vary depending on the region of the research. Temperature effecting reactor performance, but isolation technologies might solve this problem. More investigations are needed on the heat transfer calculations or simultaneous calculations with mass transfer. Also, generally, petroleum feed composites are uncertain, and might be affected by the atmospheric distillation on the main field. Feed compositions can change hourly and can affect the optimization process dramatically.

In case of higher benzene content (>10%) and sulfur content (0.1 ppm), several researchers have suggested including two reactions and exceeding the amount of the hydrogen flowrate to convert the benzene to basic paraffin and the sulfur to gas (H_2S) (Fathy and Soliman, 2019, Polanec et al., 2012, Said et al., 2014, Szoboszlai et al., 2012, Szoboszlai and Hancsók, 2010, Szoboszlai and Hancsók, 2011). However, their studies focused on specific applications other than the applications considered in this thesis.

7.2.1.3 Designing a global Superstructure flowsheet by expanding pathways

To improve the superstructure flowsheet and process pathways, it can grow to include more units such as multi distillations (i.e. DIH and DIP), combination separation technology and heat efficient distillations. In

addition, an extra pathway can be added by including intensified processes to the flowsheet. Process intensification is one the best way to enhance a process design (Boodhoo and Harvey, 2013, Keil, 2018). One way to intensify the process is by using the reactive separation method (Lutze et al., 2010, Skiborowski, 2018). Combination of a reactor-distillation process (Estrada-Villagrana et al., 2006, Giyazov and Parputs, 2013a, Giyazov and Parputs, 2013b) and a reactor-adsorption process (Al-Juhani and Loughlin, 2003, Loughlin and Al-Soudani, 2005) were studied for isomerization process to enhance the process performance. This showed a considerable potential that can be investigated and optimized beside the other options.

7.2.2 Recommendation for techno-economic analysis/objective function improvement

Material prices could vary depends on the market demands. This can change the objective function results and the financial attractiveness of the process. To sort that, another economical factor such as internal rate of return (IRR) can be used. Moreover, considering multi-objective functions by including the environmental and social impacts is suggested for sustainable solutions.

7.2.3 Recommendation for the optimization platform

The methodology can be improved by investigating in the following proposals.

7.2.3.1 Developing recycle convergence (RC)

This thesis assumed a simpler way (i.e. glitch) to solve recycle convergence (RC) problem, as the investigation was focusing on the process quality (i.e. RON) rather than quantity. However, an alternative method such as Newton-Raphson method can be used. The method tolerance can reach 0.0001% for more accurate solution.

7.2.3.2 Improving the optimization setting parameters

In this thesis, population size was limited to 100 individuals and the maximum number of generations were limited to 20 generation. Thus, more investigation is needed to explore the effect of crossover rate and mutation rate the population dynamic and finding solution in wider population sizes and wider number of generations. Also, the experimental results were based on 20% of the population were elite offspring, which is a large number and can poorer the diversity of the next generation. An investigation can be drawn toward lowering the elite count to at most 5% of the population. Moreover, the mutation function needs to be further investigated, and compared with Adaptive feasible approach. Selection function also needs to be compared with other method such as tournament and uniform (Meloni and Murroni, 2014).

In addition, the reason of finding errors after running the experiment 3 times was that distillation column and heat pump distillations including vapour compression, bottom flashing and absorption did not achieved deterministic results when sending same values input to HYSYS®. It is strongly recommended to pin the elite value by setting 'EvalElites'. Thus, elite values will pass to the next generation without been affect by the

randomness equation. This can maintain the best values through generations and can maintain finding the global optima progress steady. However, reducing the GA randomness can also reduce the population diversity, which might lead to local optima. Then, high mutation rate is recommended.

An alternative suggestion, is by using another method that can deal with stochastic problem such as simulated annealing (SA) and then implementing that method to GA. This will create a novel method of hybrid stochastic – stochastic approaches, which had never been carried out before.

7.3 Recommendations for future work

At the end of the study, the following questions need to be answered: (i) how the developed software can be extended to study/analyze different processes, as these would entail a totally different superstructure (i.e. how flexible the proposed method? (ii) what is the confidence in the results obtained, as they are a result of several modelling assumptions and the process models can contain a large number of uncertain factors? and (iii) while the proposed approach can be general, the application if the software is not.

First, to generalize the proposed method to include different processes, the main requirements will be to clearly defined decision variables (Figure 7-1). including operating conditions and superstructure parameters. Most of chemical processes identify these variables when the data have been collected. Any of superstructure representation methods (see Chapter 2), including the proposed switch method (see

Chapter 3), can be used to represent the process superstructure. This superstructure is then simulated in an equation oriented (EO) or sequential modular (SM) or combination programs. The key consideration to choose between these software is the communication stability. After this, the process will be evaluated and optimized following the proposed level sequence of Input data, master and slave convergence analysis and presentation levels as described in Chapter 3.
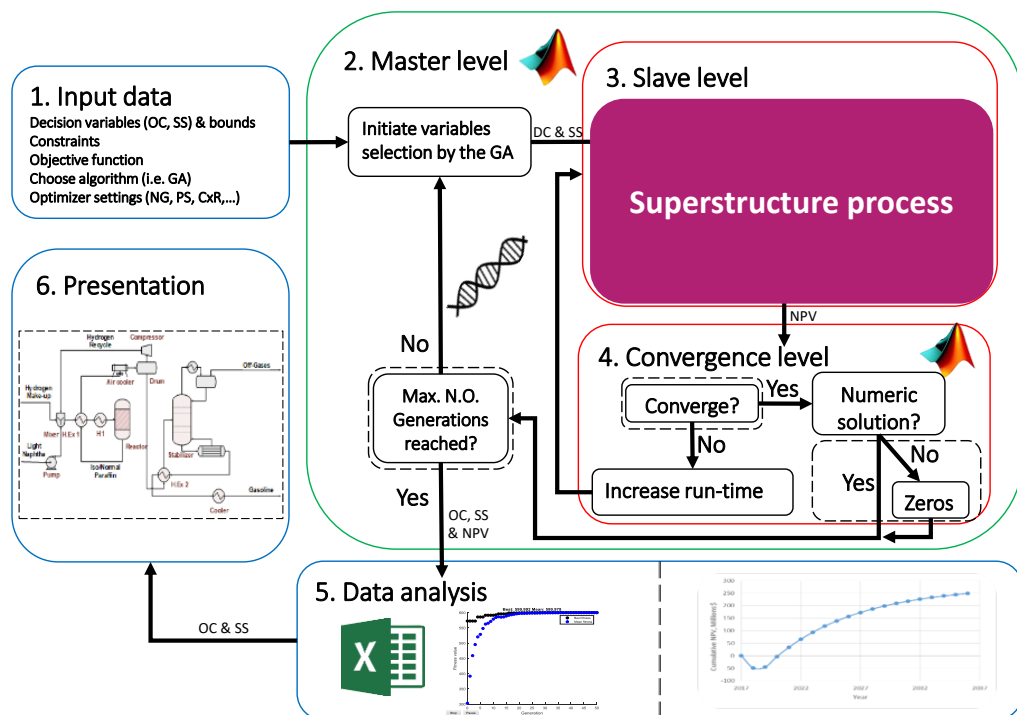
Figure 7-1 Generic hybrid optimization platform using GA

Second, as several assumptions were made to simulate the process, many error ranges were reported throughout the thesis. For neat simulation, further improvements are needed to narrow down these ranges. In addition, further investigation is needed to confirm the results obtained in the thesis. Third, the answer will be yes, as the proposed method was based on the level sequence rather than software tools, case studies or even superstructure representation method.

Appendices

Appendix A   Genetic algorithm encoding

Figure A-1 presents an example of the GA encrypted with a process model. As the GA proceed in the left hand of Figure A-1, the right hand of the figure shows the changes that occur on the decision variable and fitness function (FF) in the process model. As mentioned in Section 1.2.3,
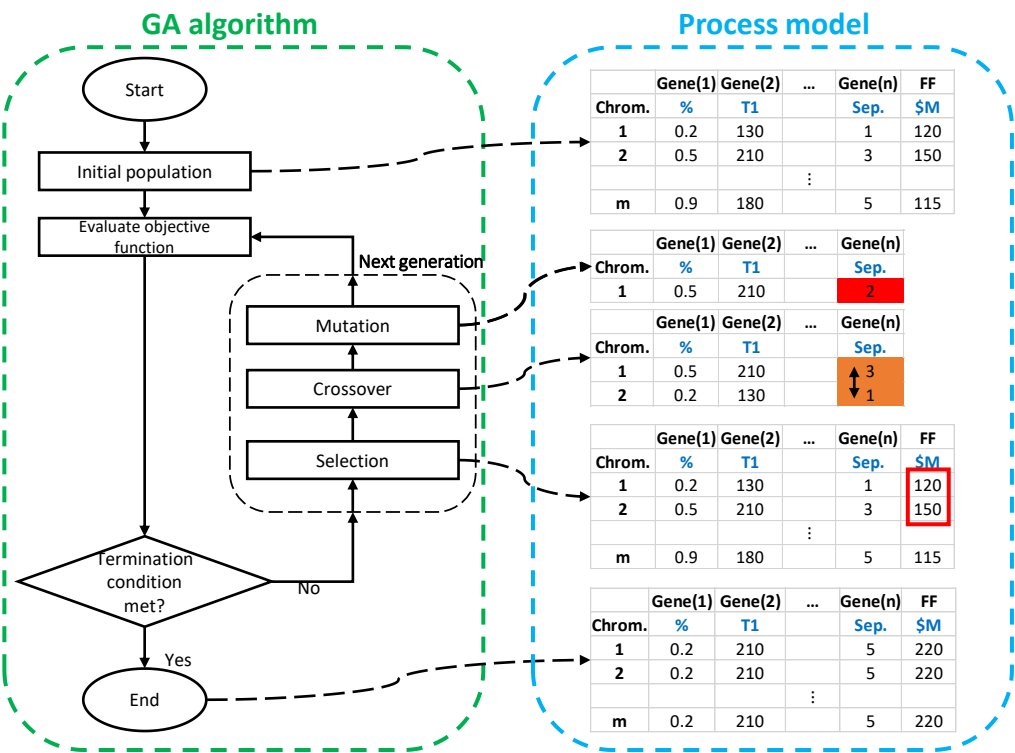
Figure A-1 GA encoding example

Appendix B   Hybrid systems

Table B-1, 2 and 3 present the integration of hybrid software in chemical process applications, i.e. modelling, optimization and control, respectively. Table B-4 presents Aspen custom modeler (ACM) in chemical process applications as the ACM also is considered as a hybrid model. In addition, Table B-1, 2, 3 and 4 summarize type of software and purpose of each publication for the last decade.

Table B-1 Chemical process applications use the direct interface and indirect interface with MS Excel®

Software	Application/ Case study	Model	Purpose	Reference
ASPEN PLUS® with Excel®-MATLAB®	Isoamyl acetate production	Hybrid Membrane	Energy integration and minimize the total annual cost	(Osorio-Viana et al., 2014)
ASPEN PLUS® with Excel®-MATLAB®	Isoamyl acetate production	Membrane reactors	Enhance performance, reduce energy consumptions, and estimate the total annual cost	(Gómez-García et al., 2016)
Aspen PLUS® with Python®	Water-ethanol separation	Flash drum	Temperature vs composition profile analysis	(Kitchin, 2013)
ASPEN PLUS® with Excel®	Hydrogen fuel production from methane reforming	Membrane reactor	Enhance the model reliability and predict performance	(Pasha et al., 2019)
Aspen HYSYS® with IDE Delphi®	Isomerisation process of light naphtha	Complex kinetic reactions	Increase the separation efficiency of normal/iso paraffin	(Chuzlov and Molotov, 2016, Chuzlov et al., 2015a, Chekantsev et al., 2014, Chuzlov et al., 2015b)
Aspen HYSYS® with IZOMER®	Isomerisation process of light naphtha	Complex kinetic reactions	Enhance the RON regarding the feed composition	(Chuzlov et al., 2014, Chuzlov et al., 2019)
PHREEQ with MATLAB®	Neodymium and cerium oxalates reactive in nitric acid media	Reactive precipitation	Thermodynamic modelling and to predict earth solubility	(Rodríguez-Ruiz et al., 2018)
ASPEN PLUS® with MATLAB®	Bisphenol A production process	Crystal tower	To build a realistic model	(Dai et al., 2017)
ASPEN PLUS® with Excel®-	Dehydration ethanol + purification of acetic acid processes	Hybrid distillation–pervaporation	To build a realistic model	(Verhoef et al., 2008)

Table B-2 Chemical process optimization applications implement hybrid model

Software	Application/ Case study	Purpose (Algorithm)	Reference
C# with Visual Studio® & FSOpt	Hydroformylation of long chain olefins process	Superstructure optimization (GA & DE)	(Steimel et al., 2013, Steimel et al., 2014)
Aspen PLUS® with MATLAB® & MS Excel®	Hybrid distillation and vapour permeation for ethanol dehydration process	Optimization the system performance	(Fontalvo, 2014)
Aspen PLUS® with MATLAB® & MS Excel®	Benzene-Toluene separation process	Energy efficient distillation (HIDiC) minimization (optimization toolbox)	(Claumann et al., 2015)
Aspen HYSYS® with C & MS Excel®	Biobutanol production process	Multi objectives optimization (DE with tabu list)	(Segovia-Hernández and Gómez-Castro, 2017)
Aspen PLUS® with MATLAB® with MS Excel®	Production of syngas	Optimization reactor network (GA)	(Martinez-Gomez et al., 2017)
COLOM© software with FORTRAN®	Natural gas separation process	Distillation systems Optimization (SA)	(Farrokhpanah, 2009)
Aspen HYSYS® with MATLAB®	LNG refrigerant process	Heat exchanger network (GA)	(Alabdulkarem et al., 2011, Abdelhamid et al., 2017)
Aspen HYSYS® with MATLAB®	Pyrolysis gasoline hydrogenation	Distillation column optimization (GA)	(Sharifzadeh and Thornhill, 2011)
Aspen HYSYS® with MATLAB®	Extractive Distillation System	Minimization of the total annual cost (TAC) (PSO)	(Javaloyes-Antón et al., 2013)
Aspen HYSYS® with MATLAB®	Methanol plant	Superstructure optimization (GDP)	(Navarro-Amorós et al., 2014, Ruiz-Femenia et al., 2020)

Software	Application/ Case study	Purpose (Algorithm)	Reference
Aspen HYSYS® with MATLAB®	Methanol, Acetone and Water separation processes	Distillation system optimization (GDP)	(Caballero, 2015)
Aspen HYSYS® with CPLEX & CONOPT	Production of Light Olefins from Natural Gas via the Methanol Intermediate	Flowsheet superstructure optimization (MILP & NLP)	(Onel et al., 2016)
Aspen PLUS® with MATLAB®	Rankine cycle using LNG cryogenic	Distillation Optimization (GA)	(Lee et al., 2017)
Aspen HYSYS® with MATLAB®	Propylene/Propane Separation	Distillation system optimization (PSO)	(Christopher et al., 2017)
Aspen HYSYS® with GCA.	Hydrogen systems	Hydrogen network (PT)	(Marques et al., 2017)
Aspen HYSYS® with MATLAB®	LNG (Liquefied Natural Gas) process	Flowsheet optimization (PSO)	(Dutta et al., 2018)
Aspen PLUS® with MATLAB®	Ethanol dehydration process	Flowsheet optimization (DE)	(Vázquez-Ojeda et al., 2013)
Aspen PLUS® with MS Excel®	Heat excahnger netwok process	Energy integration (MISQP)	(Wang et al., 2013)
Aspen PLUS® with MATLAB®	Extractive distillation systems (n-heptane/isobutanol, acetonitrile/water and isopropanol/water)	Distillation system optimization (GA)	(Cui and Sun, 2019)
Aspen PLUS® with MATLAB®	Extractive distillation system for n-hexane/ethyl acetate separation	Optimize extractive distillation (MINLP)	(Feng et al., 2020)

Table B-2 Continue

Software	Application/ Case study	Purpose (Algorithm)	Reference
Aspen HYSYS® with MATLAB®	Di-n-pentyl ether production process	Design novel reaction separation and recycle and catalytic distillation processes and minimize the total annual cost (direct search algorithm)	(Bildea et al., 2015)
Aspen HYSYS® with MATLAB®	Catalytic cracking of higher olefins on ZSM	Process optimization (fmincon with the SQP)	(Sundberg et al., 2018)
Aspen HYSYS® with MATLAB®	Azeotropic distillation processes	Data analysis	(Tabari and Ahmad, 2015)
SuperPro Designer® with MATLAB®	Sustainable design of bioprocesses	Multi-objective optimization (NIMBUS, GA)	(Taras and Woinaroschy, 2012)
ANSYS CFX® with MATLAB®	Biocatalytic microreactor configurations	Topology optimization (ESO)	(Rosinha et al., 2015)
Aspen PLUS® with MATLAB® & MS Excel®	Separation of ternary mixture (i.e. Cyclopentane Benzene and Toluene) process	Distillation sequences optimization (SA)	(Cabrera-Ruiz et al., 2012)
Aspen HYSYS® with MATLAB® & MS Excel®	Production of biofuel and petrochemicals from bio-waste	Supply chain design network model (MILP)	(Emara et al., 2016)
ChemCAD® with MATLAB®	Multi-component distillation with recycle process	Retrofit evaluation (MIPT)	(Otte et al., 2016)
Aspen HYSYS® with MS Excel®	Methanol Process	Structural and operating optimization & multi-objective optimization (DE)	(Hernandez-Perez et al., 2020)
Aspen PLUS® with MATLAB®	Petrochemical gas separation plant	Energy integration optimization ((GA) with Pattern Search (PS))	(Qian et al., 2007)

Table B-2 Continue

Software	Application/ Case study	Purpose (Algorithm)	Reference
Aspen PLUS® with MATLAB®	Chemical process	Multi-objective optimization (NSGA-II)	(De Buck et al., 2019)
Aspen HYSYS® with MATLAB®	Crude oil distillation systems with a pre-flash units design	Rigorous distillation optimization (GA)	(Ledezma-Martínez et al., 2018)
CasADi® with MATLAB®	Butyl acetate production process	Multi-objective optimization (ESO)	(Muñoz et al., 2017)
Aspen PLUS® with MATLAB®	CO_2 capture pilot plant	Superstructure optimization (GA)	(Lee et al., 2016)
Aspen PLUS® with MATLAB®	CO_2 dehydration process	Superstructure optimization (GA)	(An et al., 2018)
Aspen PLUS® with MATLAB® & MS Excel®	Biodiesel production process with a reactive dividing-wall column	Rigorous distillation optimization (SA) and Data analysis	(Kiss et al., 2012b)
Aspen PLUS® with Python®	Biomass	Superstructure optimization (BISSO)	(Mangone et al., 2019)

162

Table B-3 Process control applications use the interface model

Software	Application/ Case study	Purpose	Reference
Aspen HYSYS® With MATLAB®	Depropanizer distillation column	Implementing the MPC	(Tuan et al., 2016)
Aspen HYSYS® With MATLAB®	Depropanizer distillation column	Implementing MPC and Kalman filter	(Tuan et al., 2017)
Aspen HYSYS® With MATLAB®	Multi-component separation distillation	Implementing the CLPA	(Salahshoor and Arjomandi, 2010, Arjomandi, 2011)
Aspen HYSYS® With MATLAB®	Propylene glycol plant	Implementing the CLPA	(Salahshoor et al., 2011)
Aspen HYSYS® With MATLAB®	Acrylic acid process	Maximize profitability and decrease the environmental impact	(Duque and Ochoa, 2017)
Dynsim® With MATLAB®	Propylene/propane separation column	Implementing the RIHMPC	(Hinojosa and Odloak, 2014)
DyOS® with MATLAB® or Modelica or gPROMS®	Copolymerization process	Applying the NMPC	(Elixmann et al., 2014)
Aspen PLUS® With MATLAB®	Three ternary alcohol mixtures separation	Six different configurations of dividing-wall columns	(Tarjani et al., 2018)
Aspen PLUS® With MATLAB®	Hydrogenation process	Linear PI-based multi-loop feedback control was used	(Wu et al., 2015)

Table B-4 Chemical process applications use the ACM®

Software	Application/ Case study	Model	Purpose	Reference
Aspen HYSYS®	CO_2 removal from natural gas	Membrane	The process techno-economic assessment	(Peters et al., 2011)
Aspen HYSYS®	N/A	Electo-membrane	Model development	(Bobák et al., 2014)
Aspen HYSYS®	Distillation Process	Vacuum membrane	Determine heat and mass transfer resistances	(Cao and Mujtaba, 2015)
Aspen PLUS®	Acetone-Butanol Fermentation	Reactor	Economical evaluation	(Segovia-Hernández and Gómez-Castro, 2017)
Aspen HYSYS®	Methyl tert butyl ether process	Heterogeneous catalytic distillation	Scaling-up the process	(Bao et al., 2002)
Aspen HYSYS®	Biogas upgrading	Membrane	Techno-economic analysis using NPV comparison between polymeric and carbon membranes	(Haider et al., 2016)
Aspen PLUS®	Methyl tert butyl ether production	Multi-tubular packed-bed Reactor	Productivity maximization	(Nawaz, 2017)
Aspen HYSYS®	Production of oxygen-enriched air (OEA)	Carbon membrane separation	The process techno-economic assessment	(Haider et al., 2018)

Appendix C   Taylor series

C.1   Derivatives of the backward time centred space (BTCS)

All derivatives were taken from Ames (2014) work. Starting from Taylor series is shown as follows:

C.1.1   Fist order:

Taylor series is shown as follows for f(x+Δx) and f(x-Δx)

$$f(x + \Delta x) = f(x) + \frac{\partial f(x)}{\partial x}\frac{\Delta x}{1!} + \frac{\partial^2 f(x)}{\partial x^2}\frac{\Delta x^2}{2!} + \frac{\partial^3 f(x)}{\partial x^3}\frac{\Delta x^3}{3!} \quad \text{(C-1)}$$
$$+ \frac{\partial^4 f(x)}{\partial x^4}\frac{\Delta x^4}{4!} + \cdots$$

$$f(x - \Delta x) = f(x) - \frac{\partial f(x)}{\partial x}\frac{\Delta x}{1!} + \frac{\partial^2 f(x)}{\partial x^2}\frac{\Delta x^2}{2!} - \frac{\partial^3 f(x)}{\partial x^3}\frac{\Delta x^3}{3!} \quad \text{(C-2)}$$
$$+ \frac{\partial^4 f(x)}{\partial x^4}\frac{\Delta x^4}{4!} + \cdots$$

Subtracting Equation (C-1) from Equation (C-2)

$$f(x + \Delta x) - f(x - \Delta x) = 2\frac{\partial f(x)}{\partial x}\frac{\Delta x}{1!} + 2\frac{\partial^3 f(x)}{\partial x^3}\frac{\Delta x^3}{3!} + \cdots \quad \text{(C-3)}$$

Rearranging Equation (C-3) and substitute 3! with 6

$$2\frac{\partial f(x)}{\partial x}\frac{\Delta x}{1!} = f(x + \Delta x) - f(x - \Delta x) - 2\frac{\partial^3 f(x)}{\partial x^3}\frac{\Delta x^3}{6} + \cdots \quad \text{(C-4)}$$

Divide both sides in (C-4) by 2 Δx

$$\frac{\partial f(x)}{\partial x} = \frac{f(x + \Delta x) - f(x - \Delta x)}{2\Delta x} - \frac{\partial^3 f(x)}{\partial x^3}\frac{\Delta x^2}{3} + \cdots \quad \text{(C-5)}$$

C.1.2   Second order:

Taylor series is shown as follows for f(x+Δx) and f(x-Δx)

$$f(x + \Delta x) = f(x) + \frac{\partial f(x)}{\partial x}\frac{\Delta x}{1!} + \frac{\partial^2 f(x)}{\partial x^2}\frac{\Delta x^2}{2!} + \frac{\partial^3 f(x)}{\partial x^3}\frac{\Delta x^3}{3!} \quad \text{(C-6)}$$

$$+ \frac{\partial^4 f(x)}{\partial x^4}\frac{\Delta x^4}{4!} + \cdots$$

$$f(x - \Delta x) = f(x) - \frac{\partial f(x)}{\partial x}\frac{\Delta x}{1!} + \frac{\partial^2 f(x)}{\partial x^2}\frac{\Delta x^2}{2!} - \frac{\partial^3 f(x)}{\partial x^3}\frac{\Delta x^3}{3!} \quad \text{(C-7)}$$

$$+ \frac{\partial^4 f(x)}{\partial x^4}\frac{\Delta x^4}{4!} + \cdots$$

Adding Equation (C-6) and Equation (C-7)

$$f(x + \Delta x) + f(x - \Delta x) = 2f(x) + 2\frac{\partial^2 f(x)}{\partial x^2}\frac{\Delta x^2}{2!} \quad \text{(C-8)}$$

$$+2\frac{\partial^4 f(x)}{\partial x^4}\frac{\Delta x^4}{4!} + \cdots$$

Rearranging Equation (C-8) and substitute 4! with 24

$$\frac{\partial^2 f(x)}{\partial x^2}\Delta x^2 = f(x + \Delta x) + f(x - \Delta x) - 2f(x) \quad \text{(C-9)}$$

$$-2\frac{\partial^4 f(x)}{\partial x^4}\frac{\Delta x^4}{24} + \cdots$$

Dividing both sides in Equation (C-9) by Δx²

$$\frac{\partial^2 f(x)}{\partial x^2} = \frac{f(x + \Delta x) - 2f(x) + f(x - \Delta x)}{\Delta x^2} - \frac{\partial^4 f(x)}{\partial x^4}\frac{\Delta x^2}{12} + \cdots \quad \text{(C-10)}$$

C.2   The Derivative of the backward Euler's Method

Backward Euler is divided from Taylor series is shown as follows (Equation (C-11))

$$\frac{\partial f(t)}{\partial t} = \frac{f(t) - f(t - \Delta t)}{\Delta t} - \frac{\partial^2 f(t)}{\partial t^2}\frac{\Delta t^2}{2} + \cdots \tag{C-11}$$

C.3   Example

$$\frac{\partial f(x,t)}{\partial t} + U\frac{\partial f(x,t)}{\partial x} = D\frac{\partial^2 f(x,t)}{\partial x^2} \tag{C-12}$$

Substitute Equation (C-5), Equation (C-10) and Equation (C-11) in Equation (C-12)

$$\frac{f(t) - f(t - \Delta t)}{\Delta t} + U\frac{f(x + \Delta x) - f(x + \Delta x)}{2\Delta x} \tag{C-13}$$
$$= D\frac{f(x + \Delta x) - 2f(x) + f(x + \Delta x)}{\Delta x^2}$$

Rearranging Equation (C-13)

$$\frac{f(t) - f(t - \Delta t)}{\Delta t} = -U\frac{f(x + \Delta x) - f(x + \Delta x)}{2\Delta x} \tag{C-14}$$
$$+ D\frac{f(x + \Delta x) - 2f(x) + f(x + \Delta x)}{\Delta x^2}$$

Multiply both sides in Equation (C-14) by Δt

$$f(t) - f(t - \Delta t) = -U\frac{f(x + \Delta x) - f(x + \Delta x)}{2\Delta x}\Delta t \tag{C-15}$$
$$+ D\frac{f(x + \Delta x) - 2f(x) + f(x + \Delta x)}{\Delta x^2}\Delta t$$

Rearranging Equation (C-15)

$$f(t) = f(t - \Delta t) - U \frac{f(x + \Delta x) - f(x + \Delta x)}{2\Delta x} \Delta t \qquad \text{(C-16)}$$
$$+ D \frac{f(x + \Delta x) - 2f(x) + f(x + \Delta x)}{\Delta x^2} \Delta t$$

Appendix D   Reactor validations

Table D-1, 2 and 3 illustrate compositions, error percentages and RON for Pt/SO$_4$–ZrO$_2$, Pt/zeolite and Pt/Al$_2$O$_3$–CCl$_4$ catalysts, respectively. The average error of compositions is recorded to be less than 15%, which is acceptable because of not all reactions were included and all the reactions were assumed to be first order. It should be noted that, the error % does not represent some components such as C4, iC4 and Benzene, which have errors more than 50%, because of the difference between HYSYS model and the reference (Chekantsev et al., 2014) concentration of these components are very small. Moreover, there are no differences on the research octane number (RON).

Table D-1 Inlet and outlet validation Pt/SO$_4$–ZrO$_2$

	Feed (wt.%) (Chekantsev et al., 2014)	Product (wt.%) (Chekantsev et al., 2014)	HYSYS® model	Error%
C4	0	0.19	0.00	100.00
iC4	0	1.19	0.00	100.00
C5	34.03	13.57	13.29	2.10
iC5	10.64	36.38	33.66	7.46
nC6	18.09	5.17	5.79	-12.06
2MC5	13.83	13.54	14.71	-8.64
3MC5	7.45	8.49	8.48	0.13
22DMC4	0	11.48	13.00	-13.24
23DMC4	0	4.48	5.00	-11.61
nC7+	0	0	0.00	0.00
CC5	4.26	1.99	1.95	2.18
MCC5	7.45	2.25	2.74	-21.78
CC6	2.13	1.16	1.20	-3.75
Benzene	1.06	0.11	0.18	-65.17
Total	100	100	100	5.40
RON	65.4	81.1	81.3	

Table D-2 Inlet and outlet validation Pt/zeolite

	Feed (wt.%) (Chekantsev et al., 2014)	Product (wt.%) (Chekantsev et al., 2014)	HYSYS® model	Error%
C4	0.22	1.45	0.22	84.83
iC4	0.02	0.67	0.02	97.01
C5	24.5	19.12	19.97	-4.43
iC5	15.26	21.73	22.79	-4.86
nC6	17.68	10.87	10.35	4.77
2MC5	14.34	14.95	14.02	6.21
3MC5	10.01	9.78	10.79	-10.35
22DMC4	0.27	4.79	4.50	6.02
23DMC4	2.22	4.77	5.51	-15.51
nC7+	4.44	2.75	2.62	4.63
CC5	2.99	2.68	3.04	-13.43
MCC5	5.86	4.91	4.58	6.64
CC6	2.19	1.52	1.58	-3.95
Benzene	0.0	0.01	0.00	100.00
Total	100	100	100.00	18.40
RON	64.0	72.5	73.7	

Table D-3 Inlet and outlet validation Pt/Al$_2$O$_3$–CCl$_4$

	Feed (wt.%) (Chekantsev et al., 2014)	Product (wt.%) (Chekantsev et al., 2014)	HYSYS® model	Error%
C4	1.1	0.22	0.25	-13.89
iC4	0.18	0.21	0.04	80.59
C5	36.18	25.51	24.18	5.21
iC5	20.33	31.46	31.63	-0.54
nC6	7.15	0.04	0.05	-27.45
2MC5	15.52	9.33	9.62	-3.15
3MC5	6.73	0.44	0.47	-7.43
22DMC4	0.70	15.84	17.02	-7.46
23DMC4	1.82	7.06	7.01	0.66
nC7+	0.03	0.02	0.03	-56.67
CC5	7.81	8.99	8.93	0.66
MCC5	2.36	0.66	0.56	15.33
CC6	0.09	0.21	0.19	7.73
Benzene	0.0	0.01	0.00	100.00
Total	100	100	100.00	6.68
RON	72.2	83.6	83.6	

Appendix E Equipment purchases estimation

The estimation of equipment purchases was based on the preliminary estimate method. This method is based on individual factors method of Guthrie, 1969, 1974. All equations are taken from Seider et al (2017) to calculate equipment purchases.

E.1 Reactors

Vessel cost (Sinnott, 2005) (C_P) is calculated form:

$$C_B = 4555 * L^{0.85} Di^{1.05} \qquad \text{(E-1)}$$

$$C_P = F_P * F_M * F_L * C_B \qquad \text{(E-2)}$$

where C_B is the base cost, L is the bed length, Di is the inner diameter, F_p is the pressure factor, F_L is the length tube correction factor and F_M is the material factor.

E.2 Distillation columns

The design pressure (P_d) of the column is calculated by interpreted the operating pressure (P_o) in Equation (E-3) (Apostolakou et al., 2009, Chaves et al., 2016, Seider et al., 2017):

$$P_d = \exp[0.60608 + 0.91615 \ln(P_o) + 0.0015655 \ln(P_o)^2] \quad \text{(E-3)}$$

The wall thickness (t_p) is calculated from:

$$t_P = \frac{P_d * D_i}{2 * S * E - 1.2 * P_d} \qquad \text{(E-4)}$$

where D_i is the inner diameter, S is the maximum material stress allowable, and E is the welding efficiency.

Then, the tower weight (W) is calculated form:

$$W = \pi * (D_i + t_S) * 0.8 * D_i * t_s * \rho \qquad \text{(E-5)}$$

where t_s is the stage height and ρ is column construction material density.

Then, the empty vessel cost (C_v) is calculated from Equation (E-6), including manholes, supports, etc.

$$C_V = \exp[7.0374 + 0.18255 * \ln(W) + 0.02297 \qquad \text{(E-6)}$$
$$* (\ln(W))^2]$$

Then, the stairs and platforms costs (C_{PL}) is considered and calculated from:

$$C_{PL} = 237.1 * (D_i)^{0.63316} * L^{0.80161} \qquad \text{(E-7)}$$

The length of column (L) is calculated from:

$$L = 1.2 * t_s * (N - 1) \qquad \text{(E-8)}$$

where N is the number of trays.

The internal diameter of column (D_i) is calculated form:

$$D_i = \sqrt{\frac{4 * A_n}{0.88 * \pi}} \qquad\qquad \text{(E-9)}$$

The net area (A_n) of column is calculated from:

$$A_n = \underset{all\ tray}{max}\left(\frac{V}{2\sqrt{\rho_V}}\right) \qquad\qquad \text{(E-10)}$$

The trays cost (C_{tr}):

$$C_{tr} = 380 * N^{0.81}(D_I)^{1.55} \qquad\qquad \text{(E-11)}$$

Finally, the purchase cost (C_p) is calculated of the distillation column:

$$C_P = F_M * C_V + C_{PL} + C_{tr} \qquad\qquad \text{(E-12)}$$

E.3   Simulated moving bed adsorption (SMB)

The purchase cost (Hamelinck et al., 2004, Kamarudin et al., 2006) is calculated from:

$$C_P = 32.6\left(\frac{F}{9600}\right)^{0.7} \qquad\qquad \text{(E-13)}$$

where F is the flow rate in kmol/hr.

Base year was given at 2002 and initial cost (C_0) was 32.6 M€ (Hamelinck et al., 2004).

E.4   Flash Drum

Vessel cost (Sinnott, 2005, Chaves et al., 2016, Seider et al., 2017) (C_P) is calculated from:

$$C_V = 4555\,H^{0.85}Di^{1.05} \qquad \text{(E-14)}$$

Finally, the purchase cost is calculated:

$$C_P = F_M C_V \qquad \text{(E-15)}$$

E.5   Kettle type Heat Exchangers

The heat exchanger area (Seider et al., 2017) is calculated from:

$$Q = A * U * \Delta T_{LM} \qquad \text{(E-16)}$$

where Q is the heat transfer, A is heat transfer area, U is the heat transfer coefficient and ΔT_{LM} is the temperature logarithmic mean.

The heat transfer is calculated from:

$$Q = C_P * (T_{out} - T_{in}) \qquad \text{(E-17)}$$

where C_p is fluid heat capacity, T_{out} and T_{in} is outlet and inlet Temperature, respectively.

Substitute Equation (E-16) in Equation (E-17) to calculate the heat transfer area (A):

$$A * U * \Delta T_{LM} = C_P * (T_{out} - T_{in}) \qquad \text{(E-18)}$$

Rearrange the above equation (D-18) with respect to A:

$$A = \frac{C_P * (T_{out} - T_{in})}{U * \Delta T_{LM}} \qquad \text{(E-19)}$$

Then, the base cost of the kettle heat exchanger type can be calculated from:

$$C_B = \exp[11.967 - 0.8709 * \ln(A) + 0.090005 * (\ln(A))^2] \quad \text{(E-20)}$$

The purchase cost of the heat exchanger is calculated from:

$$C_P = F_L F_M F_P C_B \qquad \text{(E-21)}$$

where F_L is the length tube correction factor and F_M is the material type factor (Table 16.25 from Ravagnani (2010)). F_P is the pressure factor based on shell side pressure, which can be calculated as follows:

$$F_P = 0.9803 + 0.018 * \frac{P}{100} + 0.0017 * \left(\frac{P}{100}\right)^2 \qquad \text{(E-22)}$$

E.6   Pumps

The base cost (C_B) of the pump (Chaves et al., 2016, Seider et al., 2017) is calculated as follows:

$$S = QH^{0.5} \qquad \text{(E-23)}$$

where S is the size factor, Q is the volumetric flow in gpm, and H is pump head in ft. (from HYSYS).

$$C_B = \exp[9.2951 - 0.6019 * (\ln(S))^2] \qquad \text{(E-24)}$$

where C_B is the base cost of the pump.

Cost of the pump motor is calculated as follows:

$$P_C = \frac{P_T}{\eta_P * \eta_P} = \frac{P_B}{\eta_M} = \frac{Q * H * \rho}{33,000 * \eta_P * \eta_M} \qquad \text{(E-25)}$$

where P_C is the power consumed, P_T is the theoretical pump power, η_P is the pump efficiency, η_M is the electric motor efficiency, and P_B is the pump brake power.

$$\eta_P = -0.316 + 0.24015 * \ln(Q) - 0.01199 * (\ln(Q)^2) \qquad \text{(E-17)}$$

within volumetric flows (Q) between 50 and 5000 gpm:

$$\eta_M = 0.8 + 0.0319 * \ln(P_B) - 0.00182 * (\ln(P_B)^2) \qquad \text{(E-26)}$$

with P_B in a range from 1 to 1500 hp.

Base cost of the pump motor is calculated from:

$$\begin{aligned} C_B = \exp[5.4866 &+ 0.13141 * \ln(P_C) + 0.053255 \qquad \text{(E-27)} \\ &* (\ln(P_C))^2 + 0.028628 * (\ln(P_C))^3 \\ &- 0.0035549 * (\ln(P_C))^4] \end{aligned}$$

where F_T is the motor type factor.

The total base cost of the pump is summation of Equation (E-24) and Equation (E-27) and then is substituted in Equation (E-28)

$$C_P = F_T * F_M * C_B \tag{E-28}$$

where C$_P$ is the purchase cost, F$_T$ is the pump type factor (Table 16.20 from Seider and Warren (2003)) and F$_M$ is the material factor (Table 16.21 from Seider and Warren (2003)).

E.7 Compressors

Cost of the compressor (Seider et al., 2017) is calculated from:

$$S = QH^{0.5} \tag{E-29}$$

where S is the size factor, Q is the volumetric flow, and H is pump head.

$$C_B = \exp[9.2951 - 0.6019 * (\ln(S))^2] \tag{E-30}$$

where C$_B$ is the base cost of the compressor.

Cost of the compressor motor is calculated as follows:

$$P_C = \frac{P_T}{\eta_P * \eta_P} = \frac{P_B}{\eta_M} = \frac{Q * H * \rho}{33,000 * \eta_P * \eta_M} \tag{E-31}$$

where P$_C$ is the power consumed, P$_T$ is the theoretical pump power, η$_P$ is the pump efficiency, η$_M$ is the electric motor efficiency, and P$_B$ is the pump brake power.

$$\eta_P = -0.316 + 0.24015 * \ln(Q) - 0.01199 * (\ln(Q)^2) \tag{E-32}$$

within volumetric flows (Q) between 50 and 5000 gpm:

$$\eta_M = 0.8 + 0.0319 * \ln(P_B) - 0.00182 * (\ln(P_B)^2) \qquad \text{(E-33)}$$

Base cost of the compressor motor is calculated from:

$$C_B = \exp[5.4866 + 0.13141 * \ln(P_C) + 0.053255 \qquad \text{(E-34)}$$
$$* (\ln(P_C))^2 + 0.028628 * (\ln(P_C))^3$$
$$- 0.0035549 * (\ln(P_C))^4]$$

where F_T is the motor type factor.

The total base cost of the pump is summation of Equation (E-30) and Equation (E-34) and then is substituted in Equation (E-35)

$$C_P = F_T * F_M * C_B \qquad \text{(E-35)}$$

where C_P is the purchase cost of the compressor, F_T is the pump type factor (Table 16.20 from Seider and Warren (2003)) and F_M is the material factor (Table 16.21 from Seider and Warren (2003)).

Appendix F   Economic assessments

Table F-1 General parameters

Interest rate, i	0.15
Cost Index, 2018	1.0528
Operating hour	8000
Lang Factor	4.5

The reduction in value of an asset called depreciation (Seider et al., 2017). Most companies prefer to calculate the depreciation at early years of operation, when the production capacity and discount factors are at lowest value (Seider et al., 2017). There are several methods to calculate early depreciation, namely, declining balance (DB), double declining balance (DDB) and sum of years digits (SYD) methods (Seider et al., 2017). As these methods are difficult to be applied, modified accelerant cost recovery system (MACRS) was developed in 1980s (Seider et al., 2017). MACRS combines DB or DDB with straight line depreciation (SL) methods. MACRS calculations are carried out by using the plant class life (Seider et al., 2017). For example, petroleum industry class life equals 7 years. Thus, Table F-2 shows percentages are excluded from the petroleum industry cash flow. More class life and depreciation calculations are available in Seider et al. (2017).

Table F-2 Depreciation each year

Year	%
1	14.29
2	24.49
3	17.49
4	12.49
5	8.93
6	8.92
7	8.93
8	4.46

F.1 Cash flow calculations for superstructure process using Pt/Al$_2$O$_3$-CCl$_4$ catalyst

Table F-3 Equipment cost

Equipment	SMB Cost, $	DIS Cost, $	AHP Cost, $	VRC Cost, $	BF Cost, $
Stabilizer column	5.98E+05	5.98E+05	5.98E+05	5.98E+05	5.98E+05
Reactor	3.69E+04	3.69E+04	3.69E+04	3.69E+04	3.69E+04
Catalyst	1.93E+06	1.93E+06	1.93E+06	1.93E+06	1.93E+06
Air cooler	2.14E+06	5.58E+06	4.07E+06	5.07E+06	2.98E+06
Heat exchangers	2.31E+05	2.13E+05	2.15E+05	2.14E+05	2.15E+05
Flash drum	2.55E+04	2.55E+04	2.55E+04	2.55E+04	2.55E+04
Pumps	2.04E+04	2.04E+04	2.04E+04	2.04E+04	2.04E+04
Compressors	6.29E+05	1.01E+06	1.08E+06	1.08E+06	1.08E+06
Adsorption	4.22E+04	--	--	--	--
Adsorbent	5.74E+06	--	--	--	--
Distillation unit	--	1.42E+05	9.20E+06	2.01E+06	4.82E+06
Total Equipment cost ($)	5.40E+07	4.53E+07	8.14E+07	5.21E+07	5.55E+07

Table F-4 Material prices and cost

Raw material	Amount/h	$/Amount
Hydrogen	Kg/h	3.6
Light Naphtha	Kg/h	0.628
Products		
Light gases	Kg/h	15
Gasoline	M^3/h	756.64
Hydrogen	Kg/h	3.6
Utilities		
Medium Pressure steam	Kg/h	5.00E-02
Cooling water	Kg/h	6.70E-05
Electricity	Kw/h	0.15

Table F-5 Material prices and cost for each scenario

	SMB		DIS		AHP	
Raw material	Amount/h	Cost $/y	Amount/h	Cost $/y	Amount/h	Cost $/y
Hydrogen	1021.5	2.94E+07	1021.5	2.94E+07	1021.5	2.94E+07
Light Naphtha	46000.0	2.31E+08	4.60E+04	2.31E+08	4.60E+04	2.31E+08
Products						
Light gases	1672.3	2.01E+08	1672.3	2.01E+08	1672.26	2.01E+08
Gasoline	29.2	1.78E+08	29.23	1.64E+08	29.23	1.64E+08
Hydrogen	84.5	2.43E+06	84.5	2.43E+06	84.47	2.43E+06
Utilities						
Medium Pressure steam	8396.0	3.36E+06	1.08E+05	4.34E+07	1.08E+04	4.30E+06
Cooling water	4913.0	2.63E+03	1.25E+05	6.70E+01	5.25E+03	2.81E+00
Electricity	1703.5	2.04E+06	1458.15	1.75E+06	1949.75	2.34E+06
Catalyst		8.47E+05		8.47E+05		8.47E+05
Adsorbent		1.71E+06		0.00E+00		0.00E+00
Total		2.68E8		3.06E+08		2.68E+08

Table F-6 Material prices and cost for each scenario (continue)

	VRC		BF	
Raw material	Amount/h	Cost $/y	Amount/h	Cost $/y
Hydrogen	1021.5	2.94E+07	1021.5	2.94E+07
Light Naphtha	4.60E+04	2.31E+08	4.60E+04	2.31E+08
Products				
Light gases	1672.29	2.01E+08	1672.3	2.01E+08
Gasoline	29.23	1.64E+08	29.23	1.64E+08
Hydrogen	84.46	2.43E+06	84.46	2.43E+06
Utilities				
Medium Pressure steam	8.35E+03	3.34E+06	8.25E+03	3.30E+06
Cooling water	4.92E+03	2.63E+00	4.91E+03	2.63E+00
Electricity	15694.15	1.88E+07	19010.75	2.28E+07
Catalyst		8.47E+05		8.47E+05
Adsorbent		0.00E+00		0.00E+00
Total		2.84E+08		2.87E+08

Table F-7 Economic calculations summary

		SMB	DIS	AHP
Variable cost				
Selling/Transfer expenses	0.01	3.81E+06	3.67E+06	3.67E+06
Direct Research	0.048	1.83E+07	1.76E+07	1.76E+07
Allocated research	0.005	1.90E+06	1.84E+06	1.84E+06
Administrative Expense	0.02	7.62E+06	7.34E+06	7.34E+06
Management Incentive Compensation	0.0125	4.76E+06	4.59E+06	4.59E+06
	0.0955	3.64E+07	3.51E+07	3.51E+07
Total variable cost		**3.05E+08**	**3.42E+08**	**3.03E+08**
Fixed cost				
Operations				
Operators/shift	5			
Direct wages	40	4.16E+05	4.16E+05	4.16E+05
Direct salaries	0.15	6.24E+04	6.24E+04	6.24E+04
Operating supplies	0.06	2.50E+04	2.50E+04	2.50E+04
Technical Assistance	6.00E0+7	3.00E+05	3.00E+05	3.00E+05
Control laboratory	6.50E+07	3.25E+05	3.25E+05	3.25E+05
		1.13E+06	1.13E+06	1.13E+06
Maintenance				
Wages	0.035	2.45E+06	2.06E+06	3.70E+06
Salaries	0.25	6.13E+05	5.14E+05	9.25E+05
Materials and services	1	2.45E+06	2.06E+06	3.70E+06
Maintenance overhead	0.05	1.23E+05	1.03E+05	1.85E+05
		5.64E+06	4.73E+06	8.51E+06
Operating overhead	0.228	8.08E+05	6.95E+05	1.16E+06
Property taxes and insurance	0.02	1.40E+06	1.17E+06	2.11E+06
		8.97E+06	7.73E+06	1.29E+07

Table F-8 Economic calculations summary (continue)

		VRC	BF
Variable cost			
Selling/Transfer expenses	0.01	3.67E+08	3.67E+08
Direct Research	0.048	3.67E+06	3.67E+06
Allocated research	0.005	1.76E+07	1.76E+07
Administrative Expense	0.02	1.84E+06	1.84E+06
Management Incentive Compensation	0.0125	7.34E+06	7.34E+06
	0.0955	4.59E+06	4.59E+06
Total variable cost		**3.19E+08**	**3.23E+08**
Fixed cost			
Operations			
Operators/shift	5		
Direct wages	40	4.16E+05	4.16E+05
Direct salaries	0.15	6.24E+04	6.24E+04
Operating supplies	0.06	2.50E+04	2.50E+04
Technical Assistance	6.00E0+7	3.00E+05	3.00E+05
Control laboratory	6.50E+07	3.25E+05	3.25E+05
		1.13E+06	1.13E+06
Maintenance			
Wages	0.035	2.37E+06	2.52E+06
Salaries	0.25	5.91E+05	6.30E+05
Materials and services	1	2.37E+06	2.52E+06
Maintenance overhead	0.05	1.18E+05	1.26E+05
		5.44E+06	5.80E+06
Operating overhead	0.228	7.83E+05	8.27E+05
Property taxes and insurance	0.02	1.35E+06	1.44E+06
		8.70E+06	9.19E+06

Table F-9 Investment summary

Total Permanent investment		SMB	DIS	AHP
Cost of site preparation	0.05	2.70E+06	2.26E+06	4.07E+06
Cost of service facilities	0.05	2.70E+06	2.26E+06	4.07E+06
Cost of contingencies and constructor fees	0.18	1.07E+07	8.96E+06	1.61E+07
Cost of land	0.02	1.40E+06	1.17E+06	2.11E+06
Cost of plant start-up	0.1	7.00E+06	5.87E+06	1.06E+07
		7.84E+07	6.58E+07	1.18E+08
Working capital	0.15	1.38E+07	1.16E+07	2.09E+07
Total capital investment		9.23E+07	7.74E+07	1.39E+08

Table F-10 Investment summary (continue)

Total Permanent investment		VRC	BF
Cost of site preparation	0.05	2.60E+06	2.77E+06
Cost of service facilities	0.05	2.60E+06	2.77E+06
Cost of contingencies and constructor fees	0.18	1.03E+07	1.10E+07
Cost of land	0.02	1.35E+06	1.44E+06
Cost of plant start-up	0.1	6.76E+06	7.20E+06
		7.57E+07	8.06E+07
Working capital	0.15	1.34E+07	1.42E+07
Total capital investment		8.91E+07	9.49E+07

Table F-11 Cash flow summary for SMB

Year	Capacity	Sales	Capital cost	Working capital	Var. Cost	Fixed cost	Depreciation
2018	0						
2019	0		-9.23E+07	1.38E+07			
2020	0.45	1.71E+08			-1.37E+08	-8.97E+06	-1.00E+07
2021	0.68	2.59E+08			-2.07E+08	-8.97E+06	-1.72E+07
2022	1	3.81E+08			-3.05E+08	-8.97E+06	-1.22E+07
2023	1	3.81E+08			-3.05E+08	-8.97E+06	-8.75E+06
2024	1	3.81E+08			-3.05E+08	-8.97E+06	-6.25E+06
2025	1	3.81E+08			-3.05E+08	-8.97E+06	-6.25E+06
2026	1	3.81E+08			-3.05E+08	-8.97E+06	-6.25E+06
2027	1	3.81E+08			-3.05E+08	-8.97E+06	-3.12E+06
2028	1	3.81E+08			-3.05E+08	-8.97E+06	
2029	1	3.81E+08			-3.05E+08	-8.97E+06	
2030	1	3.81E+08			-3.05E+08	-8.97E+06	
2031	1	3.81E+08			-3.05E+08	-8.97E+06	
2032	1	3.81E+08			-3.05E+08	-8.97E+06	
2033	1	3.81E+08			-3.05E+08	-8.97E+06	
2034	1	3.81E+08			-3.05E+08	-8.97E+06	
2035	1	3.81E+08			-3.05E+08	-8.97E+06	
2036	1	3.81E+08			-3.05E+08	-8.97E+06	
2037	1	3.81E+08			-3.05E+08	-8.97E+06	
2038	1	3.81E+08		-1.38E+07	-3.05E+08	-8.97E+06	

Table F-12 Cash flow summary for SMB (continue)

Year	Taxale income	Taxes	Net Earning	Cash flow	Cumulative NPV
2018				0	0
2019				-7.84E+07	-6.82E+07
2020	1.53E+07	-3.05E+06	1.83E+07	2.22E+07	-5.14E+07
2021	2.56E+07	-5.12E+06	3.07E+07	3.76E+07	-2.67E+07
2022	5.49E+07	-1.10E+07	6.59E+07	5.62E+07	5.45E+06
2023	5.84E+07	-1.17E+07	7.01E+07	5.55E+07	3.30E+07
2024	6.09E+07	-1.22E+07	7.30E+07	5.50E+07	5.68E+07
2025	6.09E+07	-1.22E+07	7.31E+07	5.50E+07	7.74E+07
2026	6.09E+07	-1.22E+07	7.30E+07	5.50E+07	9.54E+07
2027	6.40E+07	-1.28E+07	7.68E+07	5.43E+07	1.11E+08
2028	6.71E+07	-1.34E+07	8.06E+07	5.37E+07	1.24E+08
2029	6.71E+07	-1.34E+07	8.06E+07	5.37E+07	1.36E+08
2030	6.71E+07	-1.34E+07	8.06E+07	5.37E+07	1.46E+08
2031	6.71E+07	-1.34E+07	8.06E+07	5.37E+07	1.54E+08
2032	6.71E+07	-1.34E+07	8.06E+07	5.37E+07	1.62E+08
2033	6.71E+07	-1.34E+07	8.06E+07	5.37E+07	1.69E+08
2034	6.71E+07	-1.34E+07	8.06E+07	5.37E+07	1.74E+08
2035	6.71E+07	-1.34E+07	8.06E+07	5.37E+07	1.79E+08
2036	6.71E+07	-1.34E+07	8.06E+07	5.37E+07	1.84E+08
2037	6.71E+07	-1.34E+07	8.06E+07	5.37E+07	1.87E+08
2038	6.71E+07	-1.34E+07	8.06E+07	3.99E+07	1.90E+08

Table F-13 Cash flow summary for DIS

Year	Capacity	Sales	Capital cost	Working capital	Var.cost	Fixed cost	Depreciation
2018	0						
2019	0		-7.74E+07	1.16E+07			
2020	0.45	1.65E+08			-1.54E+08	-7.73E+06	-8.39E+06
2021	0.68	2.50E+08			-2.32E+08	-7.73E+06	-1.44E+07
2022	1	3.67E+08			-3.42E+08	-7.73E+06	-1.03E+07
2023	1	3.67E+08			-3.42E+08	-7.73E+06	-7.34E+06
2024	1	3.67E+08			-3.42E+08	-7.73E+06	-5.25E+06
2025	1	3.67E+08			-3.42E+08	-7.73E+06	-5.24E+06
2026	1	3.67E+08			-3.42E+08	-7.73E+06	-5.25E+06
2027	1	3.67E+08			-3.42E+08	-7.73E+06	-2.62E+06
2028	1	3.67E+08			-3.42E+08	-7.73E+06	
2029	1	3.67E+08			-3.42E+08	-7.73E+06	
2030	1	3.67E+08			-3.42E+08	-7.73E+06	
2031	1	3.67E+08			-3.42E+08	-7.73E+06	
2032	1	3.67E+08			-3.42E+08	-7.73E+06	
2033	1	3.67E+08			-3.42E+08	-7.73E+06	
2034	1	3.67E+08			-3.42E+08	-7.73E+06	
2035	1	3.67E+08			-3.42E+08	-7.73E+06	
2036	1	3.67E+08			-3.42E+08	-7.73E+06	
2037	1	3.67E+08			-3.42E+08	-7.73E+06	
2038	1	3.67E+08		-1.16E+07	-3.42E+08	-7.73E+06	

Table F-14 Cash flow summary for DIS (continue)

Year	Taxale income	Taxes	Net Earning	Cash flow	Cumulative NPV
2018				0	0.00E+00
2019		2.00E-01		-6.58E+07	-5.72E+07
2020	-4.63E+06	9.25E+05	-5.55E+06	4.69E+06	-5.37E+07
2021	-4.74E+06	9.48E+05	-5.69E+06	1.06E+07	-4.67E+07
2022	7.54E+06	-1.51E+06	9.05E+06	1.63E+07	-3.74E+07
2023	1.05E+07	-2.10E+06	1.26E+07	1.57E+07	-2.96E+07
2024	1.26E+07	-2.51E+06	1.51E+07	1.53E+07	-2.29E+07
2025	1.26E+07	-2.52E+06	1.51E+07	1.53E+07	-1.72E+07
2026	1.26E+07	-2.51E+06	1.51E+07	1.53E+07	-1.22E+07
2027	1.52E+07	-3.04E+06	1.82E+07	1.48E+07	-7.98E+06
2028	1.78E+07	-3.56E+06	2.14E+07	1.43E+07	-4.46E+06
2029	1.78E+07	-3.56E+06	2.14E+07	1.43E+07	-1.39E+06
2030	1.78E+07	-3.56E+06	2.14E+07	1.43E+07	1.27E+06
2031	1.78E+07	-3.56E+06	2.14E+07	1.43E+07	3.59E+06
2032	1.78E+07	-3.56E+06	2.14E+07	1.43E+07	5.60E+06
2033	1.78E+07	-3.56E+06	2.14E+07	1.43E+07	7.36E+06
2034	1.78E+07	-3.56E+06	2.14E+07	1.43E+07	8.88E+06
2035	1.78E+07	-3.56E+06	2.14E+07	1.43E+07	1.02E+07
2036	1.78E+07	-3.56E+06	2.14E+07	1.43E+07	1.14E+07
2037	1.78E+07	-3.56E+06	2.14E+07	1.43E+07	1.24E+07
2038	1.78E+07	-3.56E+06	2.14E+07	2.64E+06	1.25E+07

Table F-15 Cash flow summary for AHP

Year	Capacity	Sales	Capital cost	Working capital	Var.cost	Fixed cost	Depreciation
2018	0						
2019	0		-1.39E+08	2.09E+07			
2020	0.45	1.65E+08			-1.36E+08	-1.29E+07	-1.51E+07
2021	0.68	2.50E+08			-2.06E+08	-1.29E+07	-2.59E+07
2022	1	3.67E+08			-3.03E+08	-1.29E+07	-1.85E+07
2023	1	3.67E+08			-3.03E+08	-1.29E+07	-1.32E+07
2024	1	3.67E+08			-3.03E+08	-1.29E+07	-9.44E+06
2025	1	3.67E+08			-3.03E+08	-1.29E+07	-9.43E+06
2026	1	3.67E+08			-3.03E+08	-1.29E+07	-9.44E+06
2027	1	3.67E+08			-3.03E+08	-1.29E+07	-4.71E+06
2028	1	3.67E+08			-3.03E+08	-1.29E+07	
2029	1	3.67E+08			-3.03E+08	-1.29E+07	
2030	1	3.67E+08			-3.03E+08	-1.29E+07	
2031	1	3.67E+08			-3.03E+08	-1.29E+07	
2032	1	3.67E+08			-3.03E+08	-1.29E+07	
2033	1	3.67E+08			-3.03E+08	-1.29E+07	
2034	1	3.67E+08			-3.03E+08	-1.29E+07	
2035	1	3.67E+08			-3.03E+08	-1.29E+07	
2036	1	3.67E+08			-3.03E+08	-1.29E+07	
2037	1	3.67E+08			-3.03E+08	-1.29E+07	
2038	1	3.67E+08		-2.09E+07	-3.03E+08	-1.29E+07	

Table F-16 Cash flow summary for AHP (continue)

Year	Taxale income	Taxes	Net Earning	Cash flow	Cumulative NPV
2018				0	0
2019		2.00E-01		-1.18E+08	-1.03E+08
2020	7.87E+05	-1.57E+05	9.44E+05	1.57E+07	-9.10E+07
2021	4.73E+06	-9.46E+05	5.67E+06	2.97E+07	-7.15E+07
2022	3.26E+07	-6.52E+06	3.91E+07	4.46E+07	-4.60E+07
2023	3.79E+07	-7.58E+06	4.55E+07	4.35E+07	-2.44E+07
2024	4.17E+07	-8.33E+06	5.00E+07	4.28E+07	-5.92E+06
2025	4.17E+07	-8.33E+06	5.00E+07	4.28E+07	1.02E+07
2026	4.17E+07	-8.33E+06	5.00E+07	4.28E+07	2.41E+07
2027	4.64E+07	-9.28E+06	5.57E+07	4.18E+07	3.60E+07
2028	5.11E+07	-1.02E+07	6.13E+07	4.09E+07	4.61E+07
2029	5.11E+07	-1.02E+07	6.13E+07	4.09E+07	5.49E+07
2030	5.11E+07	-1.02E+07	6.13E+07	4.09E+07	6.25E+07
2031	5.11E+07	-1.02E+07	6.13E+07	4.09E+07	6.92E+07
2032	5.11E+07	-1.02E+07	6.13E+07	4.09E+07	7.50E+07
2033	5.11E+07	-1.02E+07	6.13E+07	4.09E+07	8.00E+07
2034	5.11E+07	-1.02E+07	6.13E+07	4.09E+07	8.44E+07
2035	5.11E+07	-1.02E+07	6.13E+07	4.09E+07	8.82E+07
2036	5.11E+07	-1.02E+07	6.13E+07	4.09E+07	9.15E+07
2037	5.11E+07	-1.02E+07	6.13E+07	4.09E+07	9.43E+07
2038	5.11E+07	-1.02E+07	6.13E+07	2.00E+07	9.56E+07

Table F-17 Cash flow summary for VRC

Year	Capacity	Sales	Capital cost	Working capital	Var.cost	Fixed cost	Depreciation
2018	0						
2019	0		-8.91E+07	1.34E+07			
2020	0.45	1.65E+08			-1.43E+08	-8.70E+06	-9.66E+06
2021	0.68	2.50E+08			-2.17E+08	-8.70E+06	-1.66E+07
2022	1	3.67E+08			-3.19E+08	-8.70E+06	-1.18E+07
2023	1	3.67E+08			-3.19E+08	-8.70E+06	-8.44E+06
2024	1	3.67E+08			-3.19E+08	-8.70E+06	-6.04E+06
2025	1	3.67E+08			-3.19E+08	-8.70E+06	-6.03E+06
2026	1	3.67E+08			-3.19E+08	-8.70E+06	-6.04E+06
2027	1	3.67E+08			-3.19E+08	-8.70E+06	-3.01E+06
2028	1	3.67E+08			-3.19E+08	-8.70E+06	
2029	1	3.67E+08			-3.19E+08	-8.70E+06	
2030	1	3.67E+08			-3.19E+08	-8.70E+06	
2031	1	3.67E+08			-3.19E+08	-8.70E+06	
2032	1	3.67E+08			-3.19E+08	-8.70E+06	
2033	1	3.67E+08			-3.19E+08	-8.70E+06	
2034	1	3.67E+08			-3.19E+08	-8.70E+06	
2035	1	3.67E+08			-3.19E+08	-8.70E+06	
2036	1	3.67E+08			-3.19E+08	-8.70E+06	
2037	1	3.67E+08			-3.19E+08	-8.70E+06	
2038	1	3.67E+08		-1.34E+07	-3.19E+08	-8.70E+06	

Table F-18 Cash flow summary for VRC (continue)

Year	Taxale income	Taxes	Net Earning	Cash flow	Cumulative NPV
2018				0	0
2019		2.00E-01		-7.57E+07	-6.58E+07
2020	3.45E+06	-6.90E+05	4.14E+06	1.24E+07	-5.64E+07
2021	7.71E+06	-1.54E+06	9.25E+06	2.27E+07	-4.15E+07
2022	2.80E+07	-5.59E+06	3.35E+07	3.42E+07	-2.20E+07
2023	3.13E+07	-6.27E+06	3.76E+07	3.35E+07	-5.29E+06
2024	3.37E+07	-6.75E+06	4.05E+07	3.30E+07	8.98E+06
2025	3.37E+07	-6.75E+06	4.05E+07	3.30E+07	2.14E+07
2026	3.37E+07	-6.75E+06	4.05E+07	3.30E+07	3.22E+07
2027	3.68E+07	-7.35E+06	4.41E+07	3.24E+07	4.14E+07
2028	3.98E+07	-7.96E+06	4.77E+07	3.18E+07	4.93E+07
2029	3.98E+07	-7.96E+06	4.77E+07	3.18E+07	5.61E+07
2030	3.98E+07	-7.96E+06	4.77E+07	3.18E+07	6.21E+07
2031	3.98E+07	-7.96E+06	4.77E+07	3.18E+07	6.72E+07
2032	3.98E+07	-7.96E+06	4.77E+07	3.18E+07	7.17E+07
2033	3.98E+07	-7.96E+06	4.77E+07	3.18E+07	7.56E+07
2034	3.98E+07	-7.96E+06	4.77E+07	3.18E+07	7.90E+07
2035	3.98E+07	-7.96E+06	4.77E+07	3.18E+07	8.20E+07
2036	3.98E+07	-7.96E+06	4.77E+07	3.18E+07	8.46E+07
2037	3.98E+07	-7.96E+06	4.77E+07	3.18E+07	8.68E+07
2038	3.98E+07	-7.96E+06	4.77E+07	1.85E+07	8.79E+07

Table F-19 Cash flow summary for BF

Year	Capacity	Sales	Capital cost	Working capital	Var. Cost	Fixed cost	Depreciation
2018	0						
2019	0		-9.49E+07	1.42E+07			
2020	0.45	1.65E+08			-1.45E+08	-9.19E+06	-1.03E+07
2021	0.68	2.50E+08			-2.19E+08	-9.19E+06	-1.76E+07
2022	1	3.67E+08			-3.23E+08	-9.19E+06	-1.26E+07
2023	1	3.67E+08			-3.23E+08	-9.19E+06	-8.99E+06
2024	1	3.67E+08			-3.23E+08	-9.19E+06	-6.43E+06
2025	1	3.67E+08			-3.23E+08	-9.19E+06	-6.42E+06
2026	1	3.67E+08			-3.23E+08	-9.19E+06	-6.43E+06
2027	1	3.67E+08			-3.23E+08	-9.19E+06	-3.21E+06
2028	1	3.67E+08			-3.23E+08	-9.19E+06	
2029	1	3.67E+08			-3.23E+08	-9.19E+06	
2030	1	3.67E+08			-3.23E+08	-9.19E+06	
2031	1	3.67E+08			-3.23E+08	-9.19E+06	
2032	1	3.67E+08			-3.23E+08	-9.19E+06	
2033	1	3.67E+08			-3.23E+08	-9.19E+06	
2034	1	3.67E+08			-3.23E+08	-9.19E+06	
2035	1	3.67E+08			-3.23E+08	-9.19E+06	
2036	1	3.67E+08			-3.23E+08	-9.19E+06	
2037	1	3.67E+08			-3.23E+08	-9.19E+06	
2038	1	3.67E+08		-1.42E+07	-3.23E+08	-9.19E+06	

Table F-20 Cash flow summary for BF (continue)

Year	Taxale income	Taxes	Net Earning	Cash flow	Cumulative NPV
2018				0	0
2019		2.00E-01		-8.06E+07	-7.01E+07
2020	5.61E+05	-1.12E+05	6.73E+05	1.07E+07	-6.20E+07
2021	3.46E+06	-6.92E+05	4.15E+06	2.04E+07	-4.86E+07
2022	2.28E+07	-4.55E+06	2.73E+07	3.08E+07	-3.10E+07
2023	2.64E+07	-5.27E+06	3.16E+07	3.01E+07	-1.60E+07
2024	2.89E+07	-5.78E+06	3.47E+07	2.96E+07	-3.25E+06
2025	2.89E+07	-5.79E+06	3.47E+07	2.96E+07	7.86E+06
2026	2.89E+07	-5.78E+06	3.47E+07	2.96E+07	1.75E+07
2027	3.21E+07	-6.43E+06	3.86E+07	2.89E+07	2.58E+07
2028	3.53E+07	-7.07E+06	4.24E+07	2.83E+07	3.27E+07
2029	3.53E+07	-7.07E+06	4.24E+07	2.83E+07	3.88E+07
2030	3.53E+07	-7.07E+06	4.24E+07	2.83E+07	4.41E+07
2031	3.53E+07	-7.07E+06	4.24E+07	2.83E+07	4.87E+07
2032	3.53E+07	-7.07E+06	4.24E+07	2.83E+07	5.27E+07
2033	3.53E+07	-7.07E+06	4.24E+07	2.83E+07	5.62E+07
2034	3.53E+07	-7.07E+06	4.24E+07	2.83E+07	5.92E+07
2035	3.53E+07	-7.07E+06	4.24E+07	2.83E+07	6.18E+07
2036	3.53E+07	-7.07E+06	4.24E+07	2.83E+07	6.41E+07
2037	3.53E+07	-7.07E+06	4.24E+07	2.83E+07	6.61E+07
2038	3.53E+07	-7.07E+06	4.24E+07	1.40E+07	6.70E+07

F.2 Cash flow calculations for superstructure process using Pt/SO₄–ZrO₂ catalyst

Table F-21 Equipment cost

	SMB	DIS	AHP	VRC	BF
Equipment	Cost, $	Cost, $	Cost, $	Cost, $	Cost, $
Stabilizer column	5.98E+05	5.98E+05	5.98E+05	5.98E+05	5.98E+05
Reactor	3.69E+04	3.69E+04	3.69E+04	3.69E+04	3.69E+04
Catalyst	9.67E+05	9.67E+05	9.67E+05	9.67E+05	9.67E+05
Air cooler	2.14E+06	5.58E+06	4.07E+06	5.07E+06	2.98E+06
Heat exchangers	2.31E+05	2.13E+05	2.15E+05	2.14E+05	2.15E+05
Flash drum	2.55E+04	2.55E+04	2.55E+04	2.55E+04	2.55E+04
Pumps	2.04E+04	2.04E+04	2.04E+04	2.04E+04	2.04E+04
Compressors	6.29E+05	1.01E+06	1.08E+06	1.08E+06	1.08E+06
Adsorption	4.22E+04	--	--	--	--
Adsorbent	5.74E+06	--	--	--	--
Distillation unit	--	1.42E+05	5.36E+06	2.01E+06	4.82E+06
Total Equipment cost ($)	4.94E+07	4.07E+07	5.86E+07	4.75E+07	5.09E+07

Table F-22 Material/ utilities prices and cost

Raw material	Amount/h	$/Amount
Hydrogen	Kg/h	3.6
Light Naphtha	Kg/h	0.628
Products		
Light gases	Kg/h	15
Gasoline	M³/h	756.64
Hydrogen	Kg/h	3.6
Utilities		
Medium Pressure steam	Kg/h	5.00E-02
Cooling water	Kg/h	6.70E-05
Electricity	Kw/h	0.15

Table F-23 Material prices and cost for each scenarios

Raw material	SMB Amount/h	SMB Cost $/y	DIS Amount/h	DIS Cost $/y	AHP Amount/h	AHP Cost $/y
Hydrogen	1021.5	2.94E+07	1021.5	2.94E+07	1021.5	2.94E+07
Light Naphtha	4.60E+04	2.31E+08	4.60E+04	2.31E+08	4.60E+04	2.31E+08
Products						
Light gases	1672.29	2.01E+08	1672.294	2.01E+08	1672.258	2.01E+08
Gasoline	29.23	1.77E+08	29.23052	1.59E+08	29.23052	1.59E+08
Hydrogen	84.48	2.43E+06	84.46291	2.43E+06	84.46839	2.43E+06
Utilities						
Medium Pressure steam	1.53E+04	6.13E+06	9.83E+04	3.93E+07	1.77E+04	7.09E+06
Cooling water	4.93E+03	2.64E+03	1.25E+05	6.70E+01	5.28E+03	2.83E+00
Electricity	1703.51	2.04E+06	1458.15	1.75E+06	1949.75	2.34E+06
Catalyst		3.39E+05		3.39E+05		3.39E+05
Adsorbent		1.71E+06		0.00E+00		0.00E+00
		2.71E+08		**3.02E+08**		**2.70E+08**

Table F-24 Material prices and cost for each scenarios (continue)

Raw material	VRC Amount/h	VRC Cost $/y	BF Amount/h	BF Cost $/y
Hydrogen	1021.5	2.94E+07	1021.5	2.94E+07
Light Naphtha	4.60E+04	2.31E+08	4.60E+04	2.31E+08
Products				
Light gases	1672.294	2.01E+08	1672.294	2.01E+08
Gasoline	29.23052	1.59E+08	29.23052	1.59E+08
Hydrogen	84.46291	2.43E+06	84.46291	2.43E+06
Utilities				
Medium Pressure steam	1.53E+04	6.13E+06	1.53E+04	6.13E+06
Cooling water	4.92E+03	2.63E+00	4.93E+03	2.64E+00
Electricity	15694.15	1.88E+07	19010.75	2.28E+07
Catalyst		3.39E+05		3.39E+05
Adsorbent		0.00E+00		0.00E+00
		2.86E+08		**2.90E+08**

Table F-25 Economic calculations summary

		SMB	DIS	AHP
Variable cost		Cost $/y	Cost $/y	Cost $/y
Selling/Transfer expenses	0.01	3.80E+06	3.62E+06	3.62E+08
Direct Research	0.048	1.82E+07	1.74E+07	3.62E+06
Allocated research	0.005	1.90E+06	1.81E+06	1.74E+07
Administrative Expense	0.02	7.60E+06	7.25E+06	1.81E+06
Management Incentive Compensation	0.0125	4.75E+06	4.53E+06	7.25E+06
	0.0955	**3.63E+07**	**3.46E+07**	4.53E+06
Total variable cost		**3.07E+08**	**3.37E+08**	**3.05E+08**
Fixed cost				
Operations				
Operators/shift	5			
Direct wages	40	4.16E+05	4.16E+05	4.16E+05
Direct salaries	0.15	6.24E+04	6.24E+04	6.24E+04
Operating supplies	0.06	2.50E+04	2.50E+04	2.50E+04
Technical Assistance	6.00E0+7	3.00E+05	3.00E+05	3.00E+05
Control laboratory	6.50E+07	3.25E+05	3.25E+05	3.25E+05
		1.13E+06	1.13E+06	1.13E+06
Maintenance				
Wages	0.035	2.24E+06	1.85E+06	2.66E+06
Salaries	0.25	5.61E+05	4.62E+05	6.66E+05
Materials and services	1	2.24E+06	1.85E+06	2.66E+06
Maintenance overhead	0.05	1.12E+05	9.24E+04	1.33E+05
		5.16E+06	4.25E+06	6.12E+06
Operating overhead	0.228	7.48E+05	6.36E+05	8.68E+05
Property taxes and insurance	0.02	1.28E+06	1.06E+06	1.52E+06
		8.32E+06	**7.07E+06**	**9.64E+06**

Table F-26 Economic calculations summary (continue)

		VRC	BF
Variable cost		Cost $/y	Cost $/y
Selling/Transfer expenses	0.01	3.62E+08	3.62E+08
Direct Research	0.048	3.62E+06	3.62E+06
Allocated research	0.005	1.74E+07	1.74E+07
Administrative Expense	0.02	1.81E+06	1.81E+06
Management Incentive Compensation	0.0125	7.25E+06	7.25E+06
	0.0955	4.53E+06	3.46E+07
Total variable cost		**3.20E+08**	**3.24E+8**
Fixed cost			
Operations			
Operators/shift	5		
Direct wages	40	4.16E+05	4.16E+05
Direct salaries	0.15	6.24E+04	6.24E+04
Operating supplies	0.06	2.50E+04	2.50E+04
Technical Assistance	6.00E0+7	3.00E+05	3.00E+05
Control laboratory	6.50E+07	3.25E+05	3.25E+05
		1.13E+06	1.13E+06
Maintenance			
Wages	0.035	2.16E+06	2.31E+06
Salaries	0.25	5.39E+05	5.78E+05
Materials and services	1	2.16E+06	2.31E+06
Maintenance overhead	0.05	1.08E+05	1.16E+05
		4.96E+06	5.32E+06
Operating overhead	0.228	7.24E+05	7.68E+05
Property taxes and insurance	0.02	1.23E+06	1.32E+06
		8.05E+06	**8.54E+06**

Table F-27 Investment summary

Total Permanent investment		SMB	DIS	AHP
		Cost $/y	Cost $/y	Cost $/y
Cost of site preparation	0.05	2.47E+06	2.03E+06	2.93E+06
Cost of service facilities	0.05	2.47E+06	2.03E+06	2.93E+06
Cost of contingencies and constructor fees	0.18	9.78E+06	8.05E+06	1.16E+07
Cost of land	0.02	1.28E+06	1.06E+06	1.52E+06
Cost of plant start-up	0.1	6.41E+06	5.28E+06	7.61E+06
		7.18E+07	**5.91E+07**	**8.52E+07**
Working capital	0.15	**1.27E+07**	**1.04E+07**	**1.50E+07**
Total capital investment		**8.44E+07**	**6.96E+07**	**1.00E+08**

Table F-28 Investment summary (continue)

Total Permanent investment		VRC	BF
		Cost $/y	Cost $/y
Cost of site preparation	0.05	2.37E+06	2.54E+06
Cost of service facilities	0.05	2.37E+06	2.54E+06
Cost of contingencies and constructor fees	0.18	9.40E+06	1.01E+07
Cost of land	0.02	1.23E+06	1.32E+06
Cost of plant start-up	0.1	6.16E+06	6.61E+06
		6.90E+07	**7.40E+07**
Working capital	0.15	**1.22E+07**	**1.31E+07**
Total capital investment		**8.12E+07**	**8.70E+07**

Table F-29 Cash flow summary for SMB

Year	Capacity	Sales	Capital cost	Working capital	Var. Cost	Fixed cost	Depreciation
2018	0						
2019	0		-8.44E+07	1.27E+07			
2020	0.45	1.71E+08			-1.38E+08	-8.32E+06	-9.16E+06
2021	0.68	2.58E+08			-2.09E+08	-8.32E+06	-1.57E+07
2022	1	3.80E+08			-3.07E+08	-8.32E+06	-1.12E+07
2023	1	3.80E+08			-3.07E+08	-8.32E+06	-8.00E+06
2024	1	3.80E+08			-3.07E+08	-8.32E+06	-5.72E+06
2025	1	3.80E+08			-3.07E+08	-8.32E+06	-5.72E+06
2026	1	3.80E+08			-3.07E+08	-8.32E+06	-5.72E+06
2027	1	3.80E+08			-3.07E+08	-8.32E+06	-2.86E+06
2028	1	3.80E+08			-3.07E+08	-8.32E+06	
2029	1	3.80E+08			-3.07E+08	-8.32E+06	
2030	1	3.80E+08			-3.07E+08	-8.32E+06	
2031	1	3.80E+08			-3.07E+08	-8.32E+06	
2032	1	3.80E+08			-3.07E+08	-8.32E+06	
2033	1	3.80E+08			-3.07E+08	-8.32E+06	
2034	1	3.80E+08			-3.07E+08	-8.32E+06	
2035	1	3.80E+08			-3.07E+08	-8.32E+06	
2036	1	3.80E+08			-3.07E+08	-8.32E+06	
2037	1	3.80E+08			-3.07E+08	-8.32E+06	
2038	1	3.80E+08		-1.27E+07	-3.07E+08	-8.32E+06	

Table F-30 Cash flow summary for SMB (continue)

Year	Taxale income	Taxes	Net Earning	Cash flow	Cumulative NPV
2018				0	0
2019				-7.18E+07	-6.24E+07
2020	1.54E+07	-3.08E+06	1.85E+07	2.15E+07	-4.62E+07
2021	2.56E+07	-5.13E+06	3.08E+07	3.62E+07	-2.24E+07
2022	5.35E+07	-1.07E+07	6.42E+07	5.40E+07	8.48E+06
2023	5.67E+07	-1.13E+07	6.80E+07	5.34E+07	3.50E+07
2024	5.90E+07	-1.18E+07	7.08E+07	5.29E+07	5.79E+07
2025	5.90E+07	-1.18E+07	7.08E+07	5.29E+07	7.78E+07
2026	5.90E+07	-1.18E+07	7.08E+07	5.29E+07	9.50E+07
2027	6.18E+07	-1.24E+07	7.42E+07	5.23E+07	1.10E+08
2028	6.47E+07	-1.29E+07	7.76E+07	5.17E+07	1.23E+08
2029	6.47E+07	-1.29E+07	7.76E+07	5.17E+07	1.34E+08
2030	6.47E+07	-1.29E+07	7.76E+07	5.17E+07	1.44E+08
2031	6.47E+07	-1.29E+07	7.76E+07	5.17E+07	1.52E+08
2032	6.47E+07	-1.29E+07	7.76E+07	5.17E+07	1.59E+08
2033	6.47E+07	-1.29E+07	7.76E+07	5.17E+07	1.66E+08
2034	6.47E+07	-1.29E+07	7.76E+07	5.17E+07	1.71E+08
2035	6.47E+07	-1.29E+07	7.76E+07	5.17E+07	1.76E+08
2036	6.47E+07	-1.29E+07	7.76E+07	5.17E+07	1.80E+08
2037	6.47E+07	-1.29E+07	7.76E+07	5.17E+07	1.84E+08
2038	6.47E+07	-1.29E+07	7.76E+07	3.91E+07	1.86E+08

Table F-31 Cash flow summary for DIS

Year	Capacity	Sales	Capital cost	Working capital	Var. Cost	Fixed cost	Depreciation
2018	0						
2019	0		-6.96E+07	1.04E+07			
2020	0.45	1.63E+08			-1.51E+08	-7.07E+06	-7.54E+06
2021	0.68	2.46E+08			-2.29E+08	-7.07E+06	-1.29E+07
2022	1	3.62E+08			-3.37E+08	-7.07E+06	-9.23E+06
2023	1	3.62E+08			-3.37E+08	-7.07E+06	-6.59E+06
2024	1	3.62E+08			-3.37E+08	-7.07E+06	-4.71E+06
2025	1	3.62E+08			-3.37E+08	-7.07E+06	-4.71E+06
2026	1	3.62E+08			-3.37E+08	-7.07E+06	-4.71E+06
2027	1	3.62E+08			-3.37E+08	-7.07E+06	-2.35E+06
2028	1	3.62E+08			-3.37E+08	-7.07E+06	
2029	1	3.62E+08			-3.37E+08	-7.07E+06	
2030	1	3.62E+08			-3.37E+08	-7.07E+06	
2031	1	3.62E+08			-3.37E+08	-7.07E+06	
2032	1	3.62E+08			-3.37E+08	-7.07E+06	
2033	1	3.62E+08			-3.37E+08	-7.07E+06	
2034	1	3.62E+08			-3.37E+08	-7.07E+06	
2035	1	3.62E+08			-3.37E+08	-7.07E+06	
2036	1	3.62E+08			-3.37E+08	-7.07E+06	
2037	1	3.62E+08			-3.37E+08	-7.07E+06	
2038	1	3.62E+08		-1.04E+07	-3.37E+08	-7.07E+06	

Table F-32 Cash flow summary for DIS (continue)

Year	Taxale income	Taxes	Net Earning	Cash flow	Cumulative NPV
2018				0	0
2019		2.00E-01		-5.91E+07	-5.14E+07
2020	-2.96E+06	5.92E+05	-3.55E+06	5.18E+06	-4.75E+07
2021	-2.39E+06	4.78E+05	-2.87E+06	1.10E+07	-4.03E+07
2022	9.59E+06	-1.92E+06	1.15E+07	1.69E+07	-3.06E+07
2023	1.22E+07	-2.45E+06	1.47E+07	1.64E+07	-2.24E+07
2024	1.41E+07	-2.82E+06	1.69E+07	1.60E+07	-1.55E+07
2025	1.41E+07	-2.82E+06	1.69E+07	1.60E+07	-9.51E+06
2026	1.41E+07	-2.82E+06	1.69E+07	1.60E+07	-4.28E+06
2027	1.65E+07	-3.29E+06	1.98E+07	1.55E+07	1.35E+05
2028	1.88E+07	-3.77E+06	2.26E+07	1.51E+07	3.86E+06
2029	1.88E+07	-3.77E+06	2.26E+07	1.51E+07	7.10E+06
2030	1.88E+07	-3.77E+06	2.26E+07	1.51E+07	9.91E+06
2031	1.88E+07	-3.77E+06	2.26E+07	1.51E+07	1.24E+07
2032	1.88E+07	-3.77E+06	2.26E+07	1.51E+07	1.45E+07
2033	1.88E+07	-3.77E+06	2.26E+07	1.51E+07	1.63E+07
2034	1.88E+07	-3.77E+06	2.26E+07	1.51E+07	1.79E+07
2035	1.88E+07	-3.77E+06	2.26E+07	1.51E+07	1.93E+07
2036	1.88E+07	-3.77E+06	2.26E+07	1.51E+07	2.06E+07
2037	1.88E+07	-3.77E+06	2.26E+07	1.51E+07	2.16E+07
2038	1.88E+07	-3.77E+06	2.26E+07	4.63E+06	2.19E+07

Table F-33 Cash flow summary for AHP

Year	Capacity	Sales	Capital cost	Working capital	Var. Cost	Fixed cost	Depreciation
2018	0						
2019	0		-1.00E+08	1.50E+07			
2020	0.45	1.63E+08			-1.37E+08	-9.64E+06	-1.09E+07
2021	0.68	2.46E+08			-2.07E+08	-9.64E+06	-1.86E+07
2022	1	3.62E+08			-3.05E+08	-9.64E+06	-1.33E+07
2023	1	3.62E+08			-3.05E+08	-9.64E+06	-9.50E+06
2024	1	3.62E+08			-3.05E+08	-9.64E+06	-6.79E+06
2025	1	3.62E+08			-3.05E+08	-9.64E+06	-6.79E+06
2026	1	3.62E+08			-3.05E+08	-9.64E+06	-6.79E+06
2027	1	3.62E+08			-3.05E+08	-9.64E+06	-3.39E+06
2028	1	3.62E+08			-3.05E+08	-9.64E+06	
2029	1	3.62E+08			-3.05E+08	-9.64E+06	
2030	1	3.62E+08			-3.05E+08	-9.64E+06	
2031	1	3.62E+08			-3.05E+08	-9.64E+06	
2032	1	3.62E+08			-3.05E+08	-9.64E+06	
2033	1	3.62E+08			-3.05E+08	-9.64E+06	
2034	1	3.62E+08			-3.05E+08	-9.64E+06	
2035	1	3.62E+08			-3.05E+08	-9.64E+06	
2036	1	3.62E+08			-3.05E+08	-9.64E+06	
2037	1	3.62E+08			-3.05E+08	-9.64E+06	
2038	1	3.62E+08		-1.50E+07	-3.05E+08	-9.64E+06	

Table F-34 Cash flow summary for AHP (continue)

Year	Taxale income	Taxes	Net Earning	Cash flow	Cumulative NPV
2018				0	0
2019		2.00E-01		-8.52E+07	-7.41E+07
2020	5.38E+06	-1.08E+06	6.46E+06	1.52E+07	-6.26E+07
2021	1.09E+07	-2.17E+06	1.30E+07	2.73E+07	-4.47E+07
2022	3.46E+07	-6.92E+06	4.15E+07	4.10E+07	-2.12E+07
2023	3.84E+07	-7.68E+06	4.61E+07	4.02E+07	-1.23E+06
2024	4.11E+07	-8.22E+06	4.93E+07	3.97E+07	1.59E+07
2025	4.11E+07	-8.22E+06	4.93E+07	3.97E+07	3.08E+07
2026	4.11E+07	-8.22E+06	4.93E+07	3.97E+07	4.38E+07
2027	4.45E+07	-8.90E+06	5.34E+07	3.90E+07	5.49E+07
2028	4.79E+07	-9.58E+06	5.75E+07	3.83E+07	6.44E+07
2029	4.79E+07	-9.58E+06	5.75E+07	3.83E+07	7.26E+07
2030	4.79E+07	-9.58E+06	5.75E+07	3.83E+07	7.98E+07
2031	4.79E+07	-9.58E+06	5.75E+07	3.83E+07	8.60E+07
2032	4.79E+07	-9.58E+06	5.75E+07	3.83E+07	9.14E+07
2033	4.79E+07	-9.58E+06	5.75E+07	3.83E+07	9.61E+07
2034	4.79E+07	-9.58E+06	5.75E+07	3.83E+07	1.00E+08
2035	4.79E+07	-9.58E+06	5.75E+07	3.83E+07	1.04E+08
2036	4.79E+07	-9.58E+06	5.75E+07	3.83E+07	1.07E+08
2037	4.79E+07	-9.58E+06	5.75E+07	3.83E+07	1.10E+08
2038	4.79E+07	-9.58E+06	5.75E+07	2.33E+07	1.11E+08

Table F-35 Cash flow summary for VRC

Year	Capacity	Sales	Capital cost	Working capital	Var. Cost	Fixed cost	Depreciation
2018	0						
2019	0		-8.12E+07	1.22E+07			
2020	0.45	1.63E+08			-1.44E+08	-8.05E+06	-8.81E+06
2021	0.68	2.46E+08			-2.18E+08	-8.05E+06	-1.51E+07
2022	1	3.62E+08			-3.20E+08	-8.05E+06	-1.08E+07
2023	1	3.62E+08			-3.20E+08	-8.05E+06	-7.70E+06
2024	1	3.62E+08			-3.20E+08	-8.05E+06	-5.51E+06
2025	1	3.62E+08			-3.20E+08	-8.05E+06	-5.50E+06
2026	1	3.62E+08			-3.20E+08	-8.05E+06	-5.51E+06
2027	1	3.62E+08			-3.20E+08	-8.05E+06	-2.75E+06
2028	1	3.62E+08			-3.20E+08	-8.05E+06	
2029	1	3.62E+08			-3.20E+08	-8.05E+06	
2030	1	3.62E+08			-3.20E+08	-8.05E+06	
2031	1	3.62E+08			-3.20E+08	-8.05E+06	
2032	1	3.62E+08			-3.20E+08	-8.05E+06	
2033	1	3.62E+08			-3.20E+08	-8.05E+06	
2034	1	3.62E+08			-3.20E+08	-8.05E+06	
2035	1	3.62E+08			-3.20E+08	-8.05E+06	
2036	1	3.62E+08			-3.20E+08	-8.05E+06	
2037	1	3.62E+08			-3.20E+08	-8.05E+06	
2038	1	3.62E+08		-1.22E+07	-3.20E+08	-8.05E+06	

Table F-36 Cash flow summary for VRC (continue)

Year	Taxale income	Taxes	Net Earning	Cash flow	Cumulative NPV
2018				0	0
2019		2.00E-01		-6.90E+07	-6.00E+07
2020	2.05E+06	-4.10E+05	2.46E+06	1.04E+07	-5.21E+07
2021	5.42E+06	-1.08E+06	6.51E+06	1.94E+07	-3.94E+07
2022	2.32E+07	-4.64E+06	2.78E+07	2.93E+07	-2.26E+07
2023	2.63E+07	-5.25E+06	3.15E+07	2.87E+07	-8.31E+06
2024	2.85E+07	-5.69E+06	3.42E+07	2.83E+07	3.91E+06
2025	2.85E+07	-5.69E+06	3.42E+07	2.83E+07	1.45E+07
2026	2.85E+07	-5.69E+06	3.42E+07	2.83E+07	2.38E+07
2027	3.12E+07	-6.24E+06	3.75E+07	2.77E+07	3.17E+07
2028	3.40E+07	-6.79E+06	4.08E+07	2.72E+07	3.84E+07
2029	3.40E+07	-6.79E+06	4.08E+07	2.72E+07	4.42E+07
2030	3.40E+07	-6.79E+06	4.08E+07	2.72E+07	4.93E+07
2031	3.40E+07	-6.79E+06	4.08E+07	2.72E+07	5.37E+07
2032	3.40E+07	-6.79E+06	4.08E+07	2.72E+07	5.76E+07
2033	3.40E+07	-6.79E+06	4.08E+07	2.72E+07	6.09E+07
2034	3.40E+07	-6.79E+06	4.08E+07	2.72E+07	6.38E+07
2035	3.40E+07	-6.79E+06	4.08E+07	2.72E+07	6.63E+07
2036	3.40E+07	-6.79E+06	4.08E+07	2.72E+07	6.85E+07
2037	3.40E+07	-6.79E+06	4.08E+07	2.72E+07	7.04E+07
2038	3.40E+07	-6.79E+06	4.08E+07	1.50E+07	7.13E+07

Table F-37 Cash flow summary for BF

Year	Capacity	Sales	Capital cost	Working capital	Var. Cost	Fixed cost	Depreciation
2018	0						
2019	0		-8.70E+07	1.31E+07			
2020	0.45	1.63E+08			-1.46E+08	-8.54E+06	-9.44E+06
2021	0.68	2.46E+08			-2.21E+08	-8.54E+06	-1.62E+07
2022	1	3.62E+08			-3.24E+08	-8.54E+06	-1.16E+07
2023	1	3.62E+08			-3.24E+08	-8.54E+06	-8.25E+06
2024	1	3.62E+08			-3.24E+08	-8.54E+06	-5.90E+06
2025	1	3.62E+08			-3.24E+08	-8.54E+06	-5.89E+06
2026	1	3.62E+08			-3.24E+08	-8.54E+06	-5.90E+06
2027	1	3.62E+08			-3.24E+08	-8.54E+06	-2.95E+06
2028	1	3.62E+08			-3.24E+08	-8.54E+06	
2029	1	3.62E+08			-3.24E+08	-8.54E+06	
2030	1	3.62E+08			-3.24E+08	-8.54E+06	
2031	1	3.62E+08			-3.24E+08	-8.54E+06	
2032	1	3.62E+08			-3.24E+08	-8.54E+06	
2033	1	3.62E+08			-3.24E+08	-8.54E+06	
2034	1	3.62E+08			-3.24E+08	-8.54E+06	
2035	1	3.62E+08			-3.24E+08	-8.54E+06	
2036	1	3.62E+08			-3.24E+08	-8.54E+06	
2037	1	3.62E+08			-3.24E+08	-8.54E+06	
2038	1	3.62E+08		-1.31E+07	-3.24E+08	-8.54E+06	

Table F-38 Cash flow summary for BF (continue)

Year	Taxale income	Taxes	Net Earning	Cash flow	Cumulative NPV
2018				0	0
2019		2.00E-01		-7.40E+07	-6.43E+07
2020	-8.60E+05	1.72E+05	-1.03E+06	8.75E+06	-5.77E+07
2021	1.15E+06	-2.30E+05	1.38E+06	1.71E+07	-4.65E+07
2022	1.79E+07	-3.59E+06	2.15E+07	2.59E+07	-3.17E+07
2023	2.12E+07	-4.25E+06	2.55E+07	2.52E+07	-1.91E+07
2024	2.36E+07	-4.72E+06	2.83E+07	2.48E+07	-8.40E+06
2025	2.36E+07	-4.72E+06	2.83E+07	2.48E+07	9.16E+05
2026	2.36E+07	-4.72E+06	2.83E+07	2.48E+07	9.02E+06
2027	2.66E+07	-5.31E+06	3.19E+07	2.42E+07	1.59E+07
2028	2.95E+07	-5.90E+06	3.54E+07	2.36E+07	2.17E+07
2029	2.95E+07	-5.90E+06	3.54E+07	2.36E+07	2.68E+07
2030	2.95E+07	-5.90E+06	3.54E+07	2.36E+07	3.12E+07
2031	2.95E+07	-5.90E+06	3.54E+07	2.36E+07	3.50E+07
2032	2.95E+07	-5.90E+06	3.54E+07	2.36E+07	3.84E+07
2033	2.95E+07	-5.90E+06	3.54E+07	2.36E+07	4.13E+07
2034	2.95E+07	-5.90E+06	3.54E+07	2.36E+07	4.38E+07
2035	2.95E+07	-5.90E+06	3.54E+07	2.36E+07	4.60E+07
2036	2.95E+07	-5.90E+06	3.54E+07	2.36E+07	4.79E+07
2037	2.95E+07	-5.90E+06	3.54E+07	2.36E+07	4.96E+07
2038	2.95E+07	-5.90E+06	3.54E+07	1.05E+07	5.02E+07

F.3 Cash flow calculations for superstructure process using Pt/Zeolite catalyst

Table F-39 Equipment cost

Equipment	SMB Cost, $	DIS Cost, $	AHP Cost, $	VRC Cost, $	BF Cost, $
Stabilizer column	5.98E+05	5.98E+05	5.98E+05	5.98E+05	5.98E+05
Reactor	3.69E+04	3.69E+04	3.69E+04	3.69E+04	3.69E+04
Catalyst	8.46E+05	8.46E+05	8.46E+05	8.46E+05	8.46E+05
Air cooler	2.14E+06	5.58E+06	4.07E+06	5.07E+06	2.98E+06
Heat exchangers	2.31E+05	2.13E+05	2.15E+05	2.14E+05	2.15E+05
Flash drum	2.55E+04	2.55E+04	2.55E+04	2.55E+04	2.55E+04
Pumps	2.04E+04	2.04E+04	2.04E+04	2.04E+04	2.04E+04
Compressors	6.29E+05	1.01E+06	1.08E+06	1.08E+06	1.08E+06
Adsorption	4.22E+04	--	--	--	--
Adsorbent	5.74E+06	--	--	--	--
Distillation unit	--	1.42E+05	9.20E+06	2.01E+06	4.82E+06
Total Equipment cost ($)	4.88E+07	4.01E+07	7.63E+07	4.69E+07	5.03E+07

Table F-40 Material prices and cost

Raw material	Amount/h	$/Amount
Hydrogen	Kg/h	3.6
Light Naphtha	Kg/h	0.628
Products		
Light gases	Kg/h	15
Gasoline	M³/h	756.64
Hydrogen	Kg/h	3.6
Utilities		
Medium Pressure steam	Kg/h	5.00E-02
Cooling water	Kg/h	6.70E-05
Electricity	Kw/h	0.15

Table F-41 Material prices and cost for each scenario

	SMB		DIS		AHP	
Raw material	Amount/h	Cost $/y	Amount/h	Cost $/y	Amount/h	Cost $/y
Hydrogen	1021.5	2.94E+07	1021.5	2.94E+07	1021.5	2.94E+07
Light Naphtha	4.60E+04	2.31E+08	4.60E+04	2.31E+08	4.60E+04	2.31E+08
Products						
Light gases	1672.29	2.01E+08	1672.29	2.01E+08	1672.26	2.01E+08
Gasoline	29.23	1.75E+08	29.23	1.55E+08	29.23	1.55E+08
Hydrogen	84.48	2.43E+06	84.46	2.43E+06	84.47	2.43E+06
Utilities						
Medium Pressure steam	2.00E+04	8.01E+06	1.00E+05	4.01E+07	2.03E+04	8.11E+06
Cooling water	9.21E+03	4.94E+03	1.29E+05	6.92E+01	9.45E+03	5.06E+00
Electricity	1703.51	2.04E+06	1458.15	1.75E+06	1949.75	2.34E+06
Catalyst		2.52E+05		2.52E+05		2.52E+05
Adsorbent		1.71E+06		0.00E+00		0.00E+00
Total		2.73E+08		3.03E+08		2.71E+08

Table F-42 Material prices and cost for each scenario (continue)

	VRC		BF	
Raw material	Amount/h	Cost $/y	Amount/h	Cost $/y
Hydrogen	1021.5	2.94E+07	1021.5	2.94E+07
Light Naphtha	4.60E+04	2.31E+08	4.60E+04	2.31E+08
Products				
Light gases	1672.29	2.01E+08	1672.29	2.01E+08
Gasoline	29.23	1.55E+08	29.23	1.55E+08
Hydrogen	84.46	2.43E+06	84.46	2.43E+06
Utilities				
Medium Pressure steam	1.65E+04	6.59E+06	1.92E+04	7.67E+06
Cooling water	8.92E+03	4.78E+00	9.11E+03	4.88E+00
Electricity	1.57E+04	1.88E+07	1.90E+04	2.28E+07
Catalyst		2.52E+05		2.52E+05
Adsorbent		0.00E+00		0.00E+00
Total		2.86E+08		2.91E+08

Table F-43 Economic calculations summary

		SMB	DIS	AHP
Variable cost				
Selling/Transfer expenses	0.01	3.78E+06	3.58E+06	3.58E+06
Direct Research	0.048	1.82E+07	1.72E+07	1.72E+07
Allocated research	0.005	1.89E+06	1.79E+06	1.79E+06
Administrative Expense	0.02	7.56E+06	7.16E+06	7.16E+06
Management Incentive Compensation	0.0125	4.73E+06	4.47E+06	4.47E+06
	0.0955	3.61E+07	3.42E+07	3.42E+07
Total variable cost		**3.09E+08**	**3.37E+08**	**3.03E+08**
Fixed cost				
Operations				
Operators/shift	5			
Direct wages	40	4.16E+05	4.16E+05	4.16E+05
Direct salaries	0.15	6.24E+04	6.24E+04	6.24E+04
Operating supplies	0.06	2.50E+04	2.50E+04	2.50E+04
Technical Assistance	6.00E0+7	3.00E+05	3.00E+05	3.00E+05
Control laboratory	6.50E+07	3.25E+05	3.25E+05	3.25E+05
		1.13E+06	1.13E+06	1.13E+06
Maintenance				
Wages	0.035	2.22E+06	1.82E+06	3.46E+06
Salaries	0.25	5.54E+05	4.55E+05	8.66E+05
Materials and services	1	2.22E+06	1.82E+06	3.46E+06
Maintenance overhead	0.05	1.11E+05	9.11E+04	1.73E+05
		5.10E+06	4.19E+06	7.97E+06
Operating overhead	0.228	7.41E+05	6.28E+05	1.10E+06
Property taxes and insurance	0.02	1.27E+06	1.04E+06	1.98E+06
		8.24E+06	6.99E+06	1.22E+07

Table F-44 Economic calculations summary (continue)

		VRC	BF
Variable cost			
Selling/Transfer expenses	0.01	3.58E+06	3.58E+06
Direct Research	0.048	1.72E+07	1.72E+07
Allocated research	0.005	1.79E+06	1.79E+06
Administrative Expense	0.02	7.16E+06	7.16E+06
Management Incentive Compensation	0.0125	4.47E+06	4.47E+06
	0.0955	3.42E+07	3.42E+07
Total variable cost		**3.20E+08**	**3.25E+08**
Fixed cost			
Operations			
Operators/shift	5		
Direct wages	40	4.16E+05	4.16E+05
Direct salaries	0.15	6.24E+04	6.24E+04
Operating supplies	0.06	2.50E+04	2.50E+04
Technical Assistance	6.00E0+7	3.00E+05	3.00E+05
Control laboratory	6.50E+07	3.25E+05	3.25E+05
		1.13E+06	1.13E+06
Maintenance			
Wages	0.035	2.13E+06	2.29E+06
Salaries	0.25	5.33E+05	5.72E+05
Materials and services	1	2.13E+06	2.29E+06
Maintenance overhead	0.05	1.07E+05	1.14E+05
		4.90E+06	5.26E+06
Operating overhead	0.228	7.17E+05	7.61E+05
Property taxes and insurance	0.02	1.22E+06	1.31E+06
		7.97E+06	8.45E+06

Table F-45 Investment summary

Total Permanent investment		SMB	DIS	AHP
Cost of site preparation	0.05	2.44E+06	2.01E+06	3.81E+06
Cost of service facilities	0.05	2.44E+06	2.01E+06	3.81E+06
Cost of contingencies and constructor fees	0.18	9.66E+06	7.94E+06	1.51E+07
Cost of land	0.02	1.27E+06	1.04E+06	1.98E+06
Cost of plant start-up	0.1	6.33E+06	5.21E+06	9.90E+06
		7.09E+07	5.83E+07	1.11E+08
Working capital	0.15	1.25E+07	1.03E+07	1.96E+07
Total capital investment		8.35E+07	6.86E+07	1.30E+08

Table F-46 Investment summary (continue)

Total Permanent investment		VRC	BF
Cost of site preparation	0.05	2.35E+06	2.52E+06
Cost of service facilities	0.05	2.35E+06	2.52E+06
Cost of contingencies and constructor fees	0.18	9.29E+06	9.96E+06
Cost of land	0.02	1.22E+06	1.31E+06
Cost of plant start-up	0.1	6.09E+06	6.53E+06
		6.82E+07	7.32E+07
Working capital	0.15	1.20E+07	1.29E+07
Total capital investment		8.03E+07	8.61E+07

Table F-47 Cash flow summary for SMB

Year	Capacity	Sales	Capital cost	Working capital	Var. Cost	Fixed cost	Depreciation
2018	0						
2019	0		-8.35E+07	1.25E+07			
2020	0.45	1.70E+08			-1.39E+08	-8.24E+06	-9.05E+06
2021	0.68	2.57E+08			-2.10E+08	-8.24E+06	-1.55E+07
2022	1	3.78E+08			-3.09E+08	-8.24E+06	-1.11E+07
2023	1	3.78E+08			-3.09E+08	-8.24E+06	-7.91E+06
2024	1	3.78E+08			-3.09E+08	-8.24E+06	-5.66E+06
2025	1	3.78E+08			-3.09E+08	-8.24E+06	-5.65E+06
2026	1	3.78E+08			-3.09E+08	-8.24E+06	-5.66E+06
2027	1	3.78E+08			-3.09E+08	-8.24E+06	-2.83E+06
2028	1	3.78E+08			-3.09E+08	-8.24E+06	
2029	1	3.78E+08			-3.09E+08	-8.24E+06	
2030	1	3.78E+08			-3.09E+08	-8.24E+06	
2031	1	3.78E+08			-3.09E+08	-8.24E+06	
2032	1	3.78E+08			-3.09E+08	-8.24E+06	
2033	1	3.78E+08			-3.09E+08	-8.24E+06	
2034	1	3.78E+08			-3.09E+08	-8.24E+06	
2035	1	3.78E+08			-3.09E+08	-8.24E+06	
2036	1	3.78E+08			-3.09E+08	-8.24E+06	
2037	1	3.78E+08			-3.09E+08	-8.24E+06	
2038	1	3.78E+08		-1.25E+07	-3.09E+08	-8.24E+06	

Table F-48 Cash flow summary for SMB (continue)

Year	Taxale income	Taxes	Net Earning	Cash flow	Cumulative NPV
2018				0	0
2019				-7.09E+07	-6.17E+07
2020	1.40E+07	-2.80E+06	1.68E+07	2.03E+07	-4.64E+07
2021	2.35E+07	-4.71E+06	2.82E+07	3.43E+07	-2.38E+07
2022	5.02E+07	-1.00E+07	6.03E+07	5.13E+07	5.51E+06
2023	5.34E+07	-1.07E+07	6.41E+07	5.06E+07	3.07E+07
2024	5.56E+07	-1.11E+07	6.68E+07	5.02E+07	5.24E+07
2025	5.56E+07	-1.11E+07	6.68E+07	5.02E+07	7.12E+07
2026	5.56E+07	-1.11E+07	6.68E+07	5.02E+07	8.76E+07
2027	5.85E+07	-1.17E+07	7.02E+07	4.96E+07	1.02E+08
2028	6.13E+07	-1.23E+07	7.36E+07	4.90E+07	1.14E+08
2029	6.13E+07	-1.23E+07	7.36E+07	4.90E+07	1.24E+08
2030	6.13E+07	-1.23E+07	7.36E+07	4.90E+07	1.34E+08
2031	6.13E+07	-1.23E+07	7.36E+07	4.90E+07	1.42E+08
2032	6.13E+07	-1.23E+07	7.36E+07	4.90E+07	1.48E+08
2033	6.13E+07	-1.23E+07	7.36E+07	4.90E+07	1.54E+08
2034	6.13E+07	-1.23E+07	7.36E+07	4.90E+07	1.60E+08
2035	6.13E+07	-1.23E+07	7.36E+07	4.90E+07	1.64E+08
2036	6.13E+07	-1.23E+07	7.36E+07	4.90E+07	1.68E+08
2037	6.13E+07	-1.23E+07	7.36E+07	4.90E+07	1.72E+08
2038	6.13E+07	-1.23E+07	7.36E+07	3.65E+07	1.74E+08

Table F-49 Cash flow summary for DIS

Year	Capacity	Sales	Capital cost	Working capital	Var. Cost	Fixed cost	Depreciation
2018	0						
2019	0		-6.86E+07	1.03E+07			
2020	0.45	1.61E+08			-1.52E+08	-6.99E+06	-7.44E+06
2021	0.68	2.43E+08			-2.29E+08	-6.99E+06	-1.27E+07
2022	1	3.58E+08			-3.37E+08	-6.99E+06	-9.10E+06
2023	1	3.58E+08			-3.37E+08	-6.99E+06	-6.50E+06
2024	1	3.58E+08			-3.37E+08	-6.99E+06	-4.65E+06
2025	1	3.58E+08			-3.37E+08	-6.99E+06	-4.64E+06
2026	1	3.58E+08			-3.37E+08	-6.99E+06	-4.65E+06
2027	1	3.58E+08			-3.37E+08	-6.99E+06	-2.32E+06
2028	1	3.58E+08			-3.37E+08	-6.99E+06	
2029	1	3.58E+08			-3.37E+08	-6.99E+06	
2030	1	3.58E+08			-3.37E+08	-6.99E+06	
2031	1	3.58E+08			-3.37E+08	-6.99E+06	
2032	1	3.58E+08			-3.37E+08	-6.99E+06	
2033	1	3.58E+08			-3.37E+08	-6.99E+06	
2034	1	3.58E+08			-3.37E+08	-6.99E+06	
2035	1	3.58E+08			-3.37E+08	-6.99E+06	
2036	1	3.58E+08			-3.37E+08	-6.99E+06	
2037	1	3.58E+08			-3.37E+08	-6.99E+06	
2038	1	3.58E+08		-1.03E+07	-3.37E+08	-6.99E+06	

Table F-50 Cash flow summary for DIS (continue)

Year	Taxale income	Taxes	Net Earning	Cash flow	Cumulative NPV
2018				0	0
2019		2.00E-01		-5.83E+07	-5.07E+07
2020	-4.96E+06	9.92E+05	-5.95E+06	3.47E+06	-4.81E+07
2021	-5.43E+06	1.09E+06	-6.52E+06	8.40E+06	-4.25E+07
2022	4.94E+06	-9.89E+05	5.93E+06	1.31E+07	-3.51E+07
2023	7.55E+06	-1.51E+06	9.06E+06	1.25E+07	-2.88E+07
2024	9.40E+06	-1.88E+06	1.13E+07	1.22E+07	-2.36E+07
2025	9.41E+06	-1.88E+06	1.13E+07	1.22E+07	-1.90E+07
2026	9.40E+06	-1.88E+06	1.13E+07	1.22E+07	-1.50E+07
2027	1.17E+07	-2.35E+06	1.41E+07	1.17E+07	-1.17E+07
2028	1.40E+07	-2.81E+06	1.69E+07	1.12E+07	-8.93E+06
2029	1.40E+07	-2.81E+06	1.69E+07	1.12E+07	-6.51E+06
2030	1.40E+07	-2.81E+06	1.69E+07	1.12E+07	-4.41E+06
2031	1.40E+07	-2.81E+06	1.69E+07	1.12E+07	-2.58E+06
2032	1.40E+07	-2.81E+06	1.69E+07	1.12E+07	-9.94E+05
2033	1.40E+07	-2.81E+06	1.69E+07	1.12E+07	3.87E+05
2034	1.40E+07	-2.81E+06	1.69E+07	1.12E+07	1.59E+06
2035	1.40E+07	-2.81E+06	1.69E+07	1.12E+07	2.63E+06
2036	1.40E+07	-2.81E+06	1.69E+07	1.12E+07	3.54E+06
2037	1.40E+07	-2.81E+06	1.69E+07	1.12E+07	4.33E+06
2038	1.40E+07	-2.81E+06	1.69E+07	9.51E+05	4.39E+06

Table F-51 Cash flow summary for AHP

Year	Capacity	Sales	Capital cost	Working capital	Var.cost	Fixed cost	Depreciation
2018	0						
2019	0		-1.30E+08	1.96E+07			
2020	0.45	1.61E+08			-1.37E+08	-1.22E+07	-1.41E+07
2021	0.68	2.43E+08			-2.08E+08	-1.22E+07	-2.42E+07
2022	1	3.58E+08			-3.05E+08	-1.22E+07	-1.73E+07
2023	1	3.58E+08			-3.05E+08	-1.22E+07	-1.24E+07
2024	1	3.58E+08			-3.05E+08	-1.22E+07	-8.84E+06
2025	1	3.58E+08			-3.05E+08	-1.22E+07	-8.83E+06
2026	1	3.58E+08			-3.05E+08	-1.22E+07	-8.84E+06
2027	1	3.58E+08			-3.05E+08	-1.22E+07	-4.42E+06
2028	1	3.58E+08			-3.05E+08	-1.22E+07	
2029	1	3.58E+08			-3.05E+08	-1.22E+07	
2030	1	3.58E+08			-3.05E+08	-1.22E+07	
2031	1	3.58E+08			-3.05E+08	-1.22E+07	
2032	1	3.58E+08			-3.05E+08	-1.22E+07	
2033	1	3.58E+08			-3.05E+08	-1.22E+07	
2034	1	3.58E+08			-3.05E+08	-1.22E+07	
2035	1	3.58E+08			-3.05E+08	-1.22E+07	
2036	1	3.58E+08			-3.05E+08	-1.22E+07	
2037	1	3.58E+08			-3.05E+08	-1.22E+07	
2038	1	3.58E+08		-1.96E+07	-3.05E+08	-1.22E+07	

Table F-52 Cash flow summary for AHP (continue)

Year	Taxale income	Taxes	Net Earning	Cash flow	Cumulative NPV
2018				0	0
2019		2.00E-01		-1.11E+08	-9.64E+07
2020	-2.73E+06	5.47E+05	-3.28E+06	1.20E+07	-8.74E+07
2021	-7.75E+05	1.55E+05	-9.30E+05	2.36E+07	-7.18E+07
2022	2.29E+07	-4.59E+06	2.75E+07	3.57E+07	-5.15E+07
2023	2.79E+07	-5.58E+06	3.35E+07	3.47E+07	-3.42E+07
2024	3.14E+07	-6.28E+06	3.77E+07	3.40E+07	-1.95E+07
2025	3.14E+07	-6.28E+06	3.77E+07	3.40E+07	-6.76E+06
2026	3.14E+07	-6.28E+06	3.77E+07	3.40E+07	4.34E+06
2027	3.58E+07	-7.17E+06	4.30E+07	3.31E+07	1.37E+07
2028	4.02E+07	-8.05E+06	4.83E+07	3.22E+07	2.17E+07
2029	4.02E+07	-8.05E+06	4.83E+07	3.22E+07	2.86E+07
2030	4.02E+07	-8.05E+06	4.83E+07	3.22E+07	3.46E+07
2031	4.02E+07	-8.05E+06	4.83E+07	3.22E+07	3.99E+07
2032	4.02E+07	-8.05E+06	4.83E+07	3.22E+07	4.44E+07
2033	4.02E+07	-8.05E+06	4.83E+07	3.22E+07	4.84E+07
2034	4.02E+07	-8.05E+06	4.83E+07	3.22E+07	5.18E+07
2035	4.02E+07	-8.05E+06	4.83E+07	3.22E+07	5.48E+07
2036	4.02E+07	-8.05E+06	4.83E+07	3.22E+07	5.74E+07
2037	4.02E+07	-8.05E+06	4.83E+07	3.22E+07	5.97E+07
2038	4.02E+07	-8.05E+06	4.83E+07	1.26E+07	6.04E+07

Table F-53 Cash flow summary for VRC

Year	Capacity	Sales	Capital cost	Working capital	Var.cost	Fixed cost	Depreciation
2018	0						
2019	0		-8.03E+07	1.20E+07			
2020	0.45	1.61E+08			-1.44E+08	-7.97E+06	-8.70E+06
2021	0.68	2.43E+08			-2.18E+08	-7.97E+06	-1.49E+07
2022	1	3.58E+08			-3.20E+08	-7.97E+06	-1.07E+07
2023	1	3.58E+08			-3.20E+08	-7.97E+06	-7.61E+06
2024	1	3.58E+08			-3.20E+08	-7.97E+06	-5.44E+06
2025	1	3.58E+08			-3.20E+08	-7.97E+06	-5.43E+06
2026	1	3.58E+08			-3.20E+08	-7.97E+06	-5.44E+06
2027	1	3.58E+08			-3.20E+08	-7.97E+06	-2.72E+06
2028	1	3.58E+08			-3.20E+08	-7.97E+06	
2029	1	3.58E+08			-3.20E+08	-7.97E+06	
2030	1	3.58E+08			-3.20E+08	-7.97E+06	
2031	1	3.58E+08			-3.20E+08	-7.97E+06	
2032	1	3.58E+08			-3.20E+08	-7.97E+06	
2033	1	3.58E+08			-3.20E+08	-7.97E+06	
2034	1	3.58E+08			-3.20E+08	-7.97E+06	
2035	1	3.58E+08			-3.20E+08	-7.97E+06	
2036	1	3.58E+08			-3.20E+08	-7.97E+06	
2037	1	3.58E+08			-3.20E+08	-7.97E+06	
2038	1	3.58E+08		-1.20E+07	-3.20E+08	-7.97E+06	

Table F-54 Cash flow summary for VRC (continue)

Year	Taxale income	Taxes	Net Earning	Cash flow	Cumulative NPV
2018				0	0
2019		2.00E-01		-6.82E+07	-5.93E+07
2020	1.81E+05	-3.62E+04	2.17E+05	8.85E+06	-5.26E+07
2021	2.58E+06	-5.16E+05	3.10E+06	1.70E+07	-4.15E+07
2022	1.88E+07	-3.77E+06	2.26E+07	2.57E+07	-2.68E+07
2023	2.19E+07	-4.37E+06	2.62E+07	2.51E+07	-1.43E+07
2024	2.40E+07	-4.81E+06	2.88E+07	2.47E+07	-3.61E+06
2025	2.40E+07	-4.81E+06	2.89E+07	2.47E+07	5.66E+06
2026	2.40E+07	-4.81E+06	2.88E+07	2.47E+07	1.37E+07
2027	2.68E+07	-5.35E+06	3.21E+07	2.41E+07	2.06E+07
2028	2.95E+07	-5.90E+06	3.54E+07	2.36E+07	2.64E+07
2029	2.95E+07	-5.90E+06	3.54E+07	2.36E+07	3.15E+07
2030	2.95E+07	-5.90E+06	3.54E+07	2.36E+07	3.59E+07
2031	2.95E+07	-5.90E+06	3.54E+07	2.36E+07	3.97E+07
2032	2.95E+07	-5.90E+06	3.54E+07	2.36E+07	4.31E+07
2033	2.95E+07	-5.90E+06	3.54E+07	2.36E+07	4.60E+07
2034	2.95E+07	-5.90E+06	3.54E+07	2.36E+07	4.85E+07
2035	2.95E+07	-5.90E+06	3.54E+07	2.36E+07	5.07E+07
2036	2.95E+07	-5.90E+06	3.54E+07	2.36E+07	5.26E+07
2037	2.95E+07	-5.90E+06	3.54E+07	2.36E+07	5.42E+07
2038	2.95E+07	-5.90E+06	3.54E+07	1.15E+07	5.49E+07

Table F-55 Cash flow summary for BF

Year	Capacity	Sales	Capital cost	Working capital	Var. Cost	Fixed cost	Depreciation
2018	0						
2019	0		-8.61E+07	1.29E+07			
2020	0.45	1.61E+08			-1.46E+08	-8.45E+06	-9.33E+06
2021	0.68	2.43E+08			-2.21E+08	-8.45E+06	-1.60E+07
2022	1	3.58E+08			-3.25E+08	-8.45E+06	-1.14E+07
2023	1	3.58E+08			-3.25E+08	-8.45E+06	-8.16E+06
2024	1	3.58E+08			-3.25E+08	-8.45E+06	-5.83E+06
2025	1	3.58E+08			-3.25E+08	-8.45E+06	-5.83E+06
2026	1	3.58E+08			-3.25E+08	-8.45E+06	-5.83E+06
2027	1	3.58E+08			-3.25E+08	-8.45E+06	-2.91E+06
2028	1	3.58E+08			-3.25E+08	-8.45E+06	
2029	1	3.58E+08			-3.25E+08	-8.45E+06	
2030	1	3.58E+08			-3.25E+08	-8.45E+06	
2031	1	3.58E+08			-3.25E+08	-8.45E+06	
2032	1	3.58E+08			-3.25E+08	-8.45E+06	
2033	1	3.58E+08			-3.25E+08	-8.45E+06	
2034	1	3.58E+08			-3.25E+08	-8.45E+06	
2035	1	3.58E+08			-3.25E+08	-8.45E+06	
2036	1	3.58E+08			-3.25E+08	-8.45E+06	
2037	1	3.58E+08			-3.25E+08	-8.45E+06	
2038	1	3.58E+08		-1.29E+07	-3.25E+08	-8.45E+06	

Table F-56 Cash flow summary for BF (continue)

Year	Taxale income	Taxes	Net Earning	Cash flow	Cumulative NPV
2018				0	0
2019		2.00E-01		-7.32E+07	-6.36E+07
2020	-3.21E+06	6.42E+05	-3.85E+06	6.77E+06	-5.85E+07
2021	-2.42E+06	4.85E+05	-2.91E+06	1.41E+07	-4.93E+07
2022	1.25E+07	-2.50E+06	1.50E+07	2.14E+07	-3.70E+07
2023	1.58E+07	-3.16E+06	1.89E+07	2.08E+07	-2.67E+07
2024	1.81E+07	-3.62E+06	2.17E+07	2.03E+07	-1.79E+07
2025	1.81E+07	-3.62E+06	2.17E+07	2.03E+07	-1.02E+07
2026	1.81E+07	-3.62E+06	2.17E+07	2.03E+07	-3.60E+06
2027	2.10E+07	-4.21E+06	2.52E+07	1.97E+07	2.01E+06
2028	2.39E+07	-4.79E+06	2.87E+07	1.92E+07	6.74E+06
2029	2.39E+07	-4.79E+06	2.87E+07	1.92E+07	1.09E+07
2030	2.39E+07	-4.79E+06	2.87E+07	1.92E+07	1.44E+07
2031	2.39E+07	-4.79E+06	2.87E+07	1.92E+07	1.75E+07
2032	2.39E+07	-4.79E+06	2.87E+07	1.92E+07	2.03E+07
2033	2.39E+07	-4.79E+06	2.87E+07	1.92E+07	2.26E+07
2034	2.39E+07	-4.79E+06	2.87E+07	1.92E+07	2.47E+07
2035	2.39E+07	-4.79E+06	2.87E+07	1.92E+07	2.64E+07
2036	2.39E+07	-4.79E+06	2.87E+07	1.92E+07	2.80E+07
2037	2.39E+07	-4.79E+06	2.87E+07	1.92E+07	2.93E+07
2038	2.39E+07	-4.79E+06	2.87E+07	6.24E+06	2.97E+07

Appendix G   MATLAB® model

G.1   Langmuir model

```matlab
% MATLAB Program: Langmuir model. TM v1.0 2021
clc
clear all
clf
R    = 8.314e-3; % Gas constant
T    = 523;       % Temperature (K)
Pt   = [0:.05:3];% Pressure (bar)
nc   = 6; % Number of components

% Model consents from (Barcia P.S. 2010a &
Barcia P.S. 2010b)

qm_S = [.529 .329 .775 .797 .608 .491];
b0_S = [5.0*10^-10 2.0*10^-9 8.6*10^-10 1.2*10^-
9 1*10^-8 1.3*10^-8];
E_S  = [70.3 67.2 67.5 65.9 59.5 59.1];

qm_Z = [.289 .195 0 0 .082 .354];
b0_Z = [1.7*10^-9 3*10^-10 0 0 9.7*10^-9 2*10^-
8];
E_Z  = [78.8 84.8 0 0 26.2 52.8];

qm_I = [.112 .406 .155 .133 .257 .1];
b0_I = [4.6*10^-12 5*10^-12 6.8*10^-10 3.2*10^-9
8.1*10^-9 1.8*10^-8];
E_I  = [99.8 87.1 80.2 68.1 65.9 60.3];

for i=1:nc
        b_S(i)   = b0_S(i).*exp(E_S(i)/R/T);
        b_Z(i)   = b0_Z(i).*exp(E_Z(i)/R/T);
        b_I(i)   = b0_I(i).*exp(E_I(i)/R/T);
end
    f=[.98 .95 .95 1.9 .5 .9];
for j=1:length(Pt)
    p{j}      = f*Pt(j);
```

```matlab
    for i=1:nc
        q{i}(j)    =
(qm_S(i).*b_S(i).*p{j}(i))./(1 +
b_S(1)*p{j}(1)+b_S(2)*p{j}(2)+b_S(3)*p{j}(3)+b_S
(4)*p{j}(4)+b_S(5)*p{j}(5)+b_S(6)*p{j}(6))...
            +(qm_Z(i).*b_Z(i).*p{j}(i))./(1 +
b_Z(1)*p{j}(1)+b_Z(2)*p{j}(2)+b_Z(3)*p{j}(3)+b_Z
(4)*p{j}(4)+b_Z(5)*p{j}(5)+b_Z(6)*p{j}(6))...
            +(qm_I(i).*b_I(i).*p{j}(i))./(1 +
b_I(1)*p{j}(1)+b_I(2)*p{j}(2)+b_I(3)*p{j}(3)+b_I
(4)*p{j}(4)+b_I(5)*p{j}(5)+b_I(6)*p{j}(6));
    end

end

% Solution plotting and validations

Ptr=[.7 1.7 2.4];

q1=[.027 .055 .07];
q2=[.011 .027 .035];
q3=[.010 .020 .025];
q4=[.009 .019 .024];
q5=[.004 .009 .013];
q6=[.005 .011 .015];

c1=[.75 0 0];                  %Red
c2=[0 0 .75];                  %Blue
c3=[.5 .5 .5];                 %Grey
c4=[0 .5 0];                   %Green
c5=[0.8500, 0.3250, 0.0980];   %Orange
c6=[0 0 0];                    %Black
plot(Pt,q{1},'color',c1,'LineWidth', 2)
hold on
plot(Pt,q{2},'color',c2,'LineWidth', 2)
hold on
plot(Pt,q{3},'color',c3,'LineWidth', 2)
hold on
plot(Pt,q{4},'color',c4,'LineWidth', 2)
hold on
plot(Pt,q{5},'color',c5,'LineWidth', 2)
```

228

```matlab
hold on
plot(Pt,q{6},'color',c6,'LineWidth', 2)
hold on
```

```matlab
plot(Ptr,q1,'o','color',c1,'markerfacecolor',c1)
plot(Ptr,q2,'>','color',c2,'MarkerFaceColor',c2)
plot(Ptr,q3,'^','color',c3,'LineWidth',2)
plot(Ptr,q4,'>','color',c4,'MarkerFaceColor',c4)
plot(Ptr,q5,'o','color',c5,'LineWidth',2)
plot(Ptr,q6,'s','color',c6,'MarkerFaceColor',c6)
% Legend
LH(1) = plot(nan, nan, '-o','color',c1,'MarkerFaceColor',c1,'LineWidth',2);
Leg{1} = 'nC6';
LH(2) = plot(nan, nan, '->','color',c2,'MarkerFaceColor',c2,'LineWidth',2);
Leg{2} = '3M';
LH(3) = plot(nan, nan, '-^','color',c3,'LineWidth',2);
Leg{3} = '23DMB';
LH(4) = plot(nan, nan, '->','color',c4,'MarkerFaceColor',c4,'LineWidth',2);
Leg{4} = '22DMB';
LH(5) = plot(nan, nan, '-o','color',c5,'LineWidth',2);
Leg{5} = 'nC5';
LH(6) = plot(nan, nan, '-s','color',c6,'MarkerFaceColor',c6,'LineWidth',2);
Leg{6} = 'iC5';
legend(LH, Leg,'NumColumns',3);
ylabel('Loading (mmol/g)'); xlabel('Partial pressure (bar)')
ax1=gca;
legend('boxoff')
set(gca,'FontName','Arial','fontweight','bold','fontsize',10,'linewidth',2);
ax1.TickDir = 'both'; ylim([0 .095]);
% Regression calculations
```

```matlab
k(1)=regression(q{1}([15 33 49]),q1);
k(2)=regression(q{2}([15 33 49]),q2);
k(3)=regression(q{3} ([15 33 49]),q3);
k(4)=regression(q{4}([15 33 49]),q4);
k(5)=regression(q{5}([15 33 49]),q5);
k(6)=regression(q{6}([15 33 49]),q6);

disp(sum(k)/6*100)
```

G.2   Simulated moving bed – 8 bed

```matlab
% MATLAB Program: Simulated moving bed. TM v1.0
2021
function y=SMB(C6,MP3,DMB23,DMB22,C5,iC5,H2)
%('hysys.Application',"iso6.hsc");
a=actxserver('hysys.Application.V10.0');
a.Visible = 1;
e=get(a.activeDocument.Flowsheet.Operations,'Ite
m','ADS');

B2={};
% EXPORT
B2=get(e,'cell','B2');
B3=get(e,'cell','B3');
B4=get(e,'cell','B4');
B5=get(e,'cell','B5');
B6=get(e,'cell','B6');
B7=get(e,'cell','B7');
B8=get(e,'cell','B8');
B9=get(e,'cell','B9');
F1=B2.CellValue*3600;

% Feed from HYSYS
C6=B3.CellValue.*F1;
MP3=B4.CellValue.*F1;
DMB23=B5.CellValue.*F1;
DMB22=B6.CellValue.*F1;
C5=B7.CellValue.*F1;
iC5=B8.CellValue.*F1;
H21=B9.CellValue;
```

```matlab
xf=[C6 MP3 DMB23 DMB22 C5 iC5];

R   = 8.314e-3; % Gas Constant
T   = 523; % Inlet Temperature K
nc = 6; % NO. Comps
% Model conesant from (Barcia P.S. 2010a &
Barcia P.S. 2010b)
zb   =0.4;          %Voidage
mu   =0.218;        %Viscosity (N s m^-2)
dp   =1.59e-3;      %Partical diameter (m)
rou  =630;       % Bulk density (kg/m^3)
Mw   =76.3;         % Molecular weight(kg/kmol)


          %[C6 MP3 DMB23 DMB22 C5 iC5];
D        = [8.1 8.1 8.1 8.1 8.7 8.7]*1e-6;
%m/s^2
kmtc_S   = [.2668 .5549 .8689 .8464 .959 1.377];
%s-1
kmtc_Z   = [.0002 .0004 .0001 .0003 .0001 .002];
%s-1
kmtc_I   = [.0003 .0003 .0001 .0005 .0004
.003]*1e-3; %s-1
RONi     = [26 75 105 95 60 91];
%Individual RON
qm_S     = [.529 .329 .775 .797 0.608 0.491];
b0_S     = [5.0*10^-10 2*10^-9 8.6*10^-10
1.2*10^-9 1*10^-8 1.3*10^-8];
E_S      = [70.3 67.2 67.5 65.9 59.5 59.1];

qm_Z = [.289 .195 0 0 .082 .354];
b0_Z = [1.7*10^-9 3*10^-10 0 0 9.7*10^-9 2*10^-
8];
E_Z  = [78.8 84.8 0 0 26.2 52.8];

qm_I = [.112 .406 .155 .133 .257 .1];
b0_I = [4.6*10^-12 5*10^-12 6.8*10^-10 3.2*10^-9
8.1*10^-9 1.8*10^-8];
E_I  = [99.8 87.1 80.2 68.1 65.9 60.3];

for p=1:nc
        b_S(p)   = b0_S(p).*exp(E_S(p)/R/T);
```

```matlab
        b_Z(p)    = b0_Z(p).*exp(E_Z(p)/R/T);
        b_I(p)    = b0_I(p).*exp(E_I(p)/R/T);
end


x=0;            % Iintial space element
xmax=6.7*8;     % Length bed(m)
N=80;           % Number of space elements
dx=(xmax-x)/N;  % Space step

t=0;            % Iintial time element
tmax=5*60;      % Max time(s)
Ti=150;         % Number of time elements
dt=0.005;       % Time step


UF = 1e-2;        % Unit factor bars <--> kPa
xx = 2.0520e8;    % Stability factor
u  = 1;           % Velocity, m/s
nb=8;             % NO. beds

% Bed pressure (kPa)
PH=15*100;
PL=5*100;
P0=[14.5 14.5 15 15 5.5 5.5 5 5]*100;
% cyclic pressure

H2  = [.6 2.9 5.5 9.0 10 11 12 13 14];
% hydrogen amount (kmol/hr)
PFR = [1 5 10 20 30 40 60 80 100]./100;
% Purge/Feed ratio

F1=1./PFR.*H2;
F2=F1(:);
W=F2.^-1*R*T*1/.75*1.334/((1-1.334))*[(PH/PL
)^((1.334-1)/1.334)-1]; % Compressor Power(kWh)

for m=1:length(F1)

    xf = [.08 .09 .04 .05 .28 .46]*F1(m); % feed
concentrations (kmol/hr)
```

```matlab
%PFR(m)=H2(m)./F1(m);

% initial conditions
s=1;            % First bed
if s==1
    F=F1(m);
elseif s==5
    F=H2(m);
else
    F=0;
end

for p=1:nc
    c{p}=zeros(N,Ti)+xf(p);
end
ncyc=50;    % number of cycles
n=1; i=1;

for j=2:ncyc
    % Boundry conditions for each bed and
cycle
    if j==1 % 1st cycle
        for p=1:nc
            c{p}(1,1,j)=c{p}(1,1,1);
        end
    else    % 2nd and above cycle
        for p=1:nc
            c{p}(1,1,j)=c{p}(end,end,j-
1);%+c{p}(1,1,1);
        end
    end
    % pevious column concentration
    for s=1:nb
        for p=1:nc
            if s==1

                pc{p}=c{p}(i,n);
                if P0==PH
                    c{p}(i,n)=pc{p}+xf;
                    F=0;
                elseif P0==PL
```

```matlab
                        c{p}(i,n)=pc{p}+H2(m);
                    else
                        c{p}(i,n)=pc{p};
                    end
                else
                    pc{p}=c{p}((s-1)*N/nb,n);
                    if P0==PH
                        c{p}(i,n)=pc{p}+xf;
                    elseif P0==PL
                        c{p}(i,n)=pc{p}+H2(m);
                        F=H2(m);
                    else
                        c{p}(i,n)=pc{p};
                    end
                end
            end
        end
        % Tri-site Langmuir model
        for i=1:N
            for p=1:nc

q{p}(i,1,j)=kmtc_S(p)*qm_S(p)*c{p}(i,1,j)/(1+b_S
(1)*c{1}(i,1,j)+b_S(2)*c{2}(i,1,j)+...

b_S(3)*c{3}(i,1,j)+b_S(4)*c{4}(i,1,j)+...

b_S(5)*c{5}(i,1,j)+b_S(6)*c{6}(i,1,j))+...

kmtc_Z(p)*qm_Z(p)*c{p}(i,1,j)/(1+b_Z(1)*c{1}(i,1
,j)+b_Z(2)*c{2}(i,1,j)+...

b_Z(3)*c{3}(i,1,j)+b_Z(4)*c{4}(i,1,j)+...

b_Z(5)*c{5}(i,1,j)+b_Z(6)*c{6}(i,1,j))+...

kmtc_I(p)*qm_I(p)*c{p}(i,1,j)/(1+b_I(1)*c{1}(i,1
,j)+b_I(2)*c{2}(i,1,j)+...

b_I(3)*c{3}(i,1,j)+b_I(4)*c{4}(i,1,j)+...
```

```matlab
b_I(5)*c{5}(i,1,j)+b_I(6)*c{6}(i,1,j))-
c{p}(1,1,j);
                % Overall mass balance

c{p}(i,1,j)=q{p}(i,1,j)+c{p}(i,1,j);
            end
        end
        % mass balance to sorbate species

        for n=2:Ti

            for i=(s-1)*N/nb+1:s*N/nb
                if i<=2
                    i=2;
                end
                for p=1:nc

                    for p=1:nc

                        c{p}(i+1,n,j)=c{p}(i,n-
1,j);
                    end

                    c{p}(i,n,j)=c{p}(i,n-1,j)-
u*dt/dx*(c{p}(i+1,n-1,j)-c{p}(i-1,n-1,j))...

+zb*dt/dx^2*D(p)*(c{p}(i+1,n-1,j)-2*c{p}(i,n-
1,j)+c{p}(i-1,n-1,j))...
                        +q{p}(i,n-1,j);

                    q{p}(i,n,j)=q{p}(i-1,n-1,j);
                    P_drop(i)=(1.5e-3*mu*(1-
zb)^2*u/(dp^2*zb^3)+1.75e-5*Mw*rou*(1-
zb)*u^2/(dp*zb^3))*dx*UF;
                end

            end
            t=t+dt;
            x=x+dx;
            % for more stability
            for p=1:nc
```
235

```matlab
                c{p}(i,n,j)=c{p}(i,n-1,j);
            end
        end


    end

    % mass balance around each Zone
    for p=1:nc
        z1(p)=c{p}(20,end);                    %
Pressurize & adsorption
        z2(p)=abs(c{p}(80,end)*u*xx);
        z3(p)=abs(c{p}(40,end));               %
Blowdown & desorption
        z4(p)=(xf(p)-z2(p));

    end

    % RON calculations
    Re0=abs(sum(RONi.*xf/sum(abs(xf))));
    Re2(m)=abs(sum(RONi.*z2/sum(abs(z2))));
    Re3=abs(sum(RONi.*z3/sum(abs(z3))));
    Re4=abs(sum(RONi.*z4/sum(abs(z4))));

name1=['C6','3MP','23DMB','22DMB','C5','iC5','RO
N'];
%     fprintf('          Compoments : %6s %6s
%6s %6s %6s %6s
%6s\n','C6','3MP','23DMB','22DMB','C5','iC5','RO
N')
%     fprintf('The Feed      (kmol/hr): %6.2f
%6.2f %6.2f %6.2f %6.2f %6.2f %6.2f\n',
[xf,Re0]')
%     fprintf('The pressurize(kmol/hr): %6.2f
%6.2f %6.2f %6.2f %6.2f %6.2f\n', z1')
%     fprintf('The adsoption (kmol/hr): %6.2f
%6.2f %6.2f %6.2f %6.2f %6.2f %6.2f\n',
[z2,Re2(m)]')
%     fprintf('The blowdown  (kmol/hr): %6.2f
%6.2f %6.2f %6.2f %6.2f %6.2f\n', z3')
```

```matlab
%      fprintf('The desorption(kmol/hr): %6.2f
%6.2f %6.2f %6.2f %6.2f %6.2f %6.2f\n',
[z4,Re4]')
%
%      %Puriy
%
Hpur(m)=(z2(3)+z2(4)+z2(6))/(xf(3)+xf(4)+xf(6)).
*100;
%
lpur(m)=(z4(1)+z4(2)+z4(5))/(xf(1)+xf(2)+xf(5)).
*100;
%      %Recovery
%
Hrec(m)=(z2(3)+z2(4)+z2(6))/(sum(z2)).*100;
%
lrec(m)=(z4(1)+z4(2)+z4(5))/(sum(z4)).*100;
% end
%
% % yyaxis right
% % plot(PFR,Re2,'--')
% % ylim([80 100])
% figure(1)
% yyaxis left
% plot(PFR,lrec)
% ylabel('Recovery')
% hold on
% yyaxis right
% plot(PFR,lpur)
% grid on
% legend('Recovery','Purity')
% ylabel('Purity')
% xlabel('P/F ratio')
%
% figure(2)
% subplot(2,1,1)
% yyaxis left
% plot([11:19],Hrec)
% ylabel('Recovery')
% hold on
% yyaxis right
% plot([11:19],Hpur)
```

237

```matlab
% legend('Recovery','Purity')
% grid on
% ylabel('Purity')
%
% subplot(2,1,2)
% plot([11:19],-W*3600)
% xlabel('Adsorption Pressure, bar')
% ylabel('Power, kWh')
% mass balance for adsorption and elution tanks
for p=1:nc
    h{p}(1)=0;
    h1{p}(1)=0;
    Qin{p}(1)=z2(p);
    Qin1{p}(1)=z4(p);
    k=30;
    t=0;
    for i=2:Ti
        h{p}(i)=h{p}(i-1)+dt*(Qin{p}-k*h{p}(i-
1)^.5);
        h1{p}(i)=h1{p}(i-1)+dt*(Qin1{p}-
k*h1{p}(i-1)^.5);
        t(i)=t(i-1)+5*dt;

    end
    Qout{p}=k*(h{p}).^0.5;
    Qout1{p}=k*(h1{p}).^0.5;
end

% % ploting solutions
% warning off;
% figure(3)
% subplot(2,1,1)
% for p=1:nc
% plot(t,Qout{p})
% hold on
% end
% legend('C6','3MP','23DMB','22DMB','C5','iC5')
% xlabel('NO. Cycles')
% ylabel('F_(_k_m_o_l_/_h_r_)')
% title({'Adsorption
outlet',sprintf('RON=%.2f',Re2)})
```

```matlab
%
% subplot(2,1,2)
% for p=1:nc
% plot(t,Qout1{p})
% hold on
% end
% legend('C6','3MP','23DMB','22DMB','C5','iC5')
% xlabel('NO. Cycles')
% ylabel('F_(_k_m_o_l_/_hr_)')
% title({'Desorption
outlet',sprintf('RON=%.2f',Re4)})
%
% % xlswrite('B2.xlsx',[PFR;lrec;
lpur],'Sheet1',['A' num2str(4)]);
% % xlswrite('B2.xlsx',[[11:19];Hrec; Hpur;-
W'],'Sheet1',['A' num2str(8)]);
%
%
% grid on

% IMPORT
C3={};
C3=get(e,'cell','C3');
C4=get(e,'cell','C4');
C5=get(e,'cell','C5');
C6=get(e,'cell','C6');
C7=get(e,'cell','C7');
C8=get(e,'cell','C8');


D3=get(e,'cell','D3');
D4=get(e,'cell','D4');
D5=get(e,'cell','D5');
D6=get(e,'cell','D6');
D7=get(e,'cell','D7');
D8=get(e,'cell','D8');
D9=get(e,'cell','D9');

% %Product to HYSYS
C3.CellValue=real(Qout{1}(end));
C4.CellValue=real(Qout{2}(end));
```

```matlab
C5.CellValue=real(Qout{3}(end));
C6.CellValue=real(Qout{4}(end));
C7.CellValue=real(Qout{5}(end));
C8.CellValue=real(Qout{6}(end));

% %Recycle to HYSYS
D3.CellValue=real(Qout1{1}(end));
D4.CellValue=real(Qout1{2}(end));
D5.CellValue=real(Qout1{3}(end));
D6.CellValue=real(Qout1{4}(end));
D7.CellValue=real(Qout1{5}(end));
D8.CellValue=real(Qout1{6}(end));
D9.CellValue=H21;

 % % Temperture (TH)

for i=3:9
    A=sprintf('E%01d',i);
    TH=get(e,'cell',A);
    TH.CellValue=T-273;
end
% % Pressure Product(PP)

for i=3:9
    PP=sprintf('E%01d',i);
    PH_HYS=get(e,'cell',PP);
    PH_HYS.CellValue=PH;
end
% % Pressure Recycle(PR)
for i=3:9
    PR=sprintf('E%01d',i);
    PL_HYS=get(e,'cell',PR);
    PL_HYS.CellValue=PL;
end


% B3=get(e,'cell','B7');
% B3.CellValue=1-x;
%
% C40=get(e,'cell','C4');
% C4=C40.CellValue;
% C5=get(e,'cell','B8');
```

```
% C6=get(e,'cell','A4');
% A4=B3.CellValue;
% if C4==300
%     stop
% else
%     C5.CellValue=A4.*1.4;
% end

% Timer for over all process to convert
% t = timer;
% t.StartDelay = 3;
% t.TimerFcn = @(~,~) disp('t');
% start(t)
% wait(t)
```

G.3   Techno-economic analysis model

```
Techno-economic analysis model. TM v1.0 2021

function y=TA(x)
% loading HYSYS
%t1=clock;
x=[0 1 0 .5 131 131 221 2];
%x=[0 0 1 0.7825 145.9721 151.9549 260.8587 5];
x(8)=1;
xn=x;
save xfile.mat xn

a=actxserver('hysys.Application.V11.0');
%simcase =
a.SimulationCases.Open('C:\Users\enxtm8\Desktop\
iso6.hsc');
%simcase.invoke('Activate');

% Fillter
R1=[x(1:3)];
x(R1==0) = .01;
x(R1==1) = .98;
% R2=x(4:8);
```

```matlab
% xl(R2==0) = .025;
% xl(R2==1) = .90;
% x=[x(1:3) xl x(9:12)];
%%% end of the fillter

a.Visible = 1;
e=get(a.activeDocument.Flowsheet.Operations,'Ite
m','TE');
CO={};
if x(8)==1
    Ci=get(e,'cell','H2');%xr1
    Ci.CellValue=x(1);
    Ci=get(e,'cell','H3');%xr2
    Ci.CellValue=x(2);
    Ci=get(e,'cell','H4');%xr3
    Ci.CellValue=x(3);
    Ci=get(e,'cell','H5');%H2%
    Ci.CellValue=x(4);
    Ci=get(e,'cell','H6');%tr1
    Ci.CellValue=x(5);
    Ci=get(e,'cell','H7');%tr2
    Ci.CellValue=x(6);
    Ci=get(e,'cell','H8');%tr3
    Ci.CellValue=x(7);
elseif x(8)==2
    Ci=get(e,'cell','G2');%xr1
    Ci.CellValue=x(1);
    Ci=get(e,'cell','G3');%xr2
    Ci.CellValue=x(2);
    Ci=get(e,'cell','G4');%xr3
    Ci.CellValue=x(3);
    Ci=get(e,'cell','G5');%H2%
    Ci.CellValue=x(4);
    Ci=get(e,'cell','G6');%tr1
    Ci.CellValue=x(5);
    Ci=get(e,'cell','G7');%tr2
    Ci.CellValue=x(6);
    Ci=get(e,'cell','G8');%tr3
    Ci.CellValue=x(7);
elseif x(8)==3
    Ci=get(e,'cell','B2');%xr1
```

```matlab
        Ci.CellValue=x(1);
        Ci=get(e,'cell','B3');%xr2
        Ci.CellValue=x(2);
        Ci=get(e,'cell','B4');%xr3
        Ci.CellValue=x(3);
        Ci=get(e,'cell','B5');%H2%
        Ci.CellValue=x(4);
        Ci=get(e,'cell','B6');%tr1
        Ci.CellValue=x(5);
        Ci=get(e,'cell','B7');%tr2
        Ci.CellValue=x(6);
        Ci=get(e,'cell','B8');%tr3
        Ci.CellValue=x(7);
    elseif x(8)==4
        Ci=get(e,'cell','C2');%xr1
        Ci.CellValue=x(1);
        Ci=get(e,'cell','C3');%xr2
        Ci.CellValue=x(2);
        Ci=get(e,'cell','C4');%xr3
        Ci.CellValue=x(3);
        Ci=get(e,'cell','C5');%H2%
        Ci.CellValue=x(4);
        Ci=get(e,'cell','C6');%tr1
        Ci.CellValue=x(5);
        Ci=get(e,'cell','C7');%tr2
        Ci.CellValue=x(6);
        Ci=get(e,'cell','C8');%tr3
        Ci.CellValue=x(7);
    elseif x(8)==5
        Ci=get(e,'cell','I2');%xr1
        Ci.CellValue=x(1);
        Ci=get(e,'cell','I3');%xr2
        Ci.CellValue=x(2);
        Ci=get(e,'cell','I4');%xr3
        Ci.CellValue=x(3);
        Ci=get(e,'cell','I5');%H2%
        Ci.CellValue=x(4);
        Ci=get(e,'cell','I6');%tr1
        Ci.CellValue=x(5);
        Ci=get(e,'cell','I7');%tr2
        Ci.CellValue=x(6);
```

243

```matlab
    Ci=get(e,'cell','I8');%tr3
    Ci.CellValue=x(7);
end

Ci=get(e,'cell','B9');%NPV
Ci.CellValue=x(8);

C=get(e,'cell','M13');
i=x(8);

yC=[0 0 0 1 0; 0 0 1 0 0;1 0 0 0 0;0 1 0 0 0; 0
0 0 0 1 ];
if x(8)==i
    ys=yC(i,:);
end
%%%splits
Ci=get(e,'cell','E2');
Ci.CellValue=ys(1);
Ci=get(e,'cell','E3');
Ci.CellValue=ys(2);
Ci=get(e,'cell','E4');
Ci.CellValue=ys(3);
Ci=get(e,'cell','E5');
Ci.CellValue=ys(4);
Ci=get(e,'cell','E6');
Ci.CellValue=ys(5);




Hs=a.activeDocument.Solver;
SO=Hs.issolving;
D=int64(SO);

a.activeDocument.Solver.CanSolve = 0;
a.activeDocument.Solver.CanSolve = 1;



j=1;

if D==1
```

```matlab
        pause(180)
        load('xfile.mat')
        x=xn;
        run TA(x)
        if D==0
            clear x
        end
    end
end

if x(8)=5
    Fi=get(e,'cell','E20');
    Fo=get(e,'cell','E21');

    while Fi~=Fo
        SMB;
    end
end

cost(:,j) = C.CellValue;
y = -cost(:,j);

%fprintf('NPV= %6.2e, Solver= %6.2f\n' , [-
y,SO]')
persistent Count
if isempty(Count)
    Count = 0;
end
if nargin == 0  % Reply counter and reset it
    y    = Count;
    Count = 0;
    return;
end
if SO ==0
    Count = Count + 1;
else
    Count=Count;
end
%fprintf('NPV= %6.2e, Solver= %6.2f\n' , [-
y,SO]')
fprintf('Gen= %d pop= %1.0f x8=%d fn= %1.3e
Conv=
```

```
%1.2f\n',[floor(Count./100),abs(floor(Count./100
)-Count./100)*100,x(8),-y,SO])
%150 is the population number
if SO==0

ext=[floor(Count./100),abs(floor(Count./100)-
Count./100)*100,-y,x];
    xlswrite('NPV12main.xlsx',ext,'Sheet1',['A'
num2str(Count)]);
end
%t2=clock;
%ta=etime(t2,t1)
%disp(ta/60)
end
```

G.4   GA optimization model

```
GA optimization model. TM v1.0 2021

clc
clear all
close all

fcn = @TEA; % Call the function to optimise
n   = 8;    % Number of variables
lb  = [0 0 0 0.2 120 130 220 1]; % Lower
boundaries
ub  = [1 1 1 0.9 180 210 300 5]; % Upper
boundaries

% Equality equation
Aeq = [1 1 1 0 0 0 0 0;-1 -1 -1 0 0 0 0 0];
beq = [1;-1];

% Optimizer setting
opts = optimoptions(@ga,'PopulationSize',
100,'MaxGenerations', 20,...
    'EliteCount', 20,'CrossoverFraction',
0.0,'TolCon', 1e-8, 'PlotFcn', {@gaplot});

rng(1,'twister') % for reproducibility
```

```matlab
IntCon = [1 2 3 8]; % Integer numbers

[x, f, flag] =
ga(fcn,n,Aeq,beq,[],[],lb,ub,[],IntCon,opts);

% Result display x is the variables vector and f
is the optimal function results

disp(x)
disp(f)
```

Bibliography

Journal Articles

ABDELHAMID, M. I., GHALLAB, A. O., ETTOUNEY, R. S. & EL-RIFAI, M. A. 2017. Genetic Algorithm Optimization of a Small Scale Natural Gas Liquefaction Process. *World Academy of Science, Engineering and Technology International Journal of Chemical and Molecular Engineering,* 11**,** 574-578.

ABDELRASOUL, A., ZHANG, H., CHENG, C.-H. & DOAN, H. 2017. Applications of molecular simulations for separation and adsorption in zeolites. *Microporous and Mesoporous Materials,* 242**,** 294-348.

ABDULBARI, H. A., HAMADI, A. S. & KADHIM, R. A. 2017. Material Balance And Reaction Kinetics Modeling For Penex Isomerization Process In Daura Refinery. *MATEC Web of Conferences,* 111**,** 02012.

ADŽAMIĆ, T., MUŽIC, M., ADŽAMIĆ, Z. & BIONDA, K. S. 2011. Isomerization of n-hexane on Pt/SO4-ZrO2 catalyst. *GOMABN,* 50**,** 12-21.

AGUITONI, M. C., PAVÃO, L. V., SIQUEIRA, P. H., JIMÉNEZ, L. & RAVAGNANI, M. A. D. S. S. 2018. Heat exchanger network synthesis using genetic algorithm and differential evolution. *Computers & Chemical Engineering,* 117**,** 82-96.

AHMED, A. M., JARULLAH, A. T., ABED, F. M. & MUJTABA, I. M. 2018. Modeling of an industrial naphtha isomerization reactor and development and assessment of a new isomerization process. *Chemical Engineering Research and Design,* 137**,** 33-46.

AITANI, A., AKHTAR, M. N., AL-KHATTAF, S., JIN, Y., KOSEOGLO, O. & KLEIN, M. T. 2019. Catalytic Upgrading of Light Naphtha to Gasoline Blending Components: A Mini Review. *Energy & Fuels,* 33**,** 3828-3843.

AL-JUHANI, A. A. & LOUGHLIN, K. F. 2003. Simulation of a Combined Isomerization Reactor& Pressure Swing Adsorption Unit. *Adsorption,* 9**,** 251-264.

248

ALABDULKAREM, A., MORTAZAVI, A., HWANG, Y., RADERMACHER, R. & ROGERS, P. 2011. Optimization of propane pre-cooled mixed refrigerant LNG plant. *Applied Thermal Engineering,* 31**,** 1091-1098.

ALI, L. I., ALI, A.-G. A., ABOUL-FOTOUH, S. M. & K., A.-G. A. 2001. Hydroconversion of n-paraffins in light naphtha using Pt/Al2O3 catalysts promoted with noble metals and/or chlorine. *Applied Catalysis A: General,* 205**,** 129-146.

AN, J., NA, J., LEE, U. & HAN, C. 2018. Design of carbon dioxide dehydration process using derivative-free superstructure optimization. *Chemical Engineering Research and Design,* 129**,** 344-355.

APOSTOLAKOU, A. A., KOOKOS, I. K., MARAZIOTI, C. & ANGELOPOULOS, K. C. 2009. Techno-economic analysis of a biodiesel production process from vegetable oils. *Fuel Processing Technology,* 90**,** 1023-1031.

BAGAJEWICZ, M. J. & MANOUSIOUTHAKIS, V. 1992. Mass/heat-exchange network representation of distillation networks. *AIChE Journal,* 38**,** 1769-1800.

BAO, J., GAO, B., WU, X., YOSHIMOTO, M. & NAKAO, K. 2002. Simulation of industrial catalytic-distillation process for production of methyl tert-butyl ether by developing user's model on Aspen plus platform. *Chemical Engineering Journal,* 90**,** 253-266.

BÁRCIA, P. S., SILVA, J. A. C. & RODRIGUES, A. E. 2007. Separation of branched hexane isomers on zeolite BETA. *Adsorption Science & Technology,* 25**,** 169-183.

BÁRCIA, P. S., SILVA, J. A. C. & RODRIGUES, A. R. E. 2010a. Adsorption Dynamics of C5−C6Isomerate Fractions in Zeolite Beta for the Octane Improvement of Gasoline. *Energy & Fuels,* 24**,** 1931-1940.

BÁRCIA, P. S., SILVA, J. A. C. & RODRIGUES, A. R. E. 2010b. Octane Upgrading of C5/C6Light Naphtha by Layered Pressure Swing Adsorption. *Energy & Fuels,* 24**,** 5116-5130.

BILDEA, C. S., GYŐRGY, R., SÁNCHEZ-RAMÍREZ, E., QUIROZ-RAMÍREZ, J. J., SEGOVIA-HERNANDEZ, J. G. & KISS, A. A. 2015. Optimal design and plantwide control of novel processes

249

for di-n-pentyl ether production. *Journal of Chemical Technology & Biotechnology,* 90**,** 992-1001.

BOBÁK, M., SNITA, D., HRDLICKA, J., PELC, V. & KOTALA, T. 2014. Innovative process simulation software not only for electromembrane processes. *Desalination and Water Treatment,* 56**,** 3141-3145.

BROUGHTON, D. B. & GERHOLD, C. G. 1957. Continuous sorption process employing fixed bed of sorbent and moving inlets and outlets. US2985589A.

BUSTO, M., BENÍTEZ, V. M., VERA, C. R., GRAU, J. M. & YORI, J. C. 2008. Pt-Pd/WO3-ZrO2 catalysts for isomerization-cracking of long paraffins. *Applied Catalysis A: General,* 347**,** 117-125.

BUSTO, M., DOSSO, L. A., VERA, C. R. & GRAU, J. M. 2012. Composite catalysts of Pt/SO42−–ZrO2 and Pt/WO3–ZrO2 for producing high octane isomerizate by isomerization-cracking of long paraffins. *Fuel Processing Technology,* 104**,** 128-135.

BUSTO, M., VERA, C. R. & GRAU, J. M. 2011. Optimal process conditions for the isomerization–cracking of long-chain n-paraffins to high octane isomerizate gasoline over Pt/SO42—ZrO2 catalysts. *Fuel Processing Technology,* 92**,** 1675-1684.

CABALLERO, J. A. 2015. Logic hybrid simulation-optimization algorithm for distillation design. *Computers & Chemical Engineering,* 72**,** 284-299.

CAO, W. & MUJTABA, I. M. 2015. Simulation of Vacuum Membrane Distillation Process for Desalination with Aspen Plus. *Industrial & Engineering Chemistry Research,* 54**,** 672-680.

CARROLL, C. W. 1961. The created response surface technique for optimizing nonlinear, restrained systems. *Operations research,* 9**,** 169-184.

CHEKANTSEV, N. V., GYNGAZOVA, M. S. & IVANCHINA, E. D. 2014. Mathematical modeling of light naphtha (C5, C6) isomerization process. *Chemical Engineering Journal,* 238**,** 120-128.

CHEN, Q. & GROSSMANN, I. E. 2017. Recent Developments and Challenges in Optimization-Based Process Synthesis. *Annual Review of Chemical and Biomolecular Engineering,* 8**,** 249-283.

250

CHEN, Z., XU, J., FAN, Y., SHI, G. & BAO, X. 2015. Reaction mechanism and kinetic modeling of hydroisomerization and hydroaromatization of fluid catalytic cracking naphtha. *Fuel Processing Technology,* 130**,** 117-126.

CHEN, Z., YE, X. & HUANG, P. 2018. Estimating Carbon Dioxide (CO2) Emissions from Reservoirs Using Artificial Neural Networks. *Water,* 10.

CHRISTOPHER, C. C. E., DUTTA, A., FAROOQ, S. & KARIMI, I. A. 2017. Process Synthesis and Optimization of Propylene/Propane Separation Using Vapor Recompression and Self-Heat Recuperation. *Industrial & Engineering Chemistry Research,* 56**,** 14557-14564.

CHUE, K. T., KIM, J. N., YOO, Y. J., CHO, S. H. & YANG, R. T. 1995. Comparison of Activated Carbon and Zeolite 13X for CO2 Recovery from Flue Gas by Pressure Swing Adsorption. *Industrial & Engineering Chemistry Research,* 34**,** 591-598.

CHUZLOV, V. A., CHEKANTSEV, N. V. & IVANCHINA, E. D. 2014. Development of Complex Mathematical Model of Light Naphtha Isomerization and Rectification Processes. *Procedia Chemistry,* 10**,** 236-243.

CHUZLOV, V. A., DOLGANOV, I. M., DOLGANOVA, I. O., SEITENOVA, G. Z. & DUSOVA, R. M. 2019. Increase in resource efficiency of motor gasoline production with the help of mathematical models. *Petroleum and Coal,* 61**,** 6.

CHUZLOV, V. A., IVANCHINA, E. D., CHEKANTSEV, N. V. & MOLOTOV, K. V. 2015a. Efficiency Improvement of the Light Gasoline Fractions Isomerization by Mathematical Modeling. *Procedia Engineering,* 113**,** 131-137.

CHUZLOV, V. A., IVANCHINA, E. D., DOLGANOV, I. M. & MOLOTOV, K. V. 2015b. Simulation of Light Naphtha Isomerization Process. *Procedia Chemistry,* 15**,** 282-287.

CHUZLOV, V. A., IVANCHINA, E. D., SEJTENOVA, G. Z. & IVANOV, S. Y. 2017. The branched C5-C6 hydrocarbons synthesis on Pt-catalyst. *Current Organic Synthesis,* 14**,** 332-341.

CHUZLOV, V. A. & MOLOTOV, K. V. 2016. Development of computer modelling system as a tool for light naphtha isomerization improvment. *Petroleum and Coal,* 58**,** 47-55.

CLAUMANN, C. A., PARISOTTO, I. G. B., PERUZZO, T., FELICE, V. D., MARANGONI, C. & MACHADO, R. A. F. 2015. Modeling and process optimization: An approach using aspen plus and matlab in the energy integration study of distillation columns. *AAIQ Asociación Argentina de Ingenieros Químicos – CSPQ,* 8.

CUI, C. & SUN, J. 2019. Rigorous design and simultaneous optimization of extractive distillation systems considering the effect of column pressures. *Chemical Engineering and Processing - Process Intensification,* 139**,** 68-77.

DAI, T., FAN, H. M., FU, Y. J. & YANG, H. Z. 2017. Secondary Development of Aspen Plus User Model Based on Soft-Sensor. *Huadong Ligong Daxue Xuebao/Journal of East China University of Science and Technology,* 43**,** 533-539.

DHAR, A., VEKARIYA, R. L. & SHARMA, P. 2017. Kinetics and mechanistic study of n -alkane hydroisomerization reaction on Pt-doped γ-alumina catalyst. *Petroleum,* 3**,** 489-495.

DHOLE, V. R. & LINNHOFF, B. 1993. Total site targets for fuel, co-generation, emissions, and cooling. *Computers & Chemical Engineering,* 17**,** S101-S109.

DÍEZ, E., LANGSTON, P., OVEJERO, G. & ROMERO, M. D. 2009. Economic feasibility of heat pumps in distillation to reduce energy use. *Applied Thermal Engineering,* 29**,** 1216-1223.

DIPAMA, J., TEYSSEDOU, A. & SORIN, M. 2008. Synthesis of heat exchanger networks using genetic algorithms. *Applied Thermal Engineering,* 28**,** 1763-1773.

DO, D. D. & RICE, R. G. 1986. Validity of the parabolic profile assumption in adsorption studies. *AIChE Journal,* 32**,** 149-154.

DOUGLAS, J. M. 1985. A hierarchical decision procedure for process synthesis. *AIChE Journal,* 31**,** 353-362.

DUTTA, A., KARIMI, I. A. & FAROOQ, S. 2018. Heating Value Reduction of LNG (Liquefied Natural Gas) by Recovering Heavy Hydrocarbons: Technoeconomic Analyses Using Simulation-

252

Based Optimization. *Industrial & Engineering Chemistry Research,* 57**,** 5924-5932.

DZHIKIYA, O. V., SMOLIKOV, M. D., ZATOLOKINA, E. V., KAZANTSEV, K. V. & BELYI, A. S. 2016. Isomerization of n-hexane on Pd/SO42-/ZrO2/Al2O3 and Mechanical Mixtures Pd/Al2O3 (Pd/SiO2) + SO42-/ZrO2/Al2O3. *Procedia Engineering,* 152**,** 116-121.

EINI, S. S., H.R.; JAVIDI, M., SHARIFZADEH, M. & RASHTCHIAN, D. 2016. Inherently safe and economically optimal design using multi-objective optimization: The case of a refrigeration cycle. *Process. Saf. Environ. Prot,* 104**,** 254–267.

EJTEMAEI, M., CHARCHI AGHDAM, N., BABALUO, A., TAVAKOLI, A. & BAYATI, B. 2018. Isomerization of C5 isomers in the BZSM-5 membrane reactor packed with Pt/SZ nanocatalyst. *Chemical Engineering and Processing - Process Intensification,* 130**,** 185-191.

ELIXMANN, D., PUSCHKE, J., SCHEU, H., SCHNEIDER, R., WOLF, I. & MARQUARDT, W. 2014. A software environment for economic NMPC and dynamic real-time optimization of chemical processes. *at - Automatisierungstechnik,* 62.

ELLIS, M., DURAND, H. & CHRISTOFIDES, P. D. 2014. A tutorial review of economic model predictive control methods. *Journal of Process Control,* 24**,** 1156-1178.

ESTRADA-VILLAGRANA, A. D., QUIROZ-SOSA, G. B., JIMÉNEZ-ALARCÓN, M. L., ALEMÁN-VÁZQUEZ, L. O. & CANO-DOMÍNGUEZ, J. L. 2006. Comparison between a conventional process and reactive distillation for naphtha hydrodesulfurization. *Chemical Engineering and Processing: Process Intensification,* 45**,** 1036-1040.

FANG, J., CHENG, X., LI, Z., LI, H. & LI, C. 2018. A review of internally heat integrated distillation column. *Chinese Journal of Chemical Engineering.*

FATHY, D. A. N. & SOLIMAN, M. A. 2019. A Multi-Response Optimization for Isomerization of light Naphtha. *International Journal of Innovative Technology and Exploring Engineering,* 8**,** 3921-3933.

FENG, M., ZHOU, X., HU, W., WANG, W. & LI, C. 2017. Improved separation and utilization of light naphtha stock by adsorption process. *Adsorption Science & Technology,* 36**,** 732-742.

FENG, Z., SHEN, W., RANGAIAH, G. P. & DONG, L. 2018. Proportional-Integral Control and Model Predictive Control of Extractive Dividing-Wall Column Based on Temperature Differences. *Industrial & Engineering Chemistry Research,* 57**,** 10572-10590.

FENG, Z., SHEN, W., RANGAIAH, G. P. & DONG, L. 2020. Design and control of vapor recompression assisted extractive distillation for separating n-hexane and ethyl acetate. *Separation and Purification Technology.*

FONTALVO, J. 2014. Using user models in Matlab® within the Aspen Plus® interface with an Excel® link. *INGENIERÍA E INVESTIGACIÓN,* 34**,** 39-43.

FONYO, Z. & BENKO, N. 1996. Enhancement of process integration by heat pumping. *Computers chem. Engng,* 20**,** S85-S90.

FONYO, Z. & BENKÖ, N. 1998. Comparison of Various Heat Pump Assisted Distillation Configurations. *Chemical Engineering Research and Design,* 76**,** 348-360.

FONYO, Z., KURRAT, R., RIPPIN, D. W. T. & MESZAROS, I. 1995. Comparative analysis of various heat pump schemes applied to C4 splitibrs. *Computers & Chemical Engineering,* 19.

FRIEDLER, F., TARJAN, K., HUANG, Y. W. & FAN, L. T. 1992a. Combinatorial algorithms for process synthesis. *Computers & Chemical Engineering,* 16**,** S313-S320.

FRIEDLER, F., TARJAN, K., HUANG, Y. W. & FAN, L. T. 1993. Graph-theoretic approach to process synthesis: Polynomial algorithm for maximal structure generation. *Computers & Chemical Engineering,* 17**,** 929-942.

FRIEDLER, F., TARJÁN, K., HUANG, Y. W. & FAN, L. T. 1992b. Graph-theoretic approach to process synthesis: axioms and theorems. *Chemical Engineering Science,* 47**,** 1973-1988.

FU, H., QIN, H., WANG, Y., LIU, Y., YANG, C. & SHAN, H. 2018. Adsorption and separation of n/iso-pentane on zeolites: A GCMC study. *J Mol Graph Model,* 80**,** 59-66.

GÓMEZ-GARCÍA, M. Á., DOBROSZ-GÓMEZ, I. & TAQUEZ, H. N. I. 2016. Membrane reactors for isoamyl acetate production. *Chemical Engineering and Processing: Process Intensification,* 102**,** 27-36.

GOR, G. Y., PARIS, O., PRASS, J., RUSSO, P. A., RIBEIRO CARROTT, M. M. & NEIMARK, A. V. 2013. Adsorption of n-pentane on mesoporous silica and adsorbent deformation. *Langmuir,* 29**,** 8601-8.

GROSSMANN, I. E. 1989. MINLP optimization strategies and algorithms for process synthesis.

GROSSMANN, I. E., WESTERBERG, A. W. & BIEGLER, L. T. 1987. Retrofit design of processes.

HAIDER, S., LINDBRÅTHEN, A. & HÄGG, M.-B. 2016. Techno-economical evaluation of membrane based biogas upgrading system: A comparison between polymeric membrane and carbon membrane technology. *Green Energy & Environment,* 1**,** 222-234.

HAIDER, S., LINDBRÅTHEN, A., LIE, J. A. & HÄGG, M.-B. 2018. Carbon membranes for oxygen enriched air – Part II: Techno-economic analysis. *Separation and Purification Technology,* 205**,** 251-262.

HAMELINCK, C., FAAIJ, A., DENUIL, H. & BOERRIGTER, H. 2004. Production of FT transportation fuels from biomass; technical options, process analysis and optimisation, and development potential. *Energy,* 29**,** 1743-1771.

HANCSÓK, J., KASZA, T. & VISNYEI, O. 2020. Isomerization of n-C5/C6 Bioparaffins to Gasoline Components with High Octane Number. *Energies,* 13.

HASHIM, A. R. & JASSIM, A. A. A. 2014. Enhance C5+ Recovery Predicting and Maximizing The Reformate Production in Naphtha Stabilizer Using HYSYS. *Journal of Chemical, Biological and Physical Sciences,* 4**,** 14.

HASSANAT, A., ALMOHAMMADI, K., ALKAFAWEEN, E. A., ABUNAWAS, E., HAMMOURI, A. & PRASATH, V. B. S. 2019. Choosing Mutation and Crossover Ratios for Genetic

Algorithms—A Review with a New Dynamic Approach. *Information,* 10.

HASSIM, M. H., PÉREZ, A. L. & HURME, M. 2010. Estimation of chemical concentration due to fugitive emissions during chemical process design. *Process. Saf. Environ.*

HAYATI, R., ABGHARI, S. Z., SADIGHI, S. & BAYAT, M. 2014. Development of a rule to maximize the research octane number (RON) of the isomerization product from light naphtha. *Korean Journal of Chemical Engineering,* 32**,** 629-635.

HAYNES, V. O. 1979. Energy Use in Petroleum Refineries.

HEIKKILÄ, A. M. 1999. Inherent Safety in Process Plant Design. *Technical Research Centre of Finland.*

HENRIQUE, A., RODRIGUES, A. E. & SILVA, J. A. C. 2018. Separation of Hexane Isomers in ZIF-8 by Fixed Bed Adsorption. *Industrial & Engineering Chemistry Research,* 58**,** 378-394.

HERNANDEZ-PEREZ, L. G., ALSUHAIBANI, A. S., RADWAN, N., EL-HALWAGI, M. M. & PONCE-ORTEGA, J. M. 2020. Structural and Operating Optimization of the Methanol Process Using a Metaheuristic Technique. *ACS Sustainable Chemistry & Engineering,* 8**,** 3135-3150.

HINOJOSA, A. I. & ODLOAK, D. 2014. Study of the implementation of a robust MPC in a propylene/propane splitter using rigorous dynamic simulation. *The Canadian Journal of Chemical Engineering,* 92**,** 1213-1224.

HOJJATI, M. R. & NAMDARI GHAREGHANI, H. 2019. Conceptual design of distillation columns sequence for separation of pentane and hexane from C5+ stream of LPG unit. *Energy Sources, Part A: Recovery, Utilization, and Environmental Effects,* 42**,** 267-280.

HUNTER 2003. Light Naphtha isomerisation to meet 21st century gasoline specifications. *Oil Gas European Magazine,* 29**,** 97-107.

IVANOVA, A. V., VASINA, T. V., MASLOBOISHCHIKOVAA, O. V., KHELKOVSKAYA-SERGEEVAA, E. G., KUSTOVA, L. M. & HOUZVICKA, J. I. 2002. Isomerization of n-alkanes on Pt/WO3–SO4/ZrO2 systems. *Catalysis Today,* 73**,** 95-103.

JANA, A. K. 2010. Heat integrated distillation operation. *Applied Energy,* 87**,** 1477-1494.

JANA, A. K. 2014. Advances in heat pump assisted distillation column: A review. *Energy Conversion and Management,* 77**,** 287-297.

JAVALOYES-ANTÓN, J., RUIZ-FEMENIA, R. & CABALLERO, J. A. 2013. Rigorous Design of Complex Distillation Columns Using Process Simulators and the Particle Swarm Optimization Algorithm. *Industrial & Engineering Chemistry Research,* 52**,** 15621-15634.

KAMARUDIN, S. K., DAUD, W. R. W., MD.SOM, A., TAKRIFF, M. S. & MOHAMMAD, A. W. 2006. Technical design and economic evaluation of a PEM fuel cell system. *Journal of Power Sources,* 157**,** 641-649.

KAZANTSEV, K. V., BIKMETOVA, L. I., DZHIKIYA, O. V., SMOLIKOV, M. D. & BELYI, A. S. 2016. Particle Swarm Optimization for Inverse Chemical Kinetics Problem Solving as Applied to n-hexane Isomerization on Sulfated Zirconia Catalysts. *Procedia Engineering,* 152**,** 34-39.

KAZEMI, A., MEHRABANI-ZEINABAD, A. & BEHESHTI, M. 2018a. Distillation without hot utilities; development of novel distillation configurations for energy and costs saving for separation of propylene/propane mixture. *Chemical Engineering and Processing - Process Intensification,* 123**,** 158-167.

KAZEMI, A., MEHRABANI-ZEINABAD, A. & BEHESHTI, M. 2018b. Recently developed heat pump assisted distillation configurations: A comparative study. *Applied Energy,* 211**,** 1261-1281.

KAZEMI, A., RASTI, Y., MEHRABANI-ZEINABAD, A. & BEHESHTI, M. 2017. Evaluation of a novel configuration of bottom flashing on dual distillation columns for saving energy. *International Journal of Industrial Chemistry,* 9**,** 75-84.

KEIL, F. J. 2018. Process intensification. *Reviews in Chemical Engineering,* 34**,** 135-200.

KIKKINIDES, E. S., YANG, R. T. & CHO, S. H. 1993. Concentration and recovery of carbon dioxide from flue gas by pressure swing

adsorption. *Industrial & Engineering Chemistry Research,* 32**,** 2714-2720.

KIMURA, T. 2003. Development of Pt/SO42−/ZrO2 catalyst for isomerization of light naphtha. *Catalysis Today,* 81**,** 57-63.

KIRKPATRICK, S., GELATT, C. D. & VECCHI, J., M. P. 1983. Optimization by simulated annealing. *Science,* 220.

KISS, A. A., LANDAETAA, S. J. F. & FERREIRAC, C. A. I. 2012a. Mastering Heat Pumps Selection for Energy Efficient Distillation. *CHEMICAL ENGINEERING TRANSACTIONS,* 29.

KLEMEŠ, J. J. & KRAVANJA, Z. 2013. Forty years of Heat Integration: Pinch Analysis (PA) and Mathematical Programming (MP). *Current Opinion in Chemical Engineering,* 2**,** 461-474.

KLEMEŠ, J. J., VARBANOV, P. S., WALMSLEY, T. G. & JIA, X. 2018. New directions in the implementation of Pinch Methodology (PM). *Renewable and Sustainable Energy Reviews,* 98**,** 439-468.

KNAEBEL, K. S. & HILL, F. B. 1985. Pressure swing adsorption: Development of an equilibrium theory for gas separations. *Chemical Engineering Science,* 40**,** 2351-2360.

KOCIS, G. R. & GROSSMANN, I. E. 1989. A modelling and decomposition strategy for the MINLP optimization of process flowsheets. *Computers & Chemical Engineering,* 13**,** 797-819.

KONCSAG, C. I., TUTUN, I. A. & SAFTA, C. 2011. Study of C5/C6 isomerization on Pt/H-zeolite catalyst in industrial conditions. *Ovidius University Annals of Chemistry,* 22(2)**,** 102-106.

KONDILI, E., PANTELIDES, C. C. & SARGENT, R. W. H. 1993. A general algorithm for short-term scheduling of batch operations— I. MILP formulation. *Computers & Chemical Engineering,* 17**,** 211-227.

LAM, H. L., KLEMEŠ, J. J., KRAVANJA, Z. & VARBANOV, P. S. 2011. Software tools overview: process integration, modelling and optimisation for energy saving and pollution reduction. *Asia-Pacific Journal of Chemical Engineering,* 6**,** 696-712.

LAMPRECHT, D. & KLERK, A. D. 2009. Hydroisomerization of 1-Pentene to Iso-Pentane in a Single Reactor. *Chemical Engineering Communications,* 196**,** 1206-1216.

LEDEZMA-MARTÍNEZ, M., JOBSON, M. & SMITH, R. 2018. Simulation–Optimization-Based Design of Crude Oil Distillation Systems with Preflash Units. *Industrial & Engineering Chemistry Research,* 57**,** 9821-9830.

LEE, C.-G., SONG, Y. J., LEE, K. B. & MUN, S. 2019. The first attempt at continuous-mode separation of racemic and meso-2,3-butanediol with high purities using a simulated-moving-bed process. *Journal of Industrial and Engineering Chemistry,* 80**,** 677-685.

LEE, U., JEON, J., HAN, C. & LIM, Y. 2017. Superstructure based techno-economic optimization of the organic rankine cycle using LNG cryogenic energy. *Energy,* 137**,** 83-94.

LEE, U., MITSOS, A. & HAN, C. 2016. Optimal retrofit of a CO2 capture pilot plant using superstructure and rate-based models. *International Journal of Greenhouse Gas Control,* 50**,** 57-69.

LI, W., CHI, K., LIU, H., MA, H., QU, W., WANG, C., LV, G. & TIAN, Z. 2017. Skeletal isomerization of n -pentane: A comparative study on catalytic properties of Pt/WO x –ZrO 2 and Pt/ZSM-22. *Applied Catalysis A: General,* 537**,** 59-65.

LU, Z. P. & CHING, C. B. 1997. Dynamics of Simulated Moving-Bed Adsorption Separation Processes. *Separation Science and Technology,* 32**,** 1993-2010.

LUTZE, P., GANI, R. & WOODLEY, J. M. 2010. Process intensification: A perspective on process synthesis. *Chemical Engineering and Processing: Process Intensification,* 49**,** 547-558.

LUYBEN, W. L. 2011. Control of an Isomerization Column/Reactor Process. *Industrial & Engineering Chemistry Research,* 50**,** 3382-3389.

MACHT, J., CARR, R. T. & IGLESIA, E. 2009. Consequences of acid strength for isomerization and elimination catalysis on solid acids. *JACS Articles,* 131**,** 6554–6565.

MADSEN, N. & SINCOVEC, R. F. 1979. Algorithm 540: PDECOL, General Collocation Software for Partial Differential Equations [D3]. *ACM Trans. Math. Softw.,* 5**,** 326-351.

MANGONE, F., FERREIRA, J. & TORRES, A. I. 2019. BISSO: Biomass Interface for Superstructure Simulation and Optimization. *Processes,* 7.

MARQUES, J. P., MATOS, H. A., OLIVEIRA, N. M. C. & NUNES, C. P. 2017. State-of-the-art review of targeting and design methodologies for hydrogen network synthesis. *International Journal of Hydrogen Energy,* 42**,** 376-404.

MARTINEZ-GOMEZ, J., NÁPOLES-RIVERA, F., PONCE-ORTEGA, J. M. & EL-HALWAGI, M. M. 2017. Optimization of the production of syngas from shale gas with economic and safety considerations. *Applied Thermal Engineering,* 110**,** 678-685.

MASEL, R. H., SMITH, D. W. & LUYBEN, W. L. 2013. Use of Two Distillation Columns in Systems with Maximum Temperature Limitations. *Industrial & Engineering Chemistry Research,* 52**,** 5172-5176.

MCCALL, J. 2005. Genetic algorithms for modelling and optimisation. *Journal of Computational and Applied Mathematics,* 184**,** 205-222.

MENCARELLI, L., CHEN, Q., PAGOT, A. & GROSSMANN, I. E. 2020. A review on superstructure optimization approaches in process system engineering. *Computers & Chemical Engineering,* 136.

MIO, A., LIMLEAMTHONG, P., GUILLÉN-GOSÁLBEZ, G. & FERMEGLIA, M. 2018. Sustainability Evaluation of Alternative Routes for Fine Chemicals Production in an Early Stage of Process Design Adopting Process Simulation along with Data Envelopment Analysis. *Industrial & Engineering Chemistry Research,* 57**,** 7946-7960.

MIX, T. W., DWECK, J. S., WEINBERG, M. & ARMSTRONG, R. C. 1981. Energy conservation in distillation. *NASA STI/Recon Technical Report N,* 82.

MOGHADAM, N., MASOUD, S. & HOSSEINI, Z. B. M. 2012. Simulation of gas condensate stabilization unit aiming at selecting the right technique and assessing the optimized operational parameters.

International Proceedings of Chemical, Biological and Environmental Engineering, 43, 78-82.

MOGHADAM, N. & SAMADI, M. 2012. Gas Condensate Stabilization Unit: Different Design Approaches. *International Journal of Chemical Engineering and Applications*, 461-465.

MOHAMED, M. F., SHEHATA, W. M., ABDEL HALIM, A. A. & GAD, F. K. 2017. Improving gasoline quality produced from MIDOR light naphtha isomerization unit. *Egyptian Journal of Petroleum,* 26, 111-124.

MORAR, M. & AGACHI, P. S. 2010. Review: Important contributions in development and improvement of the heat integration techniques. *Computers & Chemical Engineering,* 34, 1171-1179.

NAQVI, S. R., BIBI, A., NAQVI, M., NOOR, T., NIZAMI, A.-S., REHAN, M. & AYOUB, M. 2018. New trends in improving gasoline quality and octane through naphtha isomerization: a short review. *Applied Petrochemical Research*.

NAVARRO-AMORÓS, M. A., RUIZ-FEMENIA, R. & CABALLERO, J. A. 2014. Integration of modular process simulators under the Generalized Disjunctive Programming framework for the structural flowsheet optimization. *Computers & Chemical Engineering,* 67, 13-25.

NAWAZ, Z. 2017. Methyl-Tert-Butyl-Ether Synthesis Reactor Modelling and Optimization Using an Aspen Custom Modeler. *Hungarian Journal of Industry and Chemistry,* 45, 1-7.

NISHIDA, N., STEPHANOPOULOS, G. & WESTERBERG, A. W. 1981. A review of process synthesis. *AIChE Journal,* 27, 321-351.

ONEL, O., NIZIOLEK, A. M. & FLOUDAS, C. A. 2016. Optimal Production of Light Olefins from Natural Gas via the Methanol Intermediate. *Industrial & Engineering Chemistry Research,* 55, 3043-3063.

OSORIO-VIANA, W., IBARRA-TAQUEZ, H. N., DOBROSZ-GÓMEZ, I. & GÓMEZ-GARCÍA, M. Á. 2014. Hybrid membrane and conventional processes comparison for isoamyl acetate production. *Chemical Engineering and Processing: Process Intensification,* 76, 70-82.

OTTE, D., LORENZ, H.-M. & REPKE, J.-U. 2016. A toolbox using the stochastic optimization algorithm MIPT and ChemCAD for the systematic process retrofit of complex chemical processes. *Computers & Chemical Engineering,* 84**,** 371-381.

PASHA, M. K., AHMAD, I., MUSTAFA, J. & KANO, M. 2019. Modeling of a Nickel-based Fluidized Bed Membrane Reactor for Steam Methane Reforming Process. *JOURNAL OF THE CHEMICAL SOCIETY OF PAKISTAN,* 41**,** 219-229.

PATHER, K. & LOKHAT, D. 2014. Gas-phase Hydroisomerization of n-Hexane Over Pt/SO4-ZrO2: Kinetic Modeling and Reactor Simulation. *Petroleum Science and Technology,* 32**,** 2786-2794.

PESTRYAKOV, A., CHUZLOV, V., MOLOTOV, K., KOROTKOVA, E. & VOROBEV, A. 2016. Analysis of Optimal Process Flow Diagrams of Light Naphtha Isomerization Process by Mathematic Modelling Method. *MATEC Web of Conferences,* 85**,** 01036.

PETERS, L., HUSSAIN, A., FOLLMANN, M., MELIN, T. & HÄGG, M. B. 2011. CO2 removal from natural gas by employing amine absorption and membrane technology—A technical and economical analysis. *Chemical Engineering Journal,* 172**,** 952-960.

PHAM, V. & EL-HALWAGI, M. 2012. Process synthesis and optimization of biorefinery configurations. *AIChE Journal,* 58**,** 1212-1221.

PIKULIK, A. & HE, D. 1977. COST ESTIMATING FOR MAJOR PROCESS EQUIPMENT.

POLANEC, D., BIONDA, K. S., ADŽAMIĆ, Z. & MUŽIC, M. 2012. Influence of benzene on the process of n-hexane isomerization on pt/so4 2-/zro2 catalyst. *GOMABN,* 51**,** 298-305.

QIAN, X.-H., SUN, X.-J., WANG, K.-F., DONG, H.-G. & YAO, P.-J. 2007. Energy Integration Based on Simulation Analysis and Stochastic Search. *Journal of Chemical Engineering of Chinese Universities,* 21**,** 322.

RANGAIAH, G. P., FENG, Z. & HOADLEY, A. F. 2020. Multi-Objective Optimization Applications in Chemical Process Engineering: Tutorial and Review. *Processes,* 8.

REDDY, C. C. S., FANG, Y. & RANGAIAH, G. P. 2014. Improving energy efficiency of distillation using heat pump assisted columns. *Asia-Pacific Journal of Chemical Engineering,* 9**,** 905-928.

RICARDEZ-SANDOVAL, L. A., BUDMAN, H. M. & DOUGLAS, P. L. 2009. Integration of design and control for chemical processes: A review of the literature and some recent results. *Annual Reviews in Control,* 33**,** 158-171.

RODRÍGUEZ-RUIZ, I., TEYCHENÉ, S., VITRY, Y., BISCANS, B. & CHARTON, S. 2018. Thermodynamic modeling of neodymium and cerium oxalates reactive precipitation in concentrated nitric acid media. *Chemical Engineering Science,* 183**,** 20-25.

SAID, M. M., AHMED, T. S. & MOUSTAFA, T. M. 2014. Predictive Modeling and Optimization for an Industrial Penex Isomerization Unit: A Case Study. *Energy & Fuels,* 28**,** 7726-7741.

SHACHAM, M., MACCHIETO, S., STUTZMAN, L. F. & BABCOCK, P. 1982. Equation oriented approach to process flowsheeting. *Computers & Chemical Engineering,* 6**,** 79-95.

SHARIFZADEH, M. & THORNHILL, N. F. 2011. Optimal controlled variable selection using a nonlinear simulation-optimization framework. *21st European Symposium on Computer Aided Process Engineering – ESCAPE 21,* 29**,** 597-601.

SIIROLA, J. J. & RUDD, D. F. 1971. Computer-Aided Synthesis of Chemical Process Designs. From Reaction Path Data to the Process Task Network. *Industrial & Engineering Chemistry Fundamentals,* 10**,** 353-362.

SILVA-RODRIGO, R., CRUZ-DOMÍNGUEZ, E. L., ANGEL, F. E. L.-D., NAVARRETE-BOLAÑOS, J., GARCÍA-ALAMILLA, R., OLIVAS-SARABIA, A., MELO-BANDA, J. A., CRUZ-NETRO, L. C., ZAMORA-RAMÍREZ, G. & CASTILLO-MARES, A. 2015. Studies of sulphated mixed oxides (ZrO_2–SO_4–La_2O_3) in the isomerization of n-hexane. *Catalysis Today,* 250**,** 197-208.

SILVA, J. A. C., DA SILVA, F. A. & RODRIGUES, A. E. 2000. Separation of n/iso paraffins by PSA. *Separation and Purification Technology,* 20**,** 97-110.

SILVA, J. A. C. & RODRIGUES, A. E. 1997. Fixed-Bed Adsorption of n-Pentane/Isopentane Mixtures in Pellets of 5A Zeolite. *Ind. Eng. Chem. Res.,* 36**,** 3769-3777.

SILVA, J. A. C. & RODRIGUES, A. E. 1998. Separation of n/iso-paraffins mixtures by pressure swing adsorption. *Separation and Purification Technology,* 13**,** 165-208.

SITTER, S., CHEN, Q. & E. GROSSMANN, I. 2019. An Overview of Process Intensification Methods. *Current Opinion in Chemical Engineering.*

SKIBOROWSKI, M. 2018. Process synthesis and design methods for process intensification. *Current Opinion in Chemical Engineering,* 22**,** 216-225.

SMITH, E. M. B. & PANTELIDES, C. C. 1995. Design of reaction/separation networks using detailed models. *Computers & Chemical Engineering,* 19**,** 83-88.

SMITH, R. & LINNHOFF, B. 1988. The design of separators in the context of overall processes. *Chem. Eng. Res. Of Chemical Engineering Research and Design, Rugby,* 66**,** 34.

STEIMEL, J., HARRMANN, M., SCHEMBECKER, G. & ENGELL, S. 2013. Model-based conceptual design and optimization tool support for the early stage development of chemical processes under uncertainty. *Computers & Chemical Engineering,* 59**,** 63-73.

STEIMEL, J., HARRMANN, M., SCHEMBECKER, G. & ENGELL, S. 2014. A framework for the modeling and optimization of process superstructures under uncertainty. *Chemical Engineering Science,* 115**,** 225-237.

STORN, R. & PRICE, K. 1997. Differential Evolution – A Simple and Efficient Heuristic for global Optimization over Continuous Spaces. *Journal of Global Optimization,* 11**,** 341-359.

SUBIYANTO, AHMAD, M. F., MAMAT, M. & HUSAIN, M. L. 2013. Comparison of numerical method for forward and backward time centered space for long-term simulation of shoreline evolution. *Applied Mathematical Sciences,* 7**,** 5165-5173.

SUMAN, S. K. & GIRI, V. K. 2015. Genetic Algorithms Basic Concepts and Real World Applications. *International Journal of Electrical, Electronics and Computer Systems (IJEECS),* 3.

SUNDBERG, J., STANDL, S., VON ARETIN, T., TONIGOLD, M., REHFELDT, S., HINRICHSEN, O. & KLEIN, H. 2018. Optimal process for catalytic cracking of higher olefins on ZSM-5. *Chemical Engineering Journal,* 348**,** 84-94.

SZOBOSZLAI, Z. & HANCSÓK, J. 2010. Investigation of isomerization of sulphur containing hexane fractions. *Hungarian journal of industrial chemistry veszprém,* 38**,** 71-76.

SZOBOSZLAI, Z. & HANCSÓK, J. 2011. Investigation of kinetics of hydroisomerization of C5/C6 and C6/C7 alkanes and their binary mixtures. *Hungarian journal of industrial chemistry veszprém,* 39**,** 117-120.

SZOBOSZLAI, Z., PÖLCZMANN, G. & HANCSÓK, J. 2012. Investigation of isomerisation of light naphtha fractions. *Chemical engineering transactions,* 29.

TABARI, A. & AHMAD, A. 2015. A semicontinuous approach for heterogeneous azeotropic distillation processes. *Computers & Chemical Engineering,* 73**,** 183-190.

TAILLEUR, R. G. & PLATIN, J. B. 2008. Role of Pt on PtGaZr/SiO2 catalyst in light naphtha isomerization. *Journal of Catalysis,* 255**,** 79-93.

TARAS, S. & WOINAROSCHY, A. 2012. An interactive multi-objective optimization framework for sustainable design of bioprocesses. *Computers & Chemical Engineering,* 43**,** 10-22.

TARJANI, A., TOTH, A. J., NAGY, T., HAAZ, E., FOZER, D., ANDRE, A. & MIZSEY, P. 2018. Controllability Features of Dividing-Wall Columns. *Chemical Engineering Transactions,* 69**,** 403-408.

TEH, CHUA, HONG, LING, ANDIAPPAN, FOO, HASSIM & NG 2019. A Hybrid Multi-Objective Optimization Framework for Preliminary Process Design Based on Health, Safety and Environmental Impact. *Processes,* 7.

TORAMAN, N., KAHRAMAN, K., BILLINGS, P. & SABITOV, O. 2016. Optimize isomerization reactor temperatures and component RON. *Process/Plant Optimization,* 31-35.

TUAN, T. T., TUFA, L. D., ABDUL MUTALIB, M. I. & OLAKUNLE, K. R. 2017. An Hysys Simulation of a Dynamic Process using Linear Offset Free MPC with an Empirical Model. *Indian Journal of Science and Technology,* 10, 1-5.

TUAN, T. T., TUFA, L. D., MUTALIB, M. I. A. & ABDALLAH, A. F. M. 2016. Control of Depropanizer in Dynamic Hysys Simulation Using MPC in Matlab-Simulink. *Procedia Engineering,* 148, 1104-1111.

TUFANO, V. 1997. Heat recovery in distillation by means of absorption heat pumps and heat transformers. *Applied Thermal Engineering* 17, 171-178.

TULA, A. K., BABI, D. K., BOTTLAENDER, J., EDEN, M. R. & GANI, R. 2017. A computer-aided software-tool for sustainable process synthesis-intensification. *Computers & Chemical Engineering,* 105, 74-95.

ULYEV, L., VASILIEV, M. & BOLDYRYEV, S. 2018. Process integration of crude oil distillation with technological and economic restrictions. *J Environ Manage,* 222, 454-464.

UMEDA, T., HIRAI, A. & ICHIKAWA, A. 1972. Synthesis of optimal processing system by an integrated approach. *Chemical Engineering Science,* 27, 795-804.

VALAVARASU, G. & SAIRAM, B. 2013. Light Naphtha Isomerization Process: A Review. *Petroleum Science and Technology,* 31, 580-595.

VÁZQUEZ-OJEDA, M., SEGOVIA-HERNÁNDEZ, J. G., HERNÁNDEZ, S., HERNÁNDEZ-AGUIRRE, A. & KISS, A. A. 2013. Design and optimization of an ethanol dehydration process using stochastic methods. *Separation and Purification Technology,* 105, 90-97.

VERHOEF, A., DEGRÈVE, J., HUYBRECHS, B., VAN VEEN, H., PEX, P. & VAN DER BRUGGEN, B. 2008. Simulation of a hybrid pervaporation–distillation process. *Computers & Chemical Engineering,* 32, 1135-1146.

266

VOLKOVA, G. G., RESHETNIKOV, S. I., SHKURATOVA, L. N., BUDNEVA, A. A. & PAUKSHTIS, E. A. 2007. n-Hexane skeletal isomerization over sulfated zirconia catalysts with different Lewis acidity. *Chemical Engineering Journal,* 134**,** 106-110.

VUKOVIĆ, A. 2013. Reactor temperature optimization of the light naphtha isomerization unit. *GOMABN,* 52**,** 195-206.

WANG, P., ZHANG, J., WANG, G., LI, C. & YANG, C. 2016. Nature of active sites and deactivation mechanism for n-butane isomerization over alumina-promoted sulfated zirconia. *Journal of Catalysis,* 338**,** 124-134.

WATANABE, K., KAWAKAMI, T., BABA, K., OSHIO, N. & KIMURA, T. 2004. Simultaneous isomerization and desulfurization of sulfur-containing light naphtha over metal/SO42−/ZrO2-Al2O3 catalyst. *Applied Catalysis A: General,* 276**,** 145-153.

WATANABE, K., KAWAKAMI, T., BABA, K., OSHIO, N. & KIMURA, T. 2005. Effect of metals on the catalytic activity of sulfated zirconia for light naphtha isomerization. *Catalysis Surveys from Asia,* 9**,** 17-24.

WEST, A. H., POSARAC, D. & ELLIS, N. 2008. Assessment of four biodiesel production processes using HYSYS.Plant. *Bioresour Technol,* 99**,** 6587-601.

WEYDA, H. & KÖHLER, E. 2003. Modern refining concepts—an update on naphtha-isomerization to modern gasoline manufacture. *Catalysis Today,* 81**,** 51-55.

WIERTZEMA, H., SVENSSON, E. & HARVEY, S. 2020. Bottom–Up Assessment Framework for Electrification Options in Energy-Intensive Process Industries. *Frontiers in Energy Research,* 8.

WU, W., SHAO, B. & ZHOU, X. 2015. Dynamic control of a selective hydrogenation process with undesired MAPD impurities in the C3-cut streams. *Journal of the Taiwan Institute of Chemical Engineers,* 54**,** 28-36.

XU, Z. & WANG, R. 2017. Absorption heat pump for waste heat reuse: current states and future development. *Frontiers in Energy,* 11**,** 414-436.

YASAKOVA, E. A., SITDIKOVA, A. V. & ACHMETOV, A. F. 2010. Tendency of Isomerization Process Development in Russia and Foreign Countries. *Oil and Gas Business.*

YASHIMA, T., WANG, Z. B., KAMO, A., YONEDA, T. & KOMATSU, T. 1996. Isomerization of n-hexane over Platinum loaded zeolite catalysts. *Catalysis Today,* 29**,** 279-283.

YEOMANS, H. & GROSSMANN, I. E. 1999. A systematic modeling framework of superstructure optimization in process synthesis. *Computers and Chemical Engineering,* 23**,** 709-731.

ZHANG, L., QIAN, G., LIU, Z., CUI, Q., WANG, H. & YAO, H. 2015. Adsorption and separation properties of n-pentane/isopentane on ZIF-8. *Separation and Purification Technology,* 156**,** 472-479.

Books & Book Sections

ABUALIGAH, L. M. Q. 2018. *Feature Selection and Enhanced Krill Herd Algorithm for Text Document Clustering*, Springer International Publishing.

AMES, W. F. 2014. *Numerical methods for partial differential equations*, Academic Press.

ANCHEYTA, J. 2011. *Modeling and Simulation of Catalytic Reactors for Petroleum Refining,* New Jersey.

ASPENTECH 2011. *Aspen HYSYS Customization Guide.*

BIEGLER, L. T., GROSSMANN, I. E. & WESTERBERG, A. W. 1997. *Systematic methods of chemical process design*, Prentice Hall PTR.

BIRD, R. B., STEWART, W. E. & LIGHTFOOT, E. N. 2006. *Transport Phenomena*, Wiley.

BIRNBAUM, D. & VINE, M. A. 2007. *Microsoft Excel VBA Programming for the Absolute Beginner*, Thomson Course Technology.

BOODHOO, K. & HARVEY, A. 2013. Process Intensification: An Overview of Principles and Practice. *Process Intensification for Green Chemistry.*

CABRERA-RUIZ, J., SEGOVIA-HERNANDEZ, J. G., ALCANTARA-AVILA, J. R. & HERNANDEZ, S. 2012. Optimal Dynamic Controllability in Compressor-Aided Distillation Schemes Using Stochastic Algorithms. *In:* BOGLE, I. D. L. & FAIRWEATHER, M. (eds.) *22 European Symposium on Computer Aided Process Engineering.* Amsterdam: Elsevier Science Bv.

CAMACHO, E. F. & BORDONS, C. 2007. *Model Predictive Control,* London, Springer.

CAUSON, D. M. & MINGHAM, C. G. 2010. *Introductory finite difference methods for PDEs*, Bookboon.

CHAVES, I. N. D. O. G., ZAPATA, J. L. G. A., NINO, G. R. G., LOPEZ, J. R. G. & ROBAYO, A. L. 2016. *Process Analysis and Simulation in Chemical Engineering*, Springer.

COUPER, J. R., PENNEY, W. R. & FAIR, J. R. 2012. *Chemical Process Equipment: Selection and Design*, Elsevier Science.

DE BUCK, V., LÓPEZ, C. A. M., NIMMEGEERS, P., HASHEM, I. & VAN IMPE, J. 2019. Multi-objective optimisation of chemical processes via improved genetic algorithms: A novel trade-off and termination criterion. *In:* KISS, A. A., ZONDERVAN, E., LAKERVELD, R. & ÖZKAN, L. (eds.) *Computer Aided Chemical Engineering.* Elsevier.

EMARA, I. A., GADALLA, M. & ASHOUR, F. 2016. Supply Chain Design Network Model for Biofuel and Petrochemicals from Biowaste. *In:* VARBANOV, P. S., LIEW, P. Y., YONG, J. Y., KLEMES, J. J. & LAM, H. L. (eds.) *Pres2016: 19th International Conference on Process Integration, Modeling and Optimization for Energy Savings and Pollution Reduction.* Milano: Aidic Servizi Srl.

FLETCHER, R. 2010. The Sequential Quadratic Programming Method. *In:* DI PILLO, G. & SCHOEN, F. (eds.) *Nonlinear Optimization: Lectures given at the C.I.M.E. Summer School held in Cetraro, Italy, July 1-7, 2007.* Berlin, Heidelberg: Springer Berlin Heidelberg.

FOO, D. C. Y. & NG, D. K. S. 2013. *Process Integration for Cleaner Process Design. Handbook of Process Integration (PI): Minimisation of Energy and Water Use, Waste and Emissions*, Woodhead Publishing Ltd.

GARY, J. H., HANDWERK, G. E. & KAISER, M. J. 2007. *Petroleum Refining: Technology and Economics, Fifth Edition*, CRC Press.

GEN, M. & CHENG, R. 1997. *Genetic Algorithms and Engineering Design*, Wiley.

GEN, M. & CHENG, R. 2000. *Genetic Algorithms and Engineering Optimization*, Wiley.

GONSTANTINIDES, A. & MOSTOUFI, N. 2000. *Numerical Methods for Chemical Engineers with MATLAB Applications*.

GUNDERSEN, T. 2002. *A Process Integration PRIMER*, SINTEF Energy Research.

HAUPT, R. L. & HAUPT, S. E. 2004. *Practical genetic algorithms,* Hoboken, New Jersey, A JOHN WILEY & SONS, INC.

KAISER, M. J., DE KLERK, A., GARY, J. H. & HANDWERK, G. E. 2019. *Petroleum Refining: Technology, Economics, and Markets, Sixth Edition*, CRC Press.

KHOR, C. S. & SHAH, N. 2011. A superstructure optimization approach for optimal refinery water network systems synthesis with membrane-based regenerators. *21st European Symposium on Computer Aided Process Engineering.*

KISS, A. A. 2016. Process Intensification: Industrial Applications. *Process Intensification in Chemical Engineering.*

KISS, A. A., SEGOVIA-HERNÁNDEZ, J. G., BILDEA, C. S., MIRANDA-GALINDO, E. Y. & HERNÁNDEZ, S. 2012b. Innovative biodiesel production in a reactive dividing-wall column. *22nd European Symposium on Computer Aided Process Engineering.*

KLEMES, J. 2011. Sustainability in the process industry: integration and optimization. *Handbook of process integration.* McGraw-Hill Education.

LEPRINCE, P., DESCHAMPS, A. & JULLIAN, S. 2001a. Adsorption. *Petroleum Refining. Vol. 3 Conversion Processes.* Paris.

LEPRINCE, P., DESCHAMPS, A. & JULLIAN, S. 2001b. Adsorption in the Oil and Gas Industery. *Petroleum Refining. Vol. 3 Conversion Processes.* Paris

270

LEPRINCE, P. & TRAVERS, C. 2001. Isomerization of light paraffins. *Petroleum Refining. Vol. 3 Conversion Processes.* Paris Editions Technip.

MARCHETTI, M., RAO, A. & VICKERY, D. 2001. Mixed mode simulation-Adding equation oriented convergence to a sequential modular simulation tool. *Computer Aided Chemical Engineering.* Elsevier.

MARTÍN, M. M. 2015. *Introduction to Software for Chemical Engineers*, CRC Press.

MEYERS, R. A. 2004. *handbook of petroleum refining processes.*

MOHAMED A. FAHIM, TAHER A. ALSAHHAF & ELKILANI, A. 2010. *Fundamentals of Petroleum Refining.*

MUÑOZ, C. A., TELEN, D., NIMMEGEERS, P., CABIANCA, L., LOGIST, F. & VAN IMPE, J. 2017. Investigating practical aspects of the exergy based multi-objective optimization of chemical processes. *In:* ESPUÑA, A., GRAELLS, M. & PUIGJANER, L. (eds.) *Computer Aided Chemical Engineering.* Elsevier.

PERRY, R. H. & GREEN, D. W. 1999. *Perry's chemical engineers' handbook,* McGraw-Hill Professional.

PETERS, M. S. & TIMMERHAUS, K. D. 1991. *Plant design and economics for chemical engineers.*

PONCE-ORTEGA, J. M. & HERNANDEZ-PEREZ, L. G. 2019. *Optimization of Process Flowsheets Through Metaheuristic Techniques*, Springer Nature Customer Service Center Gmbh.

RANGAIAH, G. P. 2016. *Chemical Process Retrofitting and Revamping: Techniques and Applications*, Wiley.

RICHARDSON, J. F., HARKER, J. H. & BACKHURST, J. R. 2002. Coulson and Richardson's Chemical Engineering Volume 2 - Particle Technology and Separation Processes (5th Edition). Elsevier.

ROSINHA, I. P., GERNAEY, K. V., WOODLEY, J. M. & KRUHNE, U. 2015. Topology optimization for biocatalytic microreactor configurations. *In:* GERNAEY, K. V., HUUSOM, J. K. & GANI, R.

(eds.) *12th International Symposium on Process Systems Engineering.*

ROSS, J. R. H. 2012. Some Catalytic Reactions. *Heterogeneous Catalysis.* Elsevier.

RUIZ-FEMENIA, R., JAVALOYES-ANTÓN, J., SALCEDO-DÍAZ, R., RAVAGNANI, M. A. S. S. & CABALLERO, J. A. 2020. Integration of Chemical Process Simulators with Algebraic Modeling Languages. *In:* PIERUCCI, S., MANENTI, F., BOZZANO, G. L. & MANCA, D. (eds.) *Computer Aided Chemical Engineering.* Elsevier.

RUTHVEN, D. M. 1984. *Principles of adsorption and adsorption processes*, John Wiley & Sons.

RUTHVEN, D. M., FAROOQ, S. & KNAEBEL, K. S. 1994. *Pressure Swing Adsorption*, VCH Publishers.

SCHWEFEL, H.-P. 1981. *Numerical Optimization of Computer Models*, John Wiley & Sons, Inc.

SEADER, J. D. & HENLEY, E. J. 2006. *Separation process principles.*

SEGOVIA-HERNÁNDEZ, J. G. & GÓMEZ-CASTRO, F. I. 2017. *Stochastic Process Optimization using Aspen Plus®*, CRC Press.

SEIDER, W. D., SEADER, J. D., LEWIN, D. R. & WIDAGDO, S. 2017. *Product and Process Design Principles: Synthesis, Analysis, and Evaluation*, Wiley.

SEIDER, W. D., SEADER, J. D., LEWIN, D. R. & WIDAGDO, S. 2019. *Product and Process Design Principles: Synthesis, Analysis and Design*, John Wiley & Sons, Limited.

SINNOTT, R. K. 2005. Costing and Project Evaluation. *Coulson & Richardson's chemical engineering. Volume 6, Chemical engineering design.* 4 th ed.: Oxford : Butterworth-Heinemann.

SMITH, G. D., SMITH, G. D., SMITH, G. D. S., SMITHER, M. & PRESS, O. U. 1985. *Numerical Solution of Partial Differential Equations: Finite Difference Methods*, Clarendon Press.

STINE, M. 2004. Processes to Improve The Qualities of Distillates: Isomerization. *Encyclopaedia of Hydrocarbons: Refining and Petrochemicals.* UOP LLC.

SULLIVAN, D., METRO, S. & PUJADÓ, P. R. 2015. Isomerization in Petroleum Processing. *In:* TREESE, S. A., PUJADÓ, P. R. & JONES, D. S. J. (eds.) *Handbook of Petroleum Processing.* 2 nd ed.: Springer International Publishing.

TAKAYAMA, A. & AKIRA, T. 1985. *Mathematical Economics*, Cambridge University Press.

TURTON, R., BAILIE, R. C., WHITING, W. B. & SHAEIWITZ, J. A. 2009. *Analysis, Synthesis, and Design of Chemical Processes*.

VALADI, J. & SIARRY, P. 2014. *Applications of Metaheuristics in Process Engineering*, Springer International Publishing.

WANG, D. L., FENG, X. & DENG, C. 2013. Modular Integrated Framework for Process Synthesis and Optimization Based on Sequential Process Simulator. *In:* VARBANOV, P., KLEMES, J. J., SEFERLIS, P., PAPADOPOULOS, A. I., VOUTETAKIS, S. & PIERUCCI, S. (eds.) *16th International Conference on Process Integration, Modelling and Optimisation for Energy Saving and Pollution Reduction.* Milano: Aidic Servizi Srl.

WOOD, K. R., LIU, Y. A. & YU, Y. 2018. Simulation of Adsorption Processes *In:* KGAA, W.-V. C. (ed.) *Design simulation and optimization of adsorptive and chromatographic separations: a hands-on approach.* 1 st ed.: Blackwell Verlag GmbH.

YANG, R. T. 2013. *Gas Separation by Adsorption Processes*, Elsevier Science.

ZADEH, L. & DESOER, C. 1979. *Linear system theory: the state space approach*, Courier Dover Publications.

Patents

EVANS, W. E. & STEM, S. C. 1988. *Isomerization process with recycle of mono-methyl-branched paraffins and normal paraffins*. US patent application US4804802A.

GIYAZOV, O. V. & PARPUTS, O. I. 2013a. *Hydroisomerization and isomerization process using reactive rectification column*. United States patent application.

GIYAZOV, O. V. & PARPUTS, O. I. 2013b. *Naphtha isomerisation on three catalytic reaction zones inside a distillation column*. 12715238.7.

HAENSEL, V. 1975. *Combination process of isomerization and a sorption process followed by selective frationation*. US-2966528-A.

HOLCOMBE, T. C. 1980. *Total isomerization process*.

HOLCOMBE, T. C., SAGER, T. C., VOLLES, W. K. & ZARCHY, A. 1990. *Isomerization Process*. 4,929,799.

O'BRIEN, D. E. & RICE, L. H. 2002. *Somerization process with adsorptive separation and integrated fractional distillation*.

RICE, L. & PLAINES, H. D. 2002. *Process for distillation, in a column with a dividing wall, of saturated hydrocarbons obtained by isomerisation*. US patent application.

RICE, L. H. 2007. *Isomerization process*. Unlted States patent application.

STEM, S. C. & EVANS, W. E. 1987. *Total isomerization process with mono-methyl-branched plus normal paraffin recycle stream*. US patent application US4717784A.

ZARCHY, A. S., N.Y., A., SYMONIAK, M. F. & N.C., G. 1993. *Isomerization with distillation and psa recycle streams*.

Conferences

ARJOMANDI, R. K. Statistical methods for control loop performance assessment. 2011 International Conference on Communications, Computing and Control Applications (CCCA), 3-5 March 2011 2011. 1-6.

DUQUE, A. & OCHOA, S. Dynamic optimization for controlling an acrylic acid process. 2017 IEEE 3rd Colombian Conference on Automatic Control (CCAC), 18-20 Oct. 2017 2017. 1-6.

GRAEME, S. & ROSS, J. 2004. Advanced Solutions for Paraffins Isomerization. *National Petrochemical & Refiners Association.* Marriott Rivercenter Hotel San Antonio, TX: National Petrochemical & Refiners Association.

HUMPHREY, J. L. Separation processes : playing a critical role. 1995.

KENNEDY, J. & EBERHART, R. Particle swarm optimization. Proceedings of ICNN'95 - International Conference on Neural Networks, 27 Nov.-1 Dec. 1995 1995. 1942-1948 vol.4.

KHAN, M. S., HUSNIL, Y. A., KWON, Y. S. & LEE, M. Automated optimization of process plant using particle swarm optimization. 2011 International Symposium on Advanced Control of Industrial Processes (ADCONIP), 23-26 May 2011 2011. 615-620.

LOUGHLIN, K. F. & AL-SOUDANI, T. M. Modeling and Simulation of a Combined Reactor/Pressure Swing Adsorption Unit for Isomerization of a Mixed Feed of Pentanes and Hexanes. The 2005 Annual Meeting, 2005.

MARIA, A. 1997. Introduction to modeling and simulation. *In:* ANDRADOTTIR, A., HEALY, K. J., WITHERS, D. H. & NELSON, B. L. (eds.) *Winter simulation conferance.*

MELONI, A. & MURRONI, M. On the genetic optimization of APSK constellations for satellite broadcasting. 2014 IEEE International Symposium on Broadband Multimedia Systems and Broadcasting, 25-27 June 2014 2014. 1-6.

MUHAMMED, T. A. A. & WAGIALLA, K. M. 2016. A Novel Software Application in Water Pinch Analysis for Water and Wastewater Minimization in Petroleum Refinery and Sugar Plants. *7th Annual Conference for Postgraduate Studies and Scientific Research Basic Sciences and Engineering Studies.* University of Khartoum, Sudan.

RASHEED, K. & GELSEY, A. Adaptation of genetic algorithms for engineering design optimization. Fourth International Conference on Artificial Intelligence in Design, 1996. Citeseer.

SALAHSHOOR, K. & ARJOMANDI, R. K. Comparative evaluation of control loop performance assessment schemes in an industrial chemical process plant. 2010 Chinese Control and Decision Conference, 26-28 May 2010 2010. 2603-2608.

SALAHSHOOR, K., KARIMI, I., FAZEL, E. N. & BEITARI, H. 2011. Practical Design and Implementation of a Control Loop Performance Assessment Package in an Industrial Plant. *Proceedings of the 30th Chinese Control Conference.* Yantai, China.

VOJTESEK, J., DOSTÁL, P. & MASLAN, M. Modelling And Simulation Of Water Tank. *In:* ECMS, ed. Computer Science, 2014.

Theses

FANG, X. 2007. *Engineering design using genetic algorithms.* PhD, Iowa State University.

FARROKHPANAH, S. 2009. *Design of heat integrated low temperature distillation systems.* University of Manchester.

KLERK, A. D. 2008. *Fischer-Tropsch Refining.* PhD, University of Pretoria.

LØFTEN, T. 2004. *Catalytic isomerization of light alkanes* Norwegian University of Science and Technology.

Online Sources

ASPENTECH. 2019. Available: www.AspenTech.com [Accessed].

AXENS, P. L. 2009. Isomerization: High octane C5/C6 cuts via isomerization processes. Axens IFP group technologies.

BROWNEL. 2017. Available: www.brownel.co.uk [Accessed].

CHARLIEGEFEN. 2017. *Naphtha Market By Product (Light Naphtha, Heavy Naphtha), By Application (Chemicals, Energy/Fuels) - Growth, Share, Opportunities & Competitive Analysis, 2016 - 2030* [Online]. Available: http://www.credenceresearch.com/report/naptha-market [Accessed].

KITCHIN, J. 2013. *Running Aspen via Python* [Online]. Chemical Engineering at Carnegie Mellon University. Available: https://kitchingroup.cheme.cmu.edu/blog/2013/06/14/Running-Aspen-via-Python/ [Accessed June 16 2020].

MATHWORKS. 2019. Available: www.MathWorks.com [Accessed].

OIL & GAS, J. 2018. *Oil & Gas Journal* [Online]. Available: https://www.ogj.com/index.html [Accessed].

OILS, F. 2015. Unleaded petrol 95 octane bs en 228. *In:* SHEET, S. D. (ed.).

ZAUBA TECHNOLOGIES & DATA, J. 2013. *Platinum catalyst* [Online]. Available: https://www.zauba.com/import-platinum-catalyst/hs-code-38151290-hs-code.html [Accessed 29/10/2017].